UNIVERSITY OF CALIFORNIA,
IRVINE

Optimization of Solid Sorbent CO_2 Capture and Water Usage Reduction in Advanced Power Generation

DISSERTATION

submitted in partial satisfaction of the requirements
for the degree of

DOCTOR OF PHILOSOPHY

in Mechanical and Aerospace Engineering

by

QIN CHEN

Dissertation Committee:
Professor G. Scott Samuelsen, Chair
Professor Jack Brouwer
Professor Yun Wang

2015

DEDICATION

To

my beloved wife Yingxi and my mother

for their unconditional love, constant support and encouragement

and for always believing I can make it

TABLE OF CONTENTS

LIST OF FIGURES

Page

LIST OF TABLES

NOMENCLATURE

0/1/2/3 D	Zero/One/Two/Three dimensional
AGR	Acid Gas Removal
ASU	Air separation unit
BFW	Boiler feed water
CCS	Carbon capture and storage
CFB	Circulating fluidized bed
CFD	Computational fluid dynamics
COE	Cost of electricity
CRP	Conservation Reserve Program
DCC	Directed contact cooler
DEA	Diethanolamine
DGA	Diglycolamine
DIPA	Diisopropanolamine
DOE	U.S. Department of Energy
EP	Elevated pressure
FGD	Flue gas desulfurization
F-T	Fischer-Tropsch
GE	General Electric
HHV	Higher heating value
HP/IP/MP/LP	High/ Intermediate/ Medium /Low pressure
HRSG	Heat recovery steam generator
HTS	High temperature shift

IGCC	Integrated gasification combined cycle
ITM	Ion Transport Membrane
LDF	Linear driving force
LHV	Lower heating value
LTS	Low temperature shift
MDEA	Methyldiethanolamine
MEA	Monoethanolamine
NETL	National Energy Technology Laboratory
NRCS	Natural Resources Conservation Service
O&M	Operating and maintenance
PC	Pulverized coal
PSA	Pressure swing adsorption
RPS	Renewable portfolio standard
SCR	Selective catalytic reduction
SMR	Steam methane reforming
T-S	Temperature-entropy
TS&M	Transporting, storing , and monitoring
TSA	Temperature swing adsorption
UDF	User defined functions
USDA	U.S. Department of Agriculture
VPSA	Vacuum pressure swing adsorption
VSA	Vacuum swing adsorption
WGS	Water gas shift

SYMBOLS

A	Area, m^2
B	Equilibrium concentration of bound, mol/g
c	Mole concentration (mol/m^3) or Specific heat (J/kg/K) or constant
c_p	Heat capacity, J/kg/K
C	Fluid capacity rate ratio
CoC	Cycles of concentration
COP	Coefficient of Performance
D	Mass diffusivity (m^2/s) or diameter (m)
D_T	Thermal diffusivity, m^2/s
e	Effectiveness
E	Activation energy of Arrhenius Equation or Energy (J/kg)
f	Correction factor
F	Equilibrium concentration of free (mol/g) or heat exchange area (m^2)
g	Gravity, 9.81 m/s^2
h	Heat transfer coefficient ($W/m^2/K$) or enthalpy (J/kg) or differential head (m)
h_m	Mass transfer coefficient, $kg/s/m^2$
$h_{s,out}$	Outlet enthalpy if the pressure change process is isentropic
H	Adsorption heat or desorption heat, kJ/kmol
k	Rate constant of the first order reaction (1/s) or thermal conductivity (W/m/K)
k_b	Rate constant for linear driving force model, 1/s
K	Heat transfer coefficient, $W/m^2/K$

K_0	Median binding affinity constant
K_{eq}	Equilibrium constant
L	Length, m
Le_f	Lewis factor
m	Heterogeneity index
$\dot{m}$	Mass flow rate, kg/s
$M\ or\ MW$	Molecular weight, kg/kmol
Me	Merkel number
N	Number of moles, mole
N_t	Total number of binding sites, mol/g
NTU	Number of Transfer Units
p	Pressure, Pa
P	Power, W
q	Heat flux, W/s
$\bar{q}$	Average actual amount of adsorption in sorbent, kmol/kg
q^*	Amount of adsorption in equilibrium, kmol/kg
Q	Volumetric flow rate, m^3/s
$\dot{Q}$	Heat rate, J/s
r	Rate of reaction, $mol/m^3/s$
R	Relaxation factor or universal gas constant (8.314 J/K/mol)
$R\ or\ r$	Radius, m
Re	Reynolds number
R_gT	Average kinetic energy of Arrhenius Equation

RH	Relative humidity
S	Source term
t	Time, s
T	Temperature, K
v	Velocity, m/s
V	Volume, m^3
x	Length, m
Y	Mass fraction
Z	Flow direction axis, m

Greek symbols

a	Coefficient related to the median binding affinity constant
ε	Porosity
η	Efficiency or heat exchange efficiency or effectiveness factor
μ	dynamic viscosity, N s/m^2
ρ	Density
$\bar{\bar{\tau}}$	Stress tensor, pa
υ	Kinematic viscosity, m^2/s
ϕ	Thiele modulus
ω	Humidity ratio

Subscripts

0	Standard or base condition
$1\ or\ 2$	Condition 1 or 2

$a\ or\ air$	Air
b	Bed
$cond$	Condensed water
CR	Cooling water
CT	Cooling tower
eff	Effectiveness
equ	Equilibrium
f	Fluid
i	Species i
$in\ or\ i$	Inlet
max	Maximum
$mech$	Mechanical
min	Minimum
MK	Makeup water
$out\ or\ o$	Outlet
p	Particle or packing
s	Surface
T	Total
V	Water vapor or unit volume
$w\ or\ H_2O$	Water

ACKNOWLEDGEMENTS

I would like to express my deepest gratitude to my advisor and committee chair, Professor Scott Samuelsen, for his unwavering guidance and support to complete my dissertation. His broad vision, disciplined work ethics, and genuine kindness have continuously inspired me throughout my Ph.D. study and set a role model for my future professional career.

I would also like to express my sincere appreciation to Dr. Ashok Rao for his continuous support, guidance and encouragement in my research work. His rich knowledge and creative insights about power and energy systems have been an invaluable resource to me. Without his knowledge and guidance, I would probably have stopped along the way. Many thanks for being so patient.

I warmly express gratitude to Professor Jack Brouwer and Professor Yun Wang for serving as my committee members and providing suggestions to improve my dissertation. I would also like to thank Professor Derek Dunn-Rankin and Professor Sunny Jiang for serving as my qualifying committee members.

I would also like to thank Dr. Ambalavanan Jayaraman from TDA research Inc. for his support and assistance on my research, particularly for his guidance and help with the CFD simulation of adsorption process.

My sincere appreciate to the staffs of the Advanced Power and Energy Program (APEP) at the University of California, Irvine (UCI), including Professor Vince McDonell,

Richard Hack, Dr. Li Zhao, Brendan Shaffer, Dr. Brian Tarroja, Dr. Ghazal Razeghi, Jeff Wojciechowski, Will Decker, Steven Lee, Jean Grigg, Alyssa Way and Michelle Mendez, for their assistance, support and friendship.

I would also like to appreciate the friendship and help during the journey from many of my fellow students at APEP and Department of Mechanical and Aerospace Engineering, which include Dr. Zhixuan Duan, Dr. Li Zhang, Dr. Mu Li, Jin Dang, Dr. Lei Zhan, Robert Flores, Gia Nguyen, Kersey Manliclic, Dr. Michael Mac Kinnon, Justin Chow, Dr. Howard Lee, Alicia Tan, David Page, Dr. Anh-Tuan Do, Alireza Kalantari, Dimas Avila, Andres Colorado, Derek McVay, Fabian Rosner.

Finally I acknowledge and appreciate the funding support of my research from the U.S. Department of Energy (DOE) and TDA Research Inc.

CURRICULUM VITAE

QIN CHEN

EDUCATION

Doctor of Philosophy **2010 - 2015**
Advanced Power and Energy Program GPA: 3.92/4.0
Department of Mechanical and Aerospace Engineering
University of California, Irvine
Advisor: Professor Scott Samuelsen
Dissertation: ***Optimization of Solid Sorbent CO_2 Capture and Water Usage Reduction in Advanced Power Generation***

Master of Science (in Engineering Thermophysics) **2007 -2010**
Institute of Engineering Thermophysics GPA:
Chinese Academy of Sciences (China) 81.3/100
Advisor: Professor Yue Wang
Thesis: ***A Study on Reaction Conditions and Characteristics of Mild Combustion of Gas Turbine Combustor Application***

Bachelor of Science (in Flight Vehicle Propulsion Engineering) **2003 - 2007**
School of Energy and Power Engineering GPA:
Beijing University of Aeronautics and Astronautics (China) 83.0/100

RESEARCH EXPERIENCE

Advanced Power and Energy Program at University of California, Irvine 2010 - 2015
Graduate Student Researcher

- Process simulation and optimization of advanced power generation systems (coal and biomass gasification, gas turbine, carbon capture, IGCC, pulverized coal-fired power plants, etc.).
- Established cost methodologies and economic models for power generation systems, and developed cost assessments for new power plant technologies using Aspen Process Economic Analyzer.
- Developed and validated CFD models for solid sorbent CO_2 adsorption and desorption with experimental data, using ANASYS Fluent incorporated with User Defined Functions (UDF).

- Designed an advanced reactor concept of integrated water-gas-shift and solid sorbent CO_2 adsorption using CFD simulation tools for pre-combustion CO_2 capture applications in IGCC.
- Built mathematical heat and mass transfer models of wet and dry cooling towers, successfully evaluated and optimized performance of combined wet and dry cooling system for power plant applications.

Energy Systems Laboratory, GE Global Research **Jun-Aug**
Graduate Research Intern **2014**

- Led research on heat mass transfer simulation for the project of turbine inlet chilling power generation.
- Developed and validated 1-D finite difference heat and mass transfer model of liquid desiccant regenerator, and successfully predicted its performance in turbine inlet chilling application.

Institute of Engineering Thermophysics, Chinese Academy of Sciences **2008 - 2010**
Graduate Student Researcher

- Conducted hands-on experimental research on stability and fuel flexibility of syngas combustion for IGCC applications, e.g. diffusion, premixed, flameless, and vortex combustion.
- Performed laser diagnostics (LDV and PLIF), obtained velocity distribution and OH* images of flameless flame in a 2-stage combustor, and identified O_2 content as a key factor for flameless formation.
- Developed CFD and chemical reaction networks (CRN) simulations for a 2-stage flameless combustor, and identified NO_x produced in the 1st stage is the major contributor of total NO_x emissions.

Beijing University of Aeronautics and Astronautics **Feb-Jul 2007**
Undergraduate Student Researcher

- Developed CFD simulations and evaluated the heat and mass transfer performance of various flame tube cooling structures with different multi-jet holes in jet engine combustor applications.

JOURNAL PUBLICATIONS

Journal Papers

- **Qin Chen**, Ashok Rao, Scott Samuelsen. Coproduction of transportation fuels in advanced IGCCs via coal and biomass mixtures. Applied Energy 2015; 157: 851-860

- **Qin Chen**, Ashok Rao, Scott Samuelsen. H_2 coproduction in IGCC with CCS via coal and biomass mixture using advanced technologies. Applied Energy 2014; 118: 258-270.
- **Qin Chen**, Zhedian Zhang, Jianan Zhang, Weiwei Shao, Yue Wang, Yunhan Xiao. Numerical investigation on thermodynamics and fuel conditions of mild combustion in gas turbine combustor. Gas Turbine Technology 2010; 23(4): 22-26.
- Hui Wu, **Qin Chen**, Weiwei Shao, Yongliang Zhang, Yue Wang, Yunhan Xiao. Combustion of hydrogen in an experimental trapped vortex combustor. J of Thermal Science 2009; 18(3): 256-261.
- Zhiqiang Li, Tao Tian, **Qin Chen**. Numerical simulations of flame tube cooling structure with multi-jet holes. Journal of Beijing University of Aeronautics and Astronautics 2008; 34(10): 1204-1209.

Conference Papers and others

- **Qin Chen**, Ashok Rao, Scott Samuelsen. Solid sorbent post-combustion CO_2 capture in subcritical PC power plant. Proceedings of the ASME 2015 Power and Energy Conversion Conference. San Diego, California; June 28-July 2, 2015.
- **Qin Chen**. Heat and mass transfer model for cooling tower and LiBr regenerator in turbine inlet chilling system. Proceedings of the ASME 2015 Power and Energy Conversion Conference. San Diego, California; June 28-July 2, 2015.
- **Qin Chen**, Ashok Rao, Scott Samuelsen. Combined WGS and CO_2 removal technology for pre-combustion CO2 capture. International Colloquium on Environmentally Preferred Advanced Power Generation. Irvine, California; March 23-24, 2015.
- **Qin Chen**, Ching-Jen Tang, Laura Hudy. Heat and mass transfer model of LiBr regenerator in turbine inlet chilling system. GE Global Research Annual Intern Poster Session. Niskayuna, NY; August 5, 2014.
- **Qin Chen**, Ashok Rao, Scott Samuelsen. Solid sorbent based post-combustion CO_2 capture in coal-fired power plant. International Colloquium on Environmentally Preferred Advanced Power Generation. Newport Beach, California; April 1-3, 2014.
- **Qin Chen**, Ashok Rao, Scott Samuelsen. H_2 coproduction in advanced IGCCs. International Colloquium on Environmentally Preferred Advanced Power Generation. Newport Beach, California; April 23-25, 2013.
- Ashok Rao, **Qin Chen**, and Scott Samuelsen. Design concepts for co-production of power, fuels & chemicals via coal/biomass mixtures. University Of California, Irvine, 2012.
- **Qin Chen**. A study on reaction conditions and characteristics of mild combustion of gas turbine combustor application. Beijing: Chinese Academy of Science, 2010.

- **Qin Chen**, Hui Wu, Zhedian Zhang, Yue Wang and Yunhan Xiao. Thermodynamics design of trapped vortex combustor operating on hydrogen. Proceedings of the Annual Combustion Conference of Chinese Society of Engineering Thermophysics, Hefei, Anhui; November 2009.

SKILLS

- CFD, ANSYS Fluent, Fluent UDF, ANASYS CFX, Aspen Plus®, Aspen Process Economic Analyzer, Engineering Equations Solver (EES), MATLAB, CHEMKIN, C, C++, Fortran
- Planar Laser-Induced Fluorescence (PLIF), Laser Doppler Velocimeter (LDV)

AWARDS AND HONORS

- Graduate Research Assistantship of University of California, Irvine 2010 - 2015
- Association of Energy Engineers Southern California Chapter Scholarship 2012
- Outstanding Graduate Award for BUAA Class 2007 2007
- BUAA Outstanding Undergraduate Graduate Thesis 2007

ABSTRACT OF THE DISSERTATION

Optimization of Solid Sorbent CO_2 Capture and Water Usage Reduction in Advanced Power Generation

By
QIN CHEN

Doctor of Philosophy in Mechanical and Aerospace Engineering
University of California, Irvine, 2015
Professor G. Scott Samuelsen, Chair

Greenhouse gas emissions and water usage are two major concerns in the power generation sector. Advanced clean coal technologies (i.e., solid sorbent CO_2 capture technologies and combined wet/dry cooling system) are promising for future central power generation in order to achieve sustainable, secure, and efficient system performance. This dissertation describes research associated with advanced coal derived clean power generation, from near-term pulverized coal (PC) power plant strategies retrofitted for CO_2 capture, to long-term integrated gasification combined cycle (IGCC) power generation, to co-production IGCC with carbon capture and storage (CCS) co-fueled by coal and biomass.

In this study, the post-combustion solid sorbent based CO_2 capture system for the PC power plant is optimized for integration in order to minimize plant modifications and the associated downtime. Due to significantly less steam usage in sorbent regeneration, the PC plant with advanced solid sorbent CO_2 capture has better performance and lower cost of electricity than the plant using conventional amine scrubbing technology. By employing a combined wet/dry cooling system, the PC plant with CO_2 capture reduces

water usage significantly, while the performance and water usage are a function of ambient conditions as predicted by a mathematical model, the latter of which is validated by experimental data from the literature.

Pre-combustion solid sorbent based CO_2 capture technologies used in the IGCC are evaluated by systems analysis and compared to Selexol^{TM} CO_2 capture. Compared with the Selexol^{TM} approach, solid sorbent CO_2 capture results in a power plant with significantly higher overall plant efficiency and more attractive economics.

Computational fluid dynamics (CFD) simulation models were developed for both solid sorbent CO_2 capture alone, and combined water gas shift (WGS) and solid sorbent CO_2 capture in the IGCC applications. ANSYS FLUENT and User Defined Functions (UDF) were the resources adopted to incorporate the fluid mechanics, heat and mass transfer, water vaporization, adsorption equilibrium and kinetics, and WGS reaction kinetics . The CFD models were validated by experimental data, and applied to commercial size fixed bed reactor designs and simulations. It was found that (1) the CO_2 breakthrough time or CO_2 loading capacity is independent of reactor geometry as long as the space velocity is constant, (2) the adsorption rate is the rate controlling step for CO_2 capture using solid sorbent, and (3) break through occurs before the solid sorbent near the exit of the bed is fully utilized due to bulk transfer of the CO_2 in the axial direction. However, a low space velocity can increase the loading of the sorbent. The CFD approach also assists in the design of effective thermal management strategies for the reactor in the case of combined WGS and solid sorbent CO_2 capture.

Co-feeding of biomass along with coal and the co-production of H_2 and synthetic fuels in IGCCs is evaluated for future clean coal power generation. It was determined by systems analyses that co-feeding and co-production IGCCs are preferable for renewable energy utilization and energy security, with the co-products being produced at competitive costs.

Chapter 1 Introduction

2.1 Motivation

Energy usage is an increasingly important topic world-wide, as climate change caused by greenhouse gases becomes a global concern, while energy security highlights the economic development of the world. Clean and stable energy supply has been demanded and desired in this context. Coal is a primary energy source; the world consumption of coal was 162 Quadrillion Kilojoules in 2012 which accounts for about 28.5% of the world total energy consumption and is predicted to increase to 232 Quadrillion Kilo-joules in 2040 with an average annual growth rate of 1.3%, and is expected to maintain a similar share of the total energy consumption in 2040. Particularly in the power generation sector, coal-fired plants generated 8.4 Trillion kW h of electricity in 2012 or 39.4% of total world electricity generation while 13.9 Trillion kW h of electricity or 35.6% of total world electricity generation is predicted to be generated by coal-based plants in 2040 [1]. Coal-fired power plants are the major emitters of CO_2 emissions, and various other pollutants, such as particulate matter, sulfur oxides, nitrogen oxides and mercury. For example, the US emitted 5290 Million Metric Tons of CO_2 in 2012; electrical power generation in particular accounted for 38.5% of the CO_2 emissions, and coal provided 74.3% of the electrical power for the US [2].

Pulverized coal (PC) fired boiler is one of the major coal-fired power generation technologies, and subcritical PC plant is one of the mature technologies that is widely

used in U.S. electricity generation sector. Subcritical PC plants operate the steam cycle below the critical point of water, resulting in a lower electricity efficiency than supercritical PC plants, and consequently higher CO_2 emission level at 807 kg/MWh (or 1,780 lb /MWh) [3], higher than any other non-CO_2-captured electricity generation technologies. One trend toward zero CO_2 emission power generation goal is to retrofit existing coal-fired power plants, especially subcritical PC power plants, with integration-friendly CO_2 capture technologies to reduce GHG.

Current studies on post-combustion CO_2 capture [4]–[6] are mostly focused on amine based CO_2 capture technology, while due to large amount of steam required by extraction from the steam turbine for amine regeneration, a significant modification to the steam turbine is necessary. Furthermore, such plants require a larger amount of makeup water due to the cooling of amine process when using wet cooling towers for plant heat rejection. Thus, it makes amine based CO_2 capture technology not an ideal option for retrofitting an existing PC power plant. Solid sorbent CO_2 capture technology separates CO_2 from the flue gas via strong physical adsorption followed by desorption. One advantage of solid sorbent CO_2 capture is the lower energy consumption for sorbent regeneration. A number of publications have been made investigating solid sorbents for CO_2 capture [7]–[10], while limited work has been focused on system analyses of solid sorbent CO_2 capture technology integrated into PC power plants and even lesser for retrofitting such plants and addressing the corresponding design concerns such as water usage. This proposed research of PC power plant would focus on system design of retrofitting existing subcritical PC power plant with solid sorbent based

CO_2 capture. PC power plants retrofitted with solid sorbent based CO_2 capture is supposed to consume less water than amine process, yet significantly higher than non-CO_2 captured plants, which also have been criticized for huge water usage. In addition, water shortage has been a major concern for future coal-derived electricity and a big challenge for energy-water nexus, especially in a climate change context. Considering wet cooling towers are the primary water consumer in coal fired power plants and weather/climate conditions greatly affect performance of cooling systems, another proposed research focus of PC power plant is advanced plant heat rejection strategies aimed at reducing water usage, e.g. combined wet/dry cooling systems, and the cooling system performance under various weather/climate conditions.

For future new-built coal based power generation, Integrated Gasification Combined Cycle (IGCC) is an environmentally clean approach that has drawn intense attention world-wide in the past three decades [11]. IGCC combines gasification and combined cycle to achieve the environmental benefits by converting coal into a clean synthesis gas (or syngas which is mainly H_2 and CO), utilizing it in a topping Brayton cycle gas turbine which is followed by a bottoming Rankine cycle steam turbine. Air Separation Unit (ASU) provides O_2 to the gasifier for partial oxidation of coal (and/or biomass) to produce syngas. Gas cleanup units downstream of the gasifier remove pollutants, such as sulfur compounds, particulates and mercury from the raw syngas. By adding a water gas shift reactor and a carbon capture process (coupled with sequestrating for the captured CO_2), the clean syngas could be converted into a decarbonized fuel (mostly H_2) suitable for near zero emission energy conversion in the combined cycle. Compared with a PC

power plant, water usage of an IGCC is much lower because a large fraction of the power is generated by the gas turbine. A number of advanced technologies are being studied to improve the performance of IGCC systems [12], [13]. However, research publications on component performance and integration of the advanced clean coal technologies of interest such as solid sorbent based pre-combustion CO_2 capture in an IGCC are limited. As a novel technology, reactor design, performance prediction and system integration of solid sorbent CO_2 capture are rarely reported in literature. This proposed research on IGCC would focus on evaluation of IGCCs using advanced technologies, with particular focus on solid sorbent based pre-combustion CO_2 capture using the tool of Computational fluid dynamics (CFD) simulation incorporated with physical models.

Another major advantage of IGCC is the flexibility for cofeeding (e.g., biomass) and coproduction (e.g., clean fuels or chemicals) toward renewable power generation and energy security. Cofeeding of biomass along with coal in IGCC is also an approach toward zero carbon emissions. Coproduction of electricity and H_2 and other fuels in IGCC plants [14]–[16] is a promising option for mass production of a non CO_2 emitting fuel for various applications. Currently, most research on cofeeding and coproduction in IGCCs has been focused on commercially ready or conventional technologies. The effect of cofeeding and coproduction on advanced IGCC system performance and cost has not been established yet. This dissertation research targets at integration of advanced technologies in IGCC systems with carbon capture and the evaluation of cofeeding and coproduction.

2.2 Goal

The goal of the dissertation research is to develop, characterize, and evaluate power generation systems using advanced clean coal technologies for both PC power plants and IGCC applications.

2.3 Objectives

In order to achieve the research goal, the following set of objectives was adopted:

1. Retrofit an existing subcritical PC power plant with post-combustion solid sorbent based CO_2 capture technology.
2. Investigate cooling system strategies for PC power plant retrofitting, and corresponding performance under various weather/climate conditions.
3. Design, analyze and compare conventional and advanced IGCC power systems.
4. Evaluate solid sorbent based pre-combustion CO_2 capture technologies using CFD for advanced IGCC.
5. Investigate and evaluate advanced IGCCs with biomass and coal cofeeding for electricity and H_2 / other fuels coproduction.

Chapter 2 Background

2.1 Pulverized Coal Power Generation

2.1.1 Process of PC Power Plants

Pulverized coal (PC) power plant is a conventional type of electricity generation thermal plant, which converts chemical energy of coal into electrical energy. A process schematic of a typical PC power plant is presented by Figure 2-1. Coal is ground and pulverized to fine powder, which is then blown into the boiler with air for burning [17]. The power plant steam cycle is typically a reheat Rankine Cycle [18]. High pressure (HP) boiler feed water (BFW), pumped through pipes and tubes inside the boiler, is heated up and turned into steam. The HP steam is expanded in HP steam turbine by pushing against a series of turbine blades to drive turbine shaft which is connected to generator shaft for power generation. Steam exiting HP turbine recycles to the boiler for reheat, and then flows back to intermediate pressure (IP) and low pressure (LP) turbines to generate electricity. Exhaust steam exiting LP turbine is drawn into a surface condenser and converted to liquid phase by cooling water for recycle to the boiler and complete the closed steam cycle. The cooling water exiting the surface condenser is then pumped to cooling tower to be cooled down for reuse. To cleanly utilize coal and meet environmental regulations, the exhaust combustion product from the burner goes through a series of emission control systems before venting into the atmosphere. Selective catalytic reduction (SCR) reduces NO_x into N_2 and water by using ammonia (reactions represented by Equation 2-1 through Equation 2-3) or urea (reactions

represented by Equation 2-4) [19]; particulate control devices to remove particulate matter generated during coal combustion; wet flue gas desulfurization (FGD) for SO_2 removal unit [20] consisting of a limestone-water slurry scrubber while producing a gypsum byproduct (overall reaction represented by Equation 2-5).

$$4NO + 4NH_3 + O_2 \leftrightarrow 4N_2 + 6H_2O \quad \text{Equation 2-1}$$

$$NO + NO_2 + 2NH_3 \leftrightarrow 2N_2 + 3H_2O \quad \text{Equation 2-2}$$

$$6NO_2 + 8NH_3 \leftrightarrow 7N_2 + 12H_2O \quad \text{Equation 2-3}$$

$$4NO + 2(NH_2)_2CO + O_2 \leftrightarrow 4N_2 + 4H_2O + 2CO_2 \quad \text{Equation 2-4}$$

$$CaCO_3 + SO_2 + \frac{1}{2}O_2 + 2H_2O \leftrightarrow CaSO_4 \cdot 2H_2O + CO_2 \quad \text{Equation 2-5}$$

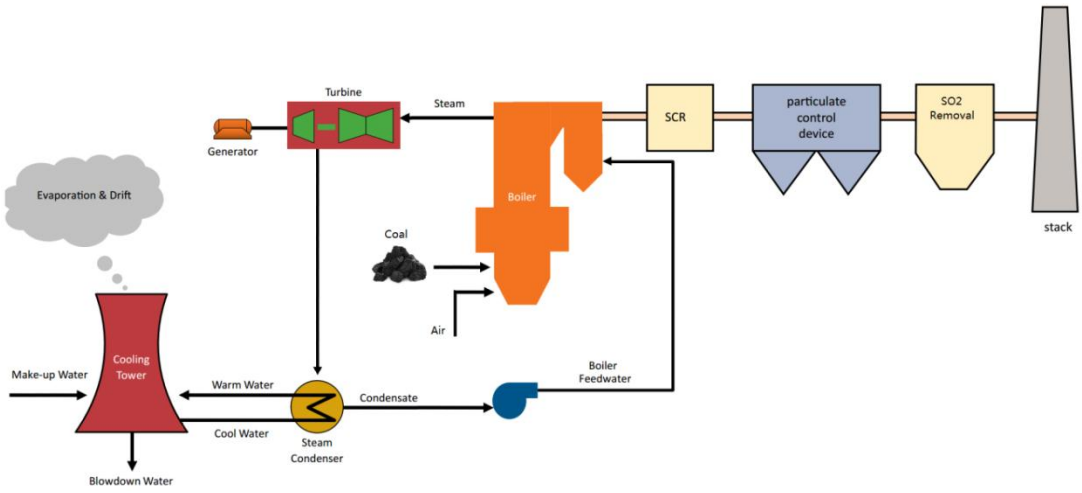

Figure 2-1 Typical pulverized coal power plant

2.1.2 Types of PC Power Plants

PC power plants are categorized into subcritical, supercritical and ultra-supercritical technologies according to the Rankine Cycle operation conditions (steam pressure and temperature),. The steam temperature-entropy (T-S) diagrams of subcritical, supercritical and ultra-supercritical are shown by Figure 2-2. Subcritical PC power plants operate at pressure below the critical point of water (374 C and 22 MPa) and temperature typically below 550 C. The efficiencies of subcritical power generation units are between 33% and 37% (Higher Heating Value / HHV) [21], depending on coal quality, operating design parameters and location. Majority of existing coal fired power generation units operated in the US are subcritical PC power plants. Supercritical operation of a reheat Rankine cycle represents a movement from subcritical to supercritical steam parameters. Supercritical technologies were not commercially available until the late 1960s after advancement in boiler materials. The efficiencies of supercritical units range from 37% to 40% (HHV). Current state-of-the-art supercritical power generation, with steam turbine inlet operating condition of24.3 MPa and 565° C, results in power generation efficiency at about 38% (HHV) for Illinois #6 coal [21]. Driven by developments in material capabilities, power industry continues to move toward higher steam pressures and temperatures, primarily higher temperatures. Defined by Electric Power Research Institute [22], the steam temperatures of ultra-supercritical steam cycles are above 593C [22]. Current research and development of ultra-supercritical operation is targeting pressures of 36.5 MPa to 38.6 MPa and temperatures

of 700C to 720C, with the possibility of raising generating efficiency to 44-46% (HHV) [21].

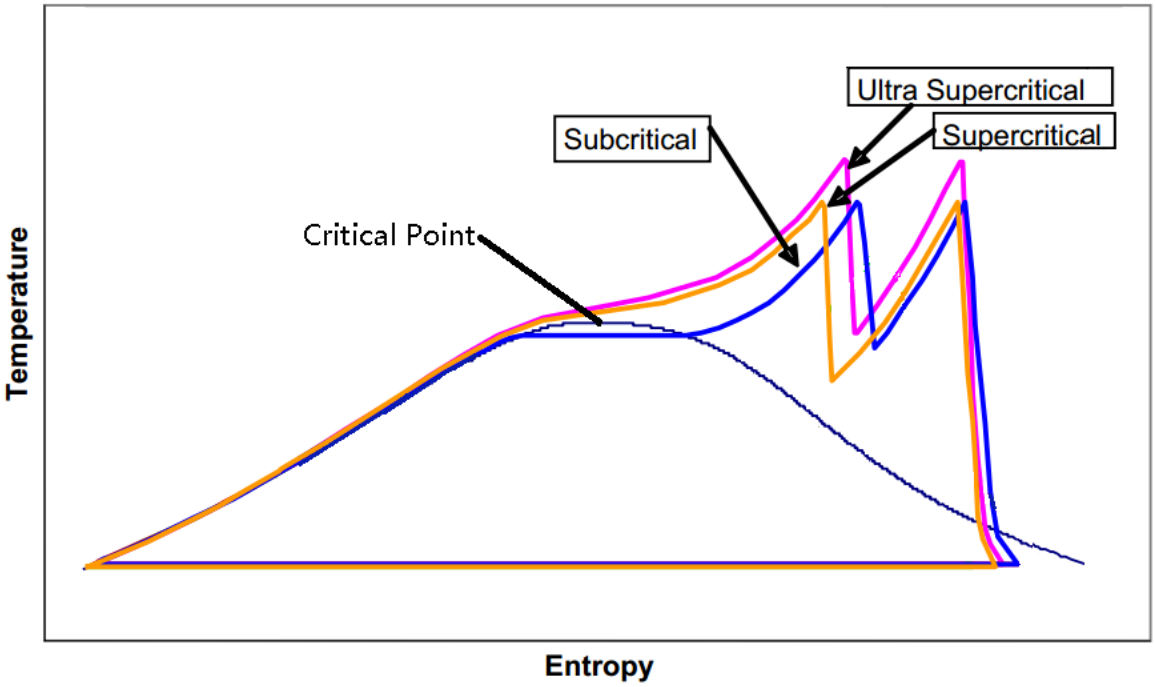

Figure 2-2 Steam T-S diagram of reheat Rankine cycles

Table 2-1 summarizes representative operating performance of subcritical, supercritical and ultra-supercritical power generation technologies on 500 MWe net power output basis using Illinois # 6 coal. Due to relatively low thermal efficiencies, subcritical PC power plants produce significantly higher CO_2 emissions on both kg/h basis and g/kWe-h basis. Therefore, CO_2 reduction from subcritical PC power plants is significantly more urgent.

Table 2-1 Representative Performance of PC Generating Technologies (Source: [21])

	Subcritical PC	Supercritical PC	Ultra-supercritical PC
Heat rate, Btu/kWe-h	9,950	8,870	7,880
Plant efficiency (HHV)	34.3%	38.5%	43.3%
Coal feed, kg/h	208,000	185,000	164,000
CO_2 emitted, kg/h	466,000	415,000	369,000
CO_2 emitted, g/kWe-h	931	830	738

Basis: 500 MWe net output. Illinois # 6 coal

Water Usage of a PC power plant is defined as the water used in the plant processes for any and all purposes, such as cooling tower makeup (majority of PC power plants employ wet cooling), BFW makeup, FGD system makeup. Water usage represents the overall impact of the process on water resource. Table 2-2 presents representative water usage of subcritical and supercritical PC power plants. The major part of water consumption is from cooling tower (mechanical draft cooling tower are utilized in both representative plants). Subcritical operation consumes 11% more water than supercritical operation due to the efficiency difference and it can be expected that number to be even larger if comparing subcritical with ultra-supercritical operation.

Table 2-2 Representative Water Usage of Subcritical and Supercritical PC Power Plants (Reproduced from source [23])

	Subcritical PC		Supercritical PC	
	Liter/s	Liter/MWh	Liter/s	Liter/MWh
FGD makeup	65.0	425	60.0	393
BFW makeup	5.0	33	0.0	0
Cooling tower	303.3	1,985	275.0	1,800
Total	371.7	2,433	335.0	2,193

Basis: 550 MWe net power output. Illinois # 6 coal

2.2 Integrated Gasification Combined Cycle Power Generation

IGCC is a technology to convert coal or other carbon based feedstock into synthesis gas or syngas for power generation. A typical IGCC system with carbon capture consists of five subsystems: air separation unit, coal gasification, syngas cleanup, CO_2 capture, and gas turbine and steam turbine combined cycle. IGCC is designed to remove impurities and pollutants before syngas is combusted. The unwanted compounds are more concentrated, and it makes them easier to be removed in IGCC than in PC power plant. Therefore, the major pollutants and energy penalty to remove pollutants in IGCC are significantly lower than those in PC power plant. Contrary to PC power plant which generates power by steam cycle, IGCC generates the major portion of the power by gas turbine and a small portion by steam cycle, so that the overall water usage of IGCC system is much lower than that of PC power generation system.

2.2.1 Air Separation Unit

Air separation unit (ASU) [24] is an important component of IGCC system using oxygen-blown gasifier to supply O_2 for coal gasification. The most common method for air separation is cryogenic distillation. The basic idea is to first compress and then cool the ambient air until liquefaction, and then selectively distill the compounds at their various bubble point temperatures. The process can provide high purity O_2 for gasification process as well as N_2 for syngas dilution for NO_x control. The disadvantage of cryogenic ASU is that it is energy-intensive since the compression/cooling process consumes large amount of power.

Membrane based ASU is an alternative air separation technology, e.g. ion transport membrane (ITM) oxygen technology. The physics of ITM oxygen is that oxygen in compressed hot air passes through the membrane in ionic form in an electrochemically driven process. The membrane consists of ion and electron mixed-conducting ceramic material. The oxygen in air is ionized on the surface of the ceramic, diffuses through the membrane as oxygen ions driven by an oxygen partial pressure gradient, and the oxygen ions then form oxygen molecules on the other side of the membrane to produce oxygen product. The schematic of the process is shown by Figure 2-3. ITM oxygen is generally integrating with the gas turbine of an IGCC system (see Figure 2-4). Portion of the compressed air from the gas turbine compressor is heated up to 800-900 C and then supplied to the membrane. Portion of the oxygen is extracted across the membrane and after cooling/heat recovery and compression it is supplied to gasification unit, while the resulting oxygen-depleted nonpermeate off-gas is mixed with the remaining portion of the gas turbine compressor discharge air and sent to the gas turbine combustor. The combustor exhaust gas expands in the gas turbine expander. Energy penalty of ITM oxygen technology is significantly lower than that of cryogenic ASU because no cooling of the depleted air occurs while its pressure is essentially conserved.

Some of the other ASU technologies, such as pressure swing adsorption (PSA) and vacuum pressure swing adsorption (VPSA), were well summarized by Castle [24]. The basic idea of adsorption based air separation is that adsorbent removes N_2 from air at relatively high pressure, releases N_2 at relatively low pressure, and O_2 is recovered at high pressures. Such technologies, however, are limited to small scale applications.

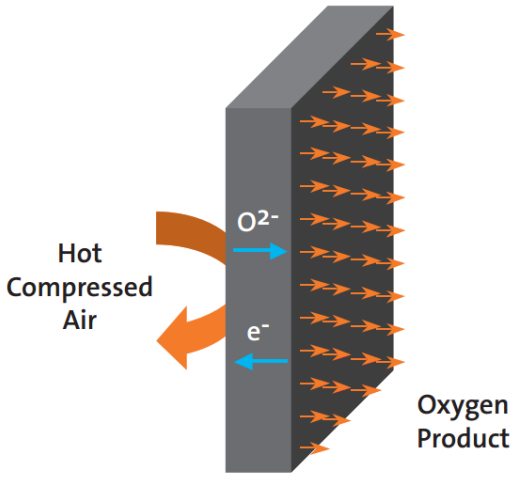

Figure 2-3 Physics of ITM xxygen (Source: [25])

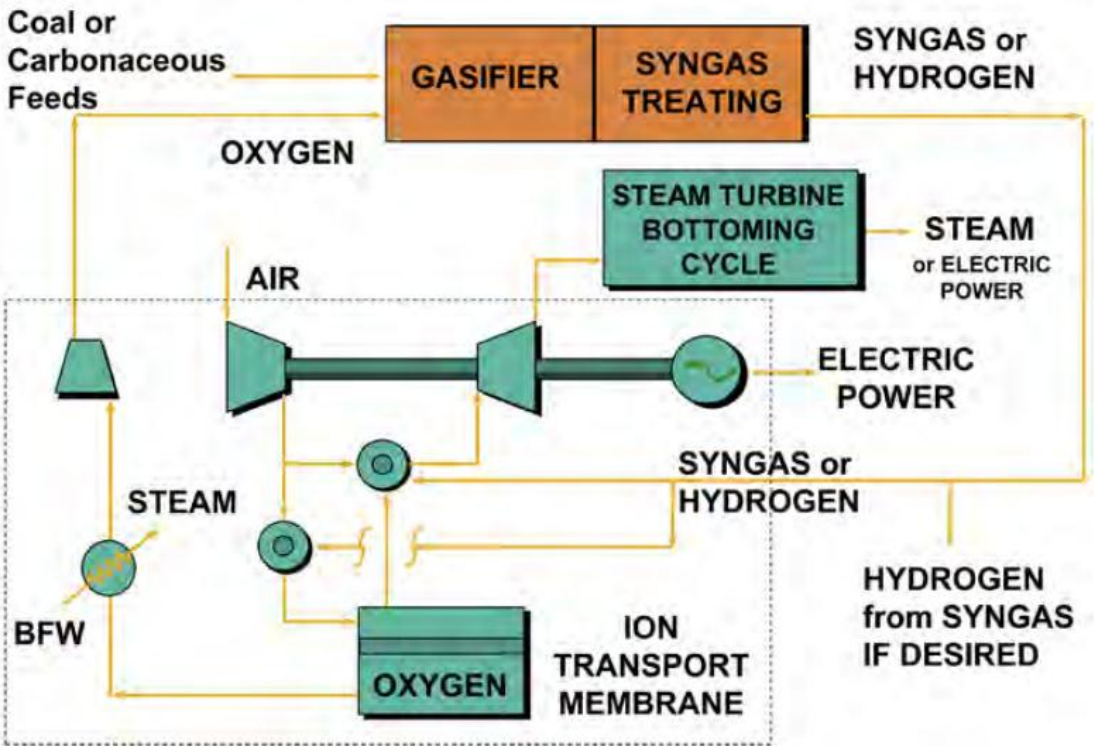

Figure 2-4 Process diagram of an ITM integrated into an IGCC (Source: [25])

2.2.2 Coal Gasification

Coal gasification is the heart of future clean coal power generation plants. Rather than burning coal directly, gasification converts coal or other carbon-based feedstock into syngas, mainly consisting of CO, H_2, CO_2, CH_4 and N_2. After cleanup, syngas can be used for power generation and/or production of H_2, chemicals or other fuel products.

The chemical reactions of gasification vary depending on the gasification conditions. Different feedstocks, the oxidant composition and operation conditions lead to different gasification products of various concentrations. Major thermodynamic reactions are those involving C, CO, CO_2, H_2, H_2O and CH_4, shown as follows [26]:

The oxidation reactions:

$$C + 0.5O_2 \rightarrow CO \quad (-111\ \mathrm{MJ/kmol}) \qquad \text{Equation 2-6}$$

$$CO + 0.5O_2 \rightarrow CO_2 \quad (-283\ \mathrm{MJ/kmol}) \qquad \text{Equation 2-7}$$

$$H_2 + 0.5O_2 \rightarrow H_2O \quad (-242\ \mathrm{MJ/kmol}) \qquad \text{Equation 2-8}$$

And other important gasification reactions:

$$C + H_2O \leftrightarrow CO + H_2 \quad (+131\ \mathrm{MJ/kmol}) \qquad \text{Equation 2-9}$$

$$C + CO_2 \leftrightarrow 2CO \quad (+172\ \mathrm{MJ/kmol}) \qquad \text{Equation 2-10}$$

$$C + 2H_2 \leftrightarrow CH_4 \quad (-75\ \mathrm{MJ/kmol}) \qquad \text{Equation 2-11}$$

Equation 2-9 through Equation 2-11 can be reduced to two homogeneous gas phase reactions of water gas shifting (Equation 2-12) and steam reforming (Equation 2-13):

$$CO + H_2O \leftrightarrow CO_2 + H_2 \quad (-41\ \text{MJ/kmol}) \qquad \text{Equation 2-12}$$

$$CH_4 + H_2O \leftrightarrow CO_2 + 3H_2 \quad (+206\ \text{MJ/kmol}) \qquad \text{Equation 2-13}$$

Three major generic types of gasifiers are fixed-bed, entrained-flow, and fluidized-bed gasifiers. Fixed- or moving-bed gasifiers typically operate under moderate pressures (25 to 30 bars). Coal particles move slowly downward through the bed, while reacting with O_2 and steam introduced at the bottom of the gasifier vessel. In an entrained-flow gasifier, coal feed, oxygen, and steam or water used as a coal slurrying medium are fed co-currently into the gasifier and operated at a high temperature and pressure which are conducive to rapid feed conversion. A fluidized-bed gasifier suspends feedstock particles in an oxygen containing gas (a mixture of oxidant, steam and fluidizing gas), and the bed within the gasifier acts as a fluid. The depiction of three types of gasifiers and their operation conditions are shown by Figure 2-5 through Figure 2-7.

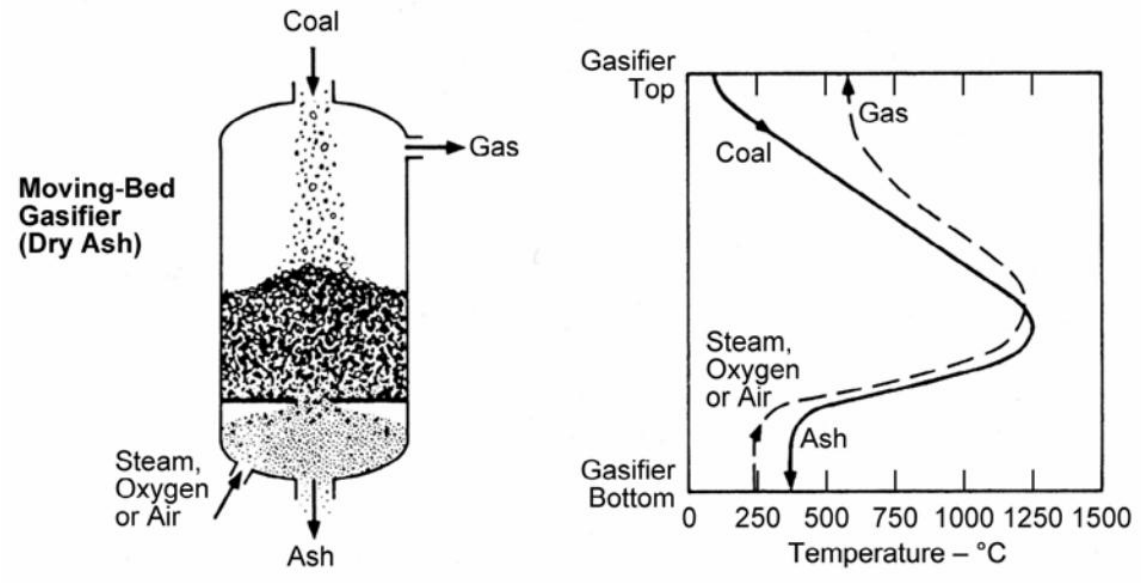

Figure 2-5 Diagram of a generic moving bed gasifier (Source: [27])

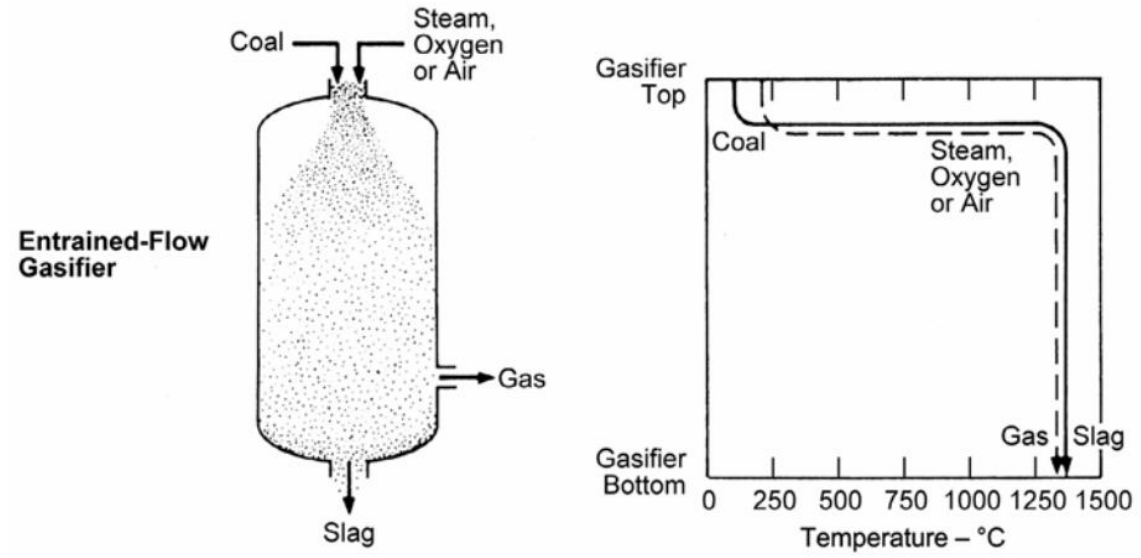

Figure 2-6 Diagram of a generic entrained-flow gasifier (Source: [27])

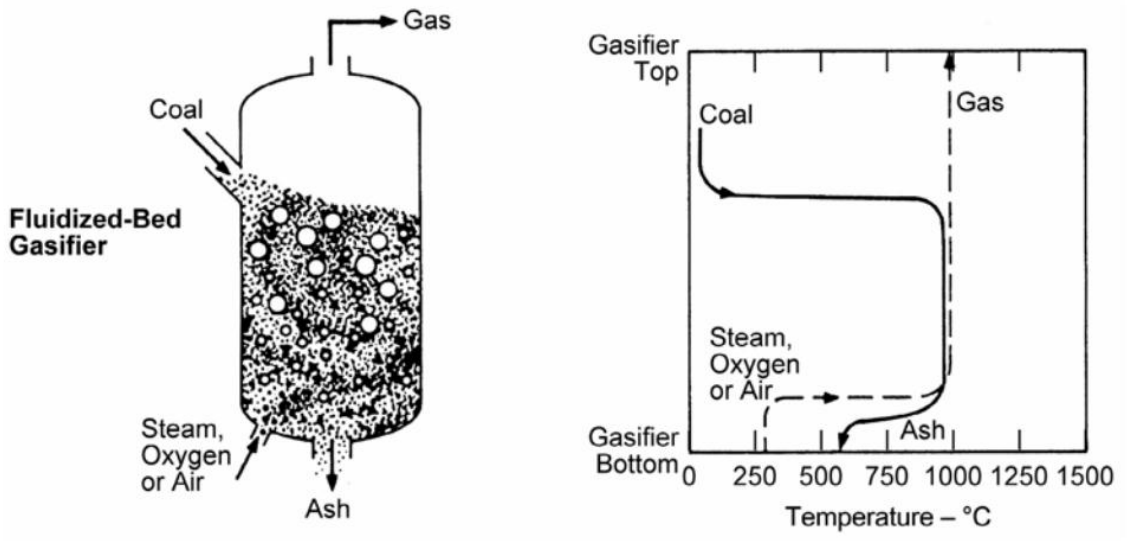

Figure 2-7 Diagram of a generic fluidized bed gasifier (Source: [27])

Gasifiers can also be classified in terms of atmospheric vs. pressurized, dry feed vs. slurry feed, and air-blown vs. oxygen-blown. Compared with atmospheric gasifirers, pressurized gasifiers are more suitable for IGCC application because it avoids downstream syngas compression to a pressure as required by the gas turbine while making the syngas cleanup system smaller, more efficient and more cost-effective. Coal can be fed as dry solids or coal-water slurry. Typically slurry feeding system has relatively lower capital cost but lower gasifier efficiency. In contrast, dry feed system results in a more efficient gasifier but more expensive, while dry gasifier is preferred for biomass gasification. Air-blown gasifiers do not require ASU but produce a much lower calorific value syngas than oxygen gasifiers and also have lower gasifier efficiency although the large parasitic load of the ASU is eliminated. Oxygen-blown gasifiers are

preferred for CO_2 capture since the concentration of CO_2 is significantly higher, which reduces the cost and increases the effectiveness of the CO_2 removal unit.

2.2.3 Syngas Cleanup

Impurities and pollutants contained in coal derived raw syngas need to be cleaned up before syngas enters power block or byproduct synthesis unit. Syngas cleanup process includes removal of particulate matters, chlorides, mercury, sulfur compounds, and CO_2. According to the operating temperature, syngas cleanup can be categorized into low temperature or cold gas cleanup technologies and high temperature or warm gas cleanup technologies.

Cold gas cleanup technologies operate at or slightly higher than ambient temperature. Water scrubbing of raw syngas exiting the gasifer can reduce particulate matters, chlorides and NH_3 to acceptable levels. Two stages of water gas shift (WGS) reactors (high temperature shift / HTS and low temperature shift / LTS) are required to convert most of the CO in the syngas into CO_2. HTS has fast reaction kinetics operating at high temperatures, around 350 C. Since shift reaction is endothermic, LTS operating at a range from 200 C to 250 C leads to higher CO conversion ratio. An activated, sulfur-impregnated, carbon bed adsorption system is used for mercury control in IGCC plants. The carbon bed is located downstream of the shift reactors and heat recovery and upstream of the desulfurization unit, and syngas enters at a temperature near 38 C [23]. An absorption system using chemical or physical washes is able to remove H_2S after COS hydrolysis (Equation 2-14) which also occurs within the shift reactors, such as Selexol^{TM}

process. The removed H_2S from Selexol™ system can be converted into elemental sulfur via Claus process (Equation 2-15 and Equation 2-16). CO_2 can be captured in cold gas cleanup system by the second stage of Selexol™ process, which is described in Session 2.4.3.1.

$$COS + H_2O \leftrightarrow CO_2 + H_2S \quad \text{Equation 2-14}$$

$$H_2S + 1.5O_2 \leftrightarrow H_2O + SO_2 \quad \text{Equation 2-15}$$

$$2H_2S + SO_2 \leftrightarrow 2H_2O + 3S \quad \text{Equation 2-16}$$

The coal gas cleanup process imposes significant efficiency penalties on an IGCC system, because the hot syngas exiting gasifier has to go through low temperature processes and heated up again for downstream applications, e.g. power generation and fuel synthesis, which creates a significant waste of thermal energy.

Warm gas cleanup can remove syngas contaminates at elevated temperature to reduce thermal penalties associated with cleanup process. The major differences of warm gas cleanup from cold gas cleanup are the removal processes of mercury, sulfur compounds and CO_2. Regenerable sorbents operating at much higher temperature have been developed to remove mercury, such as the process developed by TDA [28]. Regenerable ZnO process operating at around 260°C has been developed to remove H_2S and COS from the syngas [29], with desulfurization reactions shown by:

$$H_2S + ZnO(s) \leftrightarrow ZnS(s) + H_2O \quad \text{Equation 2-17}$$

$$COS + ZnO(s) \leftrightarrow ZnS(s) + CO_2$$ Equation 2-18

The ZnS produced in the desulfurization process can be regenerated by contacting with air and being oxidized into ZnO following the reaction below. The regenerator off-gas containing SO_2 can be processed to produce H_2SO_4 byproduct.

$$ZnS + 1.5O_2 \leftrightarrow ZnO(s) + SO_2$$ Equation 2-19

CO_2 can be captured for sequestration in warm gas cleanup system by various novel technologies, such as the solid sorbent based adsorption process, which is discussed in Session 2.4.3.2.

2.2.4 Gas Turbine and Steam Turbine Combined Cycle

Decarbonized syngas (mostly H_2) eventually enters the gas turbine and steam turbine combined cycle for power generation. For NO_x control purpose, syngas is diluted by N_2 addition and /or humidification before it is supplied to gas turbine combustor. The gas turbine works as a topping Brayton cycle to generate power. Exhaust gas enters heat recovery steam generator (HRSG), and the generated steam is sent to steam turbine to produce additional power as a bottoming Rankine cycle.

2.3 Co-Feeding and Co-Production of Integrated Gasification Combined Cycle

2.3.1 Motivation for Co-Feeding and Co-Production in IGCC

State-of-the-art gasifiers amenable to co-feeding biomass along with coal are available [30], [31] while IGCC plants are capable of co-producing clean fuels like H_2 by further processing decarbonized syngas [32]–[34], both of which make IGCC an attractive technology option given the increasing concern over global climate change caused by greenhouse gas emissions. Biomass utilization in power generation sector has been gaining increasing attention for decades due to energy security considerations and biomass' near carbon neutral benefit to lower greenhouse gas emissions. In addition, political level regulations are accelerating the trend for biomass utilization. For example, Renewable Portfolio Standard (RPS), a regulation in the U.S. to promote renewable energy, requires a substantial increased production of energy from renewable energy sources, such as wind, solar, biomass, and geothermal [35]. According to the California Energy Commission, California is to achieve 33% of renewables as its energy source by 2020 [36]. H_2 is not only needed in chemical processing industries but also for certain fuel cell [37] applications including alternative fuel vehicles in the transportation sector [38]. Thus, H_2 is a clean energy carrier for future energy systems. In addition, IGCC is also capable of co-producing alternative fuels, such as Fischer-Tropsch (F-T) liquids and ethanol, which are promising option for countries heavily dependent on petroleum imports and could enhance energy security.

2.3.2 Literature Review on Co-Feeding and Co-Production in IGCC

Though the trend of co-feeding and co-production in IGCC has been seen, the impact of co-feeding and co-production has not yet been methodologically analyzed in literature. It is significantly important to quantificationally and systematically explore the benefit or impact of co-feeding and co-production. In addition, prior investigations on co-feeding and co-production IGCC plants have been focused on current technologies (see Table 2-3) consisting of cryogenic ASU to provide oxygen to the gasifier, low temperature or cold processes for raw syngas cleanup, commercially ready gas turbine based combined cycle for power generation. And limited work has been conducted on the effects of advanced technologies that would improve the performance and economics of IGCC plants. Table 2-3 shows a summary of literature review on cofeeding and co-production in IGCC. Current research and development activity for advancing IGCC technology include: membrane based ASU [39], [40] to separate O_2 at high temperature, relatively high temperature or warm gas cleanup processes to remove pollutants and CO_2 [41], [42], and advanced gas turbines to serve as high efficiency power generators [43]. In order to fully realize the benefits of these advanced technologies, it is imperative to identify plant integration concepts that not only improve the efficiency of one single unit of the plant, but provide synergistic enhancement of the overall plant efficiency; as an example, in the case of the ASU, by achieving a better thermal integration with other high temperature and high pressure components of the plant.

Table 2-3 Summary of Literature Review on Co-Feeding and Co-Production IGCC

Year	Researchers	Feed stock	Products	Technology Features	Flow Sheet Tool
2009	Klimantos [44]	Biomass	Electricity	Dry-fed, air-blown, fixed bed gasifier; high temperature gas cleanup	Aspen Plus®
2006	Valero [45]	Coal/biomass	Electricity	Oxygen-blown gasifier	Self-developed code
2012	Mu [33]	Coal/biomass	Electricity/H_2	Dry-fed, oxygen-blown, entrained gasifier; cryogenic ASU; low temperature gas cleanup; CCS	Aspen
2009 2011	Cormos [16], [34], [46], [47]	Coal/biomass	Electricity/H_2	Dry-fed, oxygen-blown gasifier (Siemens); cryogenic ASU; low temperature gas cleanup; M701G2 (Mitsubishi Heavy Industries); CCS	ChemCAD software
2012	Tock [48]	Biomass	Electricity/H_2	Pyrolysis and CFB; low temperature gas cleanup; CCS	Self-developed code
2014	Sofia [49]	Coal/biomass	Electricity/H_2	Oxygen-blown, entrained gasifier; cryogenic ASU; low temperature gas cleanup; CCS	Aspen Plus®
2002	Tijmensen [50]	Biomass	Electricity/F-T liquids	CFB gasifier; cryogenic ASU; low temperature gas cleanup	Aspen Plus®
2008	Wang [51]	Coal	Electricity/F-T liquids	Slurry-fed, oxygen-blown, entrained bed gasifier; cryogenic ASU, low temperature cleanup; F class combined cycle	GS software, Aspen Plus®
2009	Yue [52]	Coal	Electricity/F-T liquids	Oxygen-blown entrained flow gasifier; cryogenic ASU; low temperature cleanup; F class combined cycle	PRO II
2006 2008 2009 2011	Williams [53]–[56]	Coal/biomass	Electricity/F-T liquids	Water-slurry-fed, oxygen/steam-blown, entrained-flow gasifier (GE / for coal); dry-fed, oxygen/steam-blown fluidized-bed gasifier (for biomass); cryogenic ASU; low temperature gas cleanup; F class combined cycle; CCS	Aspen Plus®

2.4 CO_2 Capture for Central Power Generation

Four major approaches for CO_2 capture in various applications [57] are:

- Post-combustion CO_2 capture
- Pre-combustion CO_2 capture
- Oxy-fuel combustion capture
- Capture from industrial process streams

Post-combustion CO_2 capture removes CO_2 from flue gas after fuel is burnt in boiler power plants, pre-combustion option captures CO_2 prior to fuel burning in IGCC applications, and in oxy-fuel combustion capture, fuel is combusted with high purity O_2 so that combustion products consist primarily of CO_2 and water vapor so that a CO_2 rich stream (for further purification) can be produced by condensing the H_2O vapor. Capture from industrial process streams mainly refers to CO_2 removal application in natural gas sweetening, and steel, cement and ammonia production, and capture technologies are usually similar to those used for post- or pre-combustion CO_2 capture. Figure 2-8 presents basic processes of the four CO_2 capture systems. Two major interests of this dissertation work are post-combustion CO_2 capture and pre-combustion CO_2 capture, while oxy-fuel combustion capture and capture from industrial process streams are beyond the research scope.

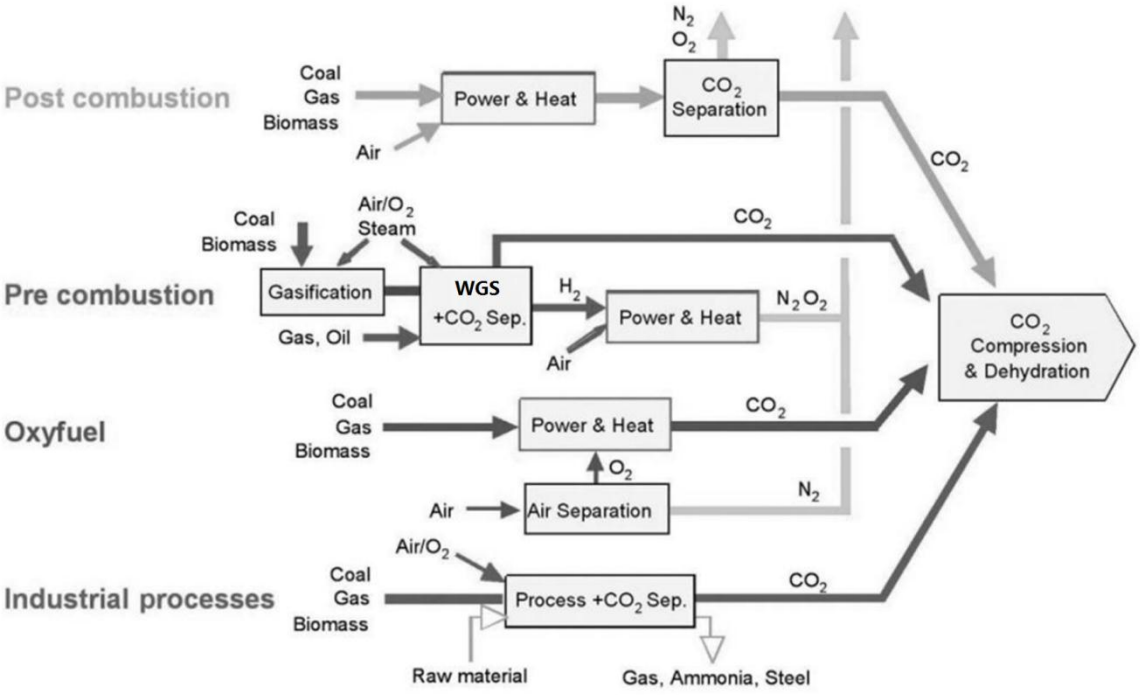

Figure 2-8 CO_2 capture systems (Source: [57])

2.4.1 CO_2 Capture Technologies

Figure 2-9 summarizes a classification of CO_2 separation and capture technologies, including absorption, adsorption, cryogenic separation, membranes and microbial/Algal systems. Regarding separation mechanisms and process characteristics, different CO_2 capture technologies are suitable for different CO_2 capture applications, which are described in this session.

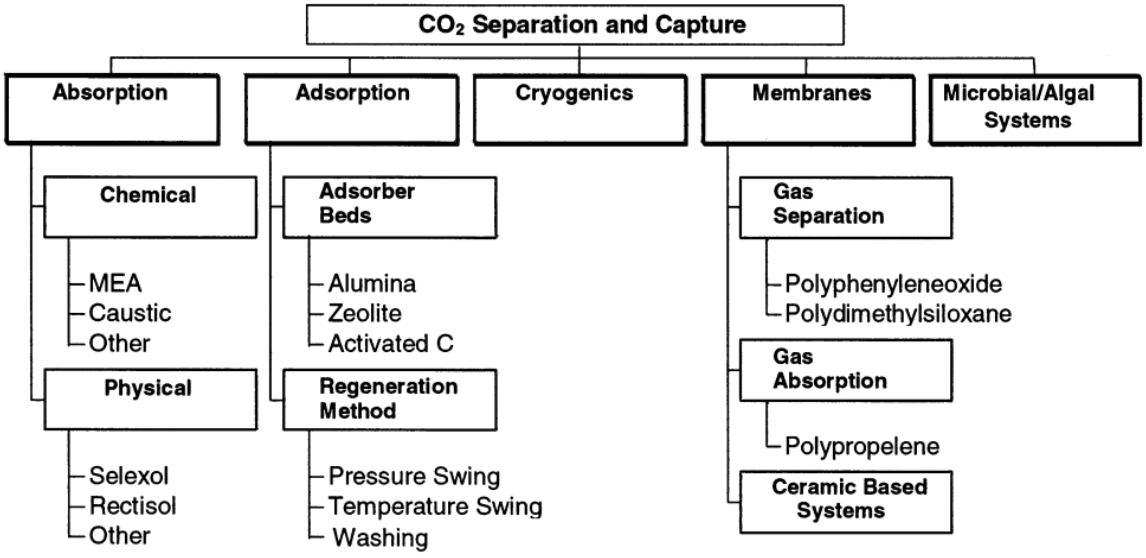

Figure 2-9 Technology options for CO_2 capture (Source: [58])

2.4.1.1 Absorption Based CO_2 Capture Technologies

Absorption in this application is defined as uptake of CO_2 into the bulk phase of another material [59]. For example, CO_2 dissolves in liquid absorbent or solvent more preferentially than other gas components.

Chemical absorption involves chemical solvent selectively reacting with CO_2 in gas mixtures to form a weakly boned intermediate compound, which can be regenerated by heat producing the original solvent and a CO_2 stream [60]. This chemical bond can be formed at low CO_2 partial pressure, and makes chemical absorption suitable for post-combustion CO_2 capture. Physical absorption involves CO_2 dissolving into solvent based on Henry's law, which effectively takes place at high CO_2 partial pressure. Since flue gas with 15 vol% or less CO_2 is emitted at atmosphere pressure in PC power generation applications, physical absorption is not suitable for post-combustion CO_2 capture [61],

while it is suitable for pre-combustion CO_2 capture from high pressure syngas produced in IGCC applications. The solvent loading versus CO_2 partial pressure is qualitatively represented in Figure 2-10 for both physical absorption and chemical absorption.

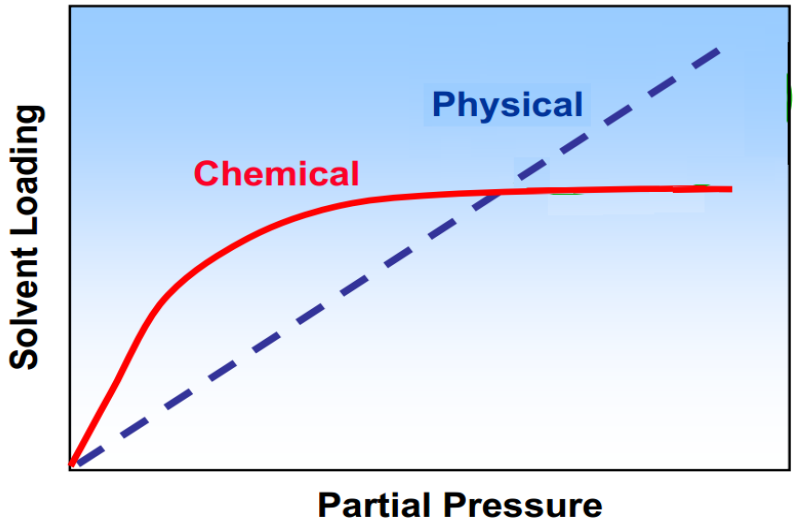

Figure 2-10 Solvent loading comparisons between physical absorption and chemical absorption (Source: [62])

The process of CO_2 capture using solvent for both PC power plant and IGCC is presented by Figure 2-11. CO_2 is continuously removed from the flue gas by passing through a column of absorber loaded with solvent. Decarbonized flue gas is vented to stack for emission in PC plant applications or decarbonized syngas is sent to power block in IGCC applications while the CO_2 loaded solvent is transported to regeneration column, where the solvent is heated up and CO_2 gets released, so that the solvent is regenerated and sent back to absorber for reuse in a cyclic process. A makeup flow of fresh solvent is required to compensate for the natural decay of activity and solvent losses. The heating

energy for solvent regeneration is large that leads to significant efficiency penalty and parasitic cost.

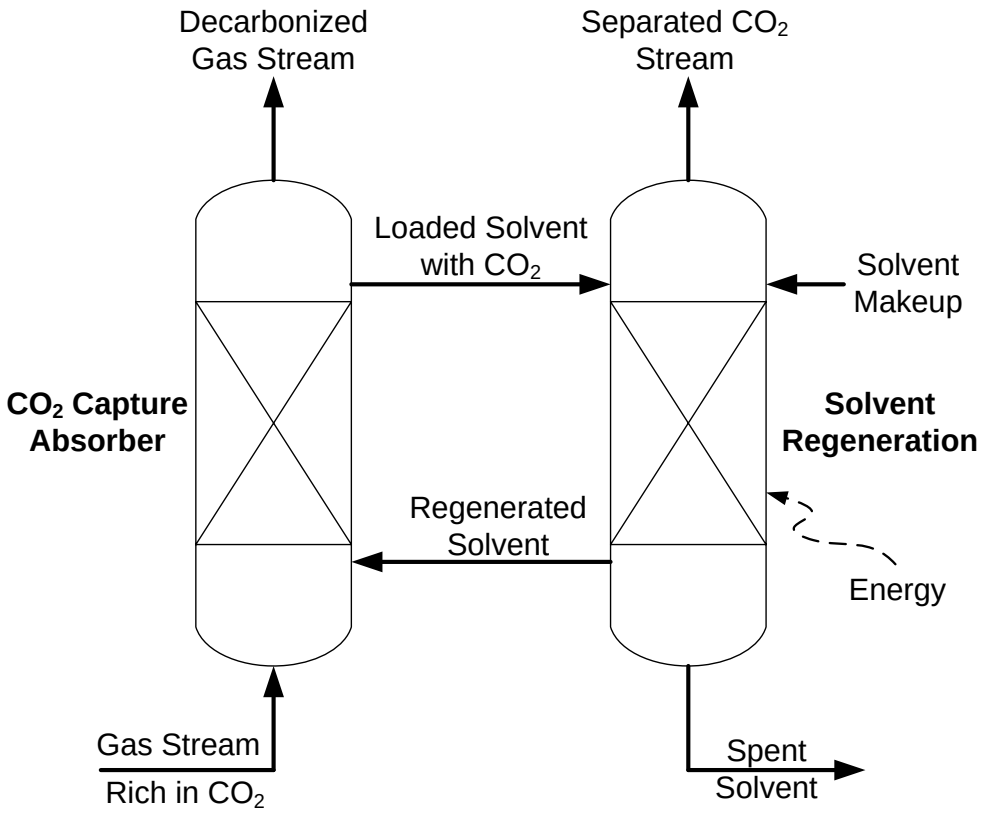

Figure 2-11 Process of CO_2 capture with solvents (Source: [63])

2.4.1.2 Adsorption Based CO_2 Capture Technologies

Adsorption refers to the process that involves the attachment of CO_2 onto the surface of a solid sorbent via weaker van der Waals forces (physical adsorption) or stronger covalent bonding (chemical adsorption) [59]. Physical sorbents can be a variety of solid physisorbent materials, including porous carbonaceous materials, crystalline materials known as zeolites, alumina, silica gels, and metal-organic frameworks (MOFs).

The high porosity of the sorbents enables the adsorption of CO_2, which can be expressed by Equation 2-20. However, the limitations of using conventional physisorbents are low CO_2 adsorption capacities at relatively low CO_2 partial pressure and the low selectivity of CO_2. Sorbents with modifications in the surface chemistry of the porous materials are considered chemisorbents; high CO_2 adsorption capacity and high selectivity for CO_2 can be achieved by incorporating basic sites capable of interacting strongly with acidic CO_2 [7]. The common modifying functional groups include alkaline carbonates and various amine groups. CO_2-loaded sorbents are typically regenerated by switching to lower pressure (PSA), and/or by switching to higher temperature (temperature swing adsorption / TSA).

$$CO_2 + surface \leftrightarrow (CO_2) \cdot (surface) \qquad \text{Equation 2-20}$$

This dissertation work particularly focuses on solid sorbents based on a TDA proprietary mesoporous carbon which consists of surface functionalized groups that remove CO_2 via physical adsorption. The relatively strong interaction between the surface group and CO_2 enables effective operation at high temperatures [64]. Because of no true covalent bond exits between CO_2 and sorbents, energy for sorbent regeneration is low, e.g. less than 5 kcal per mol of CO_2.

The adsorption process is typically implemented in fluidized beds or fixed beds [59]. In fluidized beds, gases flow upward through a column at high velocities such that the solid sorbent particles are suspended in the gas flow, and CO_2 is adsorbed onto the

porous surfaces of particles. In the case of a fixed bed, sorbent is loaded into a column, gases pass through the voids spaces between the sorbent particles while CO_2 is adsorbed. The process of CO_2 adsorption using fluidized beds is similar to the process described by Figure 2-11 where the CO_2-loaded sorbent is conveyed continuously to the regenerator column for sorbent regeneration. For fixed bed operation, the regeneration of a CO_2-loaded bed is accomplished by inert gas (e.g. steam) through the same column at lower pressure. The desorbed CO_2 from the sorbent in mixture with steam is then purified by condensing the steam at lower temperature. The process of CO_2 adsorption and regeneration in a fixed bed operation is presented by Figure 2-12.

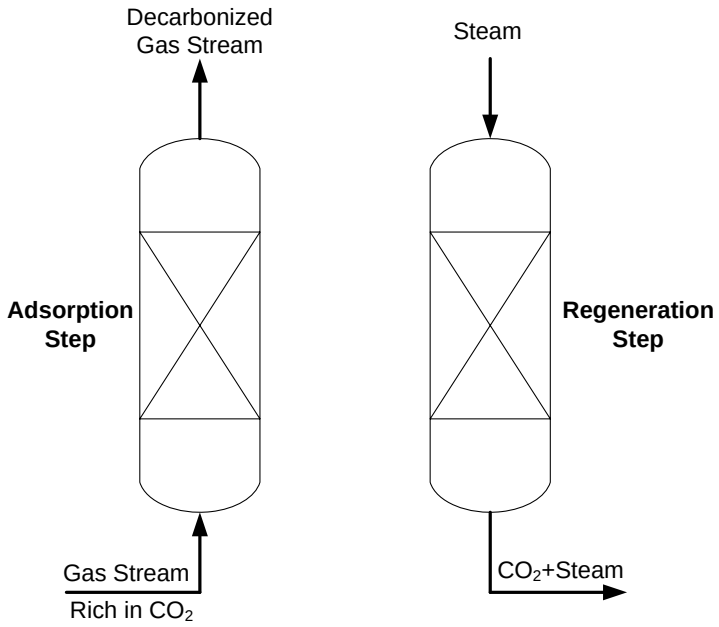

Figure 2-12 CO_2 adsorption and regeneration in fixed bed operation

2.4.1.3 Other CO_2 Capture Technologies

Cryogenic CO_2 capture is basically a refrigerated distillation process. By a series of compressing, cooling, drying and expanding steps, the stream containing CO_2 is converted to liquid phase. CO_2 is then separated from other components by distillation of the liquid mixture. Due to the cost of refrigeration, this process is typically considered suitable for highly CO_2 concentrated gases, e.g. CO_2 capture for oxy-fuel combustion [60].

Membrane based CO_2 separation generally uses thin polymeric films, which have selectivity to the permeation rate of CO_2 compared with other species. Permeation rates differ in the relative sizes of the permeating molecules (for porous membranes) or their solubilities and/or diffusion coefficients (for dense membranes) in the membrane material [65]. Permeation rates vary inversely with membrane thickness, and the permeation driving force is CO_2 partial pressure difference across the membrane. Therefore, high pressure operations, e.g. IGCC applications, are usually preferred for membrane based CO_2 capture. For post-combustion CO_2 separation from the flue gas, the required partial pressure difference of CO_2 is obtained by pressurizing the flue gas on one side of the membrane and/or by applying a vacuum on the other side [59], both of which would create significant penalty in plant efficiency.

Microbial/algal based CO_2 capture works on micro-algae's ability to transport bicarbonate into cells. Several species of algae have been reported to grow under CO_2 concentrations over 15% [66]. High purity CO_2 is not required for algae culture, which

can simplify CO_2 separation from flue gas. In addition, combustion products, e.g. NO_x or SO_x, can be used as nutrients for microalgae, which simplify flue gas scrubbing for flue gas cleanup processes. Due to the limitation of its application in large scale central power plant, this technology is beyond the scope of this dissertation study.

2.4.2 Post-Combustion CO_2 Capture System

Post-combustion CO_2 capture refers to the separation and sequestration of CO_2 from the flue gas derived from combusting carbonaceous fuels in air. In PC power plants, it is installed at the end of flue gas cleanup process, between FGD and stack, because acid gases such as SO_2 and NO_2 may enter the recovered CO_2 stream and or may affect the performance of CO_2 capture system, e.g. by forming heat stable salts with amine solvent [60] or poisoning the adsorbent. As an "end-of-pipe" technology, post-combustion CO_2 capture is flexible with respect to being switched off during periods of peak electricity demand or high market prices of electricity [67]. In addition, post-combustion CO_2 capture can also be retrofitted to existing PC power plants for CO_2 mitigation, with not very significant plant modifications as long as plot space is available for the added equipment.

2.4.2.1 Amine Based Post-Combustion CO_2 Capture System

Amines are chemical derivatives of ammonia in which one or more of the hydrogen atoms have been replaced by alkyl[2] or aryl[3] group [68]. Some of the amines most commonly used in CO_2 capture are diethanolamine (DEA), monoethanolamine (MEA), methyldiethanolamine (MDEA), diisopropanolamine (DIPA), and aminoethoxyethanol

(diglycolamine) (DGA). MEA is a proven chemical solvent for post-combustion CO_2 capture. A process flowsheet for CO_2 capture from flue gas using the amine-based system is presented by Figure 2-13. A cooler, usually directed contact cooler (DCC), cools down the flue gas before it enters the absorber to contact counter-currently with and react with an aqueous amine solution flowing from top to bottom of absorber. Decarbonized flue gas leaving the top of the absorber after washing is vented to the stack, while the CO_2 loaded solvent leaving the bottom of the absorber is sent to the regenerator via a cross heat exchanger where it gets heated up. In the regenerator, CO_2 is stripped away from the CO_2-loaded solvent by contacting it with steam produced by reboiler in a counter-current direction. A portion of the CO_2-lean solvent from the bottom of the regenerator circulates through the reboiler where auxiliary steam (typically LP steam drawn from steam cycle) is utilized to partially vaporize the amine solution, which returns to the regenerator and provides the heat needed for amine regeneration. Regenerated solvent is re-sent to the absorber after it gets cooled in the cross heat exchanger. A key feature of this system is the large amount of steam consumption to provide the regeneration heat, which significantly reduces the thermal efficiency of a power plant.

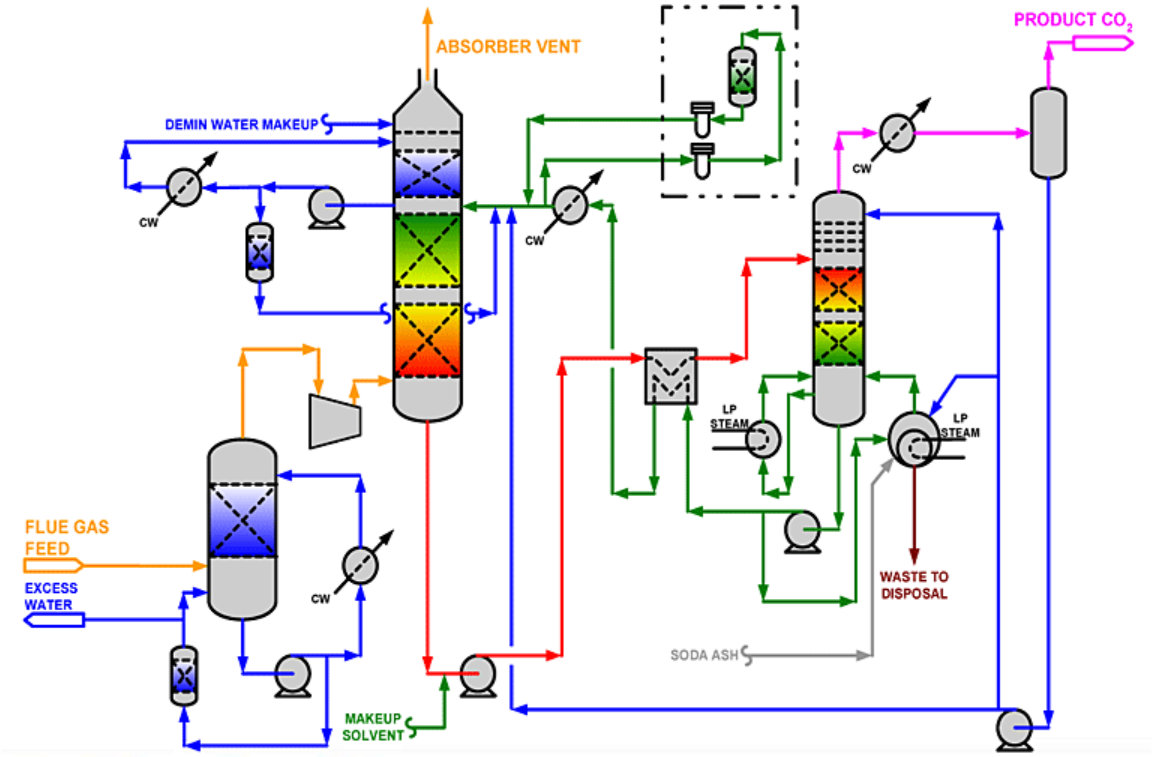

Figure 2-13 Flowsheet for CO_2 capture from flue gases using amine-based system (Source: [69])

2.4.2.2 Solid Sorbent Based Post-Combustion CO_2 Capture System

A process for solid sorbent based post-combustion CO_2 capture is similar to the depiction in Figure 2-12. Flue gas enters the fixed bed for adsorption of the CO_2 at ambient pressure. During regeneration or desorption step, CO_2 is driven off from the sorbent by switching the flow through the same bed from flue gas to steam using fast acting valves. Since the adsorption step is under ambient pressure, the regeneration step works under subatmospheric or vacuum pressure to effectively desorb CO_2. Vacuum pumps are provided downstream of the regeneration beds to pull the gases out. This mode of operation is called vacuum swing adsorption (VSA). A plant layout is

illustrated in Figure 2-14 for a post-combustion CO_2 capture system using TDA's solid sorbents.

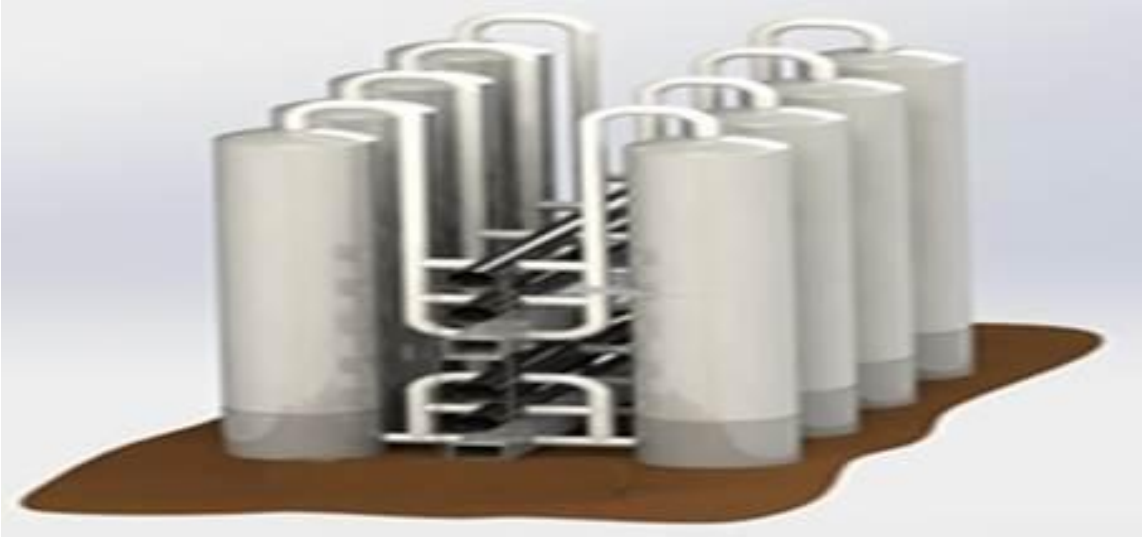

Figure 2-14 TDA's 8-bed VSA system for post combustion CO_2 capture with mesoporous carbons. Reactor ID 24 ft height 36 ft with full cycle time of 6 min (Source: TDA)

2.4.2.3 Literature Review on System Analyses of PC Power Plants Using Solid Sorbent Based Post-Combustion CO_2 Capture

System analysis of a power generation system, including techno-economic analysis and design, is of great importance for technology evaluation and development as a part of a whole power system, especially for novel technologies, e.g. solid sorbent based CO_2 capture. Extensive research [4], [70]–[73] has been carried out in literature on techno-economic analysis and design concepts of amine based post-combustion CO_2 captured PC power plant, whereas, relatively much less work has been reported on solid sorbent CO_2 capture approach. Tarka et al. [74] found that amine-functionalized solid sorbents will require less regeneration energy compared with 30% aqueous MEA (1442 kJ/kg CO_2

vs. 4498 kJ/kg CO_2). Ho et al. [75] examined the economic feasibility of PSA for recovering CO_2 from flue gas in a coal fired power plant, using commercial adsorbent zeolite 13X which has a working capacity of 2.2 mol/kg and CO_2/N_2 selectivity of 54. They reported that vacuum desorption reduces the CO_2 capture cost from US$57 to US$51 per ton of CO_2 avoided, comparable with the CO_2 capture cost using conventional MEA absorption. Zhang et al. [76] evaluated effects of process design and operating conditions under VSA, and found that the capture costs vary significantly with process configuration and operating parameters, e.g. feed gas temperature, feed concentration and evacuation pressure, which have impacts on auxiliary power consumption and CO_2 capture cost. ADA Environmental Solutions [77] tested 24 different sorbent materials for CO_2 adsorption and reported that the supported amine sorbent exhibited the highest working CO_2 capacities but was poisoned by the presence of SO_2; carbon-based materials showed excellent stability but had low CO_2 capacities; zeolites worked well under dry condition but easily became poisoned by the presence of moisture. One of the solid sorbent materials that they tested was selected for commercial-scale equipment and process evaluation, and ADA [78], [79] reported that because of the significantly low steam requirement for CO_2 desorption process, a power plant with solid sorbent CO_2 capture produces 14% more net power than the one equipped with amine based CO_2 capture. To summarize, the performance of a solid sorbent integrated PC power plant depends on material performance of adsorption and desorption, integration configuration, as well as operating conditions. A promising sorbent is TDA's

carbon based solid sorbent and is of particular interest in this study while the plant configuration and operating conditions need to be optimized correspondingly.

Another interest of this dissertation work is retrofitting an existing subcritical PC power plant for solid sorbent based CO_2 capture. Retrofit of coal fired power plants for CO_2 capture refers to necessary modifications of certain plant units and adding new carbon capture unit to exiting power plants, such that the existing plants can be capable of CO_2 capture. Minimum modification is desired for retrofit purpose, while in most of the work as reported in literature, steam is extracted from the existing steam cycle to drive sorbent regeneration process which creates significant modifications in addition to energy penalty. Thus in particular, integration strategies for solid sorbent based CO_2 capture are required for plant retrofit with minimum modifications.

2.4.3 Pre-Combustion CO_2 Capture System

Pre-combustion CO_2 capture refers to CO_2 removal from fossil fuels before combustion is completed. In IGCC applications, CO in syngas is converted into CO_2 by WGS, and CO_2 is then captured prior to entering gas turbine combustor for power generation. The high pressure shifted syngas is rich in CO_2, and allows relatively easier removal of CO_2 in comparison with post-combustion CO_2 capture technologies, which remove dilute CO_2 from flue gas at atmosphere pressure.

2.4.3.1 Selexol™ Process for Pre-Combustion CO_2 Capture System

Seleoxl™ process is widely used in acid gases removal, and Seleoxl™ is the trade name for the solvent that can separate acid gases such as H_2S and CO_2 from raw syngas

produced by gasification of coal, biomass or oils. Two-step Seleoxl^{TM} process, which uses dimethyl ether of polyethylene glycol as solvent [80], is commercially available for H_2S removal and pre-combustion CO_2 capture based on physical absorption.

The flow scheme for the two-step Seleoxl^{TM} process is illustrated in Figure 2-15. The first stage involves the sulfur absorber to remove H_2S from the raw syngas. The stripped H_2S stream is sent to a Claus plant for elemental sulfur recovery. The desulfurized syngas is then fed to the CO_2 absorber. The syngas is contacted with lean solvent to remove CO_2, with the decarbonized syngas sent to the gas turbine for power generation. A fraction of the CO_2-rich solvent exiting the CO_2 absorber is routed to the H_2S absorption section as pre-saturated solvent to minimize CO_2 cosorption. The remainder of the solvent is flash regenerated in a series of flash drums to release CO_2 which is sent to CO_2 compression and drying. Detailed process description can be found in [81]. The operation temperature of the Seleoxl^{TM} process is lower than ambient temperature and requires refrigeration of the solvent.

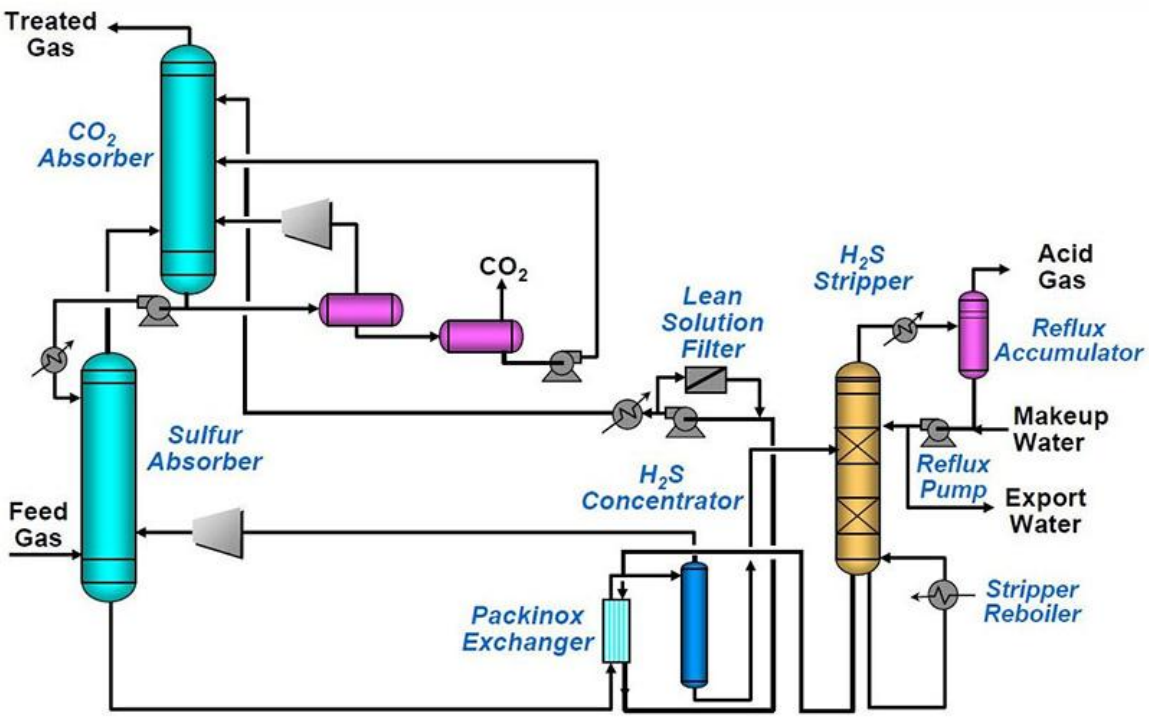

Figure 2-15 Flow diagram of two-stage Seleoxl™ process (Source: [62])

2.4.3.2 Solid Sorbent Based Pre-Combustion CO_2 Capture System

TDA's solid sorbent has also been optimized for pre-combustion CO_2 capture under high temperatures and high pressures [64]. In comparison with post-combustion application using VSA, pre-combustion CO_2 capture works under PSA mode and can also be schematically represented by Figure 2-12. The shifted syngas consisting primarily of H_2 and CO_2 is decarbonized in fixed bed absorber at high pressure, and the CO_2-loaded sorbent is regenerated at low pressure by purging steam through the fixed beds. The operating temperature of this process is above 200C. A plant layout is illustrated in Figure 2-16 for a pre-combustion CO_2 capture system using TDA's solid sorbent.

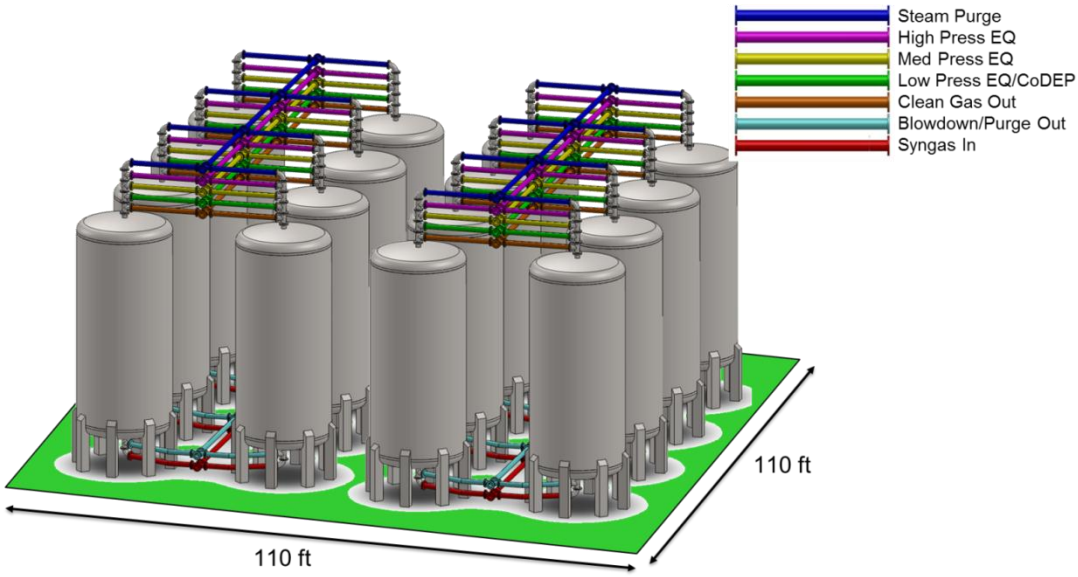

Figure 2-16 Plant layout of a pre-combustion CO_2 capture system using TDA's solid sorbent (Source: TDA)

In IGCC applications, two stages of WGS are located prior to CO_2 capture unit. Considering that the operating temperatures of the second WGS and solid sorbent based CO_2 capture unit are similar, both above 200C, TDA Inc. proposed and demonstrated a novel concept of combined WGS and CO_2 removal technology for pre-combustion CO_2 capture [82]. This technology is also referred to as sorption-enhanced water gas shift reaction [83]–[85], and similar to sorption-enhanced steam methane reforming [86], [87] consisting of combined CO_2 adsorption with steam reforming. The basic idea is packing both LTS catalyst and solid sorbent in a single fixed bed reactor, such that LTS reaction and CO_2 adsorption can occur simultaneously in the reactor. Advantages of the combination are presented as follows:

- Reduce plant capital cost by eliminating separate LTS reactors.

- Reduce steam injection into the WGS reactors and therefore improve plant thermal efficiency.

The second advantage can be illustrated by Figure 2-17 and Figure 2-18. The effects of increasing H_2O/CO ratio or removing CO_2 from gas mixtures are equivalent on CO conversion. Figure 2-17 shows the equilibrium CO conversion ratio at different carbon (CO + CO_2) capture levels under various LTS reaction temperatures. The initial reactants are H_2O and CO at mole ratio of 1:1. It may be seen that by removing CO_2 from the gas mixture CO conversion ratio increases significantly. For instance, at 250C by removing 90% carbon from the gas mixture, CO conversion ratio increases by about 7 percentage points. The contour in Figure 2-18 represents the relation between initial H_2O/CO ratio and carbon capture level to obtain the same CO conversion rate. To achieve the same CO conversion ratio at various levels of carbon capture, the required initial H_2O/CO ratio should be higher than 1:1. For instance, at 250C removing 90% carbon from the gas mixture has the equivalent effect of increasing H_2O/CO ratio by almost 40% for a given CO conversion ratio, which means steam injection would be reduced by removing CO_2 from the gas mixture.

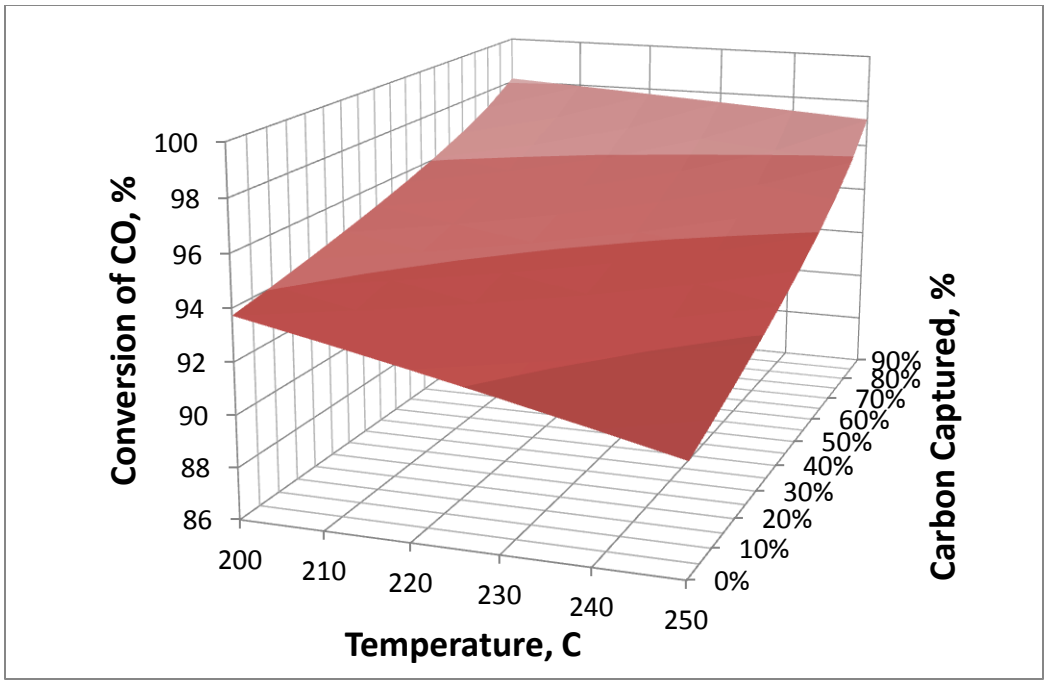

Figure 2-17 CO conversion ratio under various carbon capture level

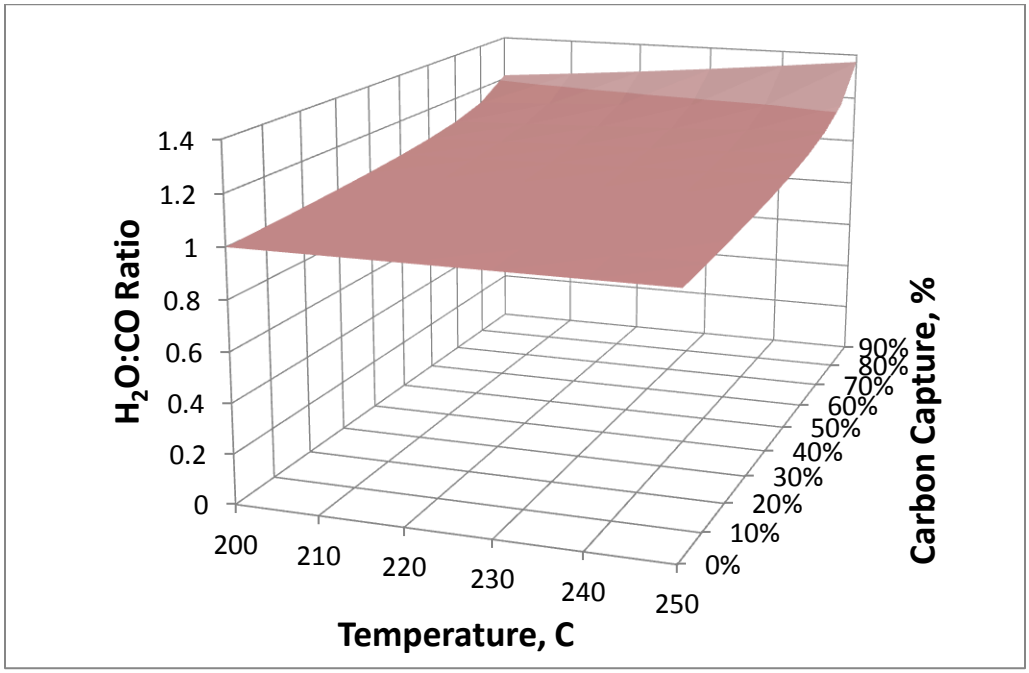

Figure 2-18 Relation between initial H_2O/CO ratio and carbon capture level

One challenge in the development of the CO_2 capture technology using combined WGS and solid adsorption is thermal management within the reactor. Both WGS reaction and CO_2 adsorption are exothermic and are most efficient under specific temperature range. Cooling strategies are required to prevent the fixed reactor beds packed with both WGS catalyst and CO_2 sorbent from localized high temperature regions ("hot spots"). Little research has been reported in literature on the thermal management of the combined WGS and CO_2 adsorption reactor.

2.4.4 Literature Review on Simulation of Solid Sorbent Based Pre-Combustion CO_2 Capture System

The design of PSA beds used to be carried out empirically through extensive experimental testing. Process development of such units however, is an expensive and time-consuming approach. Numerical simulation of the PSA process is crucial for effective and efficient process design. Simulation is also an important method for understanding of the solid sorbent based CO_2 capture technology, and a vital tool for developing its applications in pre-combustion CO_2 capture systems. A physically based simulation of the fixed bed reactors could be capable of evaluating reactor design and operation conditions such as temperature distribution, cooling strategies, CO_2 breakthrough time, peak CO_2 loading capabilities, component distribution and associated performance characteristics. Various mathematical models and simulation approaches have been reported in literatures.

Adsorption is typically described through isotherms, that is, the amount of adsorbate on the sorbent as a function of its pressure at constant temperature. The quantity adsorbed is always normalized by the mass of the sorbent to allow comparison between different materials. Thirteen different types of equilibrium isotherm models were summarized by [88]: Langmuir, Freundlich, Brunauer–Emmett–Teller, Redlich–Peterson, Dubinin–Radushkevich, Temkin, Toth, Koble–Corrigan, Sips, Khan, Hill, Flory–Huggins and Radke–Prausnitz isotherm. Langmuir isotherm refers to homogeneous monolayer adsorption and treats the adsorption process as a chemical reaction between the adsorbate molecule and empty site on solid sorbents. Freundlich isotherm describes the non-ideal and reversible adsorption, and can be applied to multilayer adsorption. Langmuir-Freundlich isotherm is a combination of the Langmuir and Freundlich isotherms, with an expression shown by Equation 2-21 [89]. It reduces to Freundlich isotherm at low pressure, and approaches Langmuir isotherm at higher pressures. Langmuir-Freundlich isotherm is demonstrated to be suitable for heterogeneous systems of adsorption with functional groups [90].

$$B = \frac{N_t a F^m}{1 + a F^m} \qquad \text{Equation 2-21}$$

where

B is equilibrium concentration of bound

F is equilibrium concentration of free

N_t is the total number of binding sites

a is related to related to the median binding affinity constant $K_0 = a^{1/m}$

m is the heterogeneity index.

Various mathematical models have been developed for gas separation processes in fixed bed columns. As comprehensively reviewed by Serbezov [91], a rigorous overall mathematical model for the simulation of adsorption fixed beds includes three sub-models: model for the bed, model for the sorbent particles, and model for adsorption kinetics. The first two sub-models can be derived by applying mass, momentum and energy balance to the bed and particles, and the third one can be obtained by applying adsorption equilibrium and adsorption rate. Various models with different levels of complexity and comprehensiveness have been reported in literatures. It is assumed for simple models that gas phase and adsorbed phase during the adsorption process are in local equilibrium using the various adsorption isotherms [92]–[97]. Another approach consists of introducing adsorption kinetics by the addition of a linear driving force (LDF) model to specific adsorption isotherms [98]–[102]. The third and most complex approach considers the detailed mass transport between the bed and sorbent particles [91], [103], [104], such as bulk diffusion, Knudsen diffusion, Knudsen flow and viscous flow as accounted in dusty-gas model [105]–[107].

The overall mass transfer rate of bulk flow travelling onto the internal surface of porous sorbents is limited to pore diffusion under practical conditions [108]. The mass transfer model can be simplified into an expression (Equation 2-22) relating the mass transfer rate with adsorption at equilibrium.

$$\frac{\partial \bar{q}}{\partial t} = f(q^*) \qquad \text{Equation 2-22}$$

where

$\bar{q}$ is average actual amount of adsorption in sorbent, kmol/kg

q^* is the amount of adsorption in equilibrium, kmol/kg.

The LDF model [109] is widely used for the prediction of mass transfer rate of cyclic gas separation processes, such as PSA or TSA. According to the LDF model, adsorption rate of a single adsorbate into a sorbent particle is given by Equation 2-23.

$$\frac{d\bar{q}}{dt} = \frac{15 D_e}{R_p^2}(q^* - \bar{q}) \qquad \text{Equation 2-23}$$

where

D_e is the diffusivity of sorbate in the particle, m^2/s

R_p is radius of spherical particle, m.

The local equilibrium model is not realistic for application in practical PSA system designs. The detailed mass transport model between the bed and sorbent particles is too complex to be employed in process simulations, while one practical application of it is to formulate a generalized LDF approximation of adsorption rate [93]. LDF approach in addition to adsorption isotherm is a widely used approach to introduce adsorption kinetics into the simulation of PSA process. Specific sorbent material and adsorbate

component correspond to particular isotherm and LDF model expressions. For novel gas separation sorbent, experiments are required to correlate new adsorption expressions for simulation purpose. Limited amount of work has been reported in literature regarding the gas loading in the solid sorbents, which is a significant design parameter for industrial scale fixed bed operation.

Nonisothermal effects are intrinsic to every adsorption process because of the heat associated with adsorption and desorption [91]. In small beds, the adsorption process is sometimes assumed isothermal in simulation because the heat generated dissipates through reactor walls quickly. In contrast, in commercial size reactors nonisothermal effects need to be strictly considered because heat conduction rate is small and temperature change dramatically affects the sorbent performance [110]. Isothermal operation is assumed for adsorption beds in some of the publications [102]–[104], [111] while others did consider nonisothermal operation [91], [92], [98]–[101].

In majority of the work reported in literature, the models for adsorbent bed and the sorbent particles are derived from mass balance and energy balance equations for 1-D plug flow, with dispersion included [92], [98], [101]–[104], [111] or without dispersion [99], [100], using finite difference or finite volume methods. Axial dispersion term can be artificially manipulated to match gas axial diffusion and component breakthrough curves. Due to relatively slow velocity of the flow passing through the bed, feasibility of plug flow assumption has been widely accepted. Pressure drop across the fixed bed is a significant operational parameter of the PSA process, which is associated with

adsorption or desorption performance as well as compression power requirement of the PSA system. In laboratory size operation the pressure drop is typically negligible and some models assumed no pressure variation across the bed in simulation [92], [99], [103], [111]. To account for pressure drop in fixed beds, Ergun's equation is typically employed in simulation work [98], [100]–[102]. Though 1-D dispersed plug flow model with Ergun's equation calculating pressure drop can well capture the flow characteristic within an adsorption-based fixed bed reactor, detailed information of the bed (such as variation in radial direction), especially for commercial size bed, cannot be well simulated and predicted due to the lack of rigorous fluid model.

More recently, due to the advances in CFD which is capable of handling both fluid dynamics and heat-mass transfer characteristics, CFD models have been used for the simulation of adsorption-based beds. Augier et al. [112] developed a CFD model for the simulation of an adsorption bed. A "Brinkman-Forchheimer" model was used for porous media simulation, and Ergun's equation was employed for pressure drop calculation. Langmuir–Freundlich isotherm and LDF model were integrated into the model for adsorption kinetics. The simulation was performed on commercial software Fluent 6.3 but it was not specified how the adsorption model was incorporated. A CFD simulation for CO_2 adsorption in fixed bed reactor was conducted by Nouh et al. [113]. Built-in porous media model in ANSYS Fluent was employed to simulate the packing characteristic and pressure drop. Langmuir isotherm and LDF model were incorporated into the simulation by UDF with mass source term, and heat associated with adsorption was introduced by energy source term. Desorption is part of a complete PSA process but

it was not included in Nouh's work. Xiao et al. [114] investigated charge-discharge cycle of cryo-adsorptive H_2 storage on activated carbon. The adsorption and desorption processes were simulated by CFD models. Dubinin-Astakhov adsorption isotherms and LDF model were also introduced by UDF. CFD models can well capture fluid characteristics using rigorous fluid models and give resolution in two dimensions or three dimensions which is important in exploring the impacts of hydrodynamics, yet limited work has been reported. CFD is a powerful tool for the design of adsorption based fixed bed, for novel sorbent utilization and bed scaling.

For the particular CFD simulation of the novel technology of combined WGS and CO_2 adsorption, little research has been reported. Challenge is expected for reaction kinetics integration, reactant mass diffusion in fixed bed and porous pellets, and its interaction with adsorption or desorption process.

To conclude, for novel technology applications including both CO_2 adsorption and combined WGS and CO_2 adsorption, a CFD model particularly developed for the specific sorbent and capable of predicting adsorption equilibrium and kinetics, component loading, shift reaction kinetics, and thermal performance is desired. Development of such CFD models is one of the research goals of this dissertation work.

2.5 Cooling System for Central Power Plants

One major disadvantage of central power plants, especially PC power plants, is extensive water usage. Wet cooling towers are widely used in central power plants to effectively reject heat to atmosphere by evaporating water, and the water makeup for the towers accounts for majority of total plant water usage. Dry cooling system is an alternative option for thermoelectric plant heat rejection which does not require water vaporization and, therefore, saves water usage. Weather or climate change will have impacts on the performance of cooling systems. Due to water shortage due to drought climate occurrence in many places of the world, research on performance change of cooling systems caused by weather or climate change is becoming increasingly important.

Multiple cooling loads are required in a central power plant, and two major cooling purposes are listed below:

1. To condensate the exhaust steam exiting steam turbine, either in a surface condenser associated with wet cooling towers, or through air-cooled condenser.
2. To reject heat from other processes in a thermoelectric plant such as CO_2 capture unit, either by cooling water which is then cooled in a cooling tower, or by air-cooled heat exchangers.

2.5.1 Wet Cooling System

In a typical wet cooling circuit of a thermoelectric power plant, turbine exhaust steam condenses in a surface condenser where heat is rejected to the cooling water. The hot water leaving the condenser is piped to the cooling tower and flows downward through the fill or packing within the tower to contact with air which is drawn through the fill, the water is cooled by a combination of vaporization and convective heat transfer. Then the cooled water is pumped back to the surface condenser in a continuous circuit.

Cooling towers are distinguished as mechanical draft or natural draft by the method of moving air through the system. Axial flow fans are used in the case of mechanical draft cooling towers while natural draft cooling towers depend on natural convection. By the arrangement of the fill section, they can be categorized as crossflow or counterflow with respect to air and water streams. Figure 2-19 shows schematic of natural draft cooling towers of both crossflow and counterflow. The airflow through the fill is created by the buoyancy via a tall chimney, which is caused by the difference in density between the heated humid air inside the tower and the denser ambient air outside the tower. The natural draft cooling towers have advantages in power saving and low cost of maintenance since no fans are used in the towers. However, natural draft towers require higher investment costs and the large overall dimensions require large plot space for tower installation.

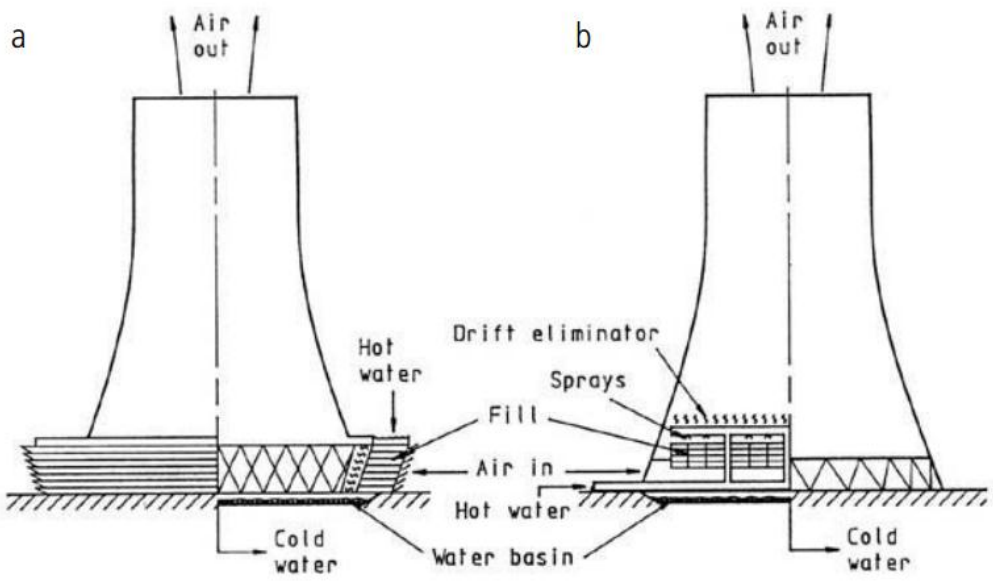

Figure 2-19 Natural draft cooling towers (a) crossflow (b) counterflow (Source: [115])

Mechanical draft cooling towers can be categorized as forced draft or induced draft design. A forced draft tower has a blower type fan at the intake, and the induced draft tower has a fan at the discharge which pulls air up through the tower. Figure 2-20 shows an induced draft counterflow cooling tower. Hot water is sprayed through nozzles located above the fill and flows downward in counterflow with the air stream which is pulled by the induced fans. Compared to natual draft cooling towers, the cooling capacity per unit fill volume of mechanical draft cooling towers is higher due to the increase in volume of the air fored through by fans, while capacity control is possible by controlling the speed of the fans; mechanical cooling towers are much smaller and flexible in the installation location, for instance, they can even be installed inside buildings. The disadvantages of using mechanical draft cooling towers is larger power

consumption and increased operating cost due to the use of fans and the associated motors and controls.

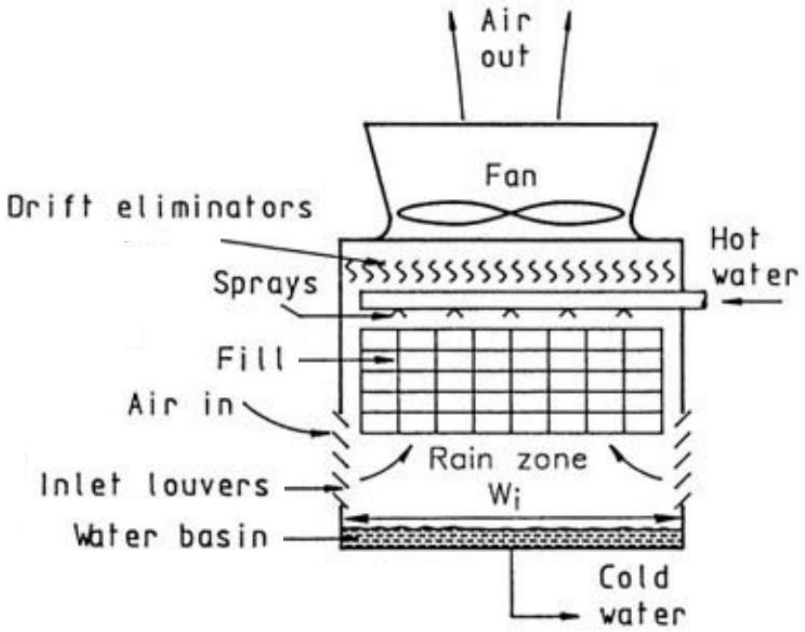

Figure 2-20 A induced draft counterflow cooling tower (Source: [115])

2.5.2 Dry Cooling System

Dry cooling system is referred to air-cooled heat exchangers, with heat transferred from the process fluid to the cooling air stream via extended surfaces or finned tubes. Therefore, it saves water usage compared to wet cooling systems. Efficiency of the power plant is compromised however, since the heat has to be rejected at a higher temperature due to the higher cooling medium (air) temperature and due to the need for larger temperature driving force to compensate for the lower heat transfer coefficient of air. Furthermore, since the performance of air-cooled heat exchangers is

determined by air temperature, the power plant performance would experience significant daily and seasonal changes. Air-cooled heat exchangers are extensively used in thermoelectric plant systems, and the one of the most water-saving application is in air-cooled condensing systems, and replaces the surface condenser and wet cooling towers. In terms of the method of steam condensation, there are two types of air-cooled condensing systems, indirect system and direct system. An indirect air-cooled system is shown in Figure 2-21, which consists of a direct contact spray condenser and a finned tube air-cooled heat exchanger which is typically incorporated into a cooling tower.

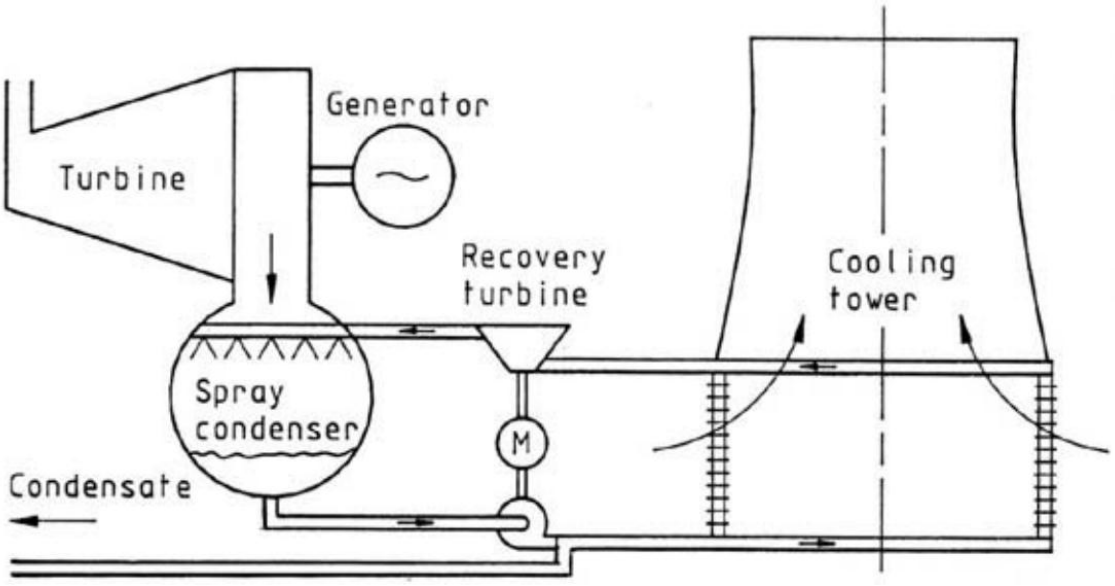

Figure 2-21 Indirect air-cooled condensing system (Source: [115])

In contrast, in a direct air-cooled condensing system (presented by Figure 2-22) the turbine exhaust steam is directly piped to the air-cooled fined tube condenser, which is

typically arranged in the form of an A-frame to reduce the required land area. Since no tower is required, the direct air-cooled condensing system requires less land use and is more cost-effective.

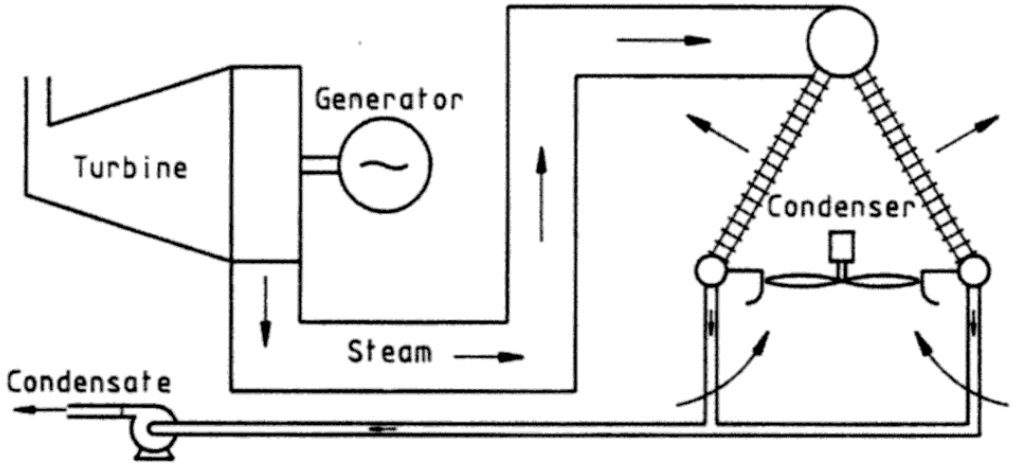

Figure 2-22 Direct air-cooled condensing system (Source: [115])

2.5.3 Wet/Dry Hybrid Cooling System

Various concepts of wet/dry hybrid cooling systems have been proposed and developed to save water while avoiding the cost of full dry-cooling systems [115]. For example, one type of hybrid cooling system has wet cooling and dry cooling in a single tower. Another integration type consisting of separate wet cooling towers and dry cooling equipment with an air-cooled condenser in parallel with a surface condenser connected to wet cooling towers (presented by Figure 2-23). A fraction of the turbine exhaust steam is condensed by the air-cooled condenser, while the remaining is condensed in the surface condenser.

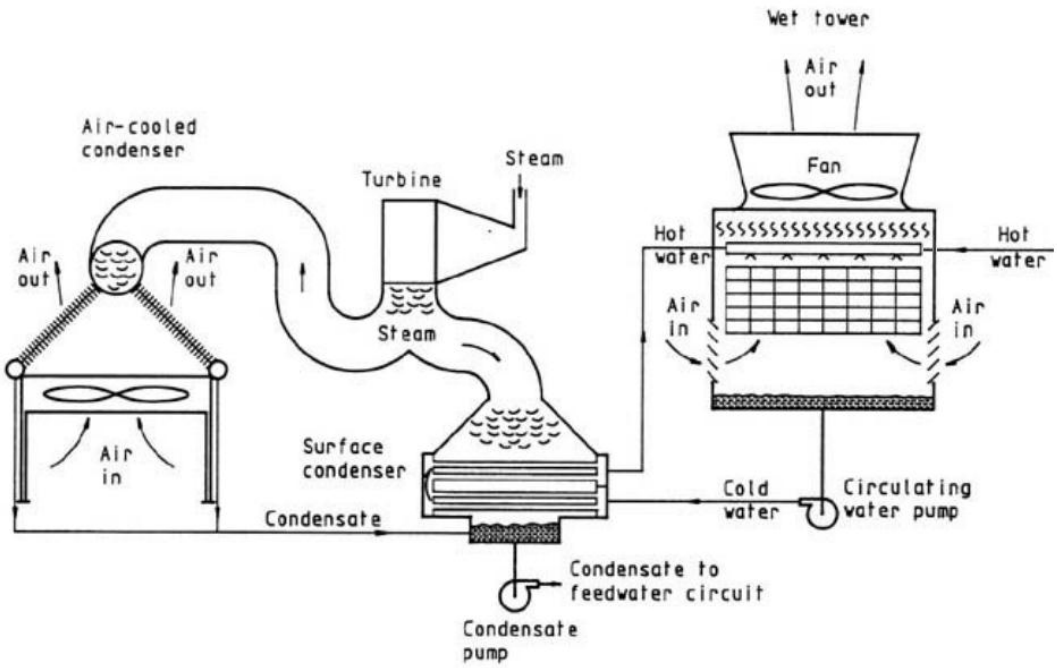

Figure 2-23 Air-cooled condenser in parallel with wet-cooling tower (Source: [115])

2.5.4 Combined Wet/Dry Cooling System

In this dissertation for advanced cooling strategies of PC power plants or specifically of retrofitted PC power plant, a combined concept of wet cooling and dry cooling is of particular interest, i.e. combined wet/dry cooling system: air-cooled condenser is employed for steam turbine exhaust steam cooling and wet cooling towers provide cooling requirements for other plant units, e.g. CO_2 capture unit. This combination cooling system can reduce plant water usage, while save capital cost compared with pure dry cooling. In addition, for plant retrofit scenario the existing cooling tower cells can be utilized rather than abandoned.

2.5.5 Literature Review on Cooling System Simulation

In terms of wet cooling simulation, Kröger et al. [115]–[117] did a comprehensive review on mathematical simulations of evaporative cooling towers in countercurrent configuration of water and air. They summarized and compared three major cooling tower models: Merkel, e-NTU and Poppe. All 3 models are based on mass and energy balances. Merkel theory [118]–[120] is based on mass and energy balance between water and air for a finite difference control volume using simplifying assumptions: the Lewis factor, Le_f, is equal to 1; the air exiting the tower is saturated with water vapor; humid air is characterized only by its enthalpy; and the water flow rate loss by vaporization is neglected in the energy balance. The assumptions cause inaccuracy in humidity of exiting air. Jaber and Webb [121] borrowed the fundamental concepts of effectiveness (e) and number of transfer units (NTU) used in heat exchanger design and developed the e-NTU method to design a cooling tower of counter, cross or parallel flow configuration. A linear saturated air enthalpy-temperature curve is assumed to obtain effectiveness. Poppe theory [122]–[124] presents detailed mass and energy balances without assumptions adopted by Merkel. A correlation for Le_f is applied to relate heat and mass transfer in heat and energy balance analyses. Governing differential equations of both Merkel and Poppe methods can be solved by finite difference methods, and e-NTU method can work as a 0-D model by treating the cooling tower as a whole and can apply to multiple finite segments in one dimensional flow direction. Detailed 2-D and 3-D CFD models are also reported in literature [125]–[127]. Gudmundsson [127] developed a CFD method for cooling tower simulation.

ANSYS Fluent was the computational platform, and thermal properties were introduced by UDF. CFD methods have good spatial resolution, but are time-consuming. To conclude, the models simulating heat and mass transfer for a countercurrent evaporative cooling tower can be categorized by dimension of the model: 0-D model such as e-NTU method; 1-D finite difference model based on mass and energy balances using Merkel, e-NTU or Poppe method; and 2-D or 3-D CFD models. 0-D models lack spatial resolution to understand detailed physics of the process, and averaged flow rate and conditions bring inaccuracy in simulation results. The 2-D or 3-D CFD model gives good spatial resolution but requires significantly more computational resource and time. The 1-D model gives reasonable spatial resolution in flow direction and reduces potential error by averaged flow rate and conditions, and does not require significant computational time. This dissertation work focuses on industrial scale wet cooling towers with particular interest in water usage and impacts of weather and climate change on cooling performance. However, most of the literate reported work focused on small scale cooling towers, and analysis on performance changes caused by ambient conditions is limited. A 1-D finite difference method based on mass and energy balances of a cooling tower is developed and applied to wet cooling tower systems in a thermoelectric power plant to address these issues.

Air-cooled condenser is integrated with steam turbines. Exhaust steam conditions, e.g. temperature and pressure not only affect the cooling performance of the air-cooled condenser but also impact the steam turbine power output. Optimum steam turbine backpressure exists to maximize the net power generation from turbine and air-cooled

condenser as a whole subsystem. In terms of the simulation of air-cooled condenser itself, a method of heat exchange efficiency (η) and NTU was reported in literature [128]–[130] to depict the heat transfer of an air-cooled condenser. With details of the air-cooled condenser unknown, e.g. material, geometry and flow conditions, $\eta - NTU$ method is an effective approach to estimate the performance of a generic air-cooled condenser. This dissertation work focuses on the application of an air-cooled condenser model in combined wet/dry cooling systems in a utility scale thermoelectric power plant.

Chapter 3 Approach

The approach of the dissertation research project includes the following tasks that are required to achieve the objectives presented in Section 2.3:

Task 1: Retrofit existing subcritical (PC) power plant with post-combustion solid sorbent based CO_2 capture technology

This task is aimed at building a system analysis model of subcritical pulverized coal (PC) power plant retrofitted with post-combustion solid sorbent based CO_2 capture technology, with the aim of evolving a retrofit design that is integration-friendly and economically feasible. A process plant simulation program, Aspen Plus®, is employed to evaluate the plant performance including plant efficiency, water usage and economics. A system model of subcritical PC power plant without CO_2 capture serves as the baseline case, and a model of PC power plant using amine CO_2 capture approach is developed as a comparison case. The PC power plant using solid sorbent based CO_2 capture is retrofitted on to the baseline plant while minimizing modifications to existing plant components, while emphasizing minimum modification complexity and plant downtime, water usage, and costs.

Task 2: Investigate cooling system strategies for PC power plant retrofitting, and corresponding performance under various weather/climate conditions.

Regarding retrofitting an existing PC power plant for CO_2 capture, water usage is a big concern particularly in dry areas since CO_2 capture unit would increase the water

demand, and it is desired to keep the same water usage or consume less water for a retrofitted plant. The wet cooling strategy would increase cooling capacity requiring additional wet cooling tower cells, which may lead to significant increase in water usage due to increased cooling tower makeup water. In this task, a particular combined wet/dry cooling strategy is proposed for the PC power plant retrofit scenarios.

Mathematical models are developed for both wet cooling towers and air-cooled condensers to understand the physics of heat and mass transfer, and the cooling performance as weather or climate change. A model for the combined wet/dry cooling system is put together to identify and understand the synergies between the wet and dry cooling systems, and the performance as a whole for this cooling strategy.

Task 3: Design, analyze and compare conventional and advanced IGCC power systems.

Integrated gasification combined cycle (IGCC) is a trend of clean coal technology for future coal based power generation systems. A number of advanced technologies are under development to improve plant performance and economics. An IGCC plant using state-of-art technologies is designed as baseline case to evaluate an advanced IGCC system using technologies that are under development. One major focus of the advanced IGCC is solid sorbent based CO_2 capture. Of particular interest are the integrated water gas shift (WGS) and solid sorbent based CO_2 capture technologies, and corresponding synergies with other subsystems of the IGCC. In this task, solid sorbent CO_2 capture unit is simulated as a black box 0-D model within the framework of the overall IGCC system model developed in Aspen Plus® with performance inputs to this

black box model being obtained from computational fluid dynamics (CFD) simulations as discussed in Task 4.

Task 4: Evaluate solid sorbent based pre-combustion CO_2 capture technologies using CFD for advanced IGCC.

In order to understand the characteristics of the solid sorbent based CO_2 capture technologies (both CO_2 capture alone technology and integrated WGS and CO_2 capture technology), 2-D transient CFD models using ANSYS FLUENT are developed. This task is divided into several steps: a) Build a CFD model of solid sorbent CO_2 capture, including both adsorption and desorption processes, and validate it with experimental data provided by the licensor (TDA Research, Inc). b) Add WGS into the CFD simulation of adsorption process, to make it capable of modeling a fixed bed of integrated WGS and CO_2 capture. c) Apply the CFD models developed in steps a) and b) into advanced IGCC applications, evaluating the effects of operating conditions of the solid sorbent based CO_2 capture technologies, and size the reactor beds and optimize thermal management strategies.

Task 5: Investigate and evaluate advanced IGCCs with biomass and coal cofeeding for electricity and H_2 / other fuels coproduction.

Co-feeding and co-production is a key advantage of IGCC over PC power generation, while limited research has been found on the evaluation of co-feeding and co-production performance especially while employing advanced technologies. This task is

to investigate performance and economics of IGCC systems with biomass and coal co-feeding for electricity and H_2 or other fuels co-production by process plant simulation program Aspen Plus®. Different feed stocks are evaluated. An incremental analysis methodology is developed to evaluate the co-feeding and co-production effects on IGCC systems.

Chapter 4 Pulverized Coal Plants for Clean Power Generation

One important goal of this dissertation work is to investigate technical approaches of PC plants for clean power generation with CO_2 emission mitigation and water usage saving. As described in Chapter 2, subcritical pulverized coal (PC) power plants are the major exiting coal fired power generation units operated in the US, which also produce the highest CO_2 emission levels on MW basis. For short term future applications, retrofitting exiting subcritical PC power plants for CO_2 capture is one of the most promising approaches toward CO_2 emission reduction, which can maximize the use of existing power generation infrastructure and minimize capital investment, as long as plot space is available for installing the equipment required for CO_2 capture and compression. CO_2 capture retrofits would play an increasingly important role until 2030 [131]. This chapter evaluates subcritical PC plants retrofitted for post-combustion CO_2 capture using solid sorbent technology, in comparison with amine CO_2 capture, from the perspectives of system integration, performance, water usage and economics. In terms of saving water usage in a PC power plant, a combined wet/dry cooling system is proposed. The performance of wet cooling tower and air-cooled condenser is investigated by mathematical models, and particular focus is effects of ambient conditions on the performance of cooling system.

4.1 Design and Analysis of PC Plants with CO_2 Capture

4.1.1 Plant Design Basis

The design ambient conditions of proposed power plant configurations are the same as ISO conditions, as presented in Table 4-1.

Table 4-1 Site conditions

Dry Bulb Temperature	15 C
Wet Bulb Temperature	11 C
Elevation	Sea Level
Air composition	
O_2	20.77%
N_2	77.22%
CO_2	0.03%
H_2O	1.04%
Ar	0.94%

The coal used in the PC power plants evaluated here is Illinois No. 6 with characteristics presented in Table 4-2.

PC Plants emissions and CO_2 capture design basis are summarized in Table 4-3.

Table 4-2 Coal properties (Source: [23])

	Bituminous	
Coal Name	Illinois No. 6 (Herrin)	
Source	Old Ben Mine	
Proximate Analysis	Dry Basis, %	As Received, %
Moisture	0	11.12
Ash	10.91	9.7
Volatile Matter	39.37	34.99
Fixed Carbon	49.72	44.19
Total	100	100
Ultimate Analysis	Dry Basis, %	As Received, %
Carbon	71.72	63.75
H_2	5.06	4.5
Nitrogen	1.41	1.25
Sulfur	2.82	2.51
Chlorine	0.33	0.29
Ash	10.91	9.7
Moisture	0	11.12
Oxygen	7.75	6.88
Total	100	100
Heating Value	Dry Basis	As Received
HHV, kJ/kg	30,531	27,135
LHV, kJ/kg	29,568	26,172

Table 4-3 Design basis for plant emissions and CCS

Parameters	
NOx emissions	< 0.070 lb/MMBtu
SOx emissions	< 0.085 lb/MMBtu
Hg emissions	< 1.14 lb/TBtu
CO_2 separation rate	90% for CO_2 captured scenario 0% for non CO_2 captured scenario
CO_2 pressure	153 bar (2215 psia)
CO_2 stream impurity level	
H_2O	< 0.015 vol.%
O_2	< 100 ppmv
Hydrocarbons	< 5 vol.%
H_2S	< 1.3 vol.%
CH_4	< 0.8 vol.%
SO_2	< 3 vol.%

4.1.2 Technical Description

The objective of Section Chapter 3 is to investigate the integration of TDA's solid sorbent CO_2 capture technology into a subcritical PC power plant by comparison with an amine solvent based CO_2 capture system. Integration concepts were evaluated using the process engineering simulation tool Aspen Plus®. Performance, water usage, and economics were then investigated. A 550 MWe subcritical PC power plant without CO_2 capture using market-ready technologies was chosen as the baseline case to represent an existing power plant.

4.1.2.1 Baseline PC Power Plant without CO_2 Capture

The plant performance and costs for the baseline case were developed using data for the subcritical PC power plant published in a DOE/NETL report [23]. The basic process is shown in Figure 4-1. Illinois No. 6 coal is the boiler fuel, which is pulverized into fine powder and conveyed to the burners by primary combustion air. Air from primary air as well as secondary air forced draft fans is heated in air preheaters against boiler exhaust gas. The PC burns in the furnace at a slightly negative pressure, and the combustion products pass through evaporator, superheater and reheater sections. The hot products then pass through economizer preheating boiler feedwater (BFW) and air preheater. An NH_3 injected selective catalytic reduction (SCR) system is installed prior to the air heater to reduce NO_x emissions. The exhaust gases then pass through a fabric filter (or baghouse) unit for particulate control. The flue gas then enters the induced draft fan followed by a limestone slurry sprayed flue gas desulfurization (FGD) system which operates at positive pressure. The FGD is designed to capture 98% of the SO_x

(ultimately forming $CaSO_4$ or gypsum) from the flue gas before it is released to the atmosphere. High pressure (HP) superheated steam generated in the boiler at 165 Bar and 566 C after expansion in the HP section of the steam turbine is reheated in the boiler to 566 C and enters intermediate pressure (IP) section of the turbine at 39 Bar. After expansion, it enters a crossover pipe leading to the two low pressure (LP) sections of the turbine. The steam exiting LP section is condensed in a water-cooled surface condenser and the condensate is pumped through four LP feedwater heaters to the deaerator. The deaerated BFW is then pumped through IP and HP feedwater heaters before it recycles to the boiler. The steam turbine has seven extraction ports to provide steam for the feedwater heaters and the deaerator.

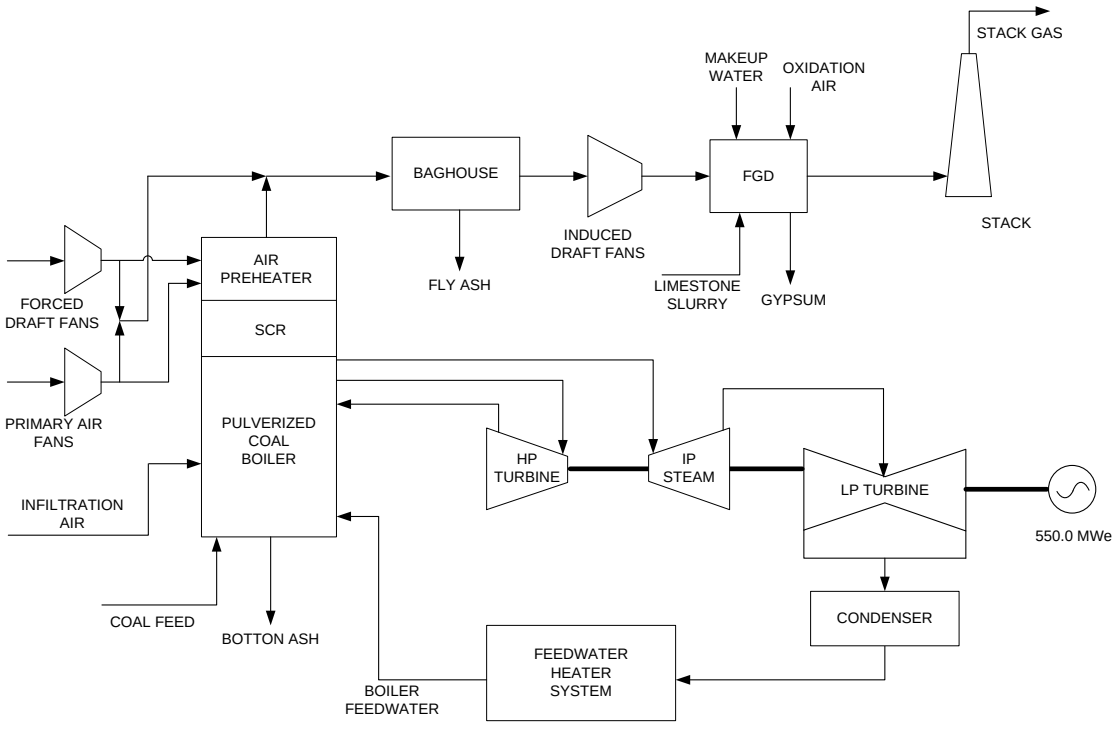

Figure 4-1 Block flow diagram of baseline subcritical PC power plant without CO_2 capture

4.1.2.2 Amine Based CO_2 Capture System

The plant with the amine CO_2 capture system consists of the flue gas supply, SO_2 polishing, CO_2 absorption, solvent stripping and reclaiming as described in detail in literature [69]. Monoethanoloamine (MEA) is the basic ingredient of the Econamine FG Plus^{SM} solvent chosen for this study, and the solvent formulation is designed to recover high-purity CO_2 from LP streams that contain oxygen, such as flue gas from coal-fired power plants.

The PC power plant equipped with the amine CO_2 capture process was developed using data for the corresponding case published in the DOE/NETL report [23]. The process schematic as shown in Figure 4-2 includes a direct contact cooler (DCC) followed by a booster fan downstream of the FGD to provide the flue gas to the downstream amine unit with sufficient pressure to overcome the losses through the CO_2 absorber. The amine solvent loaded with the absorbed CO_2 is regenerated in a stripper equipped with a reboiler which uses as much as 45% of the IP turbine exhaust steam for solvent regeneration.

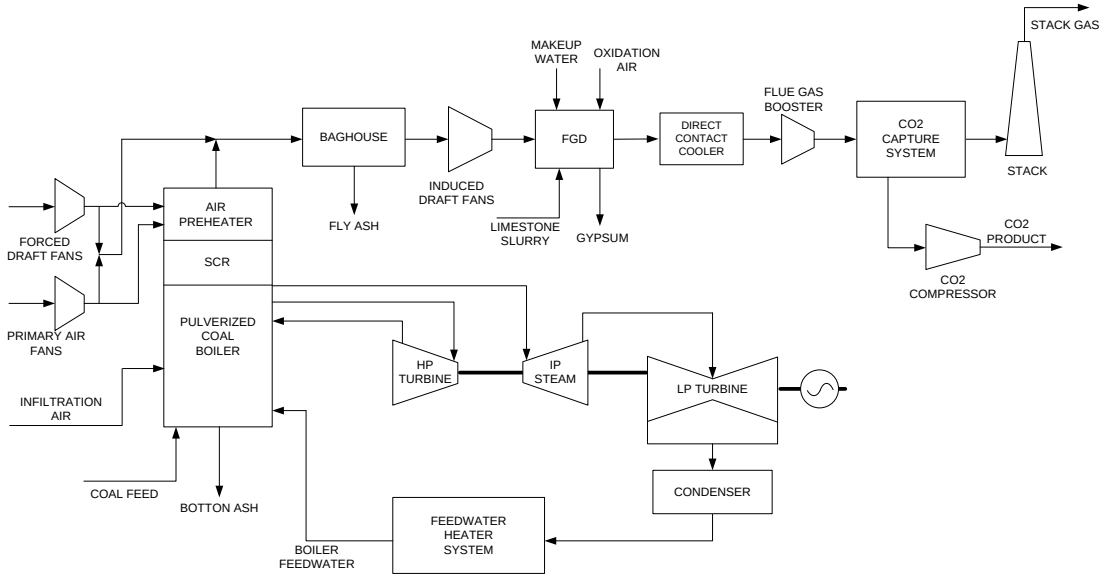

Figure 4-2 Block flow diagram of subcritical PC power plant with CO_2 capture

4.1.2.3 Solid Sorbent Based CO_2 Capture System

The fixed bed sorption process operates cyclically between adsorption and desorption of the CO_2 by alternately switching the flow of fluid entering the beds between flue gas and regeneration steam. 90% of the CO_2 is removed from flue gas when flue gas flows through the sorbent beds in the adsorption cycle. Fast acting valves switch the flow through the bed from flue gas to steam to drive off the adsorbed CO_2 under a subatmospheric pressure of 0.21 Bar while preparing the solid sorbent for reuse in the adsorption cycle. The regeneration heat is about 3.9 to 4.8 kcal/mol of CO_2 which is significantly lower than that required for amine solvent regeneration at approximately 14.4 kcal/mol [132]. Furthermore, steam at a much lower pressure is required as compared with the amine based process.

The overall plant scheme as depicted in Figure 4-2 includes a DCC and a flue gas booster fan as in the amine solvent based case downstream of the FGD and upstream of the CO_2 separation process.

4.1.2.4 CO_2 Compression and Drying

For amine based CO_2 capture, CO_2 compression system consists of a centrifugal compressor with five stages of intercooling, compressing the CO_2 to 153 Bar. The CO_2 stream at a pressure of 1.6 Bar is dehydrated with triethylene glycol to a dew point of -40 C to avoid pipeline corrosion. The compressed moisture free supercritical CO_2 stream is then pipelined to the sequestration site. For solid sorbent CO_2 capture where regeneration is accomplished with steam under a vacuum, vacuum "pumps" are installed upstream of the CO_2 compressor to maintain the subatmospheric pressure of 0.21 Bar in the vessels.

4.1.3 Integration of Sorbent CO_2 Capture into PC Power Plant

The focus here consists of PC power plant retrofitting with the solid sorbent based CO_2 capture with minimum modifications to the steam cycle.

4.1.3.1 Regeneration Steam

Two alternate design options were evaluated for providing steam required for regeneration of the sorbent. The first consisted of extracting steam from the steam turbine. Two options were considered for extraction, one in which the steam was extracted from the LP section of the turbine at a pressure of 0.8 Bar, and resulted in a 2.6% reduction in the turbine power output. The second option which would require

less modifications to the existing turbine consisted of extracting steam from the crossover pipe between IP and LP sections of the steam turbine and resulted in as much as a 4.8% reduction in the steam turbine power output. Since the decrease in turbine power output was quite significant in either case, the next design option consisted of not extracting any steam from the turbine but generating the steam by recovering heat from the CO_2/steam stream leaving the sorption beds during the regeneration step. Figure 4-3 illustrates the heat recovery scheme where two heat exchangers placed downstream of each stage of the vacuum pumps operating as heat pumps generate the LP steam required for regeneration. With this scheme the turbine power output is neither affected nor does the turbine require any modifications.

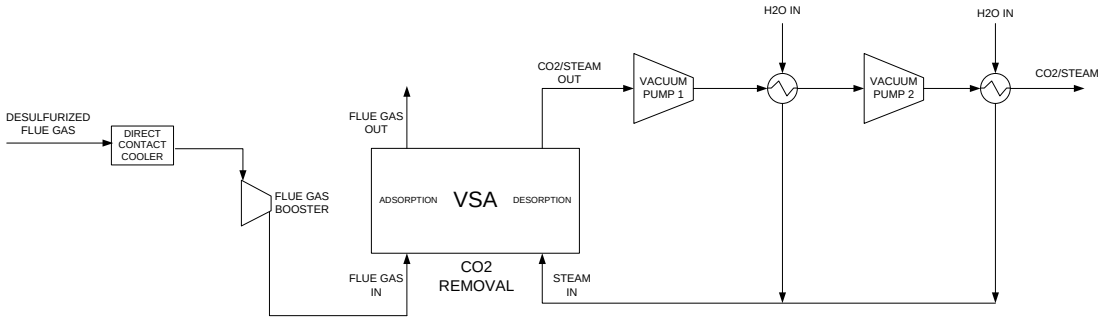

Figure 4-3 Integration of regeneration steam

4.1.3.2 Heat Exchange Loop for Adsorption and Desorption

CO_2 adsorption capacity is enhanced at lower temperatures while desorption requires relatively higher temperatures. Two alternate designs were evaluated for providing the heat in the desorption step and removing the heat from the adsorption step.

The first design alternative consisted of using a heat pump with an industrial refrigerant as the working fluid to transfer heat from the adsorption step into the desorption step (note that the system consists of multiple beds operating in cyclic manner to make the continuous transfer of heat from one step into another possible). The schematic is shown in Figure 4-4.

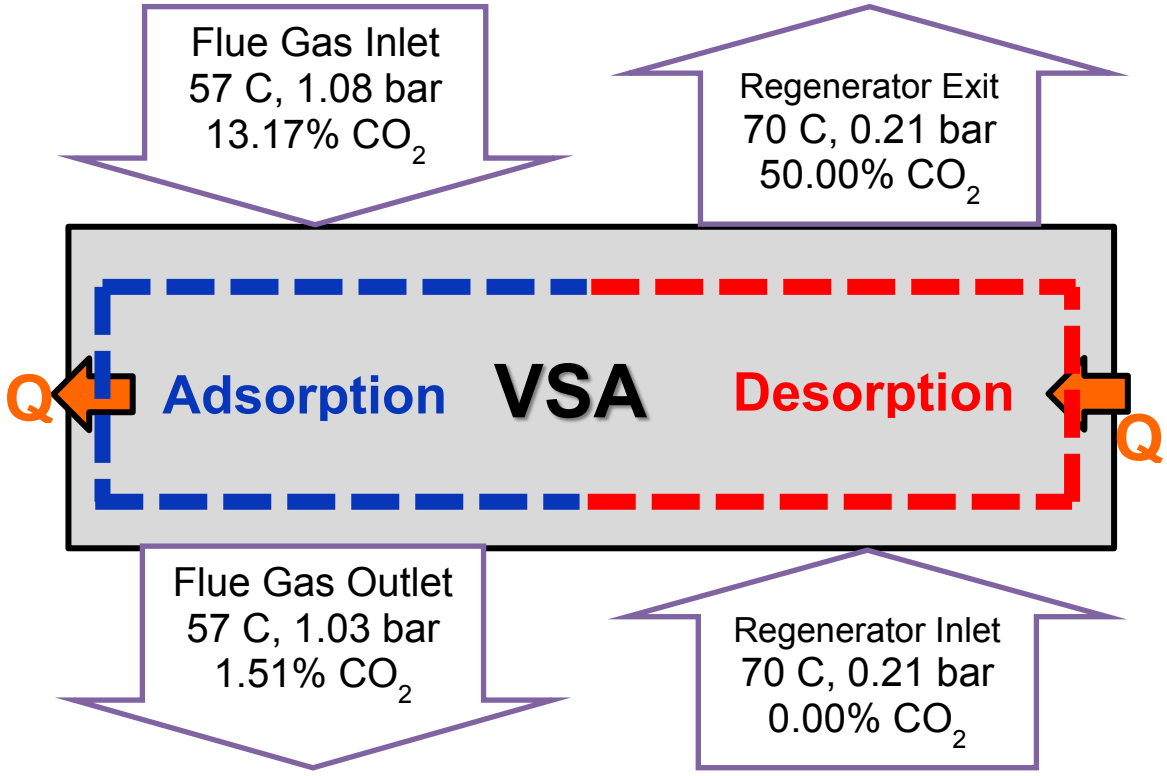

Figure 4-4 Heat exchange loop for VSA

The second design alternative consisted of using cooling water for removing the heat from the adsorption step and using steam to provide heating during the desorption step. Two options were again considered for providing the steam, one in which the steam was extracted from the LP section of the turbine at a pressure of 0.8 Bar, and

showed a 0.6% efficiency advantage over the heat pump design, and the other option which would require less modifications to the existing turbine consisted of extracting steam from the crossover pipe between IP and LP sections of the steam turbine and resulted in as much as a 1.2% reduction in the efficiency over the heat pump design.The heat pump design alternative was chosen since it required no modifications at all to the steam turbine while the efficiency penalty due to the power demand of the heat pumps was quite small.

The third design alternative is to run the VSA process adiabatically. This simplifies the reactor system design and internals. This is considered out of scope for this research. However, should be similar in performance.

4.1.4 Simulation Approach and Models

Detailed process engineering model for the power generation systems discussed in this dissertation were developed using Aspen Plus®, a commercial software package for process simulation and analysis. The purpose of Aspen Plus® model is to simulate and predict the performance of a process, involving the decomposition of the process into constituent elements (e.g. units) for individual unit performance calculation. The process characteristics (e.g. stream properties, operating conditions, etc.) are calculated using built-in physical relationships (e.g., material and energy balances, thermodynamic equilibrium, and rate equations).

Some major process models are described as follows for PC power plant simulations. Other power generation systems discussed in this dissertation were developed similarly using Aspen Plus®.

Coal combustion is a complex process due to its complicated composition. The first step of the simulation in Aspen Plus® is coal decomposition: coal is converted into its constituting components including carbon, hydrogen, oxygen, sulfur, nitrogen, and ash, by specifying the yield distribution according to the ultimate analysis. Those constituting components are then reacted with air for combustion, with major reactions shown below. The heat associated with the coal decomposition and the combustion heat for the constituting components are both accounted for as the heat of combustion of coal.

$$\mathrm{C} + O_2 \rightarrow CO_2 \qquad \text{Equation 4-1}$$

$$2H_2 + O_2 \rightarrow 2H_2O \qquad \text{Equation 4-2}$$

$$\mathrm{S} + O_2 \rightarrow SO_2 \qquad \text{Equation 4-3}$$

$$\mathrm{S} + 3/2O_2 \rightarrow SO_3 \qquad \text{Equation 4-4}$$

The fractional conversion of the limiting specie may be specified for a reaction (e.g. Equation 4-3 and Equation 4-4) while NO_x formation may be estimated using built-in correlations.

Thermodynamic models are utilized for pressure change unit operations (e.g. compressors, fans and turbines) as show below:

$$W = \dot{m}\eta_s\eta_m\left(h_{in}(T_{in}, p_{in}) - h_{s,out}(T_{out}, p_{out})\right) \quad \text{Equation 4-5}$$

where

W is work associated with the pressure change operation,

$\dot{m}$ is mass flow rate of the process fluid,

η_s is isentropic efficiency,

η_m is mechanical efficiency,

h is enthalpy,

$h_{s,out}$ is the enthalpy if the pressure change operation is isentropic,

Subscript in indicates inlet conditions, and out indicates outlet conditions.

For heaters, the thermodynamics calculation is show below:

$$Q = -\left(h_{in}(T_{in}, p_{in}) - h_{out}(T_{out}, p_{out})\right) \quad \text{Equation 4-6}$$

where Q is heat added to the operation

For heat exchangers, heat balance between hot and cold steams is calculated while keeping a specified pinch temperature:

$$-\left(h_{1,in}(T_{1,in}, p_{1,in}) - h_{1,out}(T_{1,out}, p_{1,out})\right) = \left(h_{2,in}(T_{2,in}, p_{2,in}) - h_{2,out}(T_{2,out}, p_{2,out})\right) \quad \text{Equation 4-7}$$

4.1.5 Results and Discussion

4.1.5.1 System Performance

Overall performance of the three PC plants is summarized in Table 4-4. The PC plant without CO_2 capture consumes 199,516 KG/H bituminous coal while generating 550 MW with a thermal efficiency of 36.57% (Higher Heating Value / HHV) on a net basis. Since a retrofit scenario is being considered for this study, the coal feed rate is held at this value for each of the two PC plants with CO_2 capture. With 90% CO_2 capture, the net power output of the PC plant is reduced to 391 MW with a correspondingly lower efficiency of 26.01% (HHV) using the amine capture technology. On the other hand, the reduction in net output and efficiency is less significant for the solid sorbent based plant with the power output at 431 MW and an efficiency of 28.67% (HHV) which is significantly higher, corresponding to a 9% reduction in plant heat rate over the amine based plant. The primary reason for this significant decrease in heat rate is that the amine based plant requires a significant amount of steam to be extracted from the steam turbine. As pointed out previously, the amine based plant requires as much as 45% of the steam exiting the IP section of the turbine for solvent regeneration, while the lower pressure regeneration steam required for the solid sorbent is all generated by heat recovery from the CO_2/steam stream leaving the regeneration step.

Table 4-4 Performance summary

Case No.		1	2	3
CO_2 Capture Technology	Units	No CO_2 Capture	Amine	Solid Sorbent
CO_2 Capture Level	%	0.0	90.0	90.0
Steam Turbine Power	KWe	583,686	479,040	563,966
Total Auxiliary Consumption	KWe	33,686	87,848	132,779
Net Power Output	KWe	550,000	391,192	431,187
% Net Plant Efficiency, HHV	%	36.57	26.01	28.67
Net Heat Rate	KJ/KWH	9,843	13,839	12,556
Surface Condenser Cooling Duty	10^6 KJ/H	2,565	1,451	2,581
As-Received Feed	KG/H	199,516	199,516	199,516
Thermal Input	KWT HHV	1,503,859	1,503,859	1,503,859

Detailed break-down of auxiliary power consumers for each plant is listed in Table 4-5. The major difference in the power consumption is due to that required by the flue gas booster fan, CO_2 removal and compression. The pressure drop through the amine based CO_2 capture unit is higher than that of the solid sorbent based CO_2 capture unit requiring a higher discharge pressure for the booster fan. On the other hand, the power required for pressurizing the CO_2 to pipeline pressure of 153 Bar is higher for the sorbent case because the CO_2 is regenerated at subatmospheric pressure of 0.21 Bar while the pressure of the CO_2 stream regenerated from the amine solvent is 1.6 Bar. As a result, CO_2 compression power for solid sorbent case is significantly higher than amine case, namely, 83 MWe vs. 35 MWe. The net result is that the total power consumption for the solid sorbent based plant is higher than that for the amine based plant.

Table 4-5 Auxiliary power consumptions

Case No.	1	2	3
CO2 Capture Technology	No CO_2 Capture	Amine	Solid Sorbent
Auxiliary Power Consumption, Kwe			
Feed Handling	4,395	4,395	4,395
Ash Handing	573	573	573
Primary Air Fans	1,408	1,402	1,408
Forced Draft Fans	1,790	1,788	1,790
Induced Draft Fans	7,583	8,640	7,583
SCR	50	50	50
Baghouse	70	70	70
FGD	3,193	3,188	3,193
Flue Gas Booster & CO_2 Removal	0	15,795	13,792
CO_2 Compression	0	34,896	82,734
Miscellaneous Balance of Plant	2,011	2,011	2,011
Steam Turbine Auxiliaries	401	329	387
Condensate Pumps	851	502	846
Circulating Water Pumps	6,003	7,970	7,708
Ground Water Pumps	493	710	576
Cooling Tower Fans	3,030	4,024	3,891
Transformer Losses	1,833	1,505	1,771
Total Auxiliary Consumption	33,686	87,848	132,779

4.1.5.2 Water Usage

Raw water usage is summarized in Table 4-6 for the three plants. The raw water makeup is supplied to the deminerlaizers for BFW preparation and accounts for blowdown from this unit, makeup required by the FGD unit, and by the wet cooling towers where majority of the raw water is required. As expected, the raw water consumption expressed on a MW of net power generated basis follows the same trend as the plant thermal efficiency, being lowest for the plant without CO_2 capture and highest for the plant with the amine based capture. By introducing 90% CO_2 capture, water usage of a PC power plant increases significantly; by 80% for amine approach, and

by 49% for solid sorbent approach, which is one of the concerns for the use of post-combustion CO_2 capture technology. To reduce the raw water usage in a power plant, the use of dry cooling system or combined wet/dry cooling system is investigated in Section 4.2.

Table 4-6 Raw Water Usage (Liter/MWh Basis) of PC Power Plants Using Wet Cooling System

Case No.	1		2		3	
CO2 Capture Technology	No CO_2 Capture		Amine		Solid Sorbent	
Water Use	Raw Water Usage		Raw Water Usage		Raw Water Usage	
	Liter/MWh	%	Liter/MWh	%	Liter/MWh	%
BFW Makeup	30.9	1.2	43.5	1.0	38.0	1.0
FGD Makeup	350.2	13.9	492.5	10.9	446.7	11.9
Demineralizer Blowdown	7.1	0.3	10.1	0.2	8.8	0.2
Cooling Tower Makeup						
Steam Cycle Cooling	2,157.0	85.8	1,721.1	38.0	2,767.0	73.9
CO2 Capture Cooling	0.0	0.0	2,305.4	50.9	765.7	20.5
BFW Blowdown & Flue Gas Condensate	-30.9	-1.2	-43.5	-1.0	-282.0	-7.5
Total	2,514.3	100.0	4,529.0	100.0	3,744.2	100.0

4.1.5.3 Economics

Since retrofit costs for an existing plant would be plant specific, economics were evaluated on the basis of greenfield plants in order to get generalized insights into the economics of the different CO_2 capture technologies. Total plant costs are summarized in Table 4-7 with break-down of the costs by each major plant unit for the three cases. Table 4-8 presents the development of cost of electricity as well as the operating and maintenance (O&M) costs. Cost estimations are derived primarily from NETL studies on PC plants [23]. The cost of solid sorbent based CO_2 removal unit was estimated by

Babcock and Wilcox Inc, while costs of some of the other equipment such as the DCC and heat exchange equipment were calculated by Aspen Process Economic Analyzer. The PC plant without CO_2 capture has a total plant cost of 896.1million dollars or $1,629/kW. The PC plant with the amine based unit resulted in a total plant cost of 1,265.0 million dollars or $3,234/kW and the PC plant with the solid sorbent based unit resulted in a similar total plant cost of 1291.6million dollars but due to its higher efficiency has a significantly lower cost on a per kW basis at $2,996/kW. The levelized cost of electricity without CO_2 capture was calculated at $60.5/MWh, while that for the amine based PC plant was calculated at $124.3/MWh, and that for the solid sorbent based PC plant was lower at $115.8/MWh.

Table 4-7 Total plant cost summary

Case No.	1	2	3
CO_2 Capture Technology	No CO_2 Capture	Amine	Solid Sorbent
Unit	2007 Installed Cost ($1000)	2007 Installed Cost ($1000)	2007 Installed Cost ($1000)
Coal & Sorbent Handing, Prep & Feed	59,058	59,058	59,058
Feedwater & Misc. BOP Systems	80,645	80,634	79,538
PC Boiler	268,481	268,481	268,481
Flue Gas Cleanup	136,779	136,779	136,779
CO2 Removal & Compression	0	385,947	399,268
Ductwork and Stack	36,921	33,421	31,286
Steam Turbine Generator + Auxiliaries	114,153	99,408	111,439
Cooling Water System	36,540	44,560	43,528
Ash Handling Systems	13,148	13,148	13,148
Accessory Electric Plant	52,271	45,519	51,029
Instrumentation & Controls	21,371	21,371	21,371
Improvement to Site	14,135	14,135	14,135
Buildings & Structures	62,562	62,562	62,562
Total	896,063	1,265,023	1,291,622
Total $/kW	1,629	3,234	2,996

Table 4-8 Cost of electricity

Case No.	1	2	3
CO2 Capture Technology	No CO_2 Capture	Amine	Solid Sorbent
Net Power, MW	550	391	431
Capacity Factor (CF), %	85	85	85
Total Plant Cost (TPC), $	896,063,288	1,265,023,308	1,291,622,045
6 Month Labor Cost	7,372,976	9,554,405	9,670,775
1 Month Maintenance Materials	970,735	1,370,442	1,399,257
1 Month Non-Fuel Consumables	1,137,812	1,399,291	1,792,689
1 Month Waste Disposal	252,669	252,669	252,669
25% of 1 Month Fuel Cost at 100% CF	1,532,429	1,532,429	1,532,429
2% of TPC	17,921,266	25,300,466	25,832,441
60 Day Supply of Fuel & Consumables at 100% CF	14,335,945	14,851,739	15,627,758
0.5% of TPC (Spare Parts)	4,480,316	6,325,117	6,458,110
Initial Catalyst & Chemicals Cost, $	0	1,915,465	6,178,040
Land	900,000	900,000	900,000
Other Owner's Costs	134,409,493	189,753,496	193,743,307
Financing Costs	24,193,709	34,155,629	34,873,795
Total Overnight Cost (TOC), $	1,103,570,638	1,552,334,456	1,589,883,316
Fixed Operating Cost for Initial Year of Operation (OCF), $	32,667,218	44,409,277	45,173,991
Annual Feed Cost at Above CF for Initial Year (OCV1), $	62,523,105	62,523,105	62,523,105
Other Annual Variable Operating Cost at Above CF for Initial Year (OCV2), $	24,084,400	30,828,494	35,135,075
Annual CO2 Transporting, Storing, and Monitoring Cost at Above CF for Initial Year (OCV3), $	0	31,309,149	31,288,176
1st Year Cost of Electricity (COE) w/o CO_2 TS&M[1], $/MWh	60.5	113.5	106.0
1st Year Cost of Electricity (COE), $/MWh	60.5	124.3	115.8

4.1.6 Sensitivity Studies on CO_2 Capture Level

It has been widely accepted that carbon capture should be an essential feature of a future coal fired power plant. In terms of PC power plant retrofitting for CO_2 capture, in a transitional near term future scenario because of policy drivers, economics, and tradeoff between CO_2 capture level and plant thermal efficiency, various CO_2 capture levels (30% - 90%) have been employed in previous research for amine CO_2 capture technology [133]. Due to specific integration and synergies between the CO_2 capture process, heat exchange loop and existing steam cycle, CO_2 capture level might have

[1] TS&M (transporting, storing , and monitoring) is $10/MWh.

particular impacts on the performance of a PC plant using solid sorbent CO_2 capture technology, while little work has been reported in literature so far. Using the PC plant system with integration of solid sorbent CO_2 capture process described in section 4.1.3, this section evaluates the sensitivity of performance and water usage on CO_2 capture level.

4.1.6.1 Strategy for Varying CO_2 Capture Levels

Two options can be considered to achieve various CO_2 capture levels:

1. The volumetric percentage of CO_2 in clean flue gas leaving the beds can be controlled by the space velocity in the adsorption fixed bed and duration of adsorption step. Essentially 100% CO_2 is captured if adsorption step terminates before CO_2 breaks through at bed exit. If let certain amount of CO_2 break through the bed and collected in decarbonized syngas, various CO_2 capture level can be achieved.
2. Holding the CO_2 capture rate during the adsorption step at a certain level, net CO_2 capture level of a plant can be controlled by a bypass stream of the flue gas vented directly to the stack. The block flow diagram of this strategy is shown by Figure 4-5.

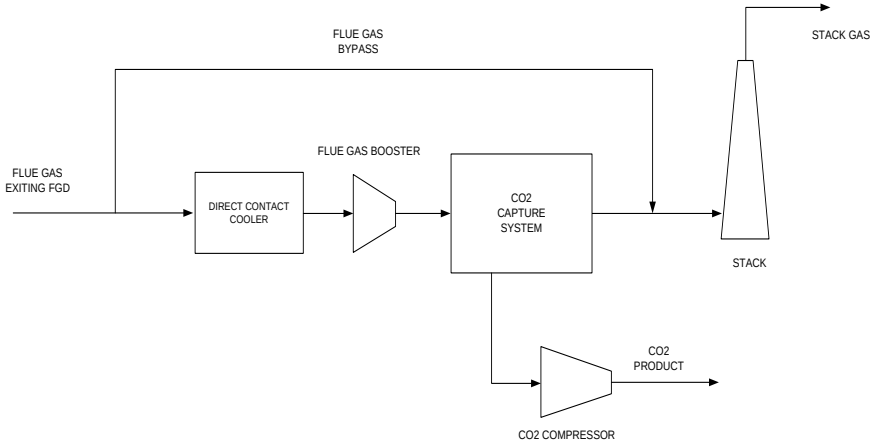

Figure 4-5 Block flow diagram of CO_2 capture with flue gas bypass

Considering that the size and number of the reactor beds are determined by the capacity of flue gas passing through the adsorption bed, and the capital investment and operating cost can be reduced at smaller reactor size and less reactors, the bypass option was chosen for the sensitivity study of CO_2 capture level.

4.1.6.2 Performance of PC Power Plants with different CO_2 capture level

Four CO_2 capture levels were evaluated using solid sorbent technology, e.g. 30%, 50%, 70% and 90%. The 90% case is the same as described previously and all CO_2 capture cases were compared with the baseline case without CO_2 capture. The case designations are as follows:

Baseline Case: 0% Capture

Case 1: 30% Capture

Case 2: 50% Capture

Case 3: 70% Capture

Case 4: 90% Capture

Table 4-9 shows the performance summaries of PC power plants with the different CO_2 capture levels, and Table 4-10 presents the breakdown of auxiliary power consumptions. Auxiliaries, e.g. flue gas booster power, CO_2 removal unit power and CO_2 compression power, increase linearly with the percentage of CO_2 captured because the flow rate entering the CO_2 related units changes linearly while other power consumptions and power generation remain at the same level for a given coal feed rate. It can be seen from Figure 4-6 that total auxiliary power increases with CO_2 capture level, and net power output correspondingly decreases. It may be seen from Figure 4-7 that net plant efficiency goes down linearly from 36.57% for the non CO_2 capture scenario to 28.67% for 90% CO_2 capture, and correspondingly net heat rate goes up from 9,843 KJ/KWH to 12,556 KJ/KWH.

Table 4-9 Performance summaries for various CO_2 capture level

Case No.	Units	Baseline	1	2	3	4
CO_2 Capture Technology		No CO_2 Capture	Solid Sorbent	Solid Sorbent	Solid Sorbent	Solid Sorbent
Steam Turbine Power	KWe	583,686	564,377	564,022	564,142	563,966
Total Auxiliary Consumption	KWe	33,686	66,839	88,826	110,789	132,779
Net Power Output	KWe	550,000	497,538	475,196	453,353	431,187
% Net Plant Efficiency, HHV	%	36.57	33.08	31.60	30.15	28.67
Net Heat Rate	KJ/KWH	9,843	10,881	11,393	11,942	12,556
Surface Condenser Cooling Duty	10^6 KJ/H	2,565	2,617	2,607	2,593	2,581
As-Received Feed	KG/H	199,516	199,516	199,516	199,516	199,516
Thermal Input	KWT HHV	1,503,859	1,503,859	1,503,859	1,503,859	1,503,859
Carbon Captured	%	0.0	30.0	50.0	70.0	90.0

Table 4-10 Auxiliary power consumptions for various CO_2 capture level

Case No.	Baseline	1	2	3	4
CO_2 Capture Technology	No CO_2 Capture	Solid Sorbent	Solid Sorbent	Solid Sorbent	Solid Sorbent
Auxiliary Power Consumption (KWe)					
Feed Handling	4,395	4,395	4,395	4,395	4,395
Ash Handing	573	573	573	573	573
Primary Air Fans	1,408	1,408	1,408	1,408	1,408
Forced Draft Fans	1,790	1,790	1,790	1,790	1,790
Induced Draft Fans	7,583	7,583	7,583	7,583	7,583
SCR	50	50	50	50	50
Baghouse	70	70	70	70	70
FGD	3,193	3,193	3,193	3,193	3,193
Flue Gas Booster	0	1,816	3,026	4,236	5,447
Solid Sorbent CO_2 Removal Unit	0	2,780	4,634	6,480	8,345
CO_2 Compression	0	27,578	45,963	64,349	82,734
Miscellaneous Balance of Plant	2,011	2,011	2,011	2,011	2,011
Steam Turbine Auxiliaries	401	387	387	387	387
Condensate Pumps	851	855	852	849	846
Circulating Water Pumps	6,003	6,677	7,026	7,364	7,708
Ground Water Pumps	493	528	545	560	576
Cooling Tower	3,030	3,371	3,547	3,718	3,891
Transformer Losses	1,833	1,773	1,772	1,772	1,771
Total Auxiliary Consumption	33,686	66,839	88,826	110,789	132,779

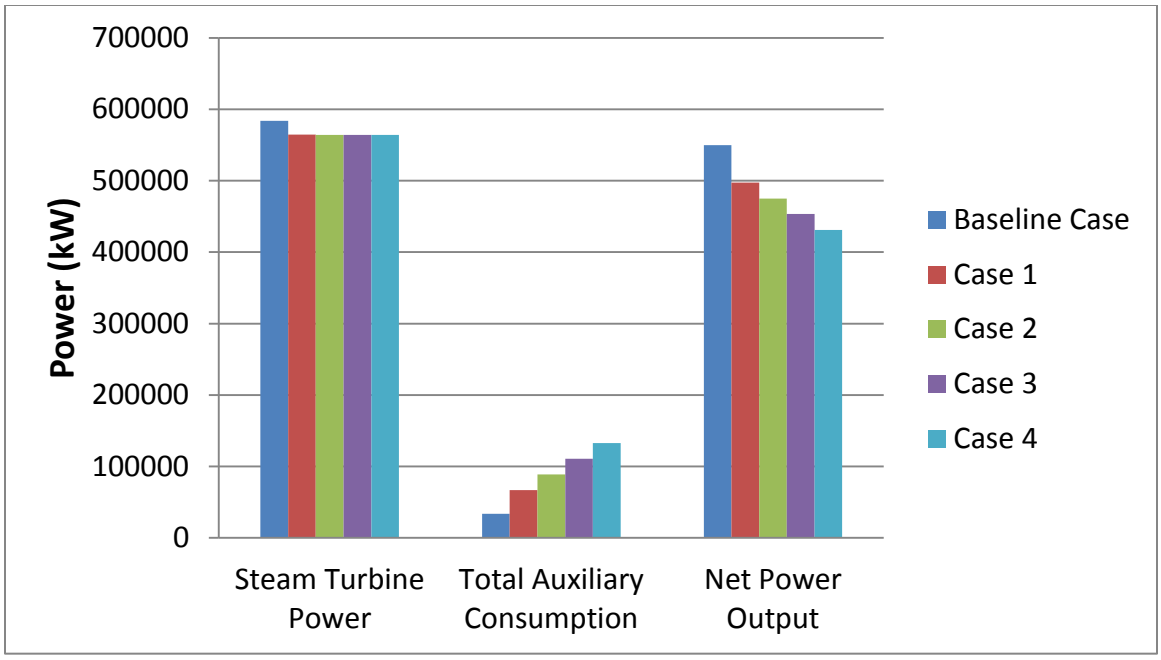

Figure 4-6 Powers for different CO_2 capture levels

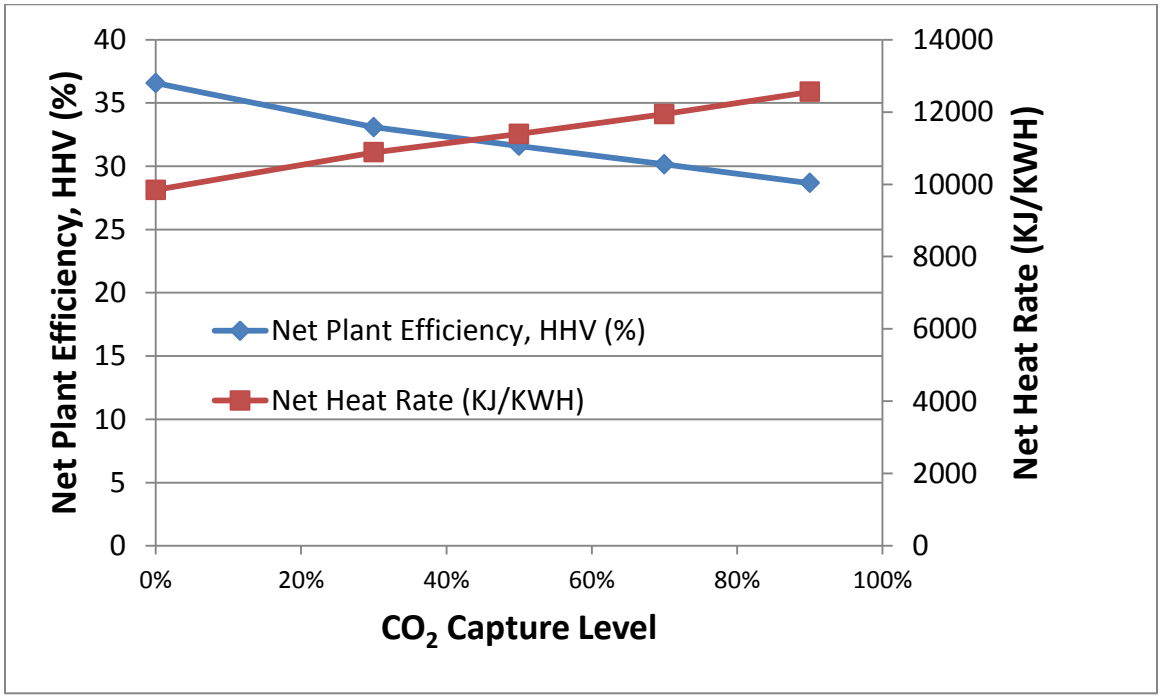

Figure 4-7 Net plant efficiency and net heat rate for different CO_2 capture levels

In terms of power consumption for CO_2 capture, power required is defined by Equation 4-5 to explore the extra power required due to CO_2 capture. It can be observed from Figure 4-8 that power required on CO_2 capture basis actually decreases from 374 kWe/Tonne CO_2 for 30% capture case to 283 kWe/Tonne for 90% case. The economies of scale for CO_2 capture are clearly observed. Higher CO_2 capture level leads to relatively smaller required power on CO_2 capture basis.

$$Power\ Requied\ \left(\frac{kWe}{Tonne\ CO_2}\right) = \frac{Reduction\ in\ Net\ Power\ (kWe)}{CO_2\ Captured\ (Tonne)} \qquad \text{Equation 4-5}$$

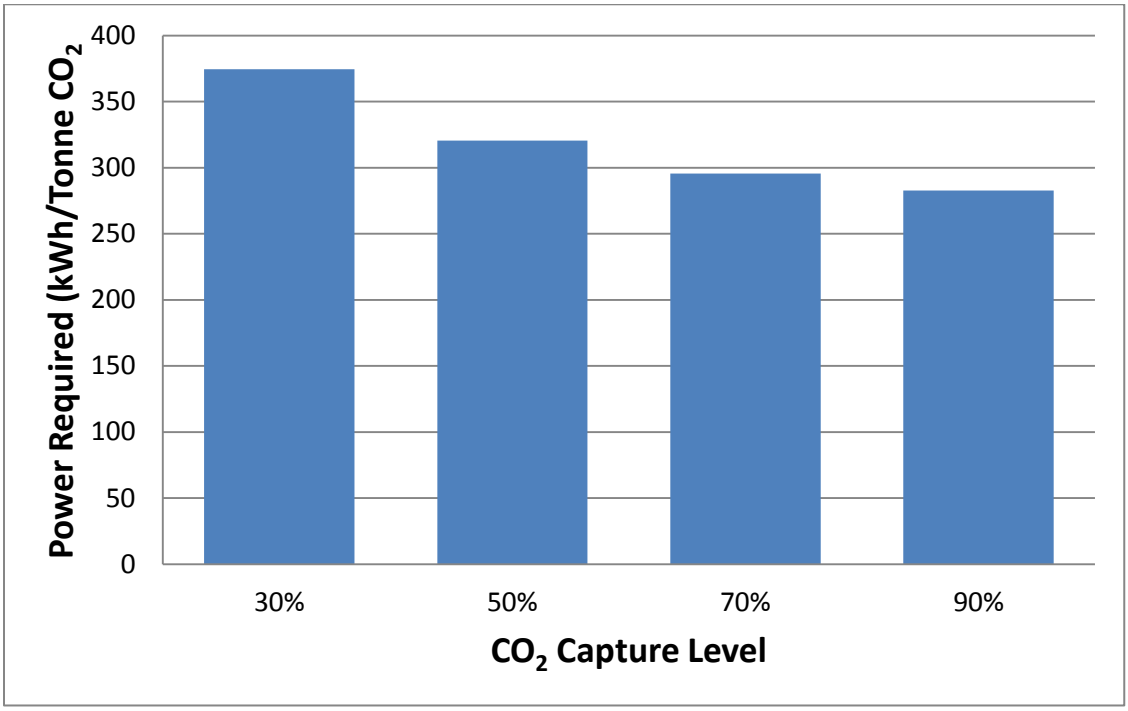

Figure 4-8 Power required for different CO_2 capture levels

4.1.6.3 Water Usage of PC Power Plants with different CO_2 capture levels

Assuming mechanical draft wet cooling towers are used for all cases, CO_2 capture level affects raw water usage of a PC power plant. Table 4-11 shows that on Liter/s basis cooling tower makeup changes due to different CO_2 capture levels while other raw water consumers remain the same. The changes are mainly caused by cooling capacity required by the CO_2 capture unit, including DCC cooling and inter-cooling of CO_2 compression, both of which are proportional to the flue gas passing through CO_2 capture unit. Taking net power output accounted in water usage calculation, the total water usages on Liter/MWh basis are shown by Table 4-12. It can be found from Figure 4-9 that for various CO_2 capture levels (30% to 90%) comparing with non CO_2 capture scenario, total water usage increases by 7% to 17% on Liter/s basis, and by 18% to by 49% on Liter/MWh basis.

Table 4-11 Raw water usage (Liter/s Basis) of PC power plants with various CO_2 capture level using wet cooling system

Case No.	Baseline		1		2		3		4	
CO_2 Capture Technology	No CO_2 Capture		Solid Sorbent		Solid Sorbent		Solid Sorbent		Solid Sorbent	
Water Use	Raw Water Usage		Raw Water Usage		Raw Water Usage		Raw Water Usage		Raw Water Usage	
	Liter/s	%	Liter/s	%	Liter/s	%	Liter/s	%	Liter/s	%
BFW Makeup	4.7	1.2	4.5	1.1	4.5	1.1	4.5	1.0	4.5	1.0
FGD Makeup	52.7	13.7	52.6	12.8	52.6	12.4	52.6	12.1	52.6	11.7
Demin Blowdown	1.1	0.3	1.0	0.3	1.0	0.2	1.0	0.2	1.0	0.2
Cooling Tower Makeup										
Steam Cycle Cooling	330.4	86.0	336.7	81.9	335.3	79.1	333.4	76.4	331.8	74.0
CO_2 Capture Cooling	0.0	0.0	30.6	7.4	51.0	12.0	71.4	16.4	91.8	20.5
BFW Blowdown & Flue Gas Condensate	-4.7	-1.2	-14.0	-3.4	-20.4	-4.8	-26.8	-6.1	-33.2	-7.4
Total	384.1	100.0	411.4	100.0	424.0	100.0	436.1	100.0	448.5	100.0

Table 4-12 Raw water usage (Liter/MWh Basis) of PC power plants with various CO_2 capture level using wet cooling system

Case No.	Baseline		1		2		3		4	
CO_2 Capture Technology	No CO_2 Capture		Solid Sorbent		Solid Sorbent		Solid Sorbent		Solid Sorbent	
CO_2 Capture Level	0%		30%		50%		70%		90%	
Water Use	Raw Water Usage		Raw Water Usage		Raw Water Usage		Raw Water Usage		Raw Water Usage	
	Liter/MWh	%	Liter/MWh	%	Liter/MWh	%	Liter/MWh	%	Liter/MWh	%
BFW Makeup	30.9	1.2	32.91	1.1	34.44	1.1	36.13	1.0	37.98	1.0
FGD Makeup	350.2	13.9	387.14	13.0	405.35	12.6	424.88	12.3	446.72	11.9
Demin Blowdown	7.1	0.3	7.60	0.3	7.96	0.2	8.35	0.2	8.77	0.2
Cooling Tower Makeup										
Steam Cycle Cooling	2,157.0	85.8	2431.11	81.7	2536.17	79.0	2643.64	76.3	2767.04	73.9
CO_2 Capture Cooling	0.0	0.0	221.17	7.4	385.75	12.0	566.47	16.4	765.74	20.5
BFW Blowdown & Flue Gas Condensate	-30.9	-1.2	-103.41	-3.5	-157.47	-4.9	-216.66	-6.3	-282.04	-7.5
Total	2,514.3	100.0	2,976.5	100.0	3,212.2	100.0	3,462.8	100.0	3,744.2	100.0

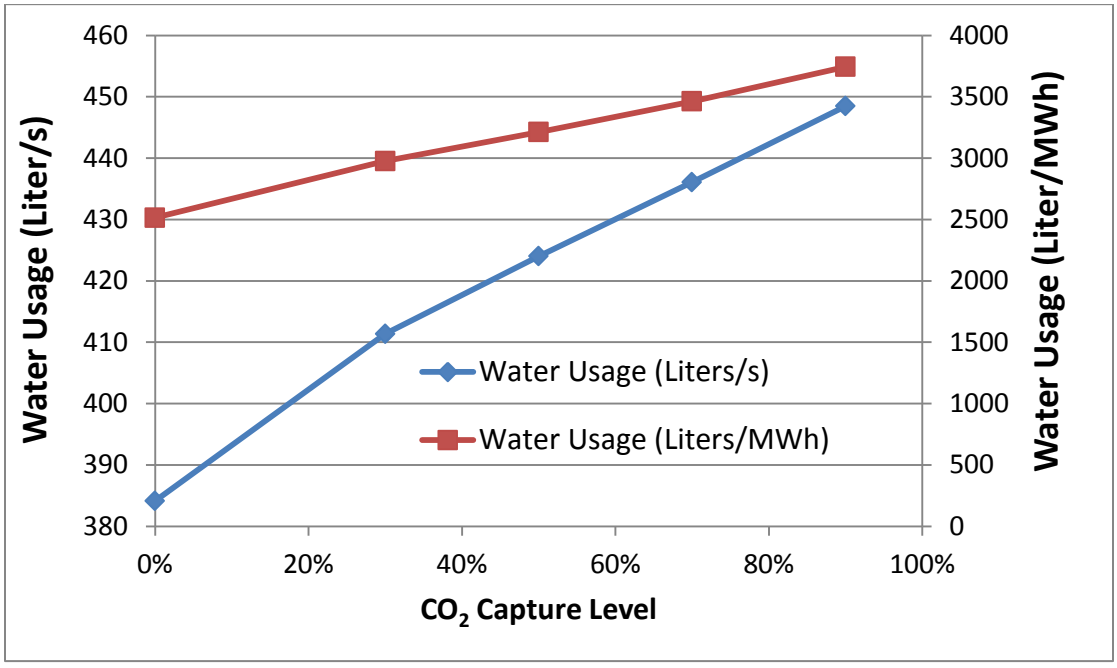

Figure 4-9 Total raw water usage for different CO_2 capture levels

4.2 Cooling Systems for PC Power Plants with CO_2 Capture

One major disadvantage of PC plants is extensive water usage, and cooling system accounts for majority of total plant water usage as described in Section Chapter 3. Advanced cooling systems with limited water usage is another desired feature for the clean power generation of a PC plant besides post-combustion CO_2 capture. Cooling tower is a key component for energy and water nexus in a power plant system, which rejects waste heat to the atmosphere through the cooling of a water stream to a lower temperature. The focus of this section is to evaluate the water usage of different cooling systems.

4.2.1 Water Usage Using Wet Cooling System

The power plants discussed in Section Chapter 3 were assumed to utilize a mechanical draft, evaporative cooling tower for waste heat rejection. A 0-D model for performance calculations of the cooling tower was developed following the same methodology adopted by DoE/NETL [23], with assumptions summarized below:

1. The design ambient wet bulb temperature is 11°C (51.5°F).
2. The cooling water is cooled from 26.7°C (80°F) to 15.6°C (60°F).
3. Evaporative losses and Drift losses are 1.6% and 0.001%, respectively, of the circulating water flow rate per cooling water range of 11.1°C (20°F).
4. Blowdown Losses = Evaporative Losses / (Cycles of Concentration - 1), Cycles of Concentration equals to 4 in this study.

5. Process blowdown streams and flue gas condensate are treated and recycled to the cooling tower.

Given the total heat duty required for the cooling tower, the circulating water flow rate can be calculated by Equation 4-6. Therefore, the total cooling water makeup flow rate can be determined by Equation 4-7 using assumptions 3 and 4 shown above.

$$\dot{m}_{CR} = \frac{\dot{Q}_{CT}}{c_w \Delta T_{CT}} \qquad \text{Equation 4-6}$$

where

$\dot{m}_{CR}$ is cooling water circulation rate, kg/s

$\dot{Q}_{CT}$ is cooling tower heat rate, kJ/s

c_w is specific heat of water, kJ/kg/K

ΔT_{CT} is temperature change of cooling water in the cooling tower, K

$$\dot{m}_{MK} = \dot{m}_{CR}\left(1.6\% + 0.001\% + \frac{1.6\%}{(CoC - 1)}\right) \qquad \text{Equation 4-7}$$

where

$\dot{m}_{MK}$ is rate of cooling tower makeup water, kg/s

CoC is Cycles of Concentration, which is assigned to be 4.

To fully understand the actual quantity of water usage for each category, raw water usage on Liter/s basis is summarized in Table 4-13 for the three plants discussed in

Section Chapter 3. Liter/s basis units are used here to compare water usage of PC power plants using wet cooling system with that using combined wet/dry cooling system. The raw water makeup is supplied to the deminerlaizers (for BFW preparation including blowdown from this unit), FGD unit, and cooling towers where majority of the raw water is consumed. Cooling tower makeup water for all the three cases were calculated using the 0-D wet cooling tower model, with results presented by Table 4-14. The quantity of cooling tower makeup water is proportional to cooling capacity as indicated by Equation 4-6 and Equation 4-7, and the cooling capacity is required for both steam cycle and CO_2 capture. Amine based CO_2 captured PC power plant requires significantly less cooling capacity for steam cycle because 45% of the LP steam is extracted for amine regeneration, while solid sorbent based CO_2 captured plant consumes the same cooling capacity as the non CO_2 capture scenario due to no modification to steam cycle. Due to the natural of CO_2 removal mechanism, amine based CO_2 capture requires much more cooling capacity than solid sorbent based CO_2 capture technology. The cooling tower makeup water required for CO_2 capture cooling is 250.5 Liter/s for amine case and 91.7 Liter/s for solid sorbent case, respectively. The total wet cooling tower capacity need to be increased by 33% for amine case and by 28% for solid sorbent case, respectively.

Table 4-13 Raw water usage (Liter/s Basis) of PC power plants using wet cooling system

Case No.	1		2		3	
CO_2 Capture Technology	No CO_2 Capture		Amine		Solid Sorbent	
CO_2 Capture Level	0%		90%		90%	
Water Use	Raw Water Usage		Raw Water Usage		Raw Water Usage	
	Liter/s	%	Liter/s	%	Liter/s	%
BFW Makeup	4.7	1.2	4.7	1.0	4.5	1.0
FGD Makeup	53.5	13.9	53.5	10.9	53.5	11.9
Demin Blowdown	1.1	0.3	1.1	0.2	1.1	0.2
Wet Cooling Tower Makeup						
Steam Cycle Cooling	329.5	85.8	187.0	38.0	331.4	73.9
CO_2 Capture Cooling	0.0	0.0	250.5	50.9	91.7	20.5
BFW Blowdown & Flue Gas Condensate	-4.7	-1.2	-4.7	-1.0	-33.8	-7.5
Total	384.1	100.0	492.1	100.0	448.5	100.0

Table 4-14 Wet cooling system water usage

Case No.	1		2		3	
CO2 Capture Technology	No CO_2 Capture		Amine		Solid Sorbent	
Wet Cooling Tower Makeup	Liter/s	Liter/MWh	Liter/s	Liter/MWh	Liter/s	Liter/MWh
Steam Cycle Cooling	329.5	2.157.0	187.0	1,721.1	331.4	2,767.0
CO_2 Capture Cooling	0.0	0.0	250.5	2,305.4	91.7	765.7
Total	329.5	2,157.0	437.5	4,026.5	423.1	3,532.7

4.2.2 Water Usage Using Combined Wet/Dry Cooling System

Increased concern over water usage motivates the investigation of dry cooling or combined wet/dry cooling systems in existing subcritical PC power plants. Special attention need to be paid to PC power plants retrofitted with CO_2 capture technology since it increases raw water usage significantly, especially on MW basis, while the plant site might not have enough water resource to compensate for the increased water

usage or even stricter regulations might be imposed on retrofitted plants. A particular combined wet/dry cooling system proposed and evaluated consists of:

1. All of the steam exhaust exiting LP steam turbine is condensed by an air-cooled condenser while the existing surface condenser remains for standby or high (summer) ambient temperature operation; again with the assumption that plot space is available in the immediate vicinity of the steam turbine for installing the air-cooled condenser.
2. Other cooling loads, such as heat rejection from the CO_2 capture system, are carried out by cooling water, which would then be cooled in wet cooling towers.

Water usage for wet cooling towers is estimated by the 0-D calculation method discussed in Section 4.2.1, while no water is used for the air-cooled condenser. This specific cooling strategy is chosen because performance of an air-cooled condenser heavily depends on ambient conditions, and at high ambient temperatures, a portion of the steam turbine exhaust may be condensed by the water-cooled surface condenser to increase plant power output. The combined wet/dry cooling system discussed further in this dissertation refers to the case where all of the steam turbine exhaust is cooled by the air-cooled condenser.

Table 4-15 presents the raw water usage on Liter/s basis of the PC power plants using the combined wet/dry cooling system. By comparing data presented in Table 4-13, the total water usage reduces by 80% for the non CO_2 capture case, by 32% for the

amine CO_2 captured case and by 68% for the solid sorbent CO_2 captured case respectively.

Table 4-15 Raw water usage (Liter/s Basis) of PC power plants using combined cooling system

Case No.	Baseline		1		2	
CO_2 Capture Technology	No CO_2 Capture		Amine		Solid Sorbent	
CO_2 Capture Level	0%		90%		90%	
Water Use	Raw Water Usage		Raw Water Usage		Raw Water Usage	
	Liter/s	%	Liter/s	%	Liter/s	%
BFW Makeup	4.7	6.1	4.7	1.4	4.5	3.1
FGD Makeup	53.5	68.6	53.5	16.0	53.5	37.0
Demin Blowdown	1.1	1.4	1.1	0.3	1.1	0.7
Wet Cooling Tower Makeup						
Steam Cycle Cooling	23.4	30.0	29.6	8.8	27.6	19.1
CO_2 Capture Cooling	0.0	0.0	250.5	74.8	91.7	63.4
BFW Blowdown & Flue Gas Condensate	-4.7	-6.1	-4.7	-1.4	-33.8	-23.4
Total	78.0	100.0	334.7	100.0	144.6	100.0

Table 4-16 shows that the air-cooled condenser saves 306.1 Liter/s (2,003.8 Liter/MWh), 157.4 Liter/s (1,448.7 Liter/MWh) and 303.9 Liter/s (2,537.4 Liter/MWh) water for Case 1, Case 2 and Case 3, respectively.

Table 4-16 Combined cooling system water usage

Case No.	1		2		3	
CO_2 Capture Technology	No CO_2 Capture		Amine		Solid Sorbent	
	Liter/s	Liter/MWh	Liter/s	Liter/MWh	Liter/s	Liter/MWh
Total Wet Cooling Tower Makeup	23.4	153.2	280.1	2,578.0	119.3	996.1
Steam Cycle Cooling	23.4	153.2	29.6	272.4	27.6	230.4
CO_2 Capture Cooling	0.0	0.0	250.5	2,305.5	91.7	765.7
Water Saved by Air-Cooled Condenser	306.1	2,003.8	157.4	1,448.7	303.9	2,537.4

4.2.3 Water Usage Using Dry Cooling System

Water usage of a PC power plant can be further reduced by using dry cooling system by employing air-cooled exchangers for heat rejection from the entire plant, i.e., for heating load of the CO_2 capture system in addition to condensing the steam turbine exhaust. The annual average overall plant performance is highly compromised, however, using such a purely dry cooling system since this mode of heat rejection is highly dependent on ambient conditions. Furthermore, a significant additional capital cost is required. Consequently, no further consideration is given to such plants employing purely dry cooling systems in this investigation.

4.3 Models of a Combined Wet/Dry Cooling System

Since the water usage of a PC power plant can be reduced significantly by the use of a combined wet/dry cooling system as seen by the results presented in Section 4.2.2, a more detailed analysis is conducted which includes sensitivity to ambient temperature, specifically for the subcritical PC power plant with the solid sorbent based CO_2 capture as described in Section Chapter 3. The simplified model for calculating the cooling tower performance as described in Section 4.2 is essentially an empirical calculation for a given set of design conditions. Due to possible variations in operating and ambient conditions, this calculation model is not capable of predicting variations in cooling tower performance including water makeup usage. Besides investigating the synergy between wet and dry cooling systems, prediction of the performance of a combined wet/dry cooling system requires detailed models for both wet cooling tower and air-cooled condenser. This section describes a physical model developed for a wet cooling tower and a performance model developed for an air-cooled condenser, followed by a case study of the combined cooling system specifically designed for the subcritical PC power plant with the solid sorbent based CO_2 capture.

4.3.1 Heat and Mass Transfer Model for Wet Cooling Tower

4.3.1.1 Governing Equations

The numerical method used in this study is similar to Poppe's theory [122], and the exit air of the cooling tower is assumed to be unsaturated for plume abatement [134]. The heat and mass transfer analysis refer to Braun's work [135], [136]. Heat and mass

balances are performed on a finite difference segment of an evaporative wet cooling tower as shown by Figure 4-10, where air and water flow in a countercurrent configuration.

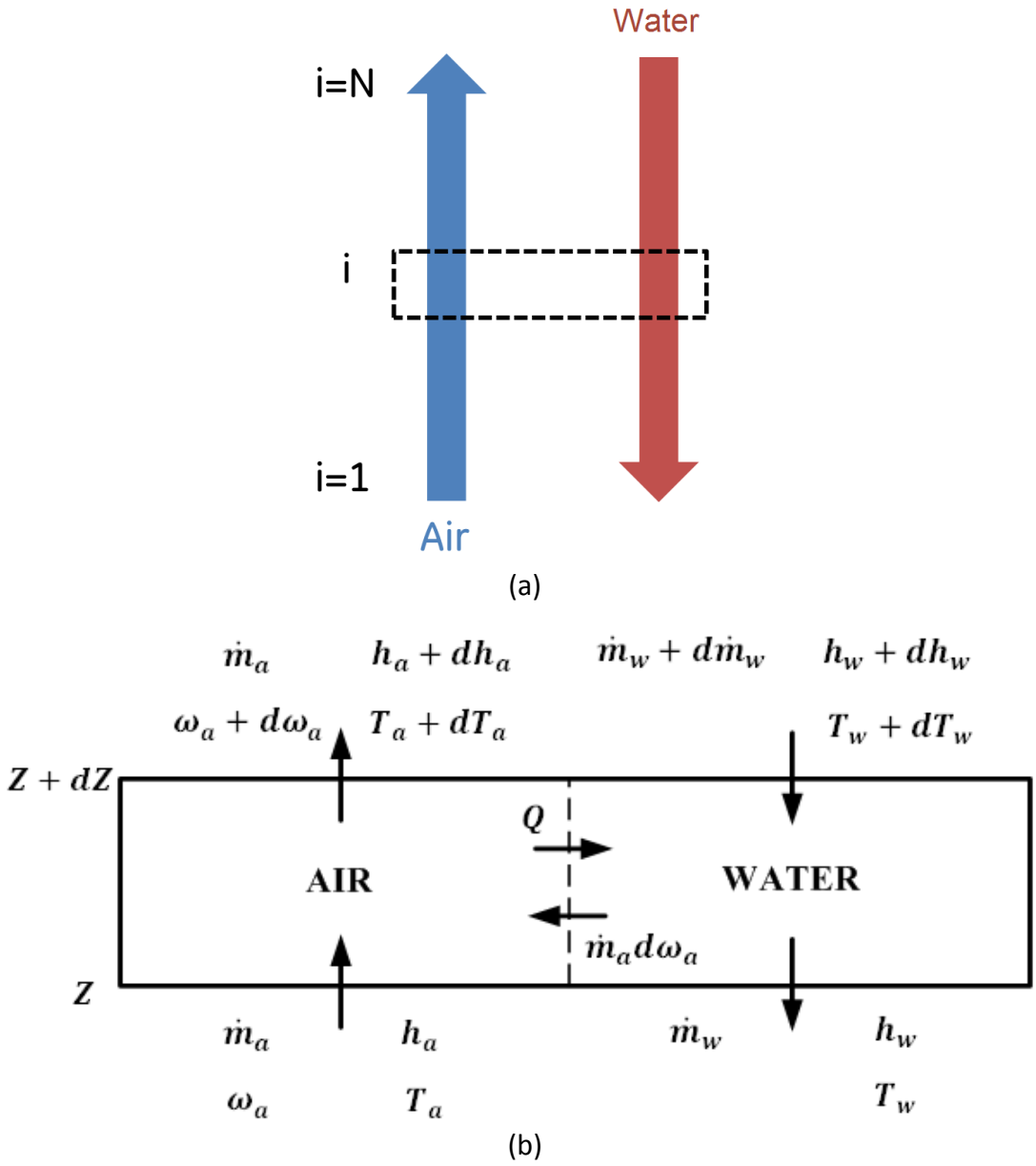

Figure 4-10 Schematic of a Finite Difference Segment for a Wet Cooling Tower

Equation 4-8 depicts the mass balance between air and water. The driving force for moisture vapor transfer from water side to air side is the vapor pressure difference between bulk air and the surface of water. Water and vapor on water surface are assumed to be in equilibrium [135], vapor pressure on water surface is a function of water temperature only and corresponds to humidity ratio (ω). This mass transfer process is expressed by Equation 4-9.

$$\frac{d\dot{m}_w}{dZ} = \dot{m}_a \frac{d\omega_a}{dZ} \qquad \text{Equation 4-8}$$

$$\frac{d\omega_a}{dZ} = \frac{h_m}{S}\left(\omega_{T_w,equ} - \omega_a\right) \qquad \text{Equation 4-9}$$

$$S = \frac{\dot{m}_a Z_{max}}{V_T A_V} \qquad \text{Equation 4-10}$$

where

Z is flow direction, m

$\dot{m}_w$ is water mass flow rate, kg/s

$\dot{m}_a$ is air mass flow rate, kg/s

ω_a is humidity ratio of bulk air

$\omega_{T_w,equ}$ is humidity ratio on water surface at water temperature of T_w

h_m is mass transfer coefficient for vapor between water side and air side, kg/s/m^2

$S = \frac{\dot{m}_a Z_{max}}{V_T A_V}$ is parameter borrowed from the heat and mass transfer model for liquid desiccant developed by Stevens [136] to simplify the equations. Z_{max} is the total height of the packing fill, V_T total volume of the packing fill, and A_V is the average surface area per unit volume of the packing fill.

Equation 4-11 and Equation 4-12 are derived from the energy balance between air and water streams. The two equations include the heat exchanged through heat convection and the vapor transfer between the water surface and air. The heat loss is assumed to be negligible in the model.

$$\frac{dh_a}{dZ} = \frac{h_V \frac{d\omega_a}{dZ} - h_a \frac{d\omega_a}{dZ} - \frac{q}{s}}{1 + \omega_a} \quad \text{Equation 4-11}$$

$$\frac{dh_w}{dZ} = \frac{\dot{m}_a}{\dot{m}_w}\left(h_V \frac{d\omega_a}{dZ} - h_w \frac{d\omega_a}{dZ} - \frac{q}{s}\right) \quad \text{Equation 4-12}$$

$$q = h(T_a - T_w) \quad \text{Equation 4-13}$$

$$h = h_m c_p Le_f \quad \text{Equation 4-14}$$

where

h_a is enthalpy of bulk air, J/kg

h_w is enthalpy of water, J/kg

h_V is enthalpy of water vapor, J/kg

q is the heat flux per unit transfer area, W/m^2

h is heat transfer coefficient, W/m^2/K

c_p is heat capacity of air, J/kg/K

Le_f is Lewis factor.

Heat transfer coefficient, h, is related to mass transfer coefficient h_m by Equation 4-14 while the Lewis factor relation (Equation 4-15) for air-water vapor systems proposed by Bosnjakovic [116], [137] is assumed in this study. The humid air at tower exit is assumed unsaturated.

$$Le_f = 0.865^{2/3}\left(\frac{\omega_{T_{w,equ}} + 0.622}{\omega_a + 0.622} - 1\right)/ln\left(\frac{\omega_{T_{w,equ}} + 0.622}{\omega_a + 0.622}\right) \qquad \text{Equation 4-15}$$

4.3.1.2 Finite Difference Model

The mass transfer coefficient, h_m, is required to obtain the heat and mass transfer performance of a cooling tower. Given h_m, the model can be solved using Equation 4-8 through Equation 4-15. In a finite difference model, the fill of a cooling tower is divided into multiple segments, as shown in Figure 4-10a, and the governing equations for each segment is solved following the simulation flow chart shown in Figure 4-11.

1. Given air inlet conditions (temperature, humidity ratio, and mass flow rate) and water inlet conditions (temperature and mass flow rate).
2. Guess an outlet temperature and mass flow rate for water stream.
3. Repeat the following calculation for each finite difference segment starting from Segment i=1 as shown in Figure 4-10a:

a. Calculate changes in water mass flow rate ($\frac{d\dot{m}_w}{dZ}$) and air humidity ratio ($\frac{d\omega_a}{dZ}$)

b. Calculate enthalpy changes in water ($\frac{dh_w}{dZ}$) and air ($\frac{dh_a}{dZ}$)

c. Calculate water mass flow ($\dot{m}_w$) and humidity ratio (ω_a) for the following segment

d. Calculate enthalpies of water (h_w) and air (h_a) for the following segment

4. Iterate until the calculated inlet conditions of water match the given water inlet conditions.

In Step 2, the new values of water temperature and mass flow rate are determined by the following two equations with a relaxation factor R.

$$T_{w,i=1}^{j+1} = T_{w,i=1}^{j} + R\left(T_{w,in} - T_{w,i=N}^{j}\right) \quad \text{Equation 4-16}$$

$$\dot{m}_{w,i=1}^{j+1} = \dot{m}_{w,i=1}^{j} + R\left(\dot{m}_{w,in} - \dot{m}_{w,i=N}^{j}\right) \quad \text{Equation 4-17}$$

The model is built by Engineering Equation Solver (EES) with comprehensive built-in thermal properties available.

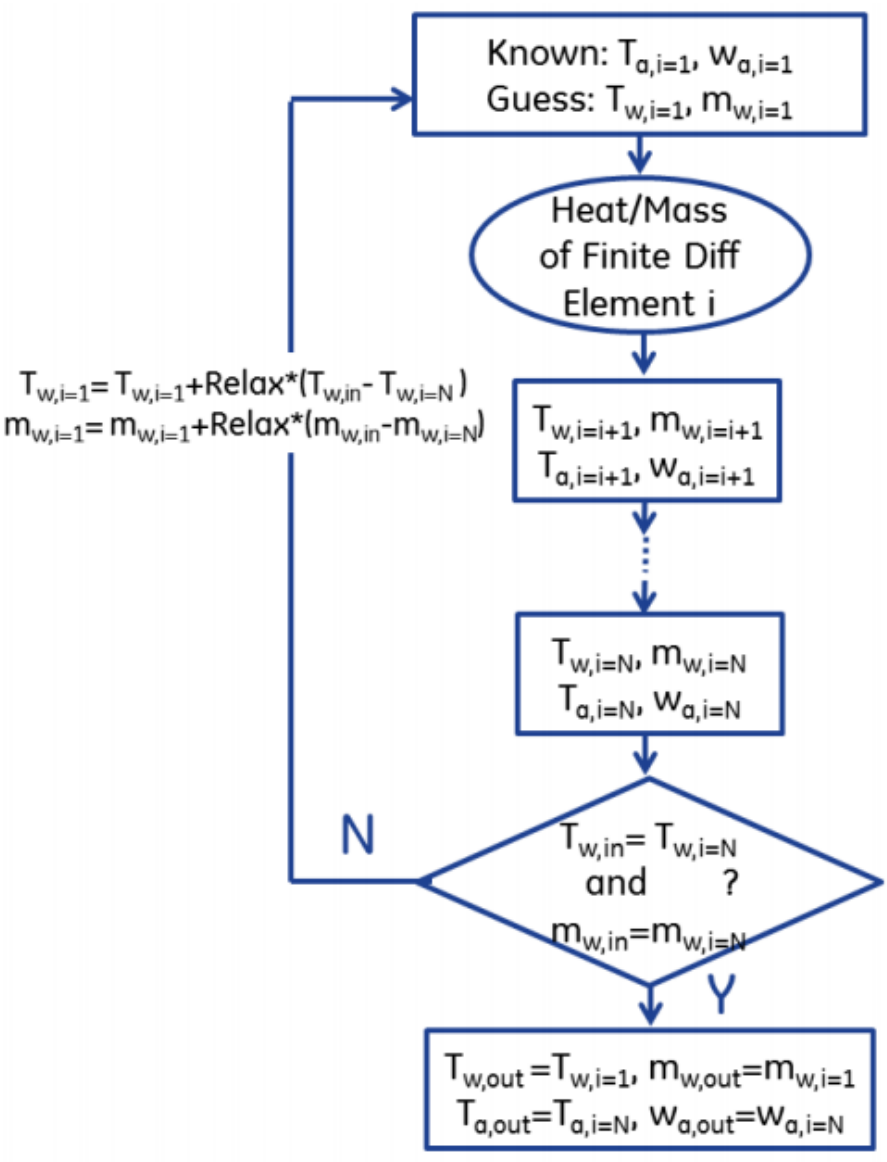

Figure 4-11 Simulation Flow Chart for a Finite Difference Cooling Tower Model

4.3.1.3 Model Validation

The experimental data provided by Simpson and Sherwood [138] for a small-sized tower has been widely used in a number of studies to validate cooling

tower models [139]–[141]. This data were also used to validate the model developed in this study.

Since a mass transfer coefficient, h_m, is required as an input to the model, h_m is determined from experimental data using the e-NTU method [116], [121]. Steps for calculating h_m for validating the models can be described as: (1) calculate effectiveness (e) of the cooling tower from experimental data using the definition Equation 4-19; (2) calculate the number of transfer units (NTU) using Equation 4-21; and (3) calculate h_m from Equation 4-22. The calculation process is similar to that conducted by Kroger [116], [117] while summarized here:

A fluid capacity rate ratio is first defined as

$$C = C_{min}/C_{max} \qquad \text{Equation 4-18}$$

Where $C_{min}$is the smaller value of $\dot{m}_w c_{p,w}$ and $\dot{m}_a \frac{dh_{a,equ,T_w}}{dT_w}$, and C_{max} is the greater value. h_{a,equ,T_w} is enthalpy of moist air on water surface in equilibrium with water at temperature T_w.

The effectiveness is expressed by:

$$e = \frac{Q}{Q_{max}} = \frac{\dot{m}_w c_{pw}\left(T_{w,in} - T_{w,out}\right)}{C_{min}\left(h_{a,equ,T_{w,out}} - f - h_{a,in}\right)} \qquad \text{Equation 4-19}$$

where f is a correction factor, according to Berman [142] given by:

$$f = \left(h_{a,equ,T_{w,out}} + h_{a,equ,T_{w,in}} - 2h_{a,equ,(T_{w,in}+T_{w,out})/2}\right)/4 \qquad \text{Equation 4-20}$$

The NTU for counter-flow cooling tower can be calculated from effectiveness and fluid capacity rate ratio, given by [116]:

$$NTU = \frac{1}{1-C} ln \frac{1-eC}{1-e} \qquad \text{Equation 4-21}$$

The NTU is also a function of h_m, and defined as [135]:

$$NTU = \frac{h_m A_V V_T}{\dot{m}_w} \qquad \text{Equation 4-22}$$

As we can see from Figure 4-12, model simulation can well predict the experimental data [138] on air outlet temperature and water outlet temperature.

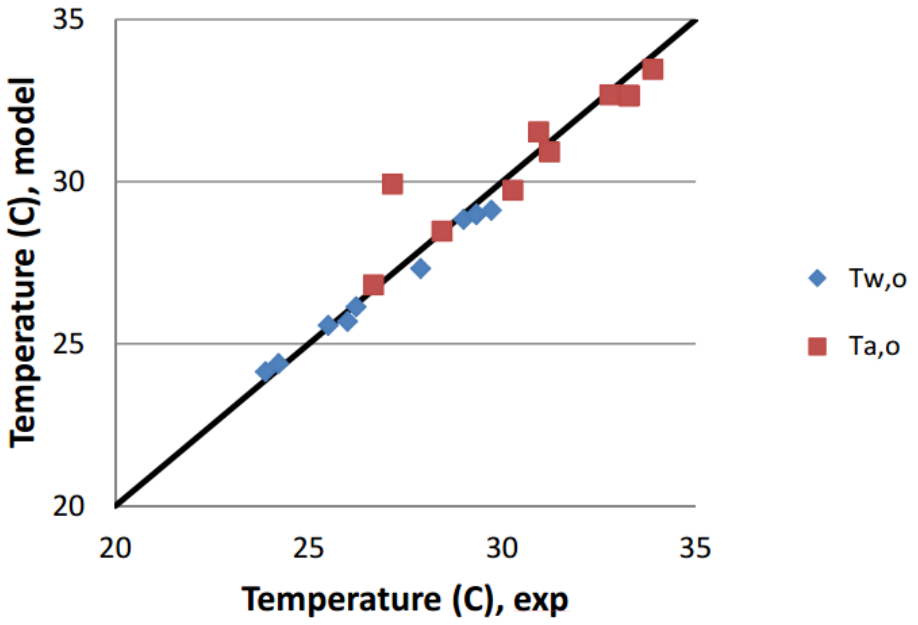

Figure 4-12 Comparison between experimental data and model predictions on air outlet temperature and water outlet temperature

4.3.2 Heat Transfer Model of Air-Cooled Condenser

4.3.2.1 Governing Equations

Heat exchange between steam side and air side can be described as:

$$\dot{Q}_{H_2O} = \dot{m}_{H_2O}(h_{steam} - h_{cond}) \quad \text{Equation 4-23}$$

$$\dot{Q}_{air} = \dot{m}_{air}\left(h_{air,in} - h_{air,out}\right) \quad \text{Equation 4-24}$$

where

$\dot{Q}_{H_2O}$ is the condensation heat duty of exhaust steam, J/s

$\dot{Q}_{air}$ is the air heat adsorption duty, J/s

$\dot{m}_{H_2O}$ is the mass flow rate of exhaust steam, kg/s

$\dot{m}_{air}$ is the mass flow rate of air, kg/s

h_{steam} is the enthalpy of exhaust steam, J/kg

h_{cond} is the enthalpy of condensed water, J/kg

$h_{air,in}$ is the enthalpy of air entering the condenser, J/kg

$h_{air,out}$ is the enthalpy of air exiting the condenser, J/kg.

Due to energy balance between two sides while neglecting heat loss,

$$\dot{Q}_{H_2O} = \dot{Q}_{air} \quad \text{Equation 4-25}$$

4.3.2.2 Heat Transfer Model Using $\eta - NTU$ Method

A relation between η and NTU is given by [130]:

$$\eta = 1 - exp(-NTU) \quad \text{Equation 4-26}$$

where η and NTU are defined as [128]:

$$\eta = \frac{T_{air,out} - T_{air,in}}{T_{cond} - T_{air,in}} \quad \text{Equation 4-27}$$

$$NTU = \frac{KF}{A_F v_F \rho_{air} C_{p,air}} \quad \text{Equation 4-28}$$

where

$T_{air,in}$ and $T_{air,out}$ are air inlet and outlet temperature, K

T_{cond} is the steam condensing temperature, K

F is the heat exchange area of the air-cooled condenser, m^2

A_F is the windward area of air-cooling condenser, m^2

v_F is the face velocity of finned tube, m/s

ρ_{air} is the average density of the cooling air, kg/m^3

$C_{p,air}$ is the specific heat capacity of cooling air, J/kg/K

K is the heat transfer coefficient, $W/m^2/K$.

In engineering applications, the K is assumed to be a function of face velocity and ambient temperature. A relation for the ratio of the heat transfer coefficients for an air-cooled condenser under two different conditions was recommended by Liu [128]:

$$\frac{K_1}{K_2} = \left(\frac{v_{F1}}{v_{F2}}\frac{v_2}{v_1}\right)^{0.6} \qquad \text{Equation 4-29}$$

where

v is kinematic viscosity and

Subscripts 1 and 2 denote conditions 1 and 2.

Equation 4-26 and Equation 4-27 may be combined to obtain:

$$NTU = ln\left(\frac{T_{cond} - T_{air,in}}{T_{cond} - T_{air,out}}\right) \qquad \text{Equation 4-30}$$

Combining Equation 4-28 and Equation 4-29, a relation for NTU of an air-cooled condenser between two conditions is obtained:

$$\frac{NTU_1}{NTU_2} = \left(\frac{\dot{m}_{air,2}}{\dot{m}_{air,1}}\right)^{0.4}\left(\frac{v_2}{v_1}\frac{\rho_{air,2}}{\rho_{air,1}}\right)^{0.6}\frac{C_{p,air,2}}{C_{p,air,1}} \qquad \text{Equation 4-31}$$

4.3.2.3 Calculation Procedure

For given steam turbine exhaust conditions (temperature, pressure and mass flow rate) with standard ambient conditions (103.35 KPa and 15C), assume an air-cooled condenser is operated at a design condition consisting of air exiting the condenser at a temperature that is 11C lower than the exhaust steam condensing temperature. At off-

design conditions (when ambient dry bulb temperature varies in the range of 10 to 20C), by employing Equation 4-30 through Equation 4-31, air exiting temperature and air flow rate can be calculated, assuming the air-cooled condenser fans are adequately sized.

4.3.3 Models of Other Components in a Combined Cooling System

In a combined cooling system besides wet cooling tower and air-cooled condenser, it comprises fans and circulating water pumps for wet (forced draft) cooling towers and fans for air-cooled condenser.

4.3.3.1 Pumps for Wet Cooling Tower

Power required for water pump is given by:

$$P_{pump} = \frac{Q\rho_w gh}{\eta_{pump}\eta_{mech}} \qquad \text{Equation 4-32}$$

where

P_{pump} is power, W

η_{pump} is pump efficiency

η_{mech} is mechanical efficiency

Q is cooling water flow capacity, m^3/s

ρ_w is density of fluid, kg/m^3

g is gravity, 9.81 m/s^2

h is differential head, m.

4.3.3.2 Fans for Wet Cooling Towers and Air-Cooled Condenser

Power required for draft fans is given by:

$$P_{fan} = \eta dpQ \qquad \text{Equation 4-33}$$

P_{fan} is power of a fan, W

η is fan efficiency

dp is pressure head, Pa

Q is air volume delivered by a fan, m^3/s.

According to the theory of similarity, the power consumptions of two fans of the same type can be expressed by the following relation:

$$\frac{P_{fan,1}}{P_{fan,2}} = \frac{\rho_{a,1}}{\rho_{a,2}}\left(\frac{Q_1}{Q_2}\right)^3 \qquad \text{Equation 4-34}$$

where

ρ_a is air density, kg/m^3

Subscripts 1 and 2 represent Fan 1 and Fan 2 of the same type, and in this case, it is the same fan at two different operating conditions.

4.3.4 A Case Study of a Combined Wet/Dry Cooling System for Subcritical PC Power Plant with Solid Sorbent CO_2 Capture

Case study of the combined wet/dry cooling system conducted for a PC power plant with solid sorbent based CO_2 capture technology to evaluate water usage and power consumption under different ambient air conditions is presented in this section. The cooling strategy as described in Section 4.2.2 consists of condensing the LP steam turbine exhaust in an air-cooled condenser, while other cooling loads such as those in the CO_2 capture system are carried out by cooling water provided by wet cooling towers.

4.3.4.1 Design Conditions and Model Calibration

A combined wet/dry cooling system is assumed to meet all reasonable design requirements discussed in this section. The cooling system is designed for ISO ambient conditions (15C dry bulb temperature, 11C wet bulb temperature or 60% relative humidity ratio, and 101.3 kPa barometric pressure).

Wet cooling tower. Since a plant retrofit scenario is considered, and since the steam water cooled condenser is replaced by an air cooled condenser, the design strategy consists of operating the required number of cooling tower cells to maintain the flow rate, and the supply and return temperatures of the cooling water for the remaining users in the plant. The design point temperature of hot water entering the cooling towers is 26.7C, which is cooled down to 15.6C, and air mass flow rate is assumed to be the same as water mass flow rate. A NTU correlation is then calibrated to achieve the design performance.

A cooling tower efficiency or Merkel number (Me) for a cooling tower as recommended by ASHRAE [143] is used to obtain a generalized relation shown by Equation 4-35.

$$Me = c\left(\frac{\dot{m}_w}{\dot{m}_a}\right)^{-0.6} \quad \text{Equation 4-35}$$

where c is an empirical constant.

A relation between NTU and M_e for a countercurrent cooling tower as recommended by Poppe's method [122] is next utilized. If $\dot{m}_w c_{p,w}$ is greater than $\dot{m}_a \frac{dh_{a,equ,T_w}}{dT_w}$,

$$NTU = Me\left(\frac{\dot{m}_w}{\dot{m}_a}\right) = c\left(\frac{\dot{m}_w}{\dot{m}_a}\right)^{0.4} \quad \text{Equation 4-36}$$

If $\dot{m}_w c_{p,w}$ is less than $\dot{m}_a \frac{dh_{a,equ,T_w}}{dT_w}$,

$$NTU = \frac{Me}{c_{p,w}} \frac{dh_{a,equ,T_w}}{dT_w} \quad \text{Equation 4-37}$$

By combining Equation 4-35 with Equation 4-36, and Equation 4-35 with Equation 4-37 we obtain:

$$NTU = c\left(\frac{\dot{m}_w}{\dot{m}_a}\right)^{0.4} \quad \text{Equation 4-38}$$

$$NTU = \frac{c\left(\frac{\dot{m}_w}{\dot{m}_a}\right)^{-0.6}}{c_{p,w}} \frac{dh_{a,equ,T_w}}{dT_w} \qquad \text{Equation 4-39}$$

By applying the finite difference model described in Section 4.3.1 together with Equation 4-38 or Equation 4-39 to meet the design conditions of the wet cooling tower, the constant c is obtained to be 11.5.

Air-cooled condenser. The design conditions of entering steam are consistent with conditions of LP steam exhaust steam in Section Chapter 3: pressure is 6.89 kPa, temperature is 38.7C, and mass flow rate is 300.6 kg/s; LP steam turbine inlet conditions are 506.76 kPa and 295.9C with turbine isentropic efficiency of 0.9 and generator efficiency (inclusive of mechanical losses) of 0.95. The air-cooled condenser outlet air temperature is assumed to be 27.7C to maintain an 11C pinch temperature (minimum heat exchange temperature difference). According to Equation 4-30, the NTU at design condition equals to 0.7678.

The cooling water circulation pump parameters are assumed to be consistent with DoE/NETL report [23] with pump pressure at 30 meter of water column, and net efficiency at 0.49.

The fans in wet cooling tower are assumed to be similar to the ones reported by DoE/NETL [23], with reference air mass flow rate at 5590 kg/s and fan power at 1734 kW.

The fans used in air-cooled condenser are assumed to be consistent with the ones referenced in literature [130]: each fan provides an air flow rate of 594 m^3/s and its motor power is 132 kW.

4.3.4.2 Performance of Wet Cooling System

Two major operating parameters of the wet cooling tower are its power consumption, which consists of auxiliary power of fans and pumps, and makeup water consumption.

Total water makeup comprises evaporative losses, drift losses and blowdown losses. Due to the finite difference model, evaporative losses equal to $\dot{m}_{w,in} - \dot{m}_{w,out}$, and two assumptions made in Section 4.2.1 were also made here in estimating drift losses (0.001% of the circulating water flow rate) and blowdown losses (1/3 of the evaporative losses). For wet cooling tower of the combined cooling system described in Section 4.2.2 for subcritical PC power plant with solid sorbent based CO_2 capture, the circulating water flow rate of the wet cooling tower is 5,590 kg/s, water make-up at design conditions is 119.3 kg/s using the 0-D calculation model, while the make-up water calculated by the 1-D model is 108.4 kg/s. The difference between the model predictions of make-up water is 9%.

Assuming the number of the wet cooling tower cells is constant, wet cooling tower that works under different ambient conditions exhibits significant different performance. As shown by Figure 4-13, increased ambient temperature (with the same relative humidity at 60%) reduces the driving force temperature for heat transfer between air

and cooling water, air mass flow rate has to increase in order to maintain an 11.1C (20F) cooling of the cooling water. Therefore, the fan power increases dramatically with the air flow rate as presented by Figure 4-14, because as indicated by Equation 4-34 fan power ratio of two operation conditions is proportional to the cube of air flow rate ratio.

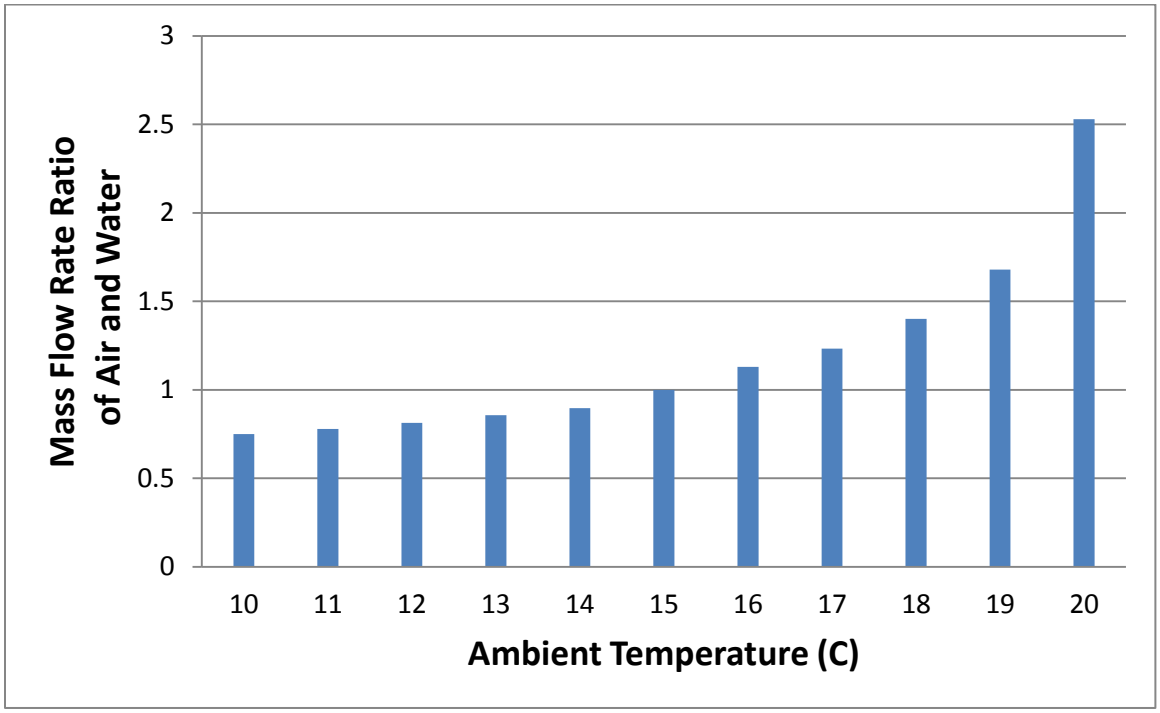

Figure 4-13 Mass flow rate ratio of air under different ambient temperatures

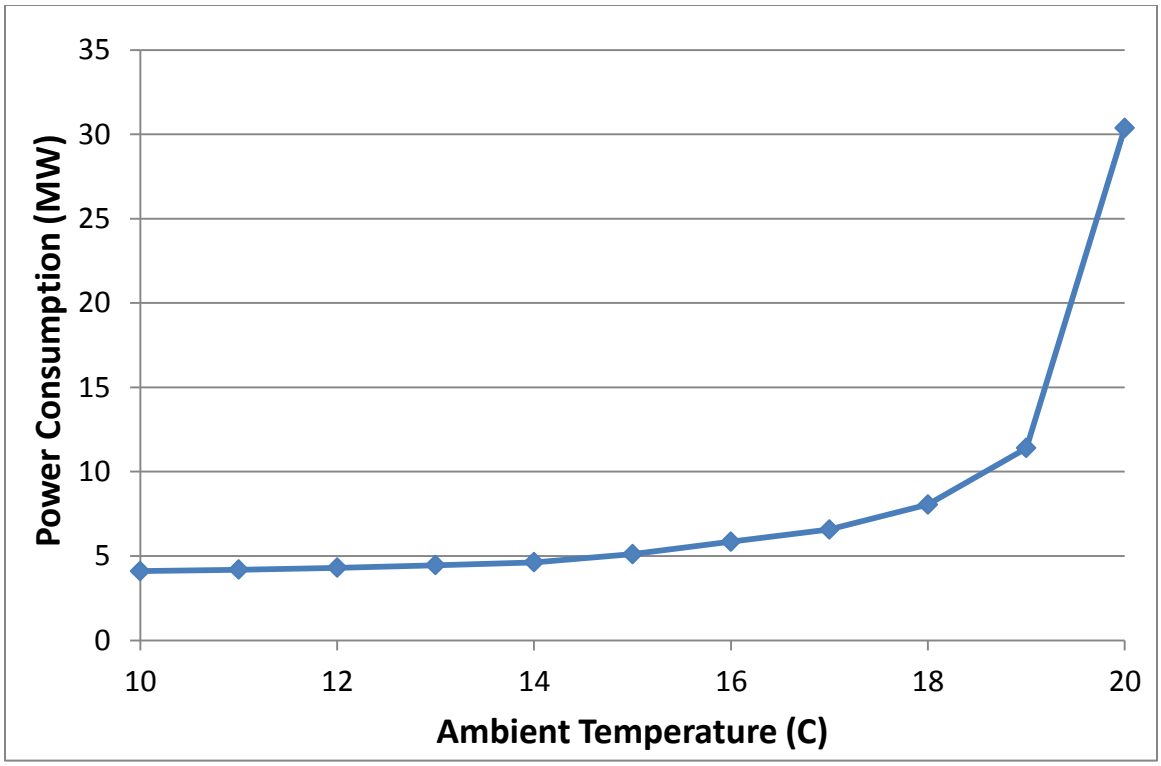

Figure 4-14 Power consumption of wet cooling towers under different ambient temperatures

Since cooling tower performance drops dramatically at high ambient temperature, in order to reduce both power consumption and water makeup a reasonable approach is to increase the temperature approach (difference between ambient wet bulb temperature and cooling water outlet temperature) by increasing the cooling water temperature. At design cooling water temperature of 26.7C, the temperature approach is 1C for ambient conditions of 20C dry bulb temperature and 60% relative humidity. If the temperature approach is increased from 1C to 5C, the power consumption decreases by 86.6%, as shown by Figure 4-15. However, this approach would affect the cooling of process streams and in this analysis was neglected. Note that process streams

cannot be cooled as much due to the increase in cooling tower temperature, and would result in some plant performance penalty.

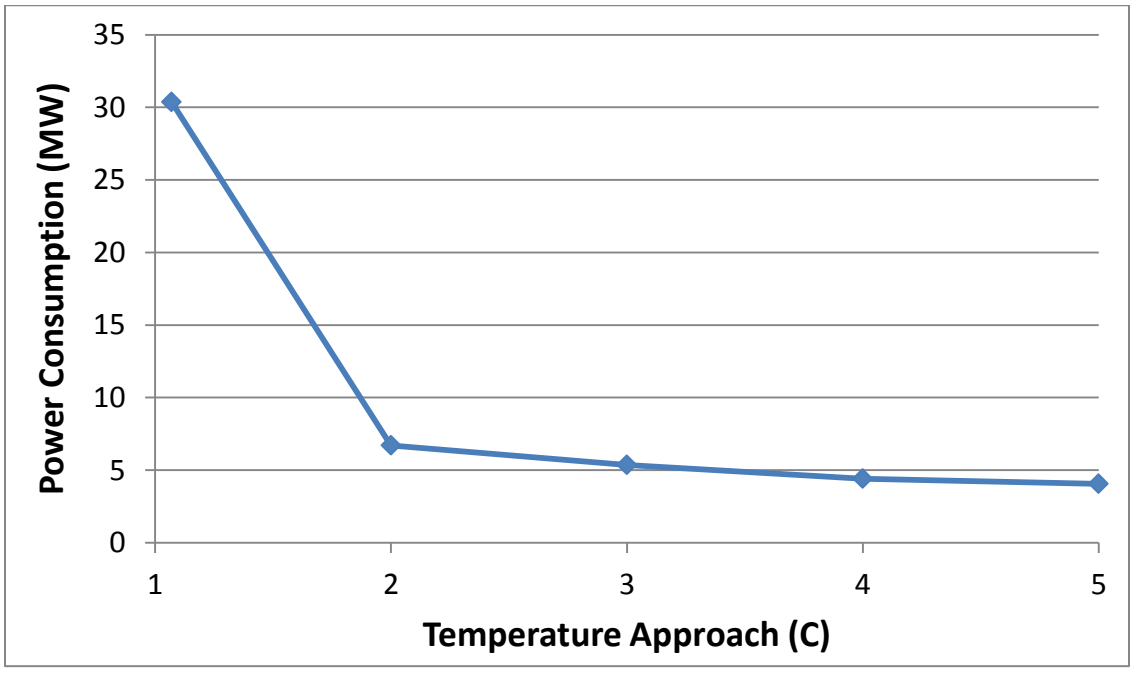

Figure 4-15 Power consumption of wet cooling towers under 20C ambient temperatures with different temperature approachs

Another variable of ambient condition is air relative humidity. Seven levels of humidity ratio, 30%, 40%, 50%, 60%, 70%, 80% and 90% were evaluated for the same ambient dry bulb temperature of 15C. The wet bulb temperatures for these seven cases are 7.2C, 8.5C, 9.7C, 10.8C, 11.9C, 13.0C and 14.0C, respectively. The changes in air flow rate and power consumption are shown by Figure 4-16 and Figure 4-17. Increased ambient air relative humidity results in a lower mass transfer driving force for moisture to transfer from water side to bulk air side, requiring larger amount of air flow and fan power for both convective heat transfer and water vaporization.

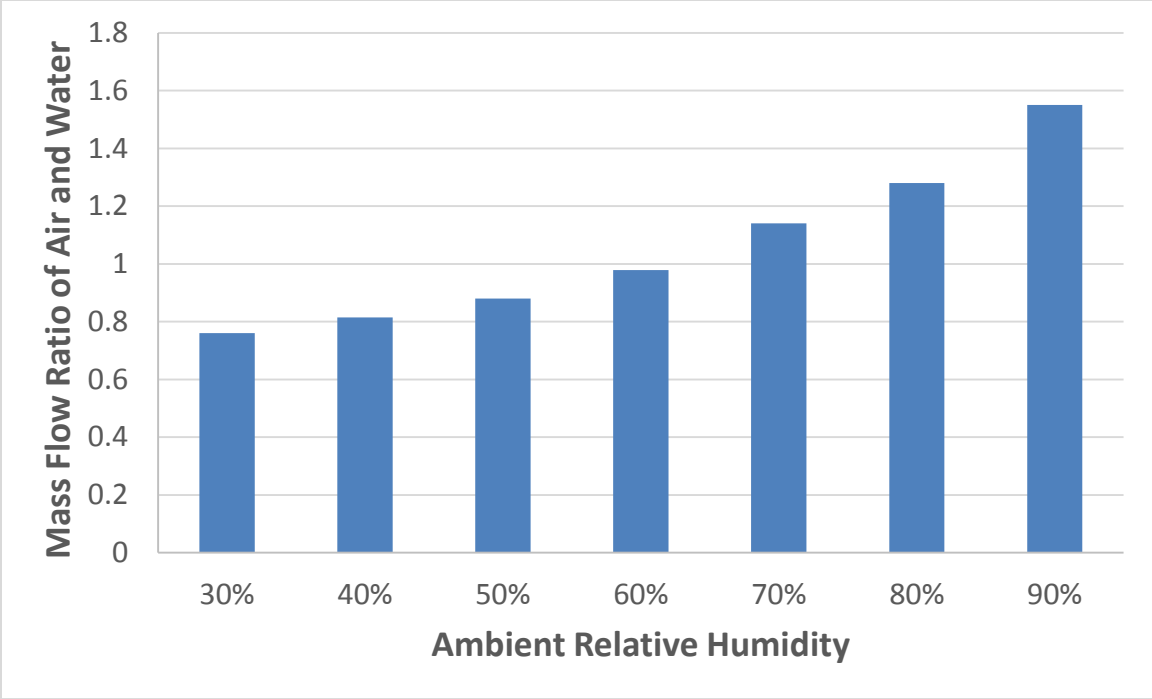

Figure 4-16 Mass flow rate ratio of air and water under different ambient air relative humidity

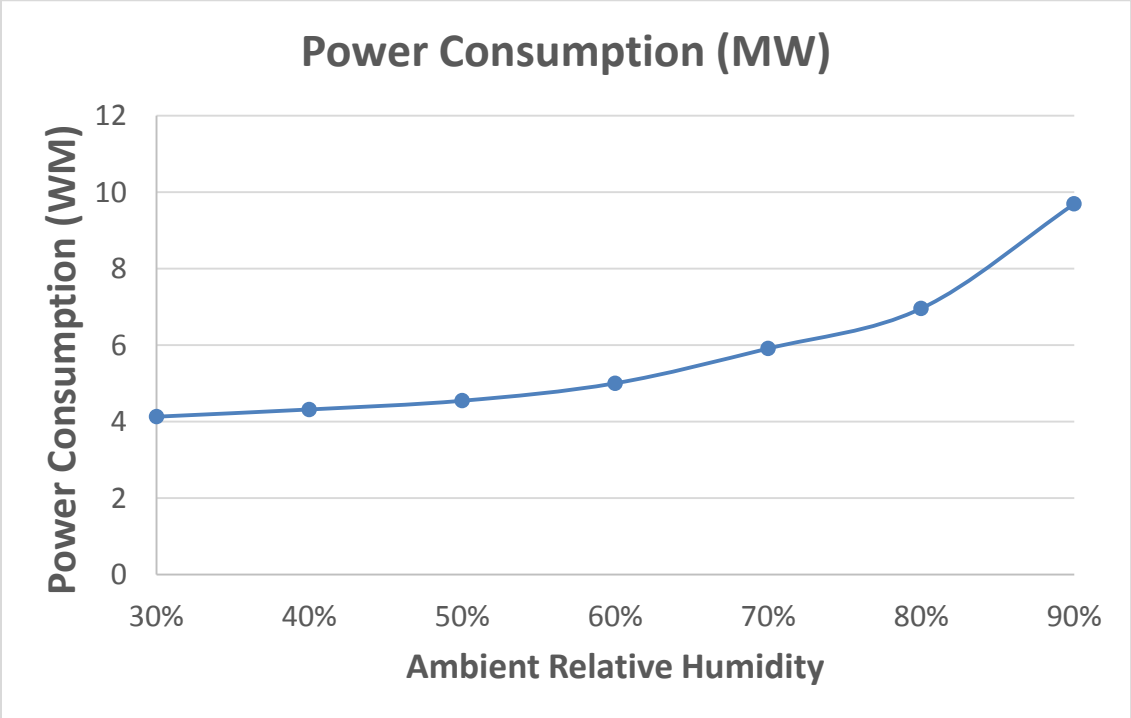

Figure 4-17 Power consumption of wet cooling towers under different ambient air relative humidity

4.3.4.3 Performance of Dry Cooling System

Steam turbine generates higher power at lower back pressure, but the power consumption of draft fans increases with back pressure. An optimal steam turbine back pressure exists for the performance of air-cooled condenser [128]–[130], at which the net power generated, i.e., difference in steam turbine power generation and fan power consumption, is maximized. An alternative optimal back pressure adopted in this study is defined by Effective Power Consumption (see), which is defined as the change in steam turbine power output over the design output at the back pressure of 6.89 kPa (same as in DoE/NETL report [23]) and the power consumed by draft fans of air-cooled condenser. Optimal back pressure is a pressure at which the Effective Power Consumption is minimized. The minimum back pressure can achieve is assumed to be 6.89 kPa.

$$Effective\ Power\ Consumption = Draft\ Fan\ Power\ Consumption + (Design\ ST\ Power\ Output - Actual\ ST\ Power\ output)$$ Equation 4-40

An example of the optimal back pressure for 20C ambient temperature is presented by Figure 4-18 and Figure 4-19. Steam flow rate is constant, and air flow rate is varied to cool down the steam turbine exhaust steam in air-cooled condenser (as pointed out previously, it is assumed that the air-cooled condenser fans are adequately sized).. Steam condensate temperature increases with increased back pressure, and temperature of the air exiting the air-cooled condenser increases correspondingly and the temperature difference between the two slightly increases from 9.5C to 13.5C. A

parabolic shape of Effective Power Consumption is observed over different back pressures, and the optimal back pressure for 20C ambient temperature is 9 kPa resulting in minimum Effective Power Consumption at 18.62 MW.

Figure 4-20 shows the optimal turbine back pressures and optimal Effective Power Consumptions under different ambient temperatures. For ambient temperatures ranged from 10C to 15C, the optimal back pressure is 6.89 kPa at the minimum pressure which is assumed that can be achieved, whereas, at ambient temperature higher beyond 15C, the optimal pressure increases linearly. To summarize, the optimal Effective Power Consumption increases from 4.21 MW to 18.62 MW as ambient temperature increases from 10C to 20C.

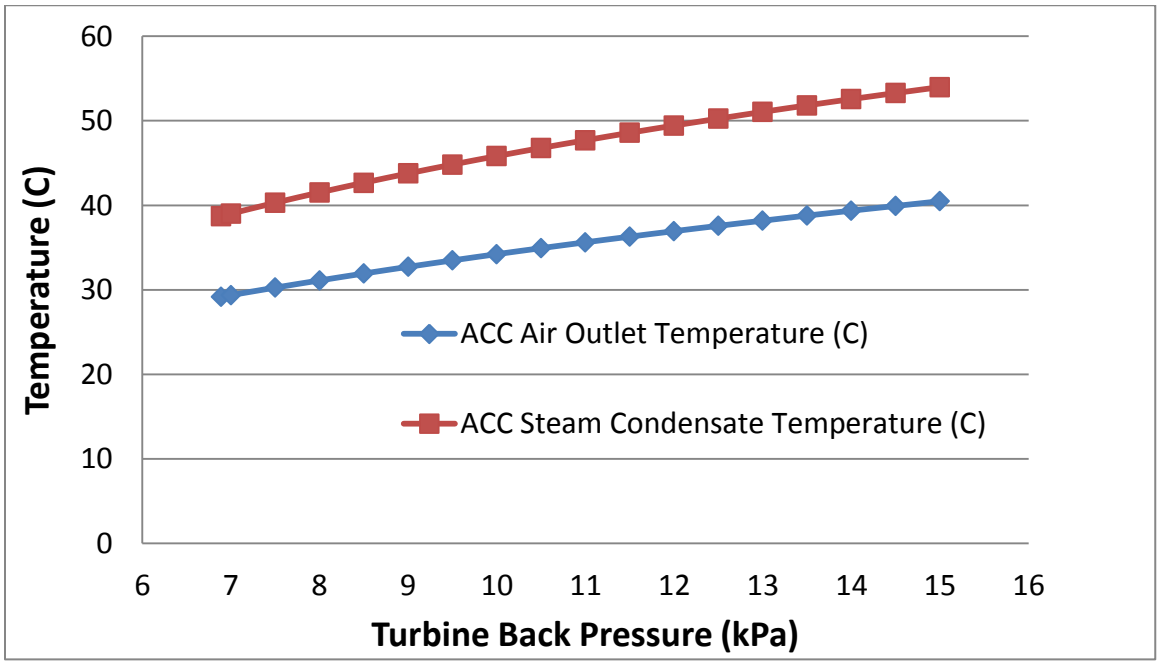

Figure 4-18 Steam condensate temperature and air outlet temperature of air-cooled condensers under 20C ambient temperature

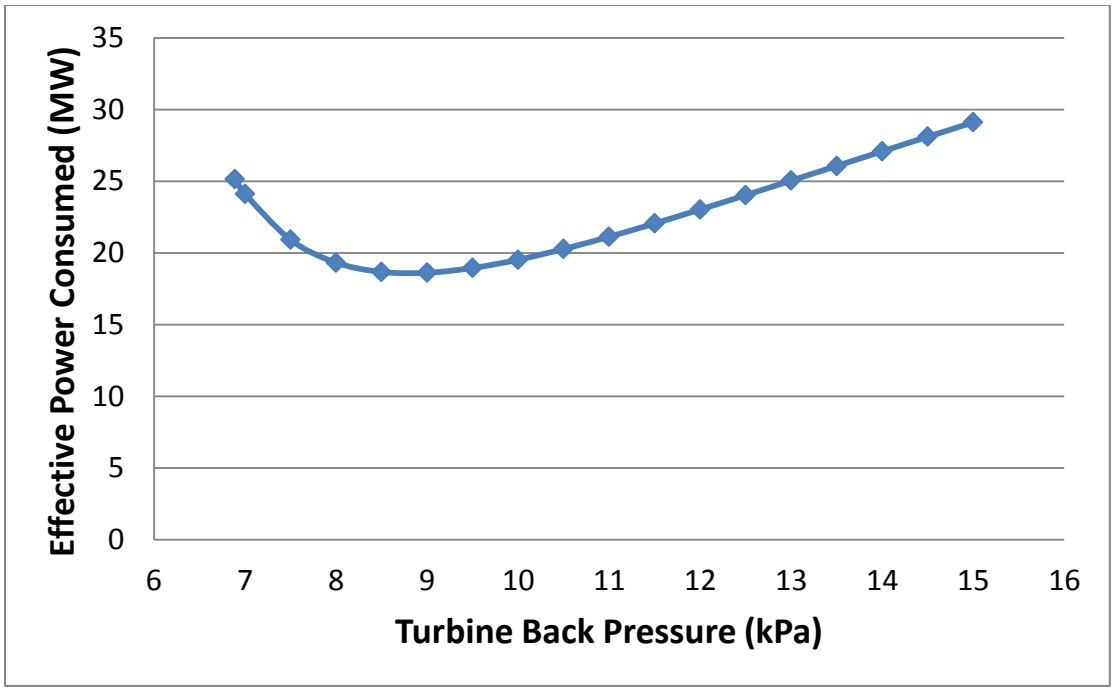

Figure 4-19 Power consumption of the drying cooling subsystem under 20C ambient temperature with different turbine back pressures

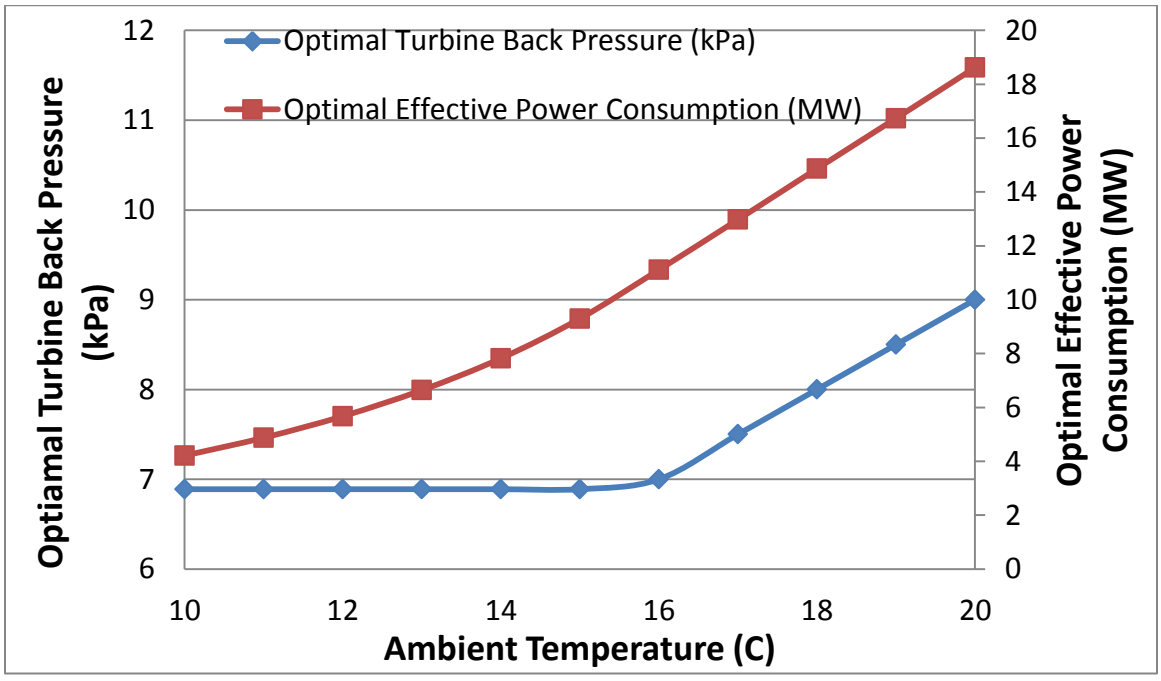

Figure 4-20 Optimal turbine back pressures and optimal effective power consumptions under different ambient temperatures

4.3.4.4 Performance of Combined Cooling System

The combined wet/dry cooling system consisting of wet cooling towers for process cooling and an air-cooled condenser is applied to the subcritical PC power plant retrofitted with solid sorbent based CO_2 capture. The plant performance can be defined by a Coefficient of Performance (COP) given by:

$$COP = \frac{Total\ Power\ Consumption}{Total\ Heat\ Rejected} \qquad \text{Equation 4-41}$$

The total power consumption in Equation 4-41 refers to the total power consumed by the combined wet/dry cooling system, including fan powers and pump powers for wet cooling tower and fan powers for air-cooled condenser.

The heat rejection of the combined wet/dry cooling system for the subcritical PC power plant using solid sorbent based CO_2 capture is 922,509 kJ/s. Total power consumptions and COPs, under different ambient temperatures, are shown in Figure 4-21. The total power consumption increases dramatically from 8.3 MW to 49.0 MW by increasing ambient temperature from 10C to 20C. By comparing it with Figure 4-14 and Figure 4-20, it is found that major part of the increased power originates from the wet cooling tower. Correspondingly, the COP reduces from 111 to 19 by increasing ambient temperature in the same range.

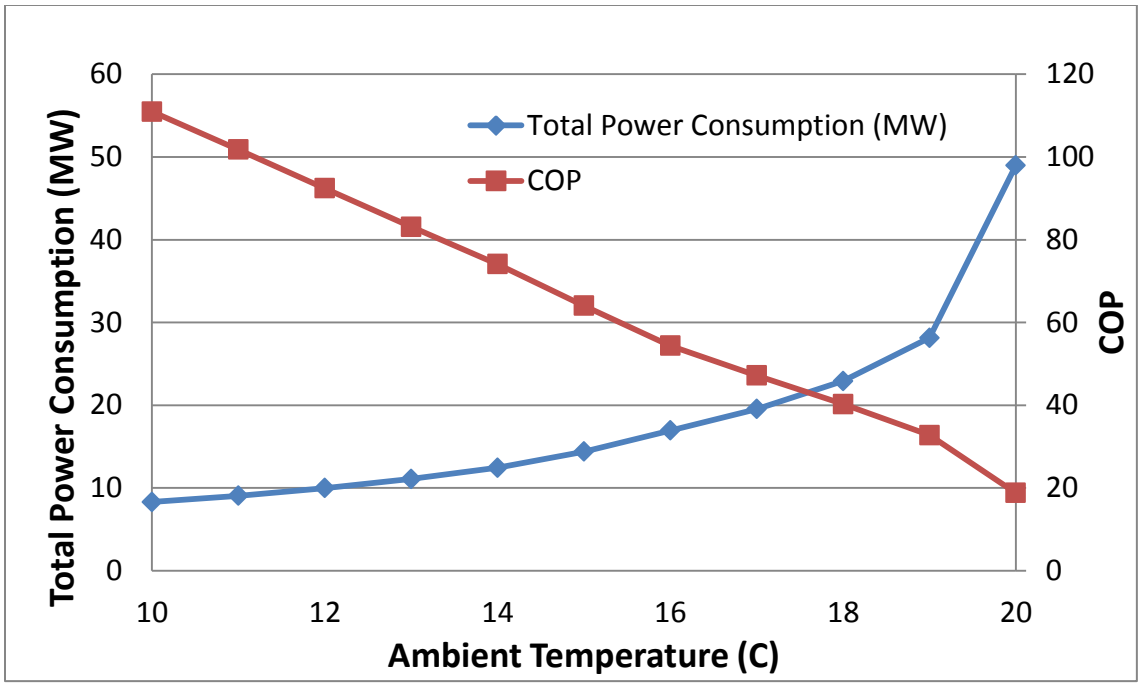

Figure 4-21 Total power consumption and COP for combined cooling system under different ambient temperatures

Total power consumptions and COPs, under different relative humidity at constant 15C ambient temperature, are shown presented by Figure 4-22. The total power consumption increases from 13.4 MW to 19.0 MW as relative humidity goes up from 30% to 90%, while COP decreases from 68.7 to 48.6. In the relative humidity range, the performance of the wet/dry combined cooling system is not significantly different as compared to changes in ambient temperature. This alternative operation is better for PC power plants retrofitted with solid sorbent CO_2 capture, not only because of increase in performance but also because that a number of existing wet cooling tower cells are available for the retrofit scenario, and those tower cells can be taken advantage of rather than be abandoned.

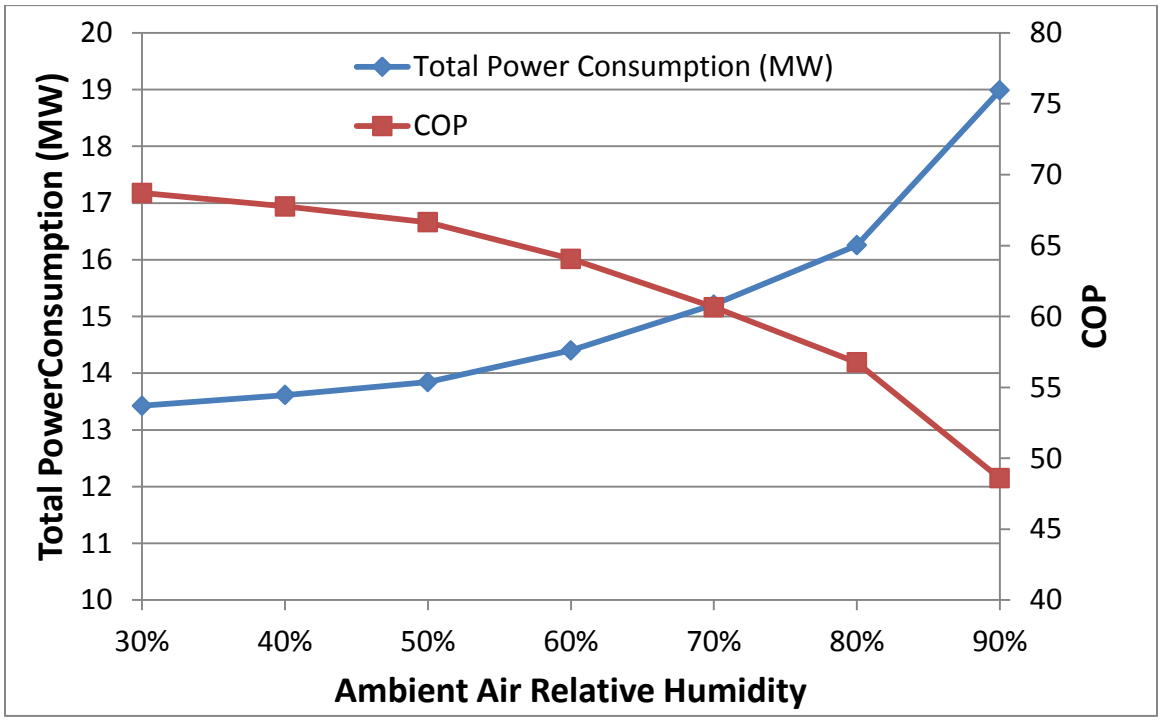

Figure 4-22 Total power consumption and COP for combined cooling system under 15C ambient temperatures of different air ambient relative humidity

If the number of wet cooling tower cells in operation is held constant, then the only strategy for the wet cooling towers responding to ambient condition change is to vary the fan speed so that the air flow rate passing through the fill can be manipulated, causing a dramatic increase in fan power consumption. Since the total number of the tower cells in the retrofitted PC power plant is much more than those required for process cooling at the design conditions, an alternative control strategy for the retrofit scenario to respond to ambient condition change is to turn on more cooling tower cells to reduce water flow rate per unit cell or shut down extra cells to increase water flow

rate per unit cell while keeping the air flow rate of each cell constant at the design condition. In this manner, the fan of each cell can operate under its design condition and the total fan power consumption can be proportional to number of cells or the total air flow rate, not cube of the total air flow rate as indicated by Equation 4-34. Therefore, it would significantly reduce the power consumption and enhance the performance of the wet cooling towers as well as the combined cooling system.

Using this new wet cooling tower operation strategy, the performance of the combined cooling system is presented by Figure 4-23 and Figure 4-24. By comparing with Figure 4-21 and Figure 4-22, it can be seen that the performance of the combined cooling system improves. Under relative lower ambient temperature or lower relative humidity, the improvement in performance is small, while under relative higher ambient temperature or higher relative humidity the performance improves significantly due to dramatically jump in fan power consumption using the fan-varying operations. For instance, at ambient temperature 20C, the total power consumption reduces to 31.5 MW from 49.0 MW, in the meanwhile, COP increases from 18.8 to 29.3.

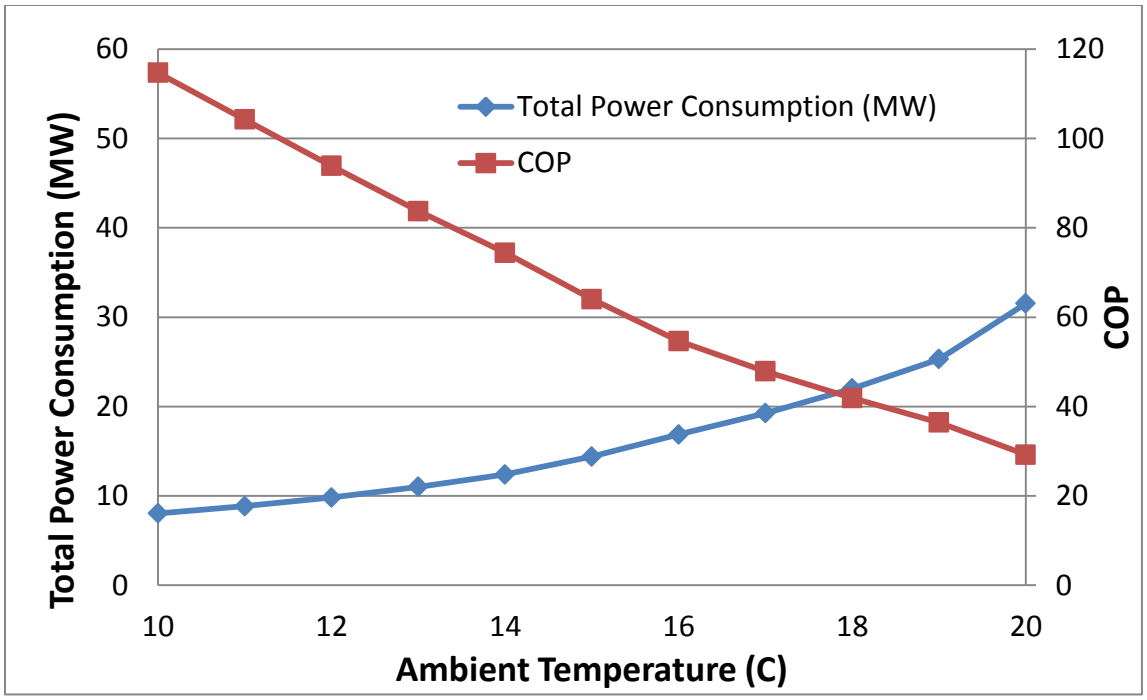

Figure 4-23 Total power consumption and COP for combined cooling system under different ambient temperatures using alternative operation strategy

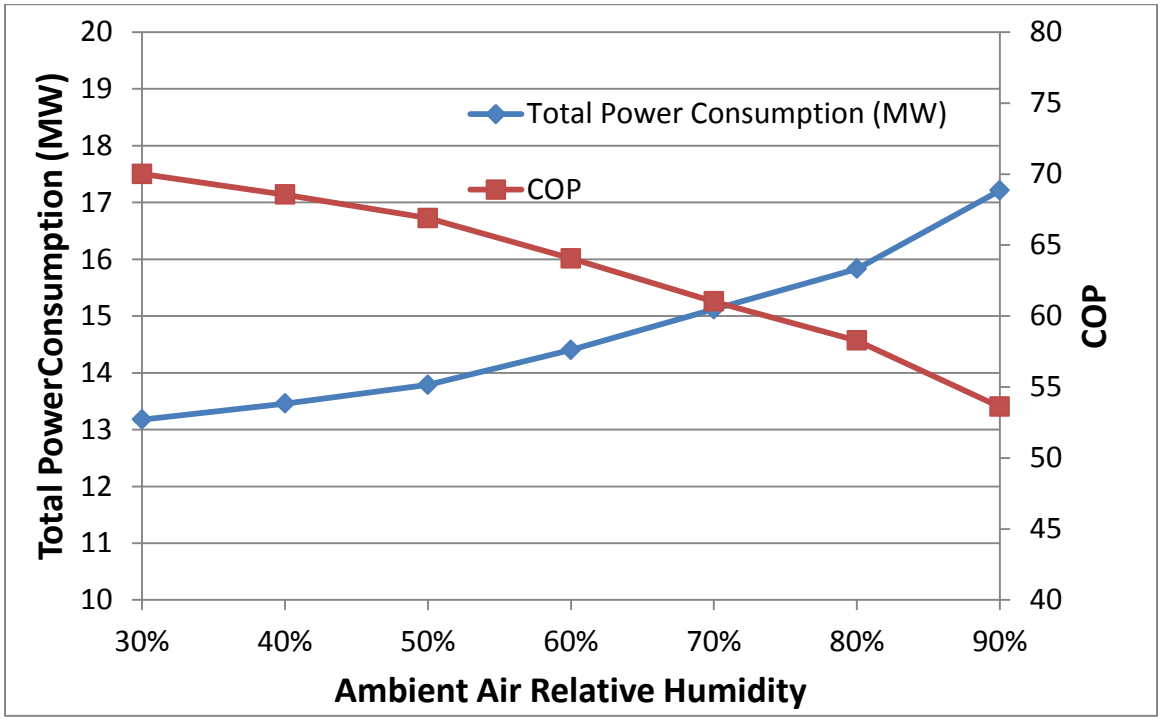

Figure 4-24 Total power consumption and COP for combined cooling system under 15C ambient temp of different air relative humidity using alternative operation strategy

4.4 Summary

This chapter presents work on retrofitting a subcritical PC power plant for solid sorbent based post combustion CO_2 capture technology, and cooling system strategies for PC power plant. Thermal performance and costs are compared with an amine based CO_2 capture plant as well as the plant with no CO_2 capture. The design of the solid sorbent based CO_2 capture system is optimized for integration to minimize plant modifications and the associated downtime. In an existing PC plant with a net output of 550 MW and thermal efficiency of 36.57%, use of the amine based capture reduces the net power output to 391 MW and thermal efficiency to 26.01% while with the solid sorbent based capture, the reduction in net power output of 431 MW and thermal efficiency of 28.67% is far less. As a consequence, the increase in plant cooling duty is significantly lower for the solid sorbent CO_2 capture case, with the water usage on a per MW basis being almost 17% lower than the amine based PC plant. The calculated levelized cost of electricity is increased from \$60.5/MWh without CO_2 capture to \$124.3/MWh for amine based capture while that with the solid sorbent based capture is much lower at \$115.8/MWh. Four levels of CO_2 capture were evaluated, 30%, 50%, 70% and 90%, respectively. The net plant efficiency decreases linearly or net heat rate increases linearly with increased CO_2 capture level, while due to economies of scale, power required decreases from 374 kWh/Tonne for 30% CO_2 capture to 283 kWh/Tonne for 90% CO_2 capture.

Another major focus of this chapter is water usage of PC power plants. By retrofitting subcritical PC power plant for 90% CO_2 capture while continuing the use of mechanical draft wet cooling system, water usage on Liter/MWh basis increases significantly, by as much as 80% for the amine approach, and by 49% for the solid sorbent approach. With 30% through 90% solid sorbent based CO_2 capture, total water usage increases by 7% to 17% on Liter/s basis, and by 18% to by 49% on Liter/MWh basis. However, a combined wet/dry cooling system proposed in this study, with the entire exhaust from the LP steam turbine condensed by an air-cooled condenser, can significantly reduce water usage.

Mathematical models were developed for the proposed combined wet/dry cooling system, and applied to a PC power plant retrofitted with solid sorbent based CO_2 capture. The wet cooling tower model was validated by experimental data in literature. It can predict power consumption of a wet cooling subsystem. The air-cooled condenser model is able to predict optimal steam turbine back pressure and power consumption of draft fans. It was predicted by the model simulation that ambient conditions have significant impacts on the performance of a combined cooling system. If using the operation strategy of fixed number of wet cooling tower cell while varying fan speed, the COP reduces from 111 to 19 by increasing ambient temperature from 10C to 20C. COP decreases from 68.7 to 48.6 for relative humidity ranged from 30% to 90% while keeping the ambient temperature at 15C. An alternative operation strategy consisting of changing the number of tower cells at fixed air flow rate for each cell showed that improved combined cooling system performance can be achieved. This alternative

operation is better for PC power plants retrofitted with solid sorbent CO_2 capture, not only because of increase in performance but also because that a number of existing wet cooling tower cells are available for the retrofit scenario, and those tower cells can be taken advantage of rather than be abandoned.

Chapter 5 IGCC Using Solid Sorbent CO_2 Capture

Toward clean coal utilization, it has been widely accepted that integrated gasification combined cycle (IGCC) is a promising technology for future central power generation with less water usage and a lower CO_2 emission level. An important goal of this dissertation is to identify the subsystem integration concepts for IGCC with advanced subsystem technologies, and its performance in comparison to conventional IGCC. A particular interest of this investigation is solid sorbent based pre-combustion CO_2 capture, including operation conditions, thermal management and reactor design of solid sorbent CO_2 capture reactors and integration of solid sorbent CO_2 capture technologies into advanced IGCC. Since this technology is currently under development and performance data as well as integration experience is limited, a major part of this investigation is the development of a computational fluid dynamics (CFD) to understand the physics and operation of the solid sorbent CO_2 capture technologies, and further used in the design of the commercial size reactors.

5.1 System Analyses of Conventional and Advanced IGCCs

An IGCC using conventional subsystem technologies is developed for comparison with the IGCC using advanced subsystem technologies to quantify the expected gain in performance and economics. Both IGCC systems discussed in this section were modeled by Aspen Plus®. The site conditions are the same as in Chapter 4, and bituminous is the coal feed with coal properties presented in Table 4-2. Table 5-1 presents the

environmental targets for the IGCCs in this study, which are more stringent than those for the PC power plants. CO_2 capture basis is the same as presented in Table 4-3.

Table 5-1 Environmental targets of IGCC

Parameters	
NO_x emissions	< 15 ppmv (dry) @ 15% O_2
SO_x emissions	< 0.0128 lb/MMBtu
Hg emissions	> 90% capture
Hg	0.0071 lb/MMBtu

5.1.1 Technical Description

5.1.1.1 IGCC Using Conventional Technologies

A conventional IGCC system was developed referring to DoE report [23] as a comparison case to evaluate the performance and economics of advanced IGCCs using solid sorbent based CO_2 capture technologies. The basic process is presented by Figure 5-1.

Air separation unit (ASU) is designed to supply high pressure and high purity O_2 (at nominal 95 mol%) for use in the gasifier. The Sulfur Recovery unit also utilizes a small quantity of O_2. Intermediate pressure (IP) N_2 is recovered as well from the ASU and compressed to dilute syngas combusted in gas turbine combustor for NO_x control and to provide additional motive fluid. Air is compressed to 13.1 bar and provided to the cold box operating at elevated pressure (EP). O_2 and N_2 in the air are separated by means of cryogenic distillation, and the O_2 stream required by the gasifier and the N_2 stream provided to the gas turbine are compressed in multistage intercooled compressors.

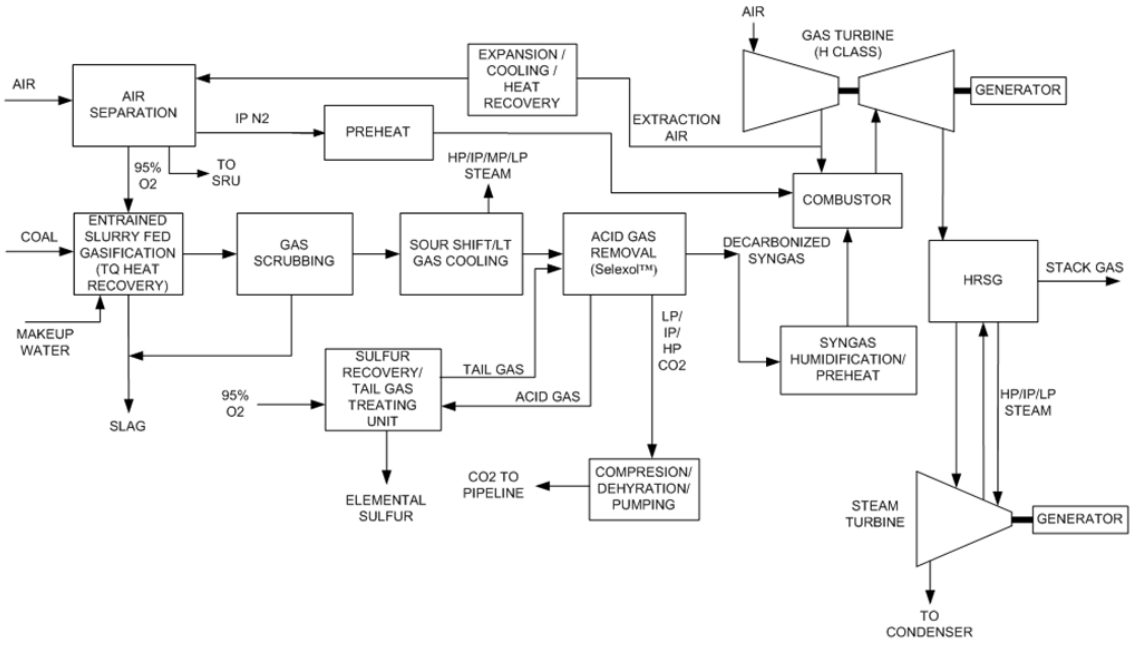

Figure 5-1 Block flow diagram of a comparison conventional IGCC

Coal-water slurry fed, pressurized, oxygen-blown, two-stage, up-flow E-Gas^{TM} gasifier [144] (shown in Figure 5-2) is designed to produce syngas. Coal slurry is pumped into the gasifier in both lower (first) and upper (second) stages. O_2 is fed to the gasifier at 4.2 MPa only into the first stage. The Gasification reactions take place at temperature of 1316C to 1427C in the first stage and 1,038C in the second stage. Hot raw syngas is cooled by quench water, and then fed to the syngas scrubber, where the particulates and the HCl are removed.

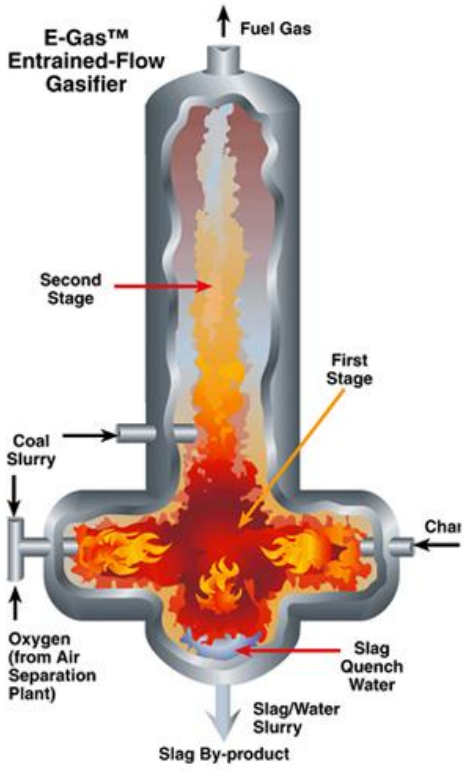

Figure 5-2 E-Gas Gasifier (Source: [145])

After scrubbing the syngas passes through two stages of water gas shift (WGS) reactors, high temperature shift (HTS) operating in the temperature range of 310C to 450C and low temperature shift (LTS) operating in the temperature range of 200C to 250C. Additional steam is injected into syngas before it enters HTS reactor to keep H_2O/CO ratio 2.25 consistent with DoE report [23] to increase CO conversion, avoid carbon deposition on the catalyst, and avoid or minimize formation of unwanted side-products such as Fisher-Tropsch liquids. Most of the CO in the syngas is shifted to H_2 by WGS reaction (Equation 5-1). The small amount of COS in the raw syngas is converted

into H_2S via hydrolysis reaction (Equation 5-2). Because syngas is shifted before it is desulfurized, both stages of WGS contain sulfur tolerant (sour shift) catalyst. The heat evolved by the exothermic shift reactions is used to generate high and intermediate pressure steam as well as to preheat the reactor feed. The remaining sensible heat is further recovered by generating steam at lower pressures and by heating several process streams to cool the shifted syngas down to a level suitable for the Acid Gas Removal unit. After shifting and cooling, the syngas flows through a mercury removal bed of Sulfided activated carbon where 95% of the mercury is captured.

$$CO + H_2O \leftrightarrow H_2 + CO_2 \qquad \text{Equation 5-1}$$

$$COS + H_2O \leftrightarrow H_2S + CO_2 \qquad \text{Equation 5-2}$$

A two-stage Selexol™ process is used in the Acid Gas Removal (AGR) unit. The syngas exiting WGS unit after heat recovery, cooling and Hg removal is first sent to the H_2S absorber, where it contacts cold, CO_2 loaded solvent and H_2S, COS and some CO_2 are transferred from the gas phase to the liquid phase. The treated gas exits the H_2S absorber and is then sent to the CO_2 absorber, where it contacts chilled, flash-regenerated solvent and CO_2 as well as low levels of other gases are transferred from the gas phase to the liquid phase. The solvent exiting the H_2S absorber is sent to stripper where it gets regenerated and acid gases are transferred into gas phase and sent out of AGR unit to the Claus Sulfur Recovery unit. The Claus process converts H_2S into elemental sulfur via reactions represented by Equation 5-3 and Equation 5-4, and the overall reaction is Equation 5-5. The solvent exiting the CO_2 absorber gets regenerated

by releasing CO_2 by decreasing the pressure in a series of flash drums. The separated CO_2 is supplied to the CO_2 compression and dehydration unit, where it is pressurized to a supercritical pressure suitable for pipeline transport to a geologic sequestration site.

$$H_2S + \frac{3}{2}O_2 \leftrightarrow H_2O + SO_2 \qquad \text{Equation 5-3}$$

$$2\,H_2S + SO_2 \leftrightarrow 2H_2O + 3S \qquad \text{Equation 5-4}$$

$$3\,H_2S + \frac{3}{2}O_2 \leftrightarrow 3\,H_2O + 3\,S \qquad \text{Equation 5-5}$$

The treated syngas exiting the AGR unit is sent to the humidification unit and humidified to 4% by contacting with water in a packed column in a counter-current manner, because the N_2 from the ASU is insufficient to provide adequate syngas dilution for the gas turbines (GE's 7FB gas turbines) for NO_x control. The moisturized syngas is then reheated and introduced into the combustor of the gas turbines along with the diluent N_2 for power generation. The exhaust gas exiting each of the gas turbines at temperature of 562C produces steam in a heat recovery steam generator (HRSG) to power a steam turbine using 12.4 MPa/534C/534C steam cycle.

5.1.1.2 IGCC Using Advanced Technologies

The major difference between advanced IGCC and conventional IGCC is syngas cleanup process and CO_2 capture. The two-stage Selexol™ process removes acid gas (mainly H_2S and CO_2) at around ambient temperature, while syngas is reheated up before it enters gas turbine, which creates penalties in thermal efficiency of IGCC system. In advanced IGCC, warm gas cleanup is adopted and CO_2 is removed at temperature

above 200C which would significantly improve the system's thermal performance. The overall block flow diagram of the advanced IGCC is presented in Figure 5-3. A brief description of the difference between the advanced IGCC and the conventional IGCC is provided in this chapter as follows.

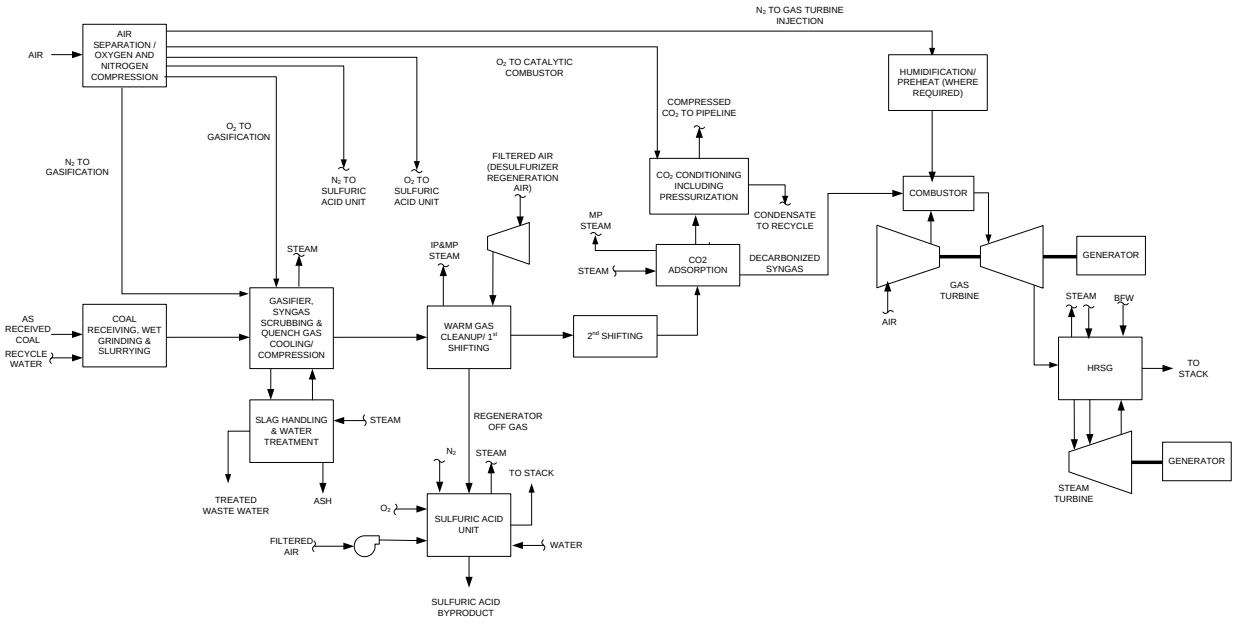

(a) CO2 capture alone

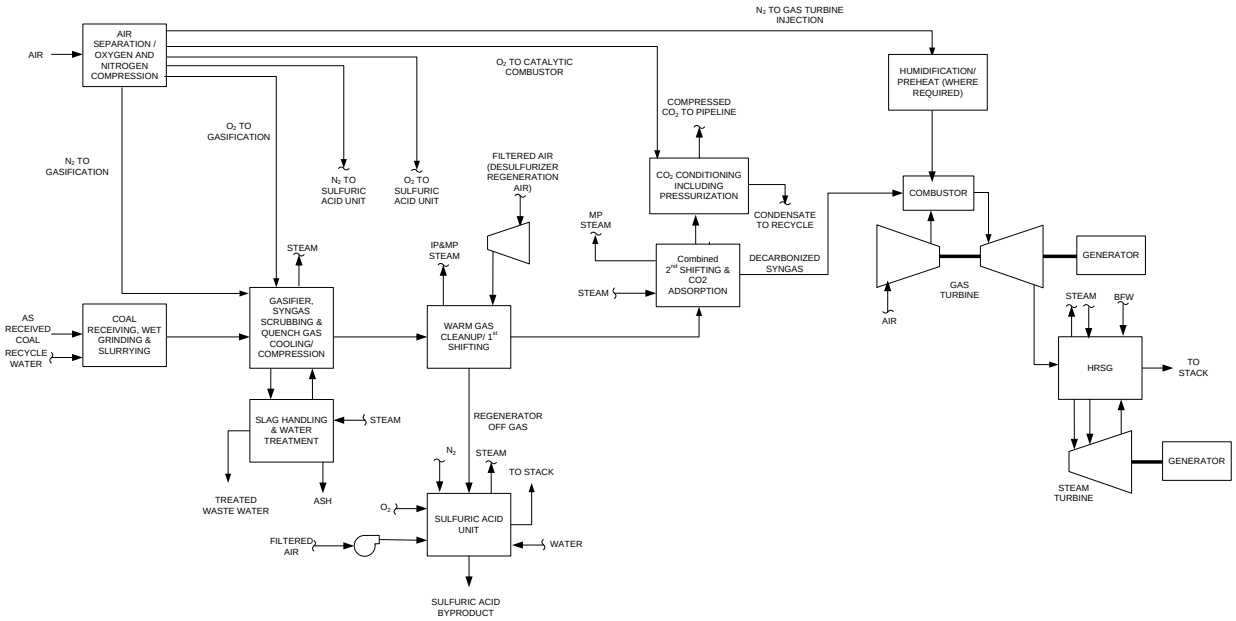

(b) Combined WGS and CO_2 capture

Figure 5-3 Block flow diagram of an advanced IGCC

For modeling purposes in Aspen Plus®, the ASU is subdivided into two sections, one consisting of an EP cryogenic section and the other consisting of a low pressure (LP) cryogenic section. The EP cryogenic section provides in addition to O_2 for the gasifier, IP N_2 for syngas dilution. Because moisture content of the syngas exiting the sorbent CO_2 capture unit is high, less N_2 diluent is required thereby limiting the size of the EP section. In order to supply enough O_2 to the gasifier and other O_2 users in the plant, the LP section is added which requires compressed air at a much lower pressure of 4.6 bar to the cryogenic distillation unit operating near atmospheric pressure with the separated N_2 and other minor components all vented to the atmosphere.

Gasification as well as coal feeding and syngas scrubbing are the same as conventional IGCC using the E-Gas™ gasifier to produce raw syngas.

Warm gas cleanup is selected to remove contaminants in the raw syngas for advanced IGCC. Sulfur components are removed by a regenerable ZnO process operating around 260°C. The scrubbed raw syngas is treated with ZnO which is converted to ZnS, this process being accomplished in a transport desulfurizer in order to make the process continuous since ZnS has to be regenerated. The regeneration is accomplished using air to release the sulfur as SO_2 from which the saleable product H_2SO_4 is made. Warm gas mercury removal process operating at around 300C to 400C [146] is employed; it uses a fixed bed reactor containing an Amended Silicates™ sorbent where the mercury is chemisorbed from the syngas.

Two WGS design options are evaluated in terms of how low temperature shift (LTS) integrates with solid sorbent CO_2 capture. HTS converts CO into CO_2 in the temperature range of 310C to 450C in both design options. For the first design option, additional steam is added to syngas entering HTS to keep H_2O/CO ratio at 2.25 in order to achieve a CO concentration of about 3% vol at HTS exit to be consistent with the conventional case. Separate LTS and CO_2 capture adsorbent are installed downstream of the desulfurization unit (regenerable ZnO process) to avoid CO_2 sorbent poisoning. LTS operating in temperature range of 200C to 250C converts CO into CO_2 with about 0.7 vol% CO left in the syngas. Shifted syngas enters solid sorbent CO_2 capture unit which operates at temperature above 200C. For the second design option, given the close

operating temperature of the two units, the second stage of WGS, the LTS, is combined with solid sorbent CO_2 capture. Both the LTS catalyst and solid sorbent are loaded into single fixed bed reactors, and WGS reaction and CO_2 adsorption occur simultaneously, driving the WGS reaction to convert more of the CO without extra steam required. Thus, in this case, no additional steam is supplied before syngas enters the HTS, with the H_2O/CO ratio at 1.24 resulting in a CO concentration of 8.2 vol% in the shifted syngas exiting the HTS.

Solid sorbent based pre-combustion CO_2 capture for cases described above is similar to post-combustion sorbent CO_2 capture to remove 90% of CO_2 in the syngas except that it operates under pressure swing adsorption (PSA) mode at elevated pressures instead of the vacuum swing adsorption (VSA) mode of operation. Adsorption step operates under pressure of 34 bar for CO_2 in syngas to be absorbed by the porous sorbent. Steam is utilized to purge the CO_2 loaded beds at lower pressure of 10 bar to desorb the CO_2. The separated CO_2 in mixture with steam is then cooled in a series of heat exchangers while condensing out most of the steam, and is then compressed for sequestration.

The decarbonized syngas contains as much as 40% water vapor which includes the water vapor originally present in the syngas fed to the adsorption unit as well as the residual purge steam remaining in the bed when the CO_2 adsorption step is initiated. Thus, humidification of syngas (in a counter-current column as is done in the conventional IGCC) is not required for syngas dilution before it is provided to the gas

turbines. The power island consisting of two GE 7FB type gas turbines and a steam turbine is similar to that used in conventional IGCC.

5.1.2 Simulation Approach and Models

In addition to the Aspen Plus® process models described in Section 4.1.4, the IGCC utilizes thermodynamic models for reactors such as the gasifier, the shift unit, as well as those in the Claus sulfur recovery unit. An approach to equilibrium may be specified for a given reaction to account for incomplete conversion. Mass transfer operations such the humidification of syngas and sour water stripping accomplished in a counter-current packed or trayed column are modeled using stage wise calculations assuming the streams leaving a stage are in mass and heat transfer equilibrium. The sizing of the columns is then performed by introducing an empirical stage efficiency.

5.1.3 System Performance

The overall performance of three IGCC plants is summarized in Table 5-2. Case 1 is IGCC using Selexol™ technology for CO_2 removal, Case 2 employs the solid sorbent technology for CO_2 capture alone, and Case 3 uses the combined WGS and solid sorbent CO_2 capture approach. The power output of a gas turbine is limited by three constrains: 1. Shaft; 2. Inlet air flow; and 3. Firing temperature. In case 1, the power output is constrained by the shaft resulting in each of the two gas turbine trains generating 232 MW of power or 464 MW total gas turbine power. In Cases 2 and 3 with the solid sorbent CO_2 capture technologies, due to higher moisture content in the decarbonized syngas, the power output is constrained by the inlet air flow as well as the firing

temperature before the shaft limitations come into play with a result that gas turbine output is considerably lower. Detailed break-down of auxiliary power consumers for each plant is listed in Table 5-3. The major difference in power consumption between Selexol™ technology and solid sorbent based technologies is due to ASU air and nitrogen compression and CO_2 removal. Due to less steam content in decarbonized syngas for Selexol™ technology, extensively more nitrogen is required for syngas dilution requiring a larger "EP section" in the ASU and correspondingly larger air and nitrogen compression power. The major power consumer in the solid sorbent CO_2 removal unit is the blow-down gas recycle compressor, while Selexol™ technology consumes larger amount of power for not only gas recycle compression but also for mechanical refrigeration to chill the solvent. The effect is that the net plant efficiency for Case 2 and Case 3 is higher than Case 1 by 2.77 and 3.27 percentage points (or in terms of heat rate, reduced by 8.2%, and 9.5%), respectively.

Table 5-2 Performance summary

Case No.		1	2	3
CO_2 Capture Technology	Units	Selexol™	Solid Sorbent CO_2 Capture Alone	Combined WGS and Solid Sorbent CO_2 Capture
CO_2 Capture Level	%	90.0	90.0	90.0
Gas Turbine Power	KWe	464,000	419,381	426,199
Steam Turbine Power	KWe	246,789	242,186	257,720
Total Power	KWe	710,789	661,567	683,920
Total Auxiliary Consumption	KWe	194,473	120,396	133,748
Net Power Output	KWe	516,316	541,171	550,172
% Net Plant Efficiency, HHV	%	31.04	33.81	34.31
Net Heat Rate	KJ/KWH	11,598	10,648	10,493
Surface Condenser Cooling Duty	10^6 KJ/H	1,354	1,299	1,426
As-Received Feed	KG/H	220,549	212,229	212,629
Thermal Input	KWT HHV	1,663,387	1,600,642	1,603,655

Table 5-3 Auxiliary power consumptions

Case No.	1	2	3
CO_2 Capture Technology	Selexol™	Solid Sorbent CO_2 Capture Alone	Combined WGS and Solid Sorbent CO_2 Capture
Coal Handling	448	431	432
Coal Milling	2,269	2,184	2,188
Coal Slurry Pumps	629	639	0
Slag Handling & Dewatering	1,118	1,084	1,086
Air Separation Unit Auxiliaries	1,071	1,034	570
Air Separation Unit Main Air Compressor	65,668	42,269	50,000
Oxygen Compressor	9,120	17,442	14,619
Nitrogen Compressor	34,525	9,828	18,675
Syngas Recycle Compressor	1,275	1,193	1,195
Tail Gas Recycle Compressor	5,420	-	-
CO_2 Purification & Compression	31,179	24,170	24,224
Boiler Feed Water & Demin Pumps	5,444	5,359	5,299
Vacuum Condensate Pump	376	378	360
Process Condensate & SWS Systems	49	80	79
Humidifier & BFW Circulating Pumps	45	93	93
Cooling Water Circulating Pumps	4,920	4,155	4,548
Cooling Tower Fans	2,484	2,098	2,296
Scrubber Pumps	397	382	382
Selexol™ Unit	21,038	-	-
Desulfurizer Unit	-	4,792	4,802
Gas Turbine Auxiliaries	1,000	904	919
Steam Turbine Auxiliaries	107	105	112
Claus & Tail Gas Treating Auxiliaries	204	-	-
H_2SO_4 unit	-	-3,612	-3,607
Miscellaneous Balance of Plant	3,054	2,938	2,944
Transformer Losses	2,633	2,450	2,533
Total Auxiliary Consumption	194,473	120,396	133,748

The difference between two solid sorbent based technologies lies in steam content in decarbonized syngas as well. One advantage of combined WGS and solid sorbent CO_2 capture technology is that no extra steam addition into syngas entering the WGS is

required resulting in larger steam cycle power generation. However, this also brings less steam in decarbonized syngas, so that relatively larger ASU air and nitrogen compression power are required to satisfy the NO_x control diluent requirement of the gas turbine feed syngas, which results in larger auxiliary power for case 3. The net effect is that the plant efficiency for Case 2 and Case 3 is brought a little closer, 33.81% for Case 2 versus 34.31% for Case 3.

5.1.4 Economic Analyses

Economics of the three IGCC plants using different CO_2 capture technologies is presented by Table 5-4. The 1st Year Cost of Electricity for Case 1, Case 2 and Case 3 are $127.8/MWh, $114.5/MWh and $112.5/MWh respectively showing that solid sorbent CO_2 capture technology is quite cost effective.

Table 5-4 Plant cost estimates and economics

Case No.	1	2	3
CO_2 Capture Technology	Selexol™	Solid Sorbent CO_2 Capture Alone	Combined WGS and Solid Sorbent CO_2 Capture
Net Power, kW	516,316	541,171	550,172
Plant Cost, $1000			
Fuel Preparation System	93,433	91,091	91,205
Air Separation Unit	233,439	224,886	225,182
Gasification System	311,390	302,832	303,245
Gas Cleanup and Conditioning Systems	347,271	274,284	268,426
Power Island	286,050	284,319	284,439
General Facilities	196,579	189,094	192,756
Total Plant Cost (TPC), $1000	1,468,162	1,366,505	1,365,252
Total Fixed Operating Cost for Initial Year, $1000/yr	55,947,663	53,049,227	53,041,793
Total Variable Operating Costs, $1000/yr	179,402,855	168,838,764	168,848,477
1st Year Cost of Electricity (COE), $/MWh	127.8	114.5	112.5

5.2 CFD Model Development for Solid Sorbent CO_2 Capture

5.2.1 Model Assumptions

Figure 5-4 schematically shows the physical and chemical processes of adsorption step in a fixed bed reactor for CO_2 capture alone. Fluid dynamics, heat and mass transfer, adsorption/desorption are simultaneously occurring in a single reactor, which makes the processes complex. To reduce the complexity of CFD simulation, simplifying assumptions have been made as shown below:

1. Transient simulation of a CO_2 capture alone fixed bed reactor.
2. The fixed bed reactor is cylindrical, and it is assumed that the computational zone is axisymmetric, so that a 2 dimensional axisymmetric model can be adopted to save computational time.
3. The CO_2-rich syngas mixture is approximated as ideal gas, and gas mixture physical properties can be estimated by mixing law.
4. Solid sorbent adsorbs only CO_2, while inert to other gases. TDA's solid sorbent material of mesoporous carbon does absorb small quantities of other gas components but the amounts are negligible compared to CO_2 [64].
5. The entering syngas in CFD simulation contains only major gas components such as CO, CO_2, H_2 and steam. Minor components such as N_2, Ar, CH_4 and NH_3 are assumed to be negligible. This assumption is acceptable because N_2, Ar and CH_4 are not absorbed by sorbent as indicated in the previous assumption while contaminants, such as particulate matter, sulfur, chlorine

and nitrogen-containing compounds, are reduced to sufficiently low concentrations by gas cleanup processes before syngas enters the combined reactor.

6. In the packed bed zone, sorbent pellets are uniformly distributed.
7. Under all operating conditions, Re number is less than 2100 and laminar flow is assumed over computational zone.
8. Radiation is neglected within the reactor due to the short beam lengths. Only heat conduction and heat convection are considered.
9. Local thermal equilibrium is assumed between gas and sorbents.
10. The external mass transfer resistance is zero. CO_2 concentration in bulk flow is the same as that on sorbent external surface.
11. The build-in porous media model in ANSYS Fluent is applied for the simulation of the fixed bed. It is assumed that the porous media and fluid flow are in thermal equilibrium.
12. The wall of bed reactor is adiabatic, a reasonable assumption for a large commercial reactor with insulation on the outside (while the experimental unit's outside wall surface is electrically traced).

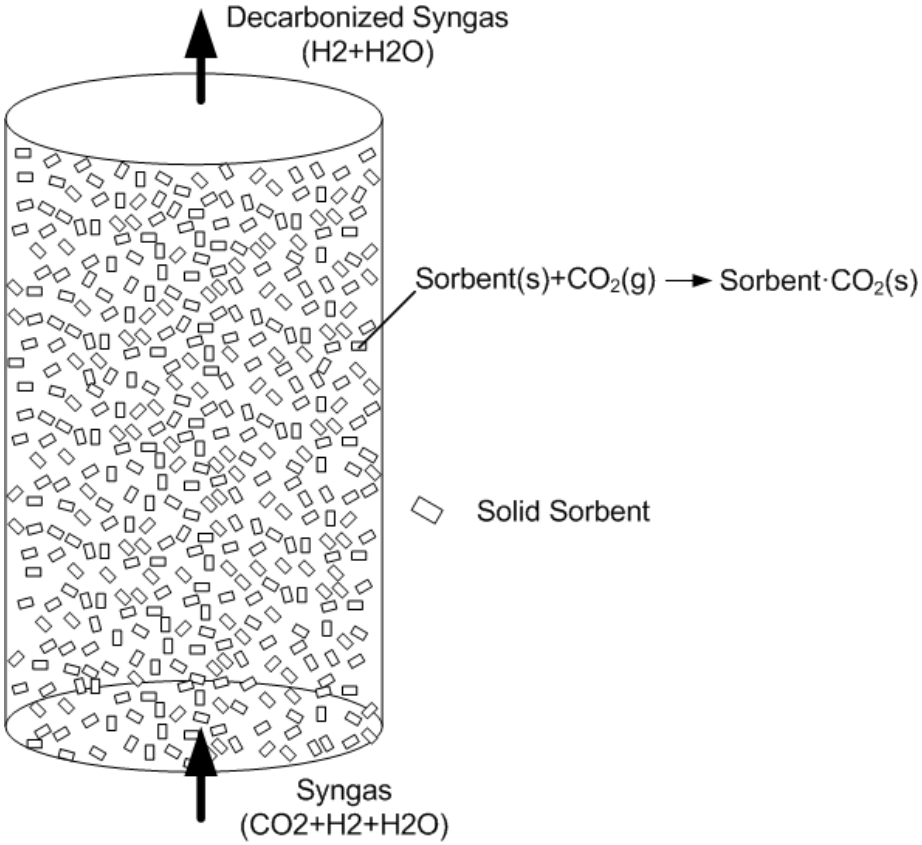

Figure 5-4 Fixed bed reactor for CO_2 capture alone

Figure 5-5 presents the schematic of the physical and chemical processes of a fixed reactor for combined WGS and CO_2 capture. The top and bottom zones are packed with only solid sorbent to avoid contaminant poisoning of WGS catalyst during adsorption and desorption processes (since the sorbent is capable of adsorbing the syngas contaminants); the middle zone of the reactor is packed with mixture of WGS catalyst and solid sorbent. Together with fluid dynamics, heat and mass transfer and adsorption/desorption, chemical reaction of WGS simultaneously occurs in the

combined packing zone. Three additional assumptions are made in the CFD simulation of the fixed bed reactor for combined WGS and CO_2 capture:

1. In sorbent packed zone, sorbent pellets are uniformly distributed. In combined packed zone, catalyst and sorbent are perfectly mixed and uniformly distributed.
2. The external mass transfer resistance is zero. Concentration of the WGS reactants in bulk flow is the same as on the catalyst external surface.
3. Catalyst and sorbent function without affecting each other.

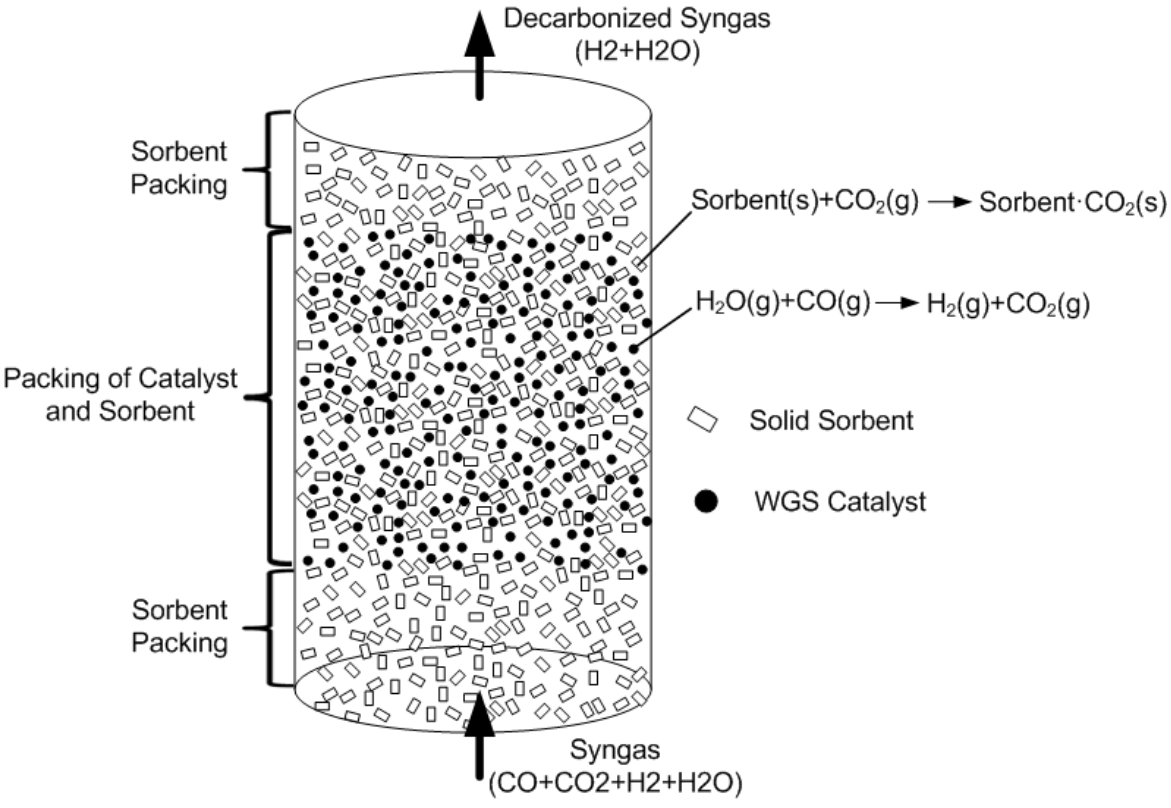

Figure 5-5 Fixed bed reactor for combined WGS and CO_2 capture

5.2.2 CO_2 Capture Model

Solid sorbent absorbs CO_2 during the adsorption step when a CO_2 containing stream passes through the bed, and desorbs CO_2 during the regeneration step when CO_2 loaded solid sorbent is exposed to an inert stream (N_2 or steam). The adsorption/desorption rate were tested and correlated at TDA Research. Inc [64]. The performance of the sorbent was evaluated in a Thermo-Gravimetric Analyzer (Shimadzu TGA-50 as shown in Figure 5-6). Adsorption and desorption were cycled by flowing pure CO_2 and N_2 at a total pressure of 82.74 kPa (12 psia) at constant temperature. The normalized CO_2 adsorption / desorption curves as measured by TGA at different temperatures are depicted in Figure 5-7.

Figure 5-6 Thermo-Gravimetric Analyzer (Shimadzu TGA-50)

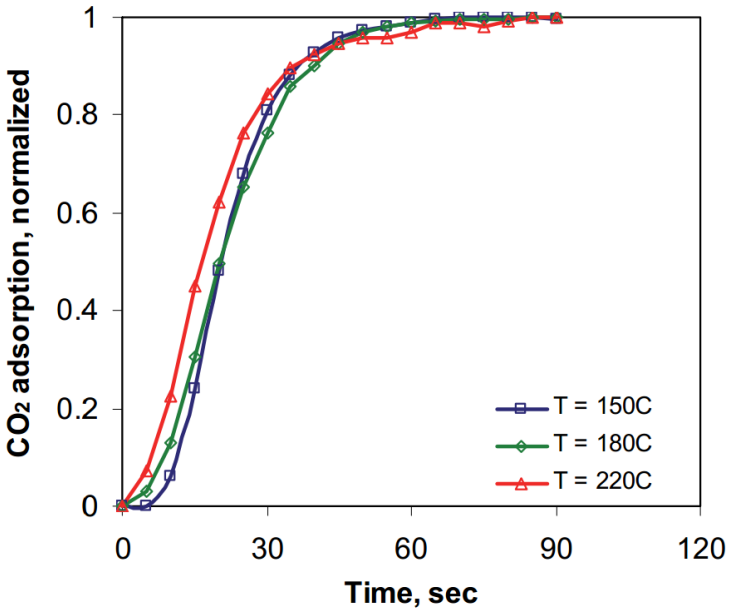

Figure 5-7 CO_2 Adsorption as a function of time at various temperatures

Adsorption process, or process of gas transporting to inside the sorbent particle from bulk flow in a fixed bed, comprises of external transport processes and internal transport processes. External transport processes consist of heat and mass transfer between a solid surface and a flowing fluid, known as film diffusion; internal transport consists of the diffusion process of gas penetrating into the porous structure during adsorption. In gas separation processes, the overall mass transfer rate is limited to pore diffusion, or internal transport, under practical conditions of gas separation [108], and film diffusion may be neglected. The CO_2 adsorption and desorption rate can be depicted by Linear Driving Force (LDF) model [108] as shown by Equation 5-6.

$$\frac{d\bar{q}}{dt} = k_b(q^* - \bar{q}) \qquad \text{Equation 5-6}$$

where

q^* is the adsorption capacity at equilibrium, kmol/kg

$\bar{q}$ is the actual adsorption capacity at a given time t, kmol/kg

k_b is rate constant (1/s) which can be approximated by $15\, D_e/r_c^2$, where D_e/r_c^2 is the diffusion time constant.

By integrating Equation 5-6, an expression for normalized adsorption is obtained as shown by Equation 5-7.

$$\frac{\bar{q}}{q^*} = 1 - exp(-k_b t) \qquad \text{Equation 5-7}$$

By fitting normalized adsorption (and desorption) curves along with Equation 5-7, the rate constant k_b can be obtained, as shown in Figure 5-8 for temperature 220 C.

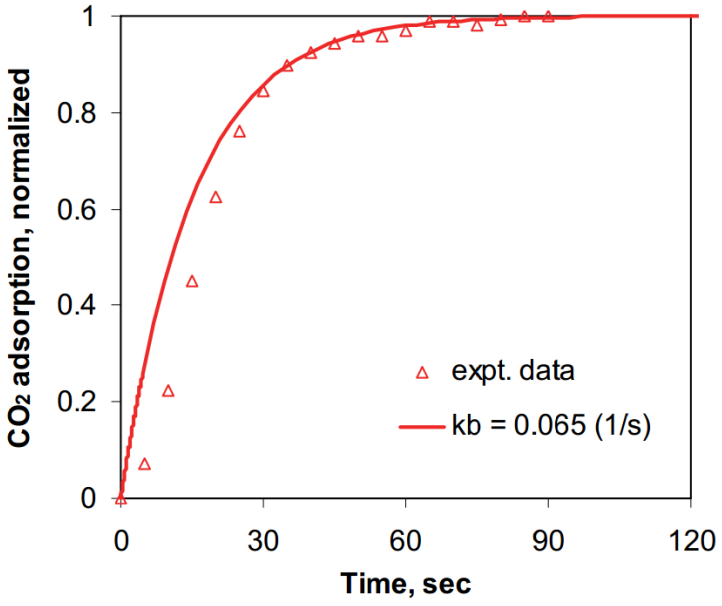

Figure 5-8 CO_2 Adsorption curves at 220°C fitted with LDF model

At pressure 82.74 kPa (12 psia), k_b at different temperatures was obtained. A correlation of Arrhenius type relationship (Equation 5-8) is used to express k_b as a function of temperature.

$$k_{b@12psia} = k_{b0@12psia}\exp(-\frac{E}{R_g T}) \qquad \text{Equation 5-8}$$

By fitting experimental data, $k_{b0@12psia} = 0.1788$, $E/R_g = 504.2$ for both adsorption and desorption.

In the CFD model, the pressure dependence of k_b was introduced by Darken theory [147] given by Equation 5-9. However a faster increase in surface diffusivity has been observed in heterogeneous surfaces [148], [149]. Sorbent used in this study (TDA's sorbent) has functionalized surface groups specifically for CO_2 adsorption, which results in surface heterogeneity, and the k_b may not strictly follow Darken theory. Due to lack of availability of k_b data as a function of surface coverage, we assumed Darken equation for TDA's CO_2 sorbent to account for variation of k_b with surface coverage.

$$k_b = \frac{k_{b@12psia}}{(1-\theta)} \qquad \text{Equation 5-9}$$

where $\theta = \frac{q^*}{q_s}$ and q_s is defined below.

In order to completely define the adsorption / desorption rate using Equation 5-6), beside rate constant k_b, adsorption capacity at equilibrium q^* is required, which can be modeled using the Langmuir-Freundlich Isotherm [150] as shown by Equation 5-10:

$$q^* = \frac{q_s B P_{CO_2}^n}{1 + B P_{CO_2}^n} \qquad \text{Equation 5-10}$$

where $q_s = k_1 e^{k_2/T}$; $B = k_3 e^{k_4/T}$; $n = k_5 e^{k_6/T}$. k_1 through k_6 are constants.

The amount of CO_2 absorbed at equilibrium was measured at TDA [151] over various CO_2 partial pressures at different temperatures. Experimental data from the tests was fitted with Langmuir-Freundlich Isotherm as shown by Figure 5-9, and the constants in Figure 5-8 are presented in Table 5-5.

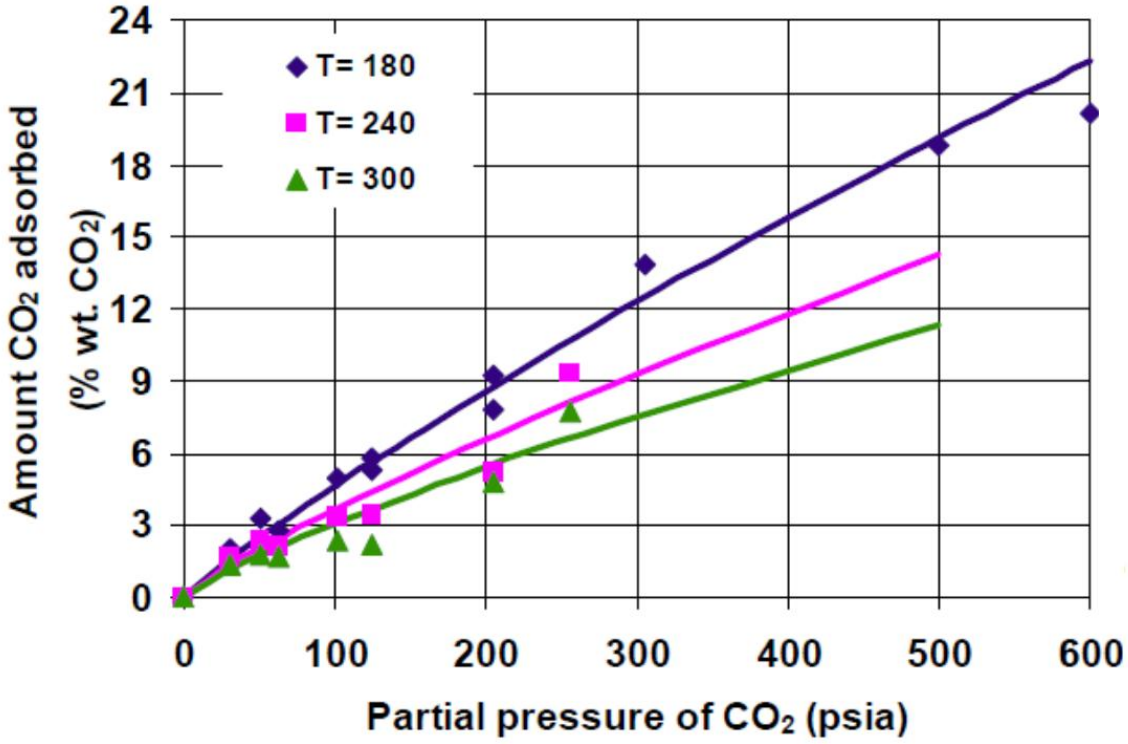

Figure 5-9 CO_2 isotherms at different temperatures

Table 5-5 Constants of Langmuir-Freundlich Isotherm

q^* (mol CO_2/kg); P_{CO_2} (psia); T (K)	
$k_1 = 58.05$	$k_4 = 47.07$
$k_2 = 46.55$	$k_5 = 0.59$
$k_3 = 2.2E\text{-}04$	$k_6 = 201.46$

A differential scanning calorimeter (Shimadzu DSC-50) was employed to measure the heat of adsorption and desorption of CO_2 normalized on unit mass of the sorbent. A TGA under similar test conditions measured the amount of CO_2 absorbed and desorbed. Combining these two measurements, it was calculated that CO_2 adsorption heat is 4.9 kcal/mol, and CO_2 desorption heat is 4.3 kcal/mol [64]. Measurements of the heat of adsorption and desorption are shown in Figure 5-10.

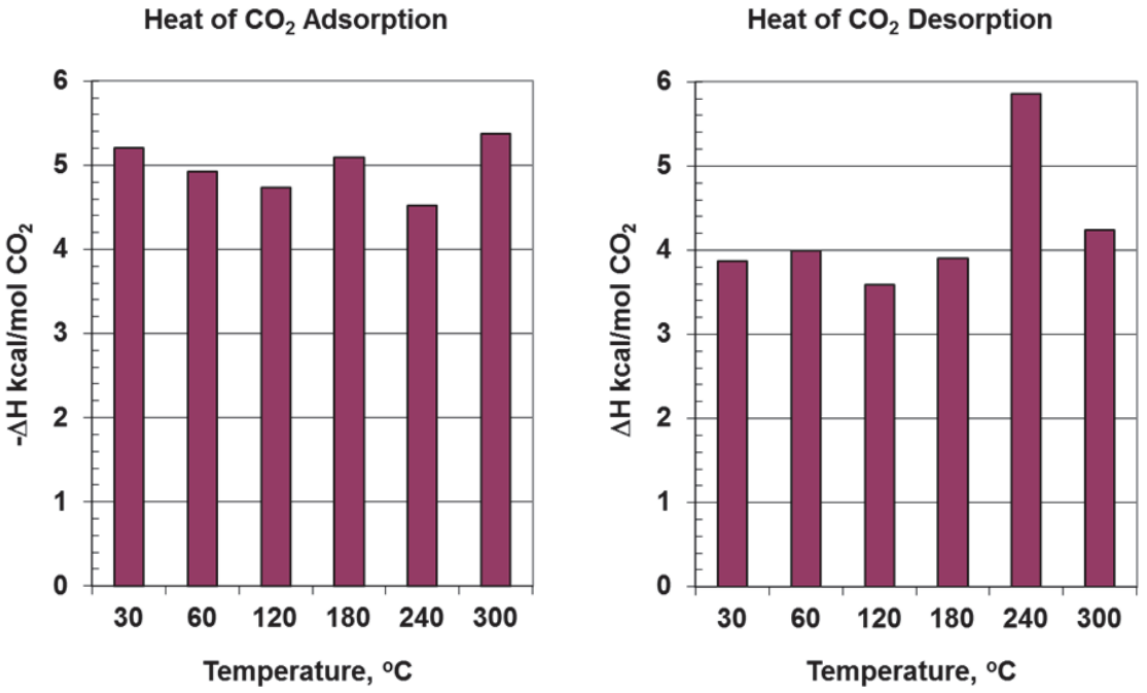

Figure 5-10 Heat of adsorption and desorption of CO_2

5.2.3 Shift Reaction Model

The water-gas shift (WGS) reaction is moderately exothermic reversible reaction and can be expressed by Equation 5-11. In pre-combustion CO_2 capture applications (as described previously for the conventional IGCC), two adiabatic stages of WGS are typically employed consisting of HTS followed by LTS. HTS is utilized for bulk CO conversion to CO_2 in the temperature range of 310 C to 450 C. The WGS reaction is kinetically favored at these high reaction temperatures but conversion is limited by equilibrium for this exothermic reaction. The LTS operating at much lower temperatures (ranging from 200 C to 250 C) converts significant fraction of the remaining CO since the WGS reaction is thermodynamically favored at the low temperatures. The reaction equilibrium is not affected by pressure due to constant volume shifting from reactants to products.

$$CO + H_2O\ (g) \leftrightarrow H_2 + CO_2 \qquad \Delta H = -41.09\ kJ/mol \qquad \text{Equation 5-11}$$

In a reactor for combined WGS and CO_2 capture, CO_2 adsorption and desorption by solid sorbent occurs at temperature around 200 C while a higher temperature would weaken CO_2 adsorption capability of the sorbent, as implied by Equation 5-10. Thus, for simple but effective thermal management within the reactor, CO_2 adsorption is combined with LTS.

In this research project, Sud-Chemie ShiftMax 230 was selected as the LTS catalyst. Composition of the catalyst is shown in Table 5-6. The WGS reaction kinetics is modeled using a rate equation (Equation 5-12) developed by Choi [152].

According to Choi, this particular LTS catalyst is active between temperature 120C and 250C.

Table 5-6 Composition of Sud-Chemie ShiftMax 230 (Source: [153])

CuO	58.0 wt.%
ZnO	31.0 wt.%
Al_2O_2	11.0 wt%

$$r = 2.88 \times 10^{-5} exp(-\frac{47400}{RT})(P_{CO}P_{H_2O} - \frac{P_{CO_2}P_{H_2}}{K_{eq}}) \quad \text{Equation 5-12}$$

where

r is the rate of reaction, mol/gcat/h

P_i is partial pressure of component, pa

T is temperature, K

R is universal gas constant, J/mol K

K_{eq} is equilibrium constant. An empirical model derived by Moe [152] is to represent K_{eq} as shown by Equation 5-13.

$$K_{eq} = exp\left(\frac{4577.8}{T} - 4.33\right) \quad \text{Equation 5-13}$$

From Equation 5-12, the rate of reaction in unit mol/m^3/s can be obtained as:

$$r = 8.01 \times 10^{-6} \rho_{cat} exp(-\frac{47400}{RT})(P_{CO}P_{H_2O} - \frac{P_{CO_2}P_{H_2}}{K_{eq}})$$ Equation 5-14

where ρ_{cat} is the density of catalyst for combined bed (kg/m^3)

Both external and internal mass transfer resistance exist for reactant travelling from bulk gas into porous structures of a catalyst pellet as shown in Figure 5-11. Reactants first transport from bulk flow to external surface of the catalyst pellet, and then diffuse further into the pores inside the pellet, with reaction taking place on the catalytic surface of the porous structures. Equation 5-14 was formulated for Sud-Chemie ShiftMax 230 that was ground and sieved to a particle diameter of 200 - 250 µm to eliminate internal diffusion resistance but allow good gas distribution [152]. Since the catalyst particle size used in this research project is significantly larger, e.g. 3000 – 5000 µm, and the internal diffusion needs to be considered when calculating actual reaction rate, an internal effectiveness factor (η) is introduced to correct the actual reaction rate of a catalytic reaction. η is defined by Equation 5-15 [154].

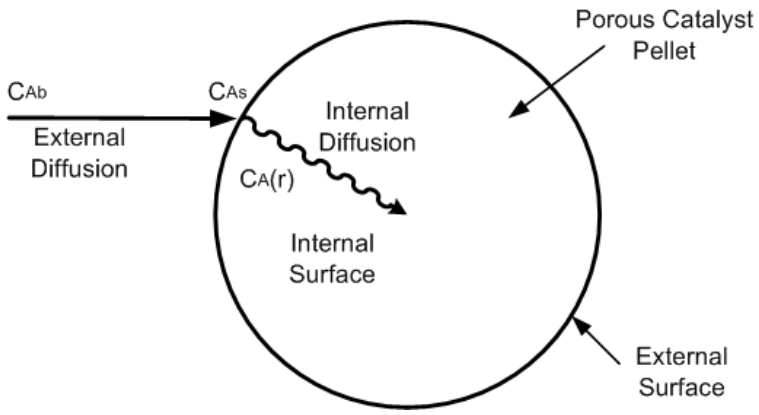

Figure 5-11 Mass transfer for a catalyst pellet

$$\eta = \frac{Actual\ overall\ rate\ of\ reaction}{\begin{matrix} Rate\ of\ reaction\ that\ would\ result\ if\ entire\ interior\ surface \\ were\ exposed\ to\ the\ external\ pellet\ surface\ conditions, C_{As}, T_s \end{matrix}} \quad \text{Equation 5-15}$$

where

C_{As} is the concentration at the external surface of the pellet

T_s is the temperature of the external surface of the pellet

According to Davis [155] for first order reactions, η for all pellet shapes can be expressed by Equation 5-16 as a function of Thiele modulus, ϕ.

$$\eta = \frac{tanh(\phi)}{\phi} \quad \text{Equation 5-16}$$

Thiele modulus, ϕ, is a dimensionless number, equals the ratio of the square root of the characteristic reaction rate and the characteristic diffusion rate. Figure 5-12 shows the dependence of η on ϕ. At small ϕ values, internal diffusion resistance is negligible; at large ϕ values, actual reaction rate is limited by internal diffusion. For cylindrical catalyst pellets as used in this study, ϕ is given by Equation 5-17 [155].

$$\phi = \frac{R_{pellet}}{\left(\frac{R_{pellet}}{x_{pellet}} + 2\right)}\sqrt{\frac{k}{D_{eff}}} \quad \text{Equation 5-17}$$

where

R_{pellet} is the radius of the pellet, m

x_{pellet} is half of the cylinder length, m

k is the rate constant of the first order reaction, 1/s

D_{eff} is effectiveness diffusivity, m^2/s.

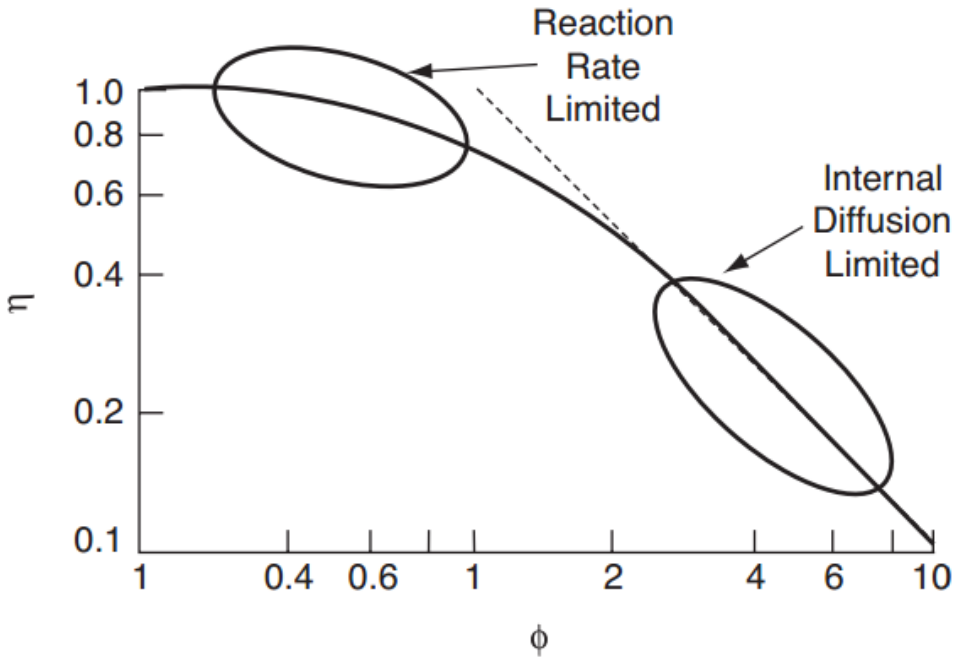

Figure 5-12 Dependence of $\boldsymbol{\eta}$ on $\boldsymbol{\phi}$ for first-order reactions (Source: [154])

For the LTS reaction combined with CO_2 capture, concentration of CO is significantly lower than H_2O by one order of magnitude. CO is the rate-controlling component of the reaction, and the WGS can be treated as a first-order reaction. To obtain the rate constant k for WGS, ideal gas law for both CO ($p_{CO} = RT\frac{N_{CO}}{V} = RTc_{CO}$) and CO_2 ($p_{CO_2} = RT\frac{N_{CO_2}}{V} = RTc_{CO_2}$) are incorporated into Equation 5-14:

$$r = 8.01 \times 10^{-6}\rho_{cat}exp(-\frac{47400}{RT})(RTP_{H_2O}c_{CO} - \frac{RTP_{H_2}c_{CO_2}}{K_{eq}}) \qquad \text{Equation 5-18}$$

$$r = 8.01 \times 10^{-6} RTP_{H_2O}\rho_{cat} exp(-\frac{47400}{RT})(c_{CO} - \frac{c_{CO_2}}{\frac{P_{H_2O}}{P_{H_2}}K_{eq}}) \quad \text{Equation 5-19}$$

where

N is number of moles, mole

V is volume, m^3

c is mole concentration, mol/m^3.

Due to constant volume shifting of WGS and carbon balance, c_{CO+CO_2} is constant. By rearrange Equation 5-19, a first-order reaction rate in terms of CO can be obtained:

$$r = 8.01 \times 10^{-6} RTP_{H_2O}\rho_{cat} exp(-\frac{47400}{RT})\left(1 + \frac{P_{H_2}}{P_{H_2O}K_{eq}}\right)(c_{CO} - \frac{P_{H_2}}{P_{H_2} + P_{H_2O}K_{eq}} c_{CO+CO_2}) \quad \text{Equation 5-20}$$

so that first-order rate constant k in Equation 5-17 is given by:

$$k = 8.01 \times 10^{-6} RTP_{H_2O}\rho_{cat} exp(-\frac{47400}{RT})\left(1 + \frac{P_{H_2}}{P_{H_2O}K_{eq}}\right) \quad \text{Equation 5-21}$$

To obtain ϕ in Equation 5-17, another parameter to be obtained is the effective diffusivity D_{eff}. The mean pore diameter of the catalyst pellets is of the order of the length scale of the molecular mean free path of the gas species, thus both ordinary

diffusion and Knudsen diffusion occur simultaneously. The diffusivity in porous media is given by [156]:

$$D_{1,eff} = \frac{\varepsilon}{\tau}\left(\frac{1}{D_{12}} + \frac{1}{D_{K1}}\right)^{-1} \qquad \text{Equation 5-22}$$

where

ε is the porosity of the porous catalyst pellet

τ is the tortuosity of the porous catalyst pellet

D_{12} is binary diffusivity, which can be estimated by Fuller Equation [157] as shown below (M_i is molecular weight of species i; $M_{12} = 2\left[\left(\frac{1}{M_1}\right) + \left(\frac{1}{M_2}\right)\right]^{-1}$ is mean molecular weight of species 1 and 2; $(\sum v)_i$ is the diffusion volume of species i):

$$D_{12} = \frac{0.00143T^{1.75}}{pM_{12}^{0.5}\left[(\sum v)_1^{\frac{1}{3}} + (\sum v)_2^{\frac{1}{3}}\right]^2} \qquad \text{Equation 5-23}$$

D_{K1} is Knudsen diffusivity. According to Kast [158] and Cunningham [156], D_{K1} can be given by the following equation (d_{pore} is the diameter of the pore structure; M_1 is molecular weight of species 1):

$$D_{K1} \approx 48.5 d_{pore}\left(\frac{T}{M_1}\right)^{0.5} \qquad \text{Equation 5-24}$$

5.2.4 Governing Equations

Both the sorbent reactor and the combined reactor (sorbent plus catalyst) consist of fixed beds and a CFD model using a porous media was employed to simulate the reactors. General governing equations of fluid dynamics modified for porous media model are discussed in this section.

Mass continuity equation for unsteady state flow in porous media is as following:

$$\frac{\partial \varepsilon_b \rho_f}{\partial t} + \nabla\left(\varepsilon_b \rho_f \vec{v}\right) = S_m \qquad \text{Equation 5-25}$$

where

ε_b is porosity of the fixed bed

ρ_f is gas density, kg/m^3

t is time, s

$\vec{v}$ is physical velocity vector, m/s

S_m is mass source term due to chemical reactions or other mass sources, e.g. gas adsorption or desorption, as shown by Equation 5-26. R_i is the production rate of species i by WGS reaction, S_i is the rate of adsorption/desorption of species i.

$$S_m = \sum (R_i + S_i) \qquad \text{Equation 5-26}$$

To predict local mass fraction of each species, Y_i, a species transport equation (Equation 5-27 and Equation 5-28) based on convection-diffusion for the i th species is employed. The first term on the left hand side of Equation 5-27is concentration change of i th species, the second is convection term, and the third is diffusion term. The right hand side is source term, which is composed of reaction production and species adsorption or desorption as shown by Equation 5-28.

$$\frac{\partial\left(\varepsilon_b \rho_f Y_i\right)}{\partial t} + \nabla\left(\varepsilon_b \rho_f \vec{v} Y_i\right) - \nabla\left(\varepsilon_b \rho_f D_{i,m} \nabla Y_i + \varepsilon_b D_{T,i} \frac{\nabla T}{T}\right) = S_i \qquad \text{Equation 5-27}$$

$$S_i = R_i - MW_i \rho_b \frac{\partial q_i}{\partial t} \qquad \text{Equation 5-28}$$

where

Y_i is mass fraction of species i

$D_{i,m}$ is the mass diffusion coefficient for species i in the mixture, m^2/s

$D_{T,i}$ is the thermal diffusion coefficient, m^2/s

S_i is source term of species i

R_i is source term of species i due to reactions

MW_i is molar mass of species i, kg/kmol

ρ_b is density of the bed, kg/m^3

ε_b is porosity of the bed

q_i is the amount of adsorption of species i, kmol/kg.

In porous media model, a momentum sink is added to the general momentum equation. Momentum equation is expressed by Equation 5-29.

$$\frac{\partial(\varepsilon_b \rho_f \vec{v})}{\partial t} + \nabla(\varepsilon_b \rho_f \vec{v}\vec{v}) = -\varepsilon_b \nabla p + \nabla(\varepsilon_b \bar{\bar{\tau}}) + \varepsilon_b \rho_f \vec{g} + \vec{S} \qquad \text{Equation 5-29}$$

where

p is the static pressure, pa

$\bar{\bar{\tau}}$ is the stress tensor, pa

$\rho_f \vec{g}$ is gravitational body force, kg/m^2/s^2

$\vec{S}$ is the momentum source term, consisting of a viscous loss term (the first term on the right hand side) and inertial loss term (the second term on the right hand side), as shown by Equation 5-30.

$$\vec{S} = -\mu \frac{\vec{v}}{\alpha} - C_2 \frac{1}{2} \rho_f |\vec{v}| \vec{v} \qquad \text{Equation 5-30}$$

Ergun Equation (Equation 5-31) is applied to calculate pressure drop through the fixed bed:

$$\Delta p = \frac{150\mu(1-\varepsilon)^2 V_s L}{\varepsilon^3 D_p^2} + \frac{1.75(1-\epsilon)\rho_f v_s^2 L}{\varepsilon^3 D_p} \qquad \text{Equation 5-31}$$

where

α is viscous resistant coefficient, given by:

$$\alpha = \frac{D_p^2 \varepsilon^3}{150(1-\varepsilon)^2} \qquad \text{Equation 5-32}$$

C_2 is inertia resistance, given by:

$$C_2 = \frac{1.75(1-\varepsilon)}{D_p \varepsilon^3} \qquad \text{Equation 5-33}$$

μ is dynamic viscosity of the fluid, N s/m^2

v_s is superficial velocity, m/s

L is length of the bed, m

D_p is diameter of the packing, m.

As assumed previously, the porous media and fluid flow are in thermal equilibrium. The conduction flux in the porous medium uses an effective conductivity and the transient term includes the thermal inertia of the solid region on the medium. Energy transport equation can be written as:

$$\frac{\partial}{\partial \mathrm{t}}\left(\varepsilon_b \rho_f E_f + (1-\varepsilon_b)\rho_b E_s\right) + \nabla\left(\vec{v}\left(\rho_f E_f + p\right)\right) = \nabla\left[k_{eff}\nabla T - \left(\sum_i h_i J_i\right) + (\bar{\bar{\tau}}\vec{v})\right] + S_f^h \qquad \text{Equation 5-34}$$

where

E_f is total fluid energy, J/kg

E_s is total solid medium energy, J/kg

k_{eff} effective thermal conductivity of the medium, W/m/K

$S_f^h = \sum H_R + \rho_b \sum \Delta H_i \frac{\partial q_i}{\partial t}$, which is fluid enthalpy source term

$\Delta H_{CO_2} = -20501.6\ kj/kmol\ co_2$ for adsorption or $\Delta H_{CO_2} = 17991.2\ kj/kmol\ co_2$ for desorption.

5.2.5 Model Formulation

5.2.5.1 Model Configuration

The fixed bed for CO_2 capture alone and fixed bed reactor for combined WGS and CO_2 capture are of both cylindrical geometry, with flow entering evenly from bottom side and exiting at the top side during adsorption step, and entering from top side and exiting at the bottom side during desorption step. Two dimensional (2-D) axisymmetric CFD models were developed to simulate the cycles of adsorption and desorption steps. Figure 5-13 shows a schematic of the reactor geometry and a 2-D axisymmetric calculation domain, and both CO_2 capture alone reactor and combined reactor for WGS and CO_2 capture share the same bed configuration.

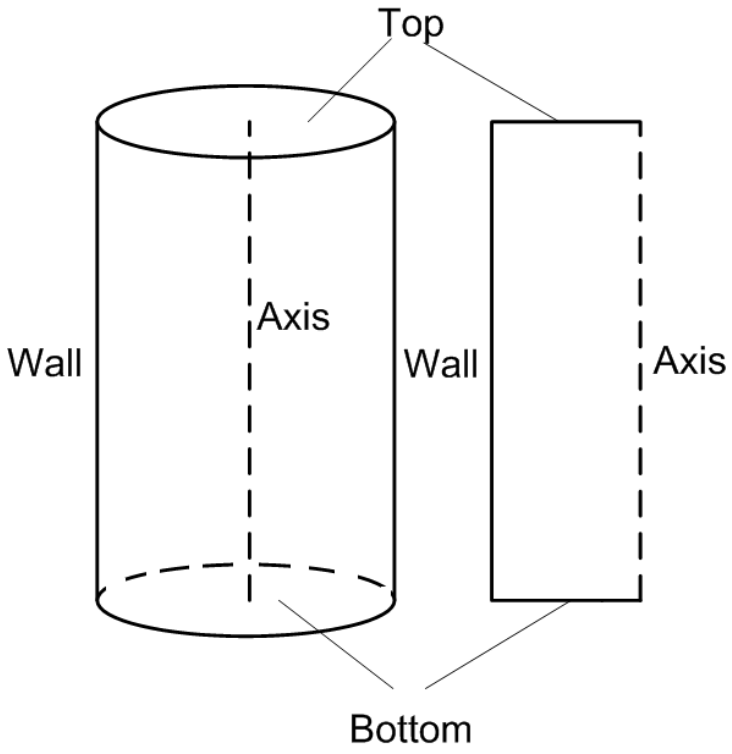

Figure 5-13 Schematic of fixed bed reactors

5.2.5.2 Mesh Generation

Due to relatively simple reactor geometry, meshes of quadrilateral cells have been considered, with higher mesh density at the wall surface (part of the mesh can be seen in Figure 5-14). Mesh sensitivity study was conducted to determine a suitable mesh size considering both computational time and accuracy of results. Details of mesh sensitivity study are discussed in Section 5.3.

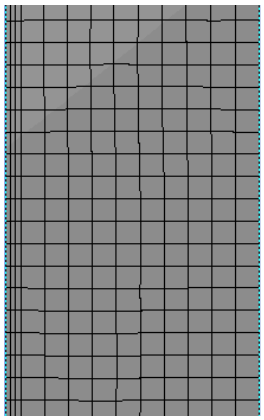

Figure 5-14 Snapshot of 2 dimensional CFD mesh

5.2.5.3 Other Features of the Model

The physical models of CO_2 adsorption and desorption are incorporated into the simulation by user defined functions (UDF). For combined reactor, WGS reaction rate is incorporated into ANSYS as volumetric reaction rate by UDF.

Some other features of the model are:

1. Laminar flow.
2. Pressure based solver SIMPLE algorithm.
3. Second order upwind as discretization scheme.
4. First order implicit scheme for transient formulation.
5. Mass diffusivity and thermal diffusion coefficient of gases are calculated by kinetic theory.
6. Specific heats of gases are calculated by mixing law.
7. Thermal conductivity and viscosity are calculated by ideal gas mixing law.

5.3 CFD Model Validation

Demonstration (demo) fixed bed reactors for CO_2 sorption/desorption and combined WGS reaction and CO_2 sorption were tested by TDA. The experimental data collected were utilized to validate the CFD models.

5.3.1 Experimental Setup and Testing Procedure

Figure 5-15 shows the geometry of a demo test reactor bed. Thermocouples were installed at three positions: bottom, middle and top, to measure and monitor the bed temperatures. Field tests were conducted by TDA for multi reactor beds in cyclic operations on syngas at National Carbon Capture Center (NCCC) and Wabash River IGCC. Figure 5-16 and Figure 5-17 show the field test units.

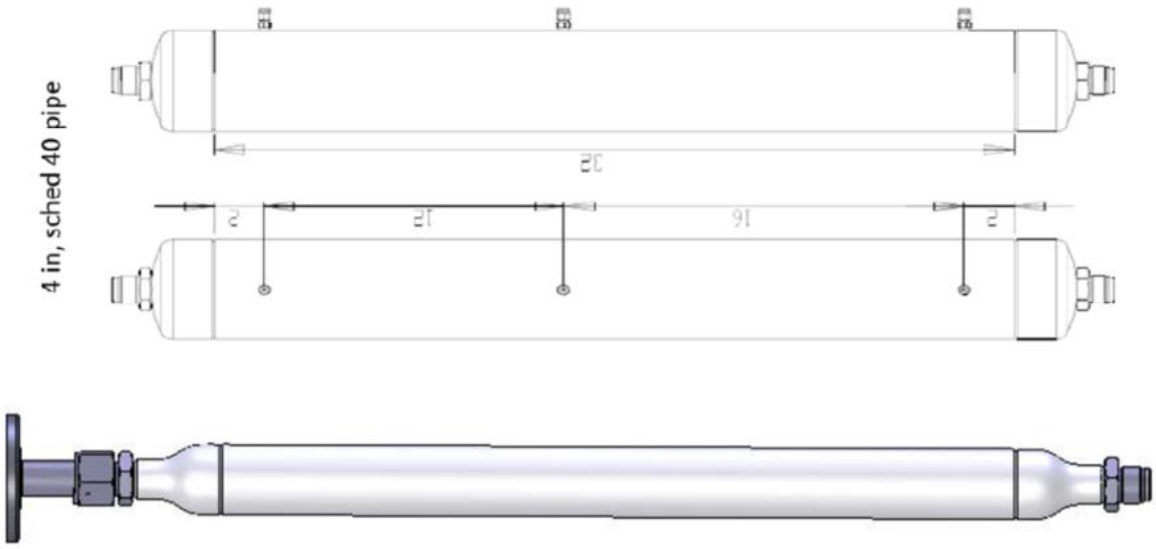

Figure 5-15 Geometry of a demo reactor

Figure 5-16 Field test units installed at NCCC

Figure 5-17 Field test units installed at Wabash River IGCC

For both CO_2 capture alone reactor and combined reactor for WGS and CO_2 capture, multiple reactor beds, connected by manifolds, were operated in cycles, with each bed operating in different PSA phase. The sequence of a 3-bed PSA operation for instance, is shown in Figure 5-18 and operation of one single bed is depicted by Figure 5-19. Taking Bed 1 for example to illustrate one cycle of a single bed, adsorption step (ADS) works under high pressure with syngas entering the reactor bed from the bottom, CO_2 is absorbed within the bed, and decarbonized syngas exits at the reactor top (in the combined reactor, CO is converted to CO_2 while CO_2 is adsorbed). At the end of adsorption step, valves are opened in the manifolding to connect the top of Bed 1 to top of bed Bed 3, which has completed its purge step at low pressure, while keeping inlet to Bed 1 closed at the bottom, so that Bed 1 goes through depressurization equalization step (EQ1) to descrease pressure of the bed to a medium level. The pressure of Bed 1 further decreased by blowing down (BD) of the remaining gases in the bed from top to bottom, with the bed outlet at the top closed. Next step is purge or sorbent regeneration in which at certain low pressure, inert gas (steam or N_2) flows from top to bottom and the CO_2 trapped in the sorbent is released. Next, Bed 1 goes through a pressurization equalization (EQ2) step accomplished by connecting with Bed 2 which has just undergone the adsorption step at high pressure. After a hold step to match phases of different beds, Bed 1 is pressurized to high pressure by blowing decarbonized syngas into the bed from the top while keeping the bed bottom closed.

Bed 1	ADS			EQ1	BD	PURGE	EQ2	HOLD	PRESS
Bed 2	EQ2	HOLD	PRESS	ADS			EQ1	BD	PURGE
Bed 3	EQ1	BD	PURGE	EQ2	HOLD	PRESS	ADS		

Figure 5-18 Sequence of a three-bed PSA operation

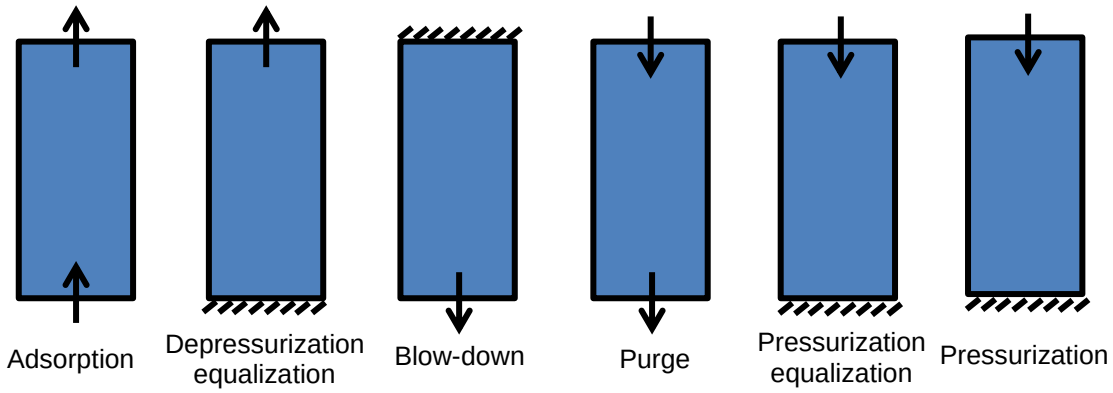

Figure 5-19 PSA cycle scheme of a single fixed bed of combined WGS and CO_2 capture

5.3.2 Boundary Conditions

Boundary conditions for each step are summarized in Table 5-7:

Table 5-7 Summary of boundary conditions

Step	Top	Bottom
Adsorption	Pressure outlet	Mass flow inlet
Depressurization equalization	Pressure outlet	Wall
Blow-down	Wall	Pressure outlet
Purge	Mass flow inlet	Pressure outlet
Pressurization equalization	Pressure inlet	Wall
Pressurization	Pressure inlet	Wall

The pressure boundary condition was assumed to follow the expression below:

$$p(t) = p_{final} + (p_{initial} - p_{final}) exp\left(\frac{-t}{0.25 t_{step}}\right) \qquad \text{Equation 5-35}$$

where

p_{final} is the pressure at the end of the process step

$p_{initial}$ is the pressure at the beginning of the process step

t_{step} is the duration of the process step

5.3.3 Mesh Sensitivity Study

For both fixed bed reactor for CO_2 capture alone and combined fixed bed reactor for WGS and CO_2 capture, knowledge of the CO_2 breakthrough curve at bed exit is critical, which determines the operating time, percentage of CO_2 captured and size of reactor. CO_2 breakthrough was selected as a criterion for mesh sensitivity study. Various mesh sizes were evaluated for the simulation of the adsorption process of the demo reactor for CO_2 capture alone. For a 2 dimensional CFD model, four mesh numbers (100, 400, 800 and 1300) were evaluated and the dependence of simulated CO_2 breakthrough curve and tested CO_2 breakthrough are presented in Figure 5-20. The simulation result with mesh number 100 is slightly off the experimental CO_2 breakthrough curve between 260 sec and 300 sec, whereas predictions of mesh numbers of 400, 800 and 1300 have a good agreement with experimental data.

The 400-mesh, 800-mesh and 1300-mesh cases were further compared with a case of much finer meshes (10000) on velocity contour. All of the simulations show a similar plug-flow pattern as shown by Figure 5-21 but the 800-mesh was selected since it shows a slight improvement over the 400-mesh. For simulations of demo reactor bed for combined WGS and CO_2 capture and simulation of commercial size beds (for both CO_2 capture alone and combined WGS and CO_2 capture), similar sensitivity studies were conducted to choose suitable mesh sizes.

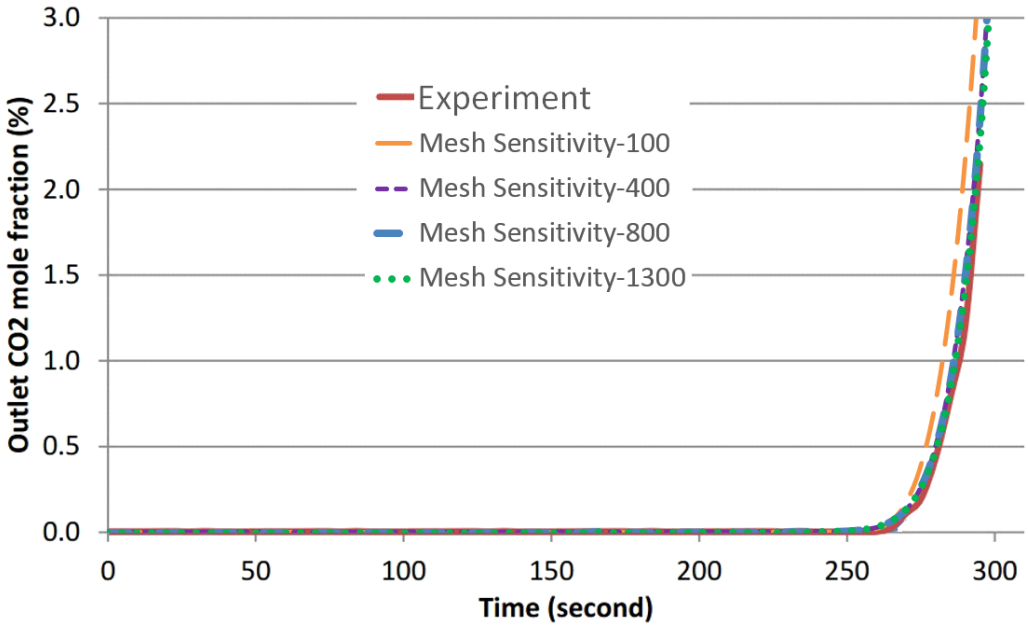

Figure 5-20 Mesh sensitivity on CO_2 breakthrough curve

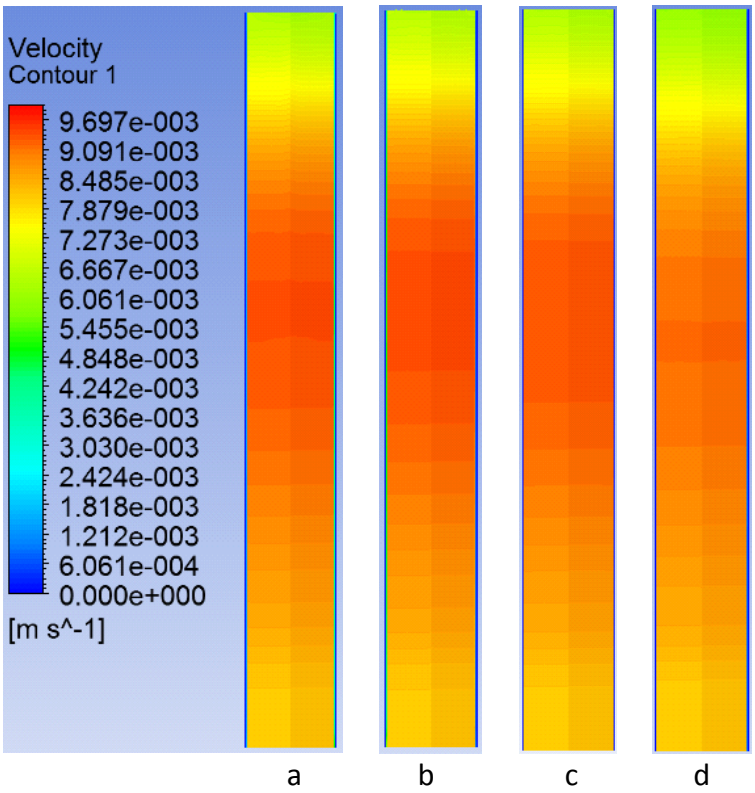

Figure 5-21 Mesh sensitivity on velocity contour (a is 400-mesh, b is 800-mesh, c is 1300-mesh, d is 10000-mesh)

5.3.4 Validation of CO_2 Adsorption

Porosity (or voidage) ϕ is the fraction of bulk volume of the porous media that is occupied by pores or void space [159]. Within a fixed bed reactor packed with porous solid sorbent, two types of porosity are identified. One is bed porosity ϕ_{bed}, which is the fraction of bulk volume of the bed that is not occupied by sorbent particles; the other is sorbent particle porosity $\phi_{particle}$, which is the fraction of bulk volume of a single solid sorbent particle that is occupied by pore space. Combining both bed porosity and particle porosity results in the nominal total porosity ϕ_{total} as given by Equation 5-36. Porosity is a critical parameter for a porous media fixed bed which affects the flow

pattern in a reactor. For the demo bed with fixed bed density, rates of CO_2 adsorption and desorption are affected by the interaction between fluid mechanics and the physical process of adsorption/desorption, which effect CO_2 breakthrough time. CO_2 breakthrough time determines the operating time for the adsorption step, percentage of CO_2 remaining in clean syngas, and size of reactor for a given flow rate of un-decarbonized syngas. Porous media model of ANSYS Fluent is employed to simulate the porous fixed bed reactor. However, only a single effective total porosity can be identified in ANSYS, without distinguishing bed porosity and particle porosity. Due to viscous and film effects on particle and pore surfaces, the effective total porosity will be lower than the nominal total porosity. Using the nominal total porosity as effective total porosity would artificially increase CO_2 breakthrough time.

$$\phi_{total} = \phi_{bed} + \phi_{particle}(1 - \phi_{bed}) \qquad \text{Equation 5-36}$$

Table 5-8 shows parameters of the demo bed column for CO_2 capture alone tested at Wabash River IGCC, including porosities and bed density. The nominal total porosity of the bed was 0.699 calculated from Equation 5-36. CO_2 breakthrough test was conducted for 300 seconds on a single demo bed with fresh solid sorbent. Four effective total porosities were evaluated in the CFD simulation and both experimental data and simulation results of CO_2 breakthrough are presented by Figure 5-22. As expected, nominal total porosity of 0.699 led to larger CO_2 breakthrough time than test result. A larger effective total porosity value of 0.8 resulted in even longer CO_2 breakthrough time. The CO_2 breakthrough curve with porosity of 0.6 matched the experimental data

well with CO_2 breakthroughs occurring at around 260 second. With smaller effective porosity, e.g. 0.4, since volume occupied by or available to gas, which is the volume of voids in the porous bed, is lower, the actual gas velocity is larger for a given superficial velocity and so the CO_2 reaches the bed exit or breaks through the bed faster. The effective porosity of 0.6 as validated by the experimental CO_2 breakthrough curve is selected for CFD simulations. Empirical fitting of porosity implies that any deviation of kb from Darken's equation is also included in this fitted porosity value.

Table 5-8 Parameters of demo bed column

Column Parameters	
Bed Porosity (ϕ_{bed})	0.3
Sorbent Particle Porosity ($\phi_{particle}$)	0.57
Nominal Total Porosity (ϕ_{total})	0.699
Density of Bed, kg/m^3	354

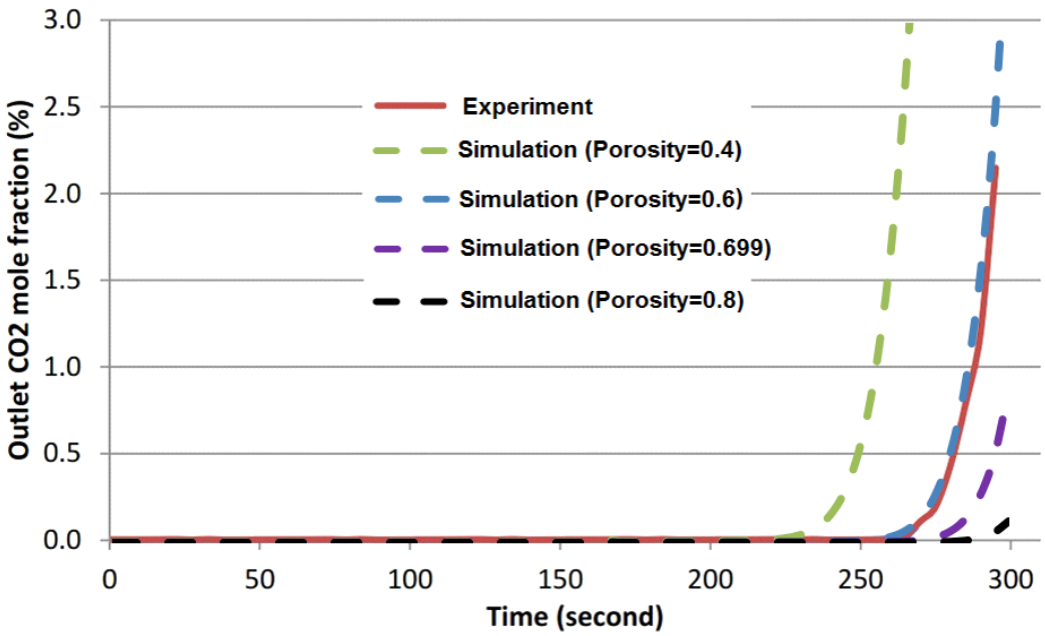

Figure 5-22 CO_2 breakthrough of an adsorption alone fixed bed

In the adsorption step, heat is released while CO_2 is absorbed; in desorption step, heat is required to activate CO_2 release from the loaded sorbent. Thermal management of the bed is important to maintain the bed in a preferred temperature range. By precisely predicting temperature distribution, an appropriate thermal strategy could be determined.

Since, in practice the fixed bed reactor operates in cycles, the thermal distribution eventually reaches a dynamic equilibrium for each step. To make the simulation effective, thermal validation was done by assuming a parabolic shape initial temperature distribution of an adsorption step, which matched the temperature measurements at three thermocouple locations (top, middle and bottom) at the beginning of the step. Temperature evolution over 180 seconds' adsorption time at three thermocouple locations is presented by Figure 5-23 for both experiments and simulations. CFD simulations can capture the temperature trends over time. The flow pattern in fixed bed is basically plug flow, syngas flows in from the bed bottom and the CO_2 adsorption front moves upwards. It can be clearly seen for the bottom temperature evolution that temperature increases as CO_2 gets adsorbed, and when saturated with CO_2 it starts to be cool down by incoming syngas. Since CO_2 saturation moves from bottom to top, there is a delay in temperature rise at the middle of the bed. By observing the CO_2 loading distribution, it may be inferred that the sorbent is not fully utilized at the top of the bed due to the axial mass transfer effect (due to bulk flow of syngas containing CO_2 in the axial direction) with CO_2 breakthrough occurring. Temperature increase at the bed top is caused by heat migration from upstream to

downstream. Due to column external heating and inaccuracy caused by thermal equilibrium assumptions, the difference between CFD simulation and experimental results was deemed acceptable.

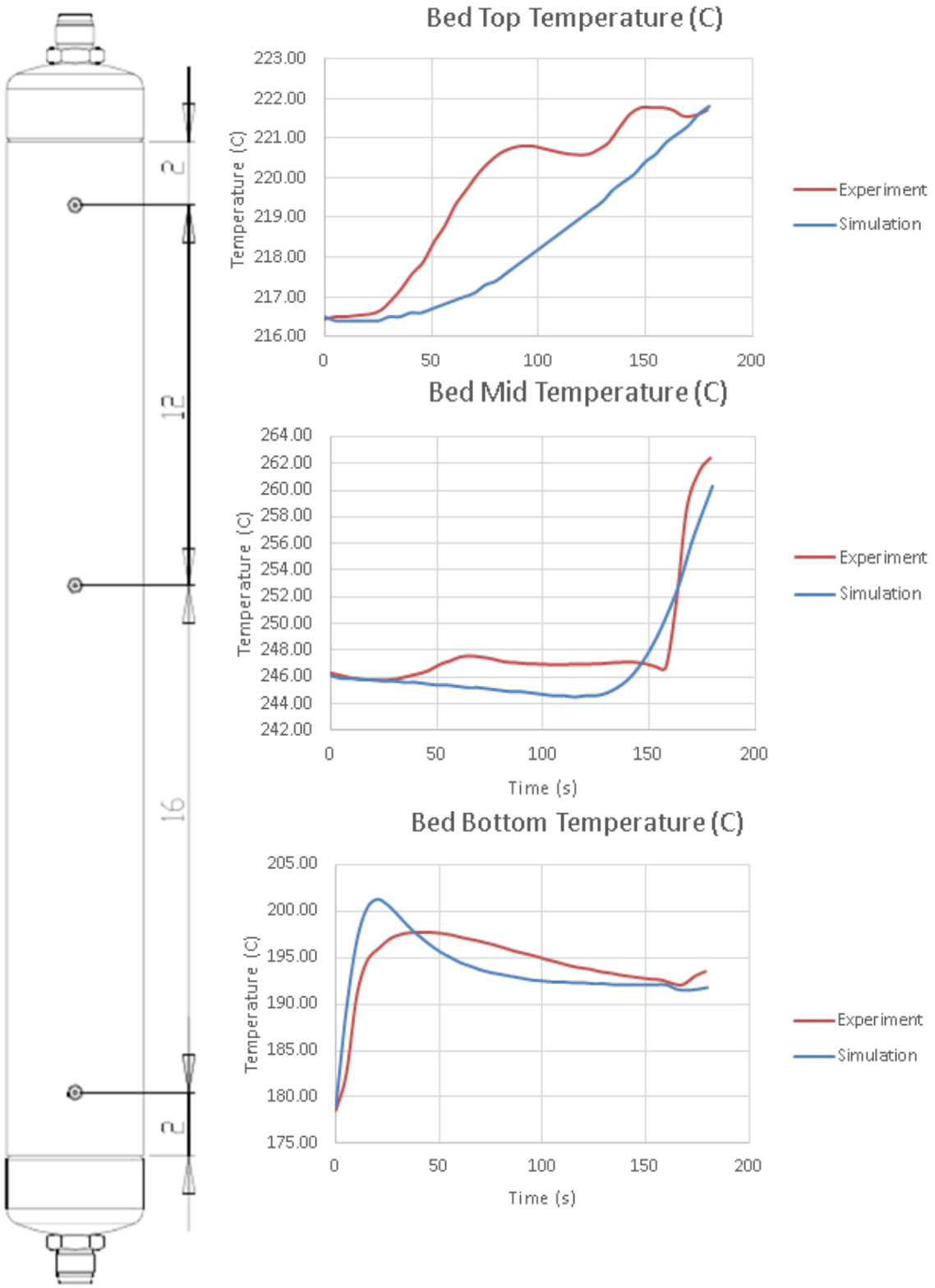

Figure 5-23 Temperature validation of an adsorption alone fixed bed

The 6-step process was simulated for a single bed reactor for a number of cycles, starting with adsorption in a bed packed with fresh sorbent till steady state was reached. The fifth cycle appeared to reach a steady state because the composition distribution was the same as that of the forth cycle for each of the steps. Figure 5-24 and Figure 5-25 show CO_2 distribution and CO_2 loading in the sorbent, respectively for the adsorption step. Because the sorbents are not fully regenerated during the last cyclic run, before the adsorption step starts, a small amount of CO_2 remains at the bottom of the bed. Syngas enters the bed from the bottom, and while CO_2 starts to be absorbed by the sorbents. The real flow pattern is not plug flow. CO_2 adsorption rate is lower than the CO_2 flow rate or axial mass transfer (due to bulk flow of syngas containing CO_2 in the axial direction), resulting in CO_2 remaining in the gas downstream of the saturated sorbent. Thus, when CO_2 breaks through at bed exit, the bed is not fully loaded with CO_2. Therefore, adsorption rate is the control step for CO_2 capture. Figure 5-26 shows the CO_2 loading along the axis of the bed at the end of adsorption step, at the end of desorption step, as well as the CO_2 loading at saturation if the overall bed is under the same CO_2 partial pressure as bed inlet conditions. At the end of adsorption step, around 50% of the total CO_2 loading potential is used up. To fully utilize the sorbent bed's CO_2 adsorption capability with practical cycle time, a tradeoff between CO_2 loading capacity and quantity of the sorbent is required.

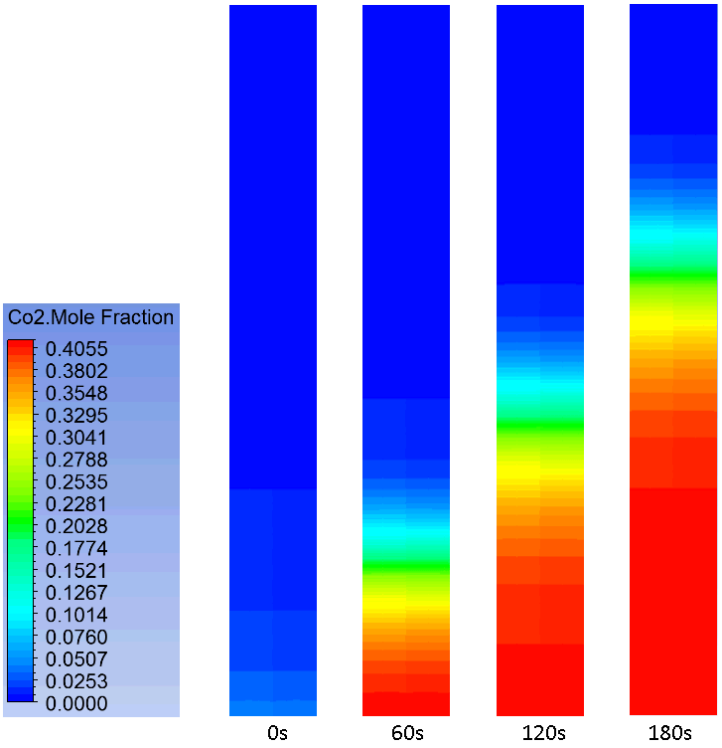

Figure 5-24 CO_2 distribution of adsorption step (5th cycle) for CO_2 capture alone

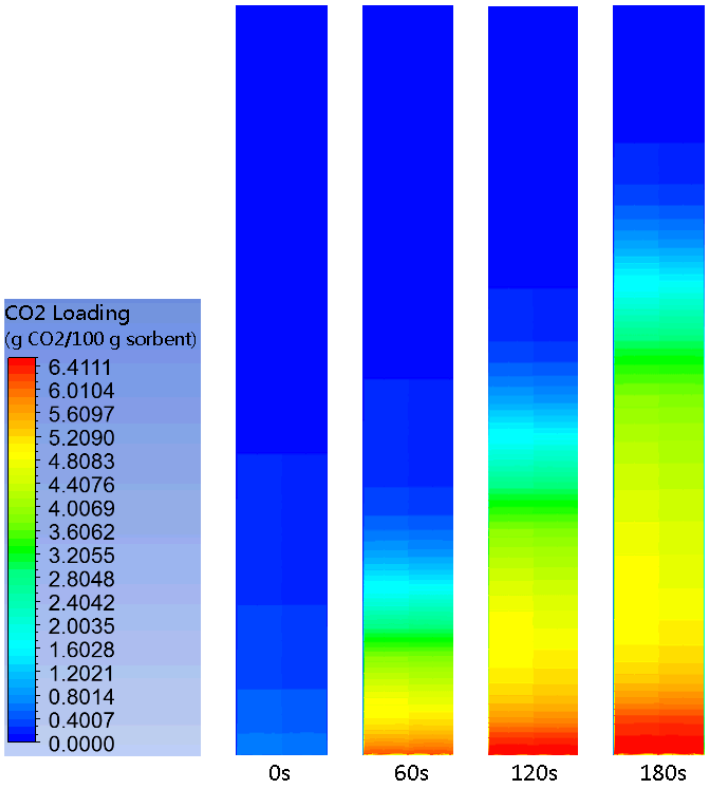

Figure 5-25 CO_2 loading of adsorption step (5th cycle) for CO_2 capture alone

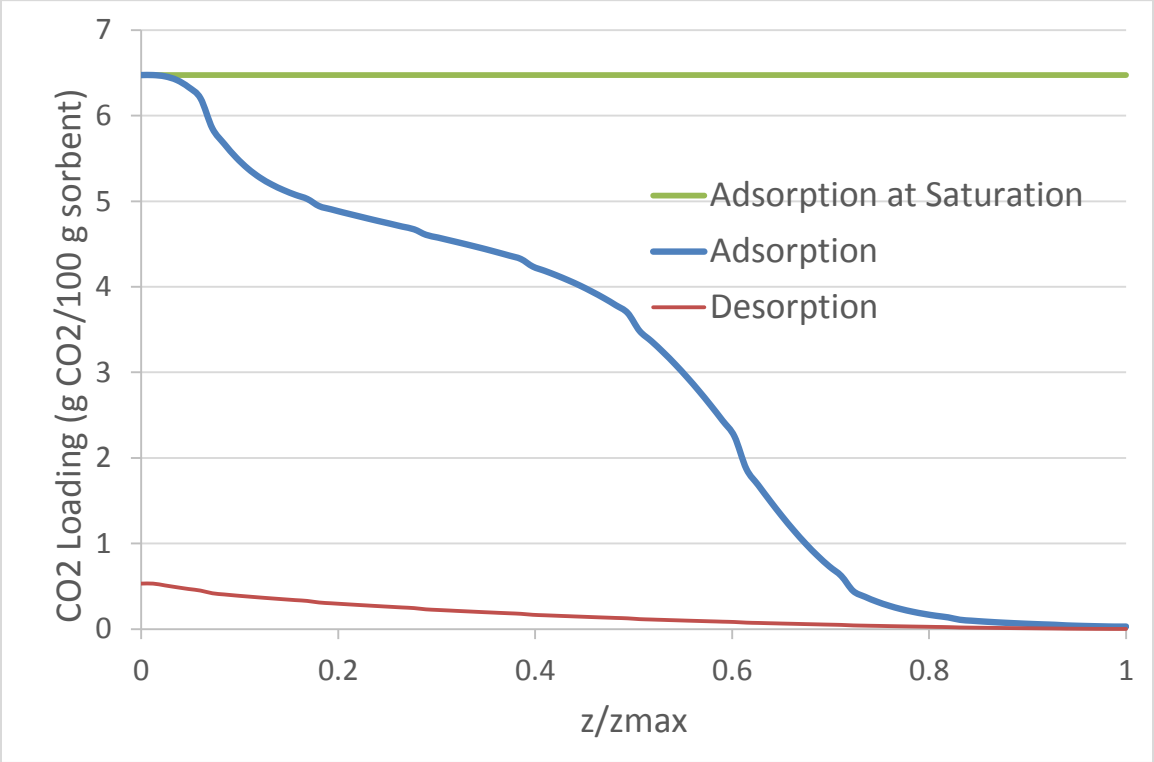

Figure 5-26 CO_2 loading along axis of the bed (5^{th} cycle) for CO_2 capture alone

Figure 5-27 and Figure 5-28 show the CO_2 distribution and CO_2 loading in sorbent, respectively, for purge step. Recall that depressurization equalization step and blow-down step follow adsorption step before purge step. Some of the CO_2 is released and blown out of the bed during depressurization equalization and blow-down processes; thus at the beginning of the purge step, CO_2 loading is smaller than that at the end of adsorption step. When steam purges the bed from top to bottom, more CO_2 is released from the sorbent. However, the bed sorbent is not fully regenerated at the end of the purge as we can see from the last CO_2 loading contour in Figure 5-28. The curve in red in

Figure 5-26 shows that CO_2 loading along the axis at the end of purge process. Around 93% of the total CO_2 loading is released when purged with steam for sorbent regeneration, while the remaining 7% of the CO_2 stays in the sorbent. A longer purge time or higher steam flow rate would be beneficial to release the CO_2 residual. Higher steam flow rate, however, reduces the steam available for power generation.

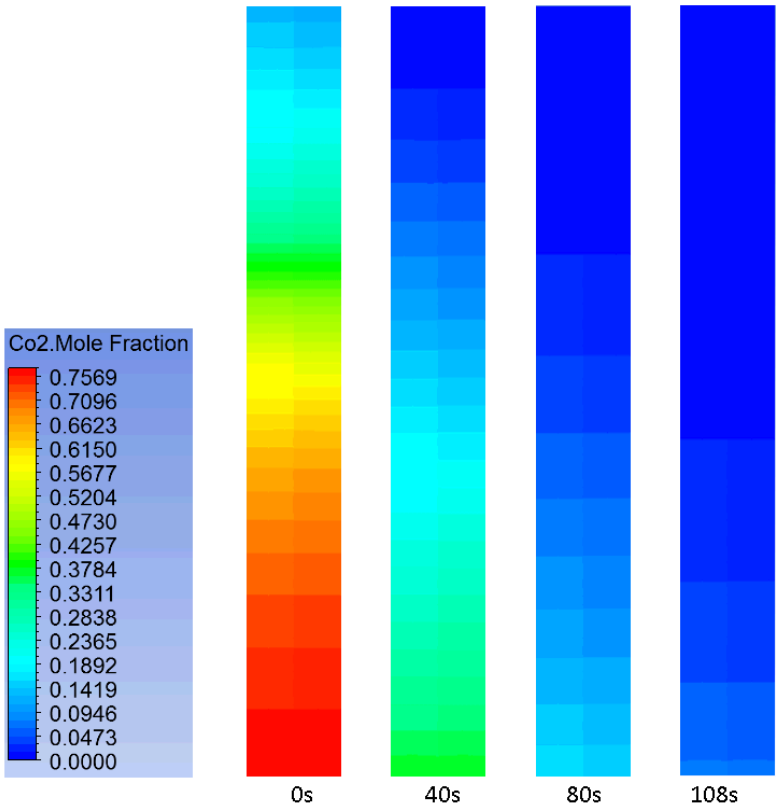

Figure 5-27 CO_2 Distribution of purge step (5^{th} cycle) for CO_2 capture alone

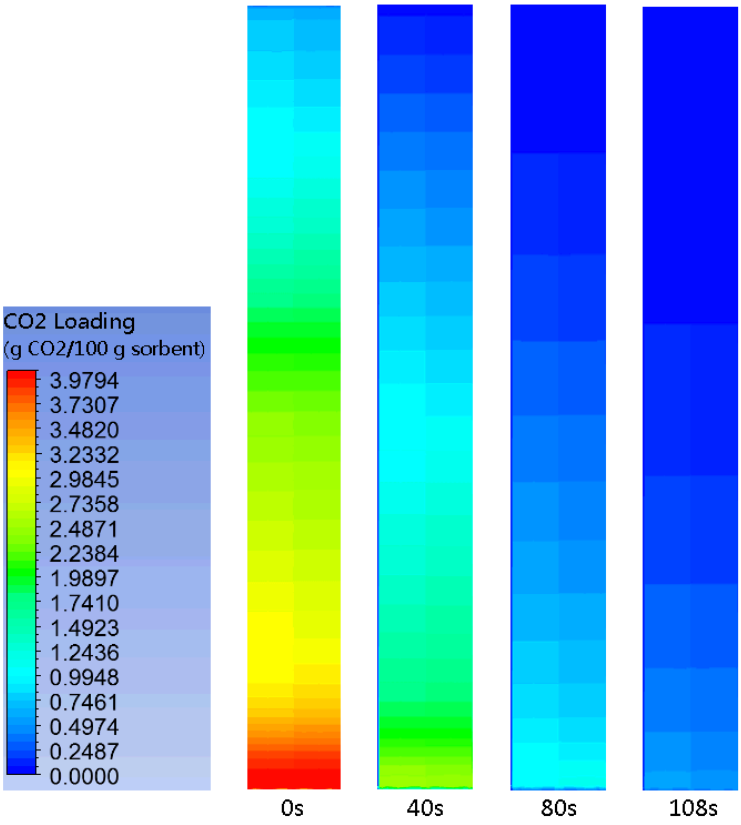

Figure 5-28 CO_2 loading of purge step (5th cycle) for CO_2 capture alone

5.3.5 Validation of Combined WGS and CO_2 Capture

For the simulation of the demo reactor bed of combined WGS and CO_2 capture, effective total porosity is kept at 0.6 to be consistent with the simulation of CO_2 capture alone process. Plots of CO_2 breakthrough are presented in Figure 5-29 for both test and simulation. It shows that despite the inaccuracy of the test data collected (as the curve representing the experimental data is not smooth), simulation can basically predict the CO_2 break through curve. As shown by Figure 5-30, the simulation results can match quite well with the experimental measurements of temperature at both the top and in the middle of the bed. At the bottom thermocouple location, the simulation prediction

follows the same temperature trend as the experimental data. Because of heat addition from the reactor walls in the experimental unit, the temperature rise is steeper than simulation results where the walls were assumed adiabatic.

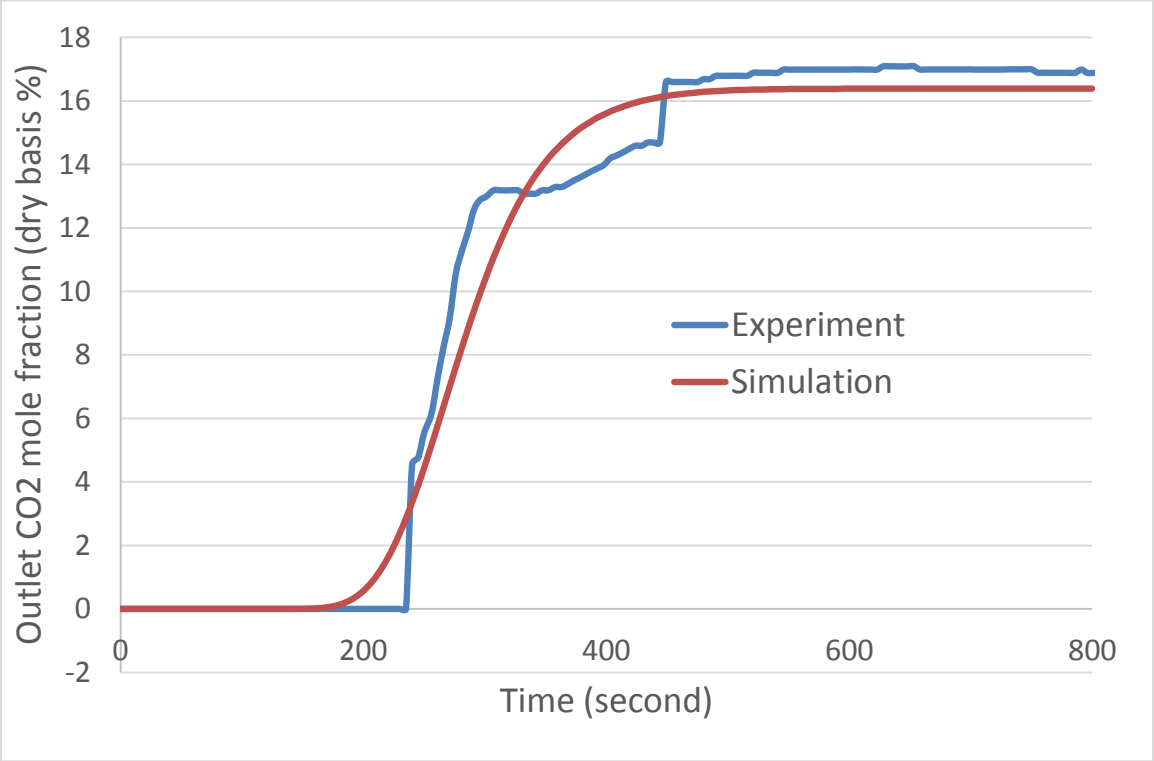

Figure 5-29 CO_2 breakthrough of a fixed bed of combined WGS and CO_2 capture

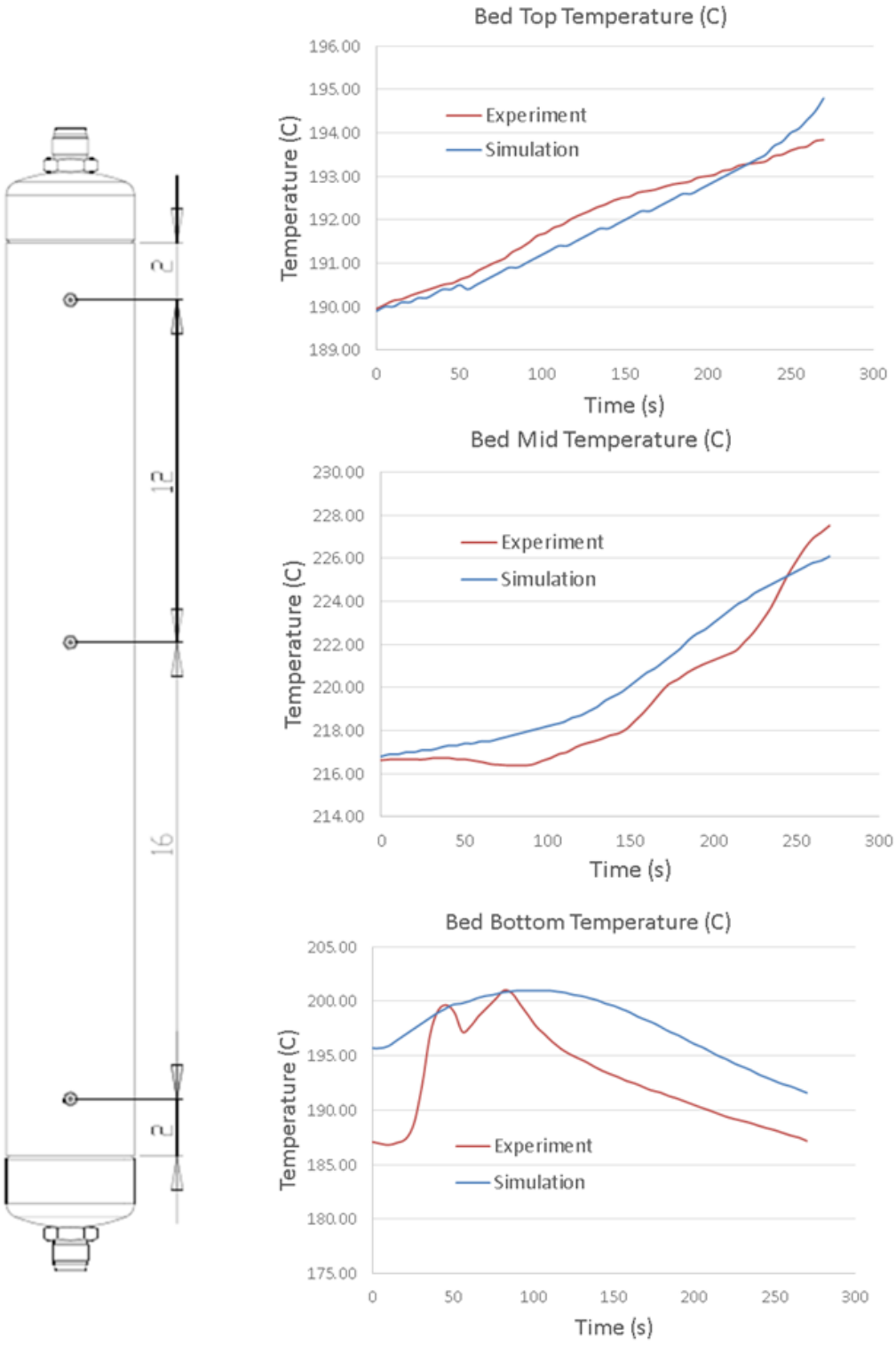

Figure 5-30 Temperature validation of a fixed bed of combined WGS and adsorption

During combined WGS and CO_2 capture tests, the demo bed temperature was maintained above 200C, so that WGS reaction remained active for all 6 steps. Figure 5-31 shows a typical contour of kinetic rate of WGS reaction during the adsorption step. Unconverted syngas containing CO enters the bed from bottom. Conversion of CO into CO_2 by the WGS reaction occurs almost immediately as the syngas comes into contact with the catalyst. It can be seen from the CO_2 distribution contour (Figure 5-32) that a jump in CO_2 mole fraction occurs at the lower interface between the sorbent alone zone and the combined catalyst and sorbent mixed zone. CO_2 loading correspondingly increases due to higher CO_2 partial pressure as shown in Figure 5-33.

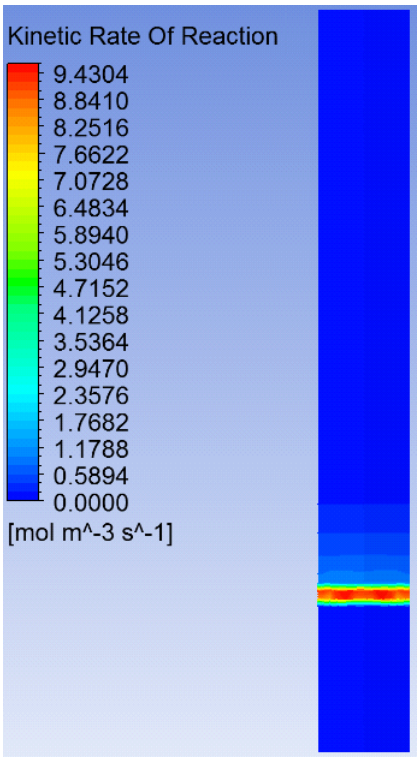

Figure 5-31 Kinetic rate of WGS reaction for adsorption step (100^{th} s)

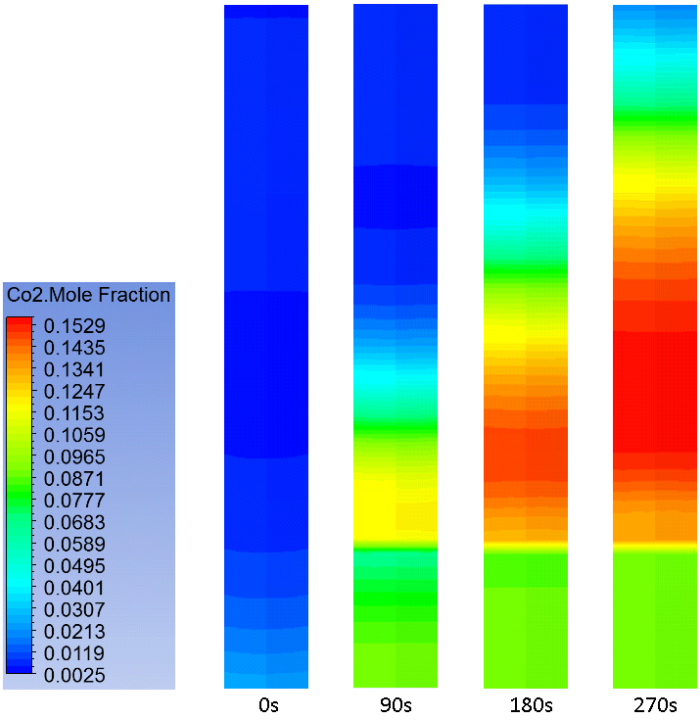

Figure 5-32 CO_2 Distribution of adsorption step (5th cycle) for combined WGS and CO_2 capture

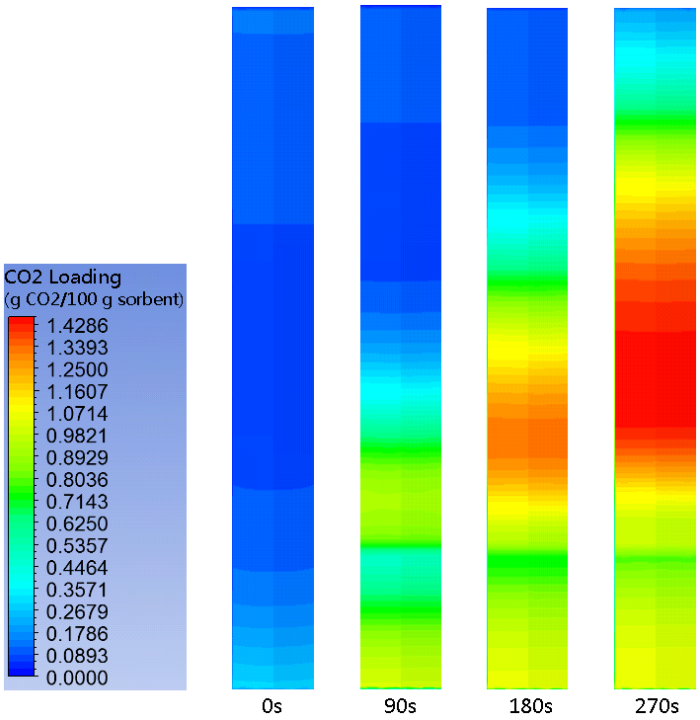

Figure 5-33 CO_2 loading of adsorption step (5th cycle) for combined WGS and CO_2 capture

Figure 5-34 and Figure 5-35 show the CO_2 distribution and CO_2 loading during the purge step for combined WGS and CO_2 capture. At the end of purge step, a small amount of CO_2 remains loaded in the sorbents. It is quantitatively presented by Figure 5-36, around 10% of the loaded CO_2 remains in the sorbent.

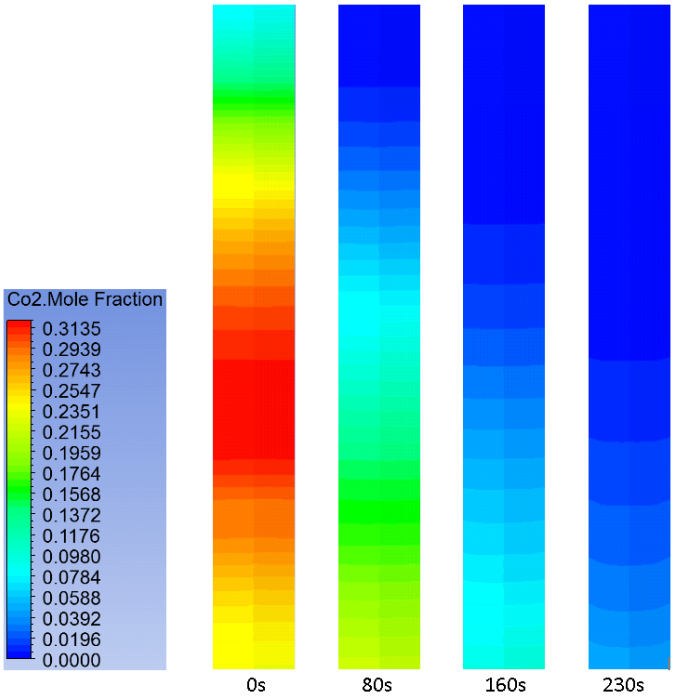

Figure 5-34 CO_2 distribution of purge step (5^{th} cycle) for combined WGS and CO_2 capture

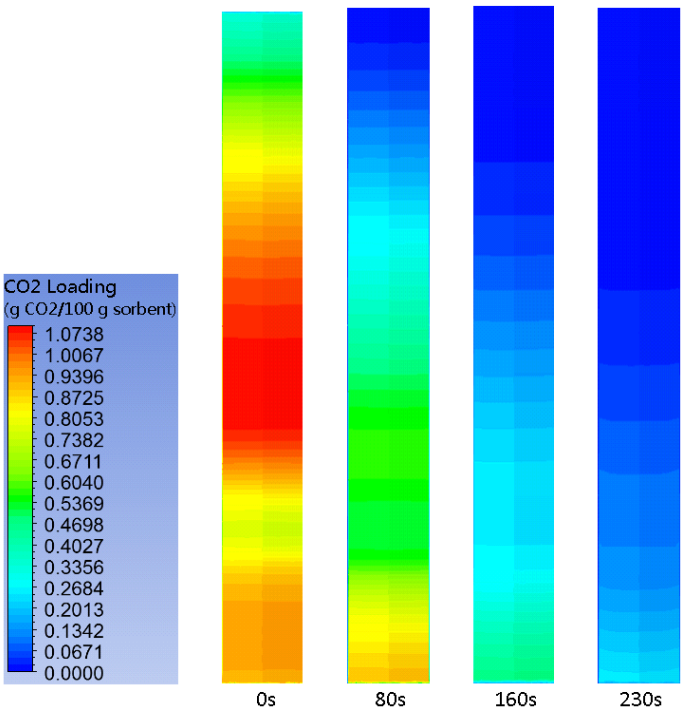

Figure 5-35 CO_2 loading of purge step (5th cycle) for combined WGS and CO_2 capture

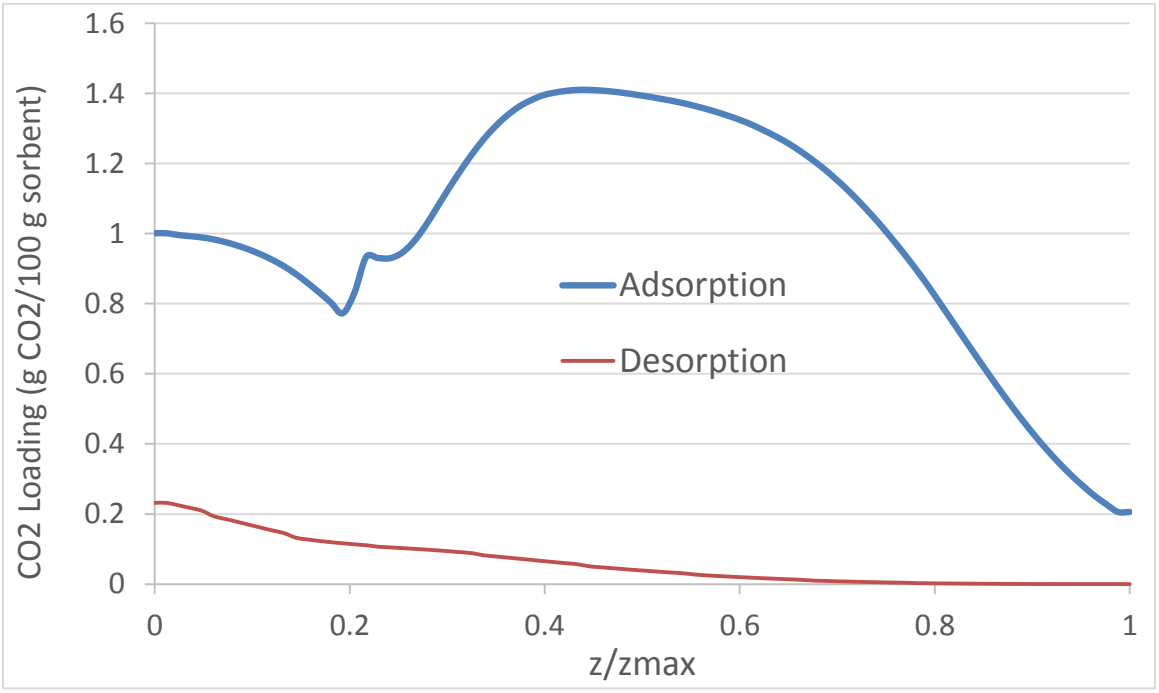

Figure 5-36 CO_2 loading at the end of adsorption and the end of desorption steps (5th cycle) for combined WGS and CO_2 capture

Heat generation by the exothermic WGS reaction is illustrated by temperature contour shown in Figure 5-37. The CFD simulation results show that a significant increase in temperature occurs near the bottom region of the combined catalyst and sorbent mixed zone because majority of the reaction occurs over a small region as the unconverted syngas reaches the WGS catalyst. The temperature of 390C predicted by the model is much higher than 250C, the LTS catalyst's upper temperature limit and sustained operation over long periods of time would deactivate the catalyst. Thus this high temperature zone should be avoided in the commercial reactor design, and cooling strategies are investigated to keep the temperatures lower to protect both catalyst and sorbent.

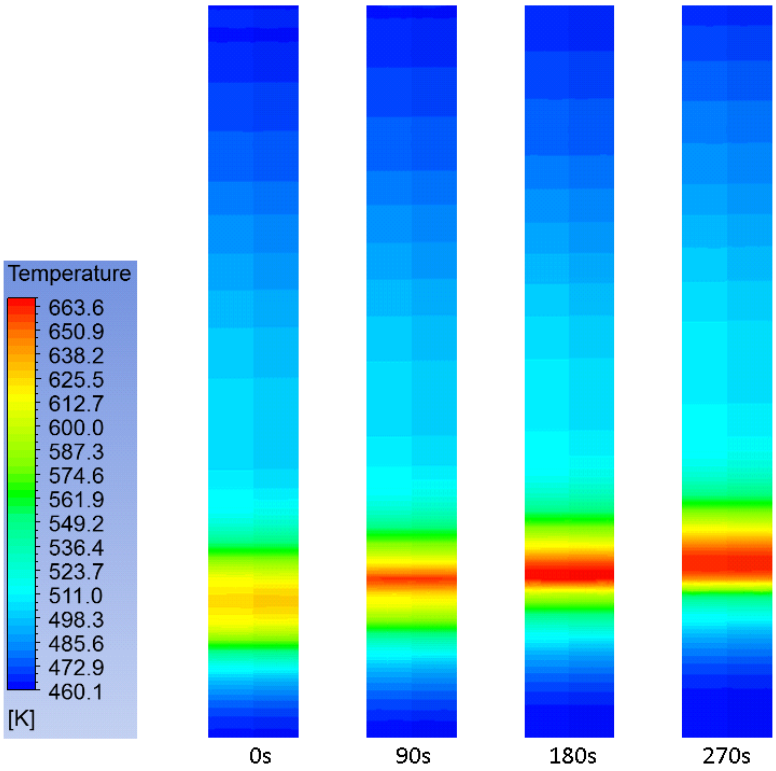

Figure 5-37 Temperature distribution of adsorption step for combined WGS and CO_2 capture

5.4 CFD Model Results and Discussion

This section presents and discusses CFD simulation results for the design of a commercial size solid sorbent based CO_2 capture unit for IGCC applications. CO_2 capture capacity, operating conditions and thermal management are investigated. The CFD models developed and validated as described in previous sections are used for design of the commercial size units for both CO_2 capture alone and for the combined WGS and CO_2 capture.

5.4.1 Results and Discussions for CO_2 Capture Alone Technology

Cylindrical columns packed with solid sorbent for CO_2 capture are assumed to be used in IGCC plants. Bed density of the sorbent is assumed to be consistent with the demo reactor. Specific bed inlet conditions for the IGCC with CO_2 capture alone discussed in Section Chapter 5 and simulated by Aspen Plus® are presented in Table 5-9. As mentioned, steam is added to the syngas to keep the H_2O/CO ratio at 2.25 before it enters the HTS reactor, and significant amount of the CO in syngas is converted into CO_2 in the HTS reactor followed by the LTS reactor prior to feeding into the solid sorbent bed.

Table 5-9 Bed Inlet conditions for CO_2 capture alone

Temperature	196C
Pressure	34.3 bar
Mole fraction	
CO_2	0.325
CO	0.007
H_2O	0.247
H_2	0.388
N_2	0.033

5.4.1.1 Sensitivity Study of Bed Geometry

Bed geometry was first examined to understand the dependency of CO_2 loading capacity on aspect ratio and reactor size. Three aspect ratios, 2, 4, and 6, and three levels of reactor volume, 49 m^3, 85 m^3 and 135 m^3, were investigated, with the bed geometry shown in Table 5-10.

Table 5-10 Geometry of bed reactors

Volume (m^3)	49			85			135		
Aspect Ratio	2	4	6	2	4	6	2	4	6
Diameter (m)	3.15	2.50	2.18	3.78	3.00	2.62	4.41	3.50	3.06
Height (m)	6.30	10.00	13.08	7.56	12.00	15.72	8.82	14	18.36

CFD simulations of the adsorption step were performed on beds packed with fresh solid sorbent. Figure 5-38 presents the CO_2 breakthrough curves for various geometry parameters while keeping the space velocity constant at 0.01 s^{-1} for all beds. For all geometries, CO_2 breaks through at 120 s which indicates that CO_2 loading is

independent of bed aspect ratio or volume in the range investigated, as long as space velocity is fixed. For all cases the CO_2 loading capacity is about 3.06 g CO_2 / 100 g sorbent. For an assumed bed space velocity and duration of the adsorption step, the CO_2 loading capacity may be obtained from the CFD simulation and the total quantity of solid sorbent required may be calculated. The total number of CO_2 capture columns and size of each of the columns for a given total syngas flow rate may then be optimized in terms of operational feasibility taking into consideration the number of valves required and their cycle times, and overall economics.

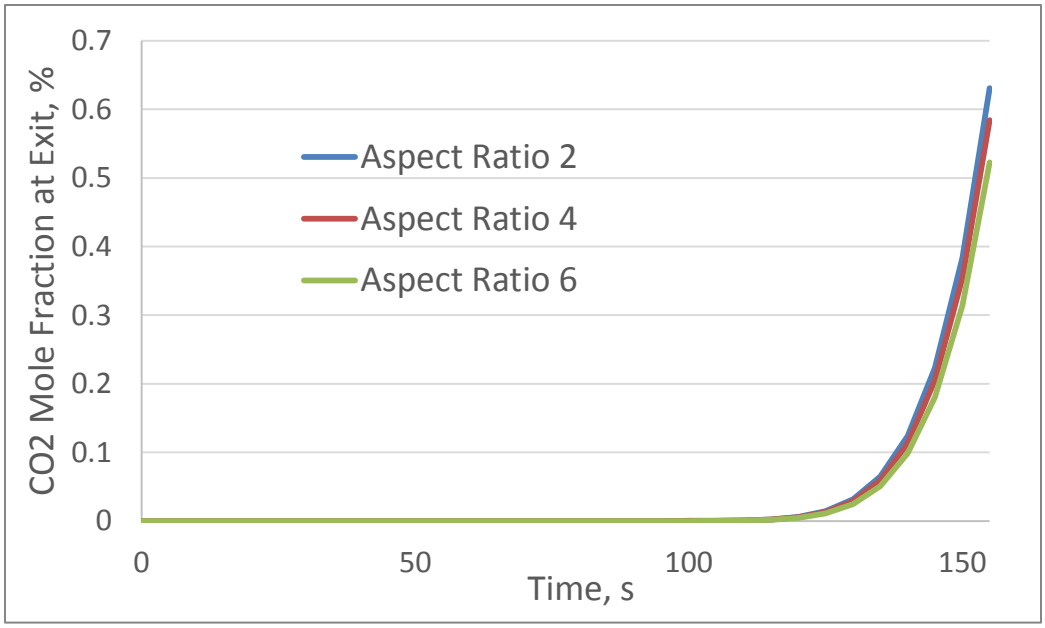

(a) Reactor Volume 49 m^3

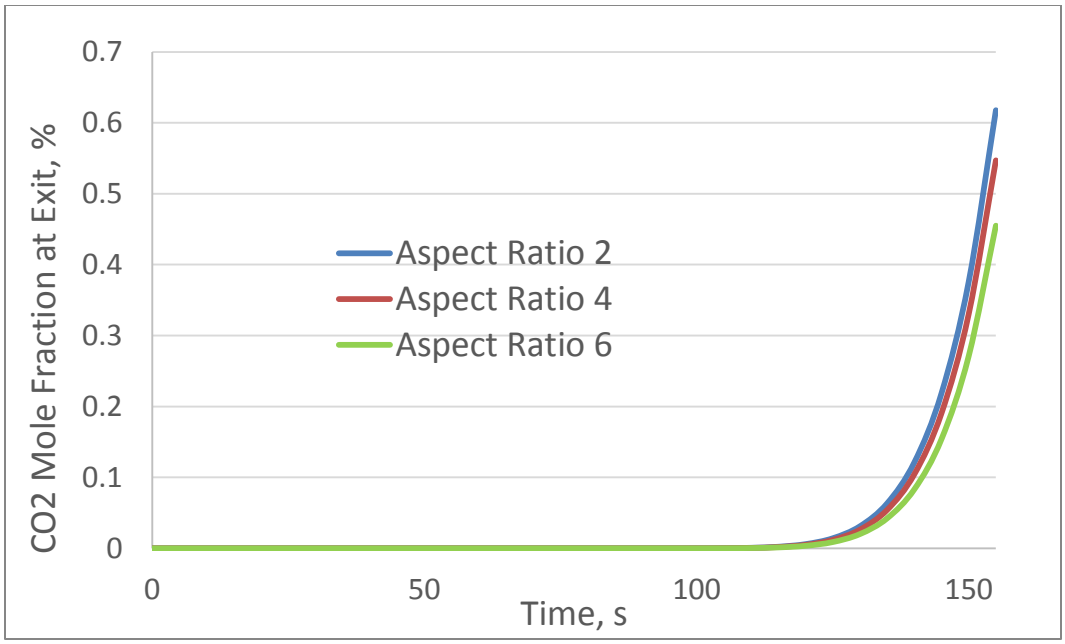

(b) Reactor Volume 85 m^3

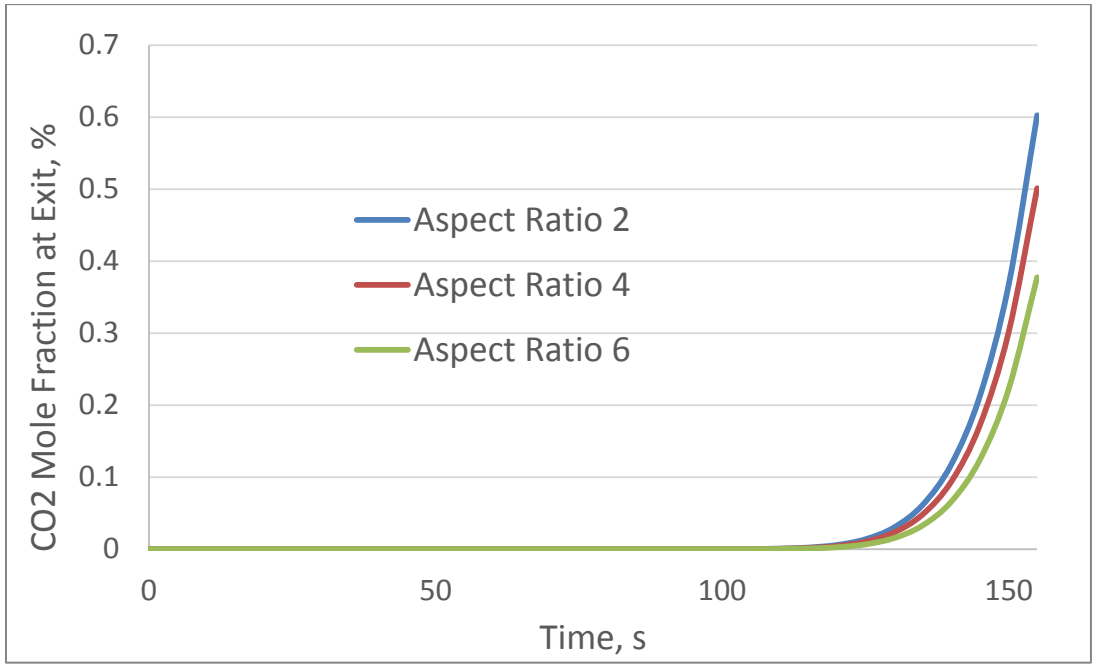

(c) Reactor Volume 135 m^3

Figure 5-38 CO_2 Breakthrough curve vs. bed geometry

5.4.1.2 Sensitivity Study of Space Velocity

CO_2 is absorbed while it travels across the fixed bed packed with solid sorbent. As discussed previously, the adsorption rate is the controlling step for CO_2 capture using fixed bed reactors, and break through occurs by mass transfer of the CO_2 due to bulk flow in the axial direction preventing the downstream sorbent from being fully utilized. Low reactor space velocity enables enough residence time for CO_2 in the syngas to be transported to and absorbed by the solid sorbent, and can increase overall bed utilization (CO_2 loading capacity). Figure 5-39 depicts the CO_2 breakthrough curves for a reactor with volume of 85 m^3 and aspect ratio of 4. CO_2 breakthrough time occurs at 60 s, 120 s and 330 s as space velocity is decreased from 0.015 s^{-1} to 0.010 s^{-1} to 0.005 s^{-1}, respectively. It can also be seen by Figure 5-40 that for all three space velocities investigated, solid sorbent at bottom of the bed is fully loaded with CO_2, while moving downstream it may be seen that CO_2 is absorbed in the solid sorbent reduces as the space velocity increases. At lower space velocity, a larger portion of the solid sorbent in the bed is loaded with the CO_2. As shown by Table 5-11, the average CO_2 loading on g CO_2 / 100 g sorbent basis is 4.31, 3.06 and 2.24 for space velocities at 0.005 s^{-1}, 0.010 s^{-1} and 0.015 s^{-1} respectively.

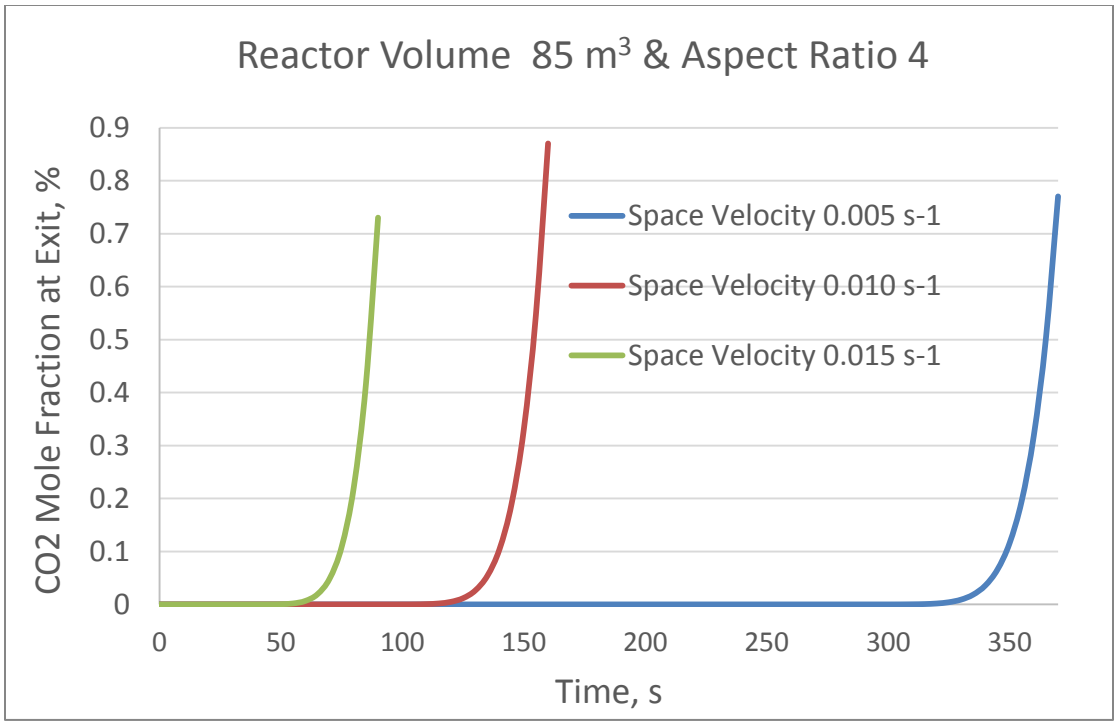

Figure 5-39 CO_2 breakthrough curve for various space velocities

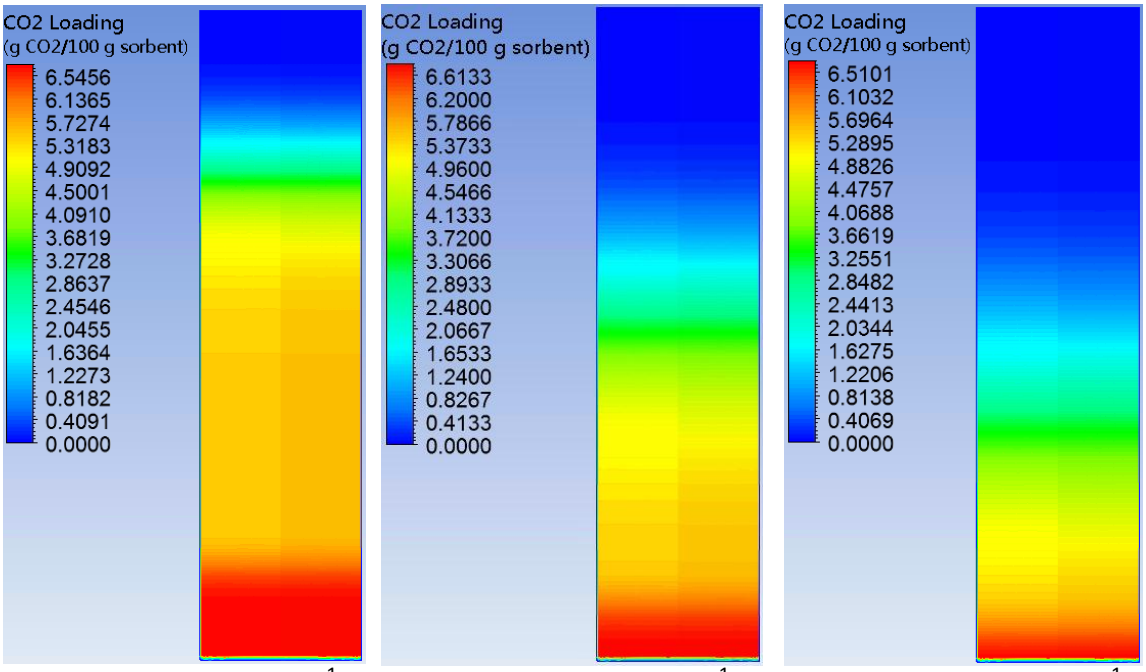

Space Velocity 0.005 s^{-1} Space Velocity 0.010 s^{-1} Space Velocity 0.015 s^{-1}

Figure 5-40 CO_2 loading contour at breakthrough for various space velocities

Table 5-11 Average CO_2 loading at breakthrough for various space velocities

Space Velocity (s-1)	0.005	0.01	0.015
CO_2 breakthrough time (s)	330	120	60
Average CO_2 Loading (g CO_2 / 100 g sorbent) @ Breakthrough	4.31	3.06	2.24

Reduced space velocity for a given bed size increases CO_2 loading capacity of the bed but a larger number of reactors are required resulting in a similar or possibly lager total quantity of sorbent and plant cost. A tradeoff study is required to select the optimum space velocity while setting a lower limit on the space velocity to avoid mass transfer resistance across the gas film surrounding the sorbent particles from becoming significant.

5.4.1.3 Sensitivity Study of Adsorption Kinetics

In order to increase the economic performance in terms of sorbent usage cost, a reasonable approach would be to improve the adsorption kinetics of the solid sorbent (k_b in Equation 5-6 and q* in Equation 5-10). In this sensitivity study, a reactor of volume = 85 m^3, aspect ratio = 4, space velocity = 0.01 s^{-1} with different adsorption kinetics is evaluated. As indicated by Figure 5-41,by doubling k_b the CO_2 breakthrough time increases from 120s to 160s because increase in adsorption rate makes the amount of CO_2 adsorbed move closer to the equilibrium value. Doubling q* has a much more significant impact on CO_2 breakthrough time, which goes up to 250s because the potential CO_2 adsorption capacity is doubled. Figure 5-42 presents the CO_2 loading in the sorbent. Improvements in the sorbent performance (large k_b and/or q*) lead to significantly better utilization of the sorbent. As shown by Table 5-12, the CO_2 loading

on wt% basis increases from 3.06 to 4.15 by doubling k_b and increases to 7.56 by doubling q*. TDA is working toward this approach by increasing mass diffusion rate within the porous structures and increasing functional groups in the porous surfaces which is expected to make a better use of the sorbent bed. TDA has made significant improvements recently and increased the breakthrough time by more than 40% for the new formulations, which will results in 40% smaller beds.

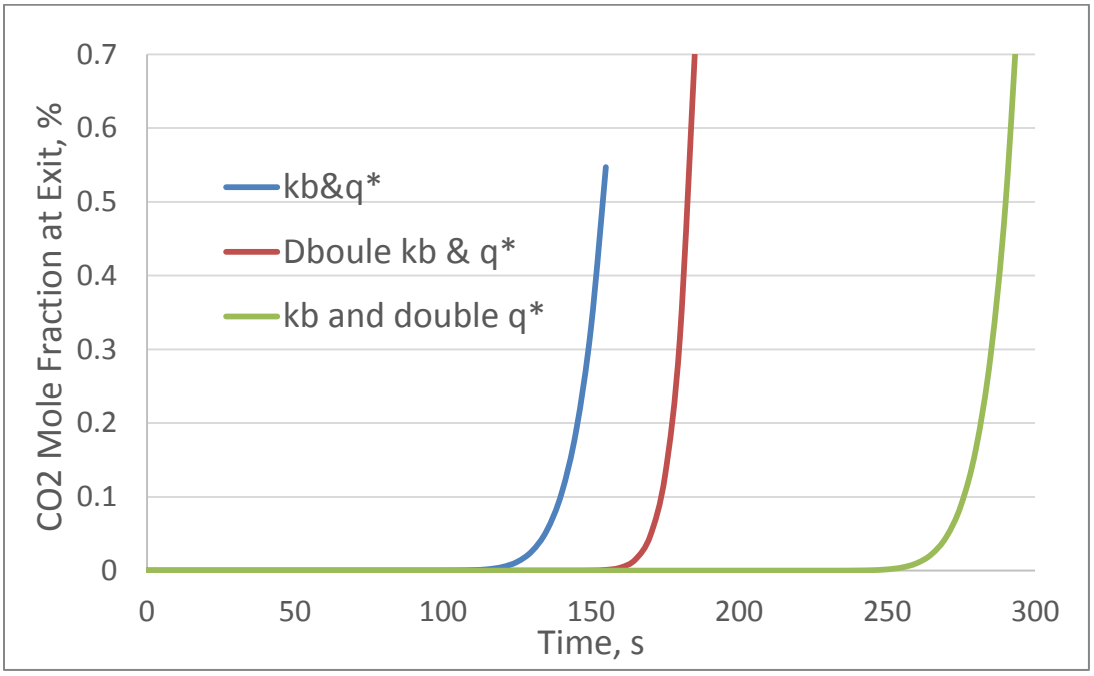

Figure 5-41 CO_2 Breakthrough curve for various adsorption kinetics

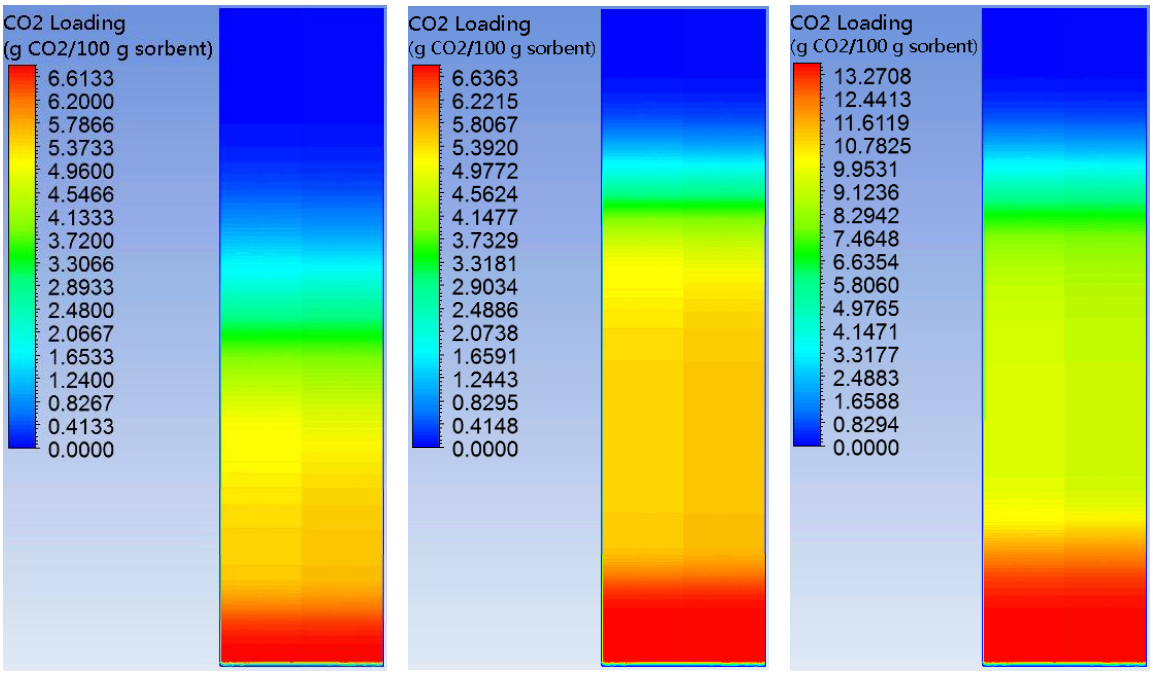

k_b & q* double k_b & q* k_b & double q*

Figure 5-42 CO_2 loading contour at breakthrough for various adsorption kinetics

Table 5-12 Average CO_2 loading at breakthrough for various adsorption kinetics

	k_b & q*	Double k_b & q*	k_b & Double q*
CO_2 breakthrough time (s)	120	160	255
Average CO2 Loading (g CO_2 / 100 g sorbent) @ breakthrough	3.06	4.15	7.56

5.4.1.4 Discussion on Bed Operation and Performance

Figure 5-43 shows the CO_2 molar concentration of an adsorption step for CO_2 capture alone case with volume = 85 m^3, aspect ratio = 4 and space velocity = 0.01 s^{-1}. Figure 5-44 presents the CO_2 loading and temperature profile. CO_2 propagates from inlet toward exit as it is absorbed by the sorbent with a temperature peak occurring in bottom section of the bed. Once the sorbent reaches equilibrium and is saturated, no

more CO_2 is absorbed, and so no heat is generated, and the sorbent is cooled down by incoming fresh syngas.

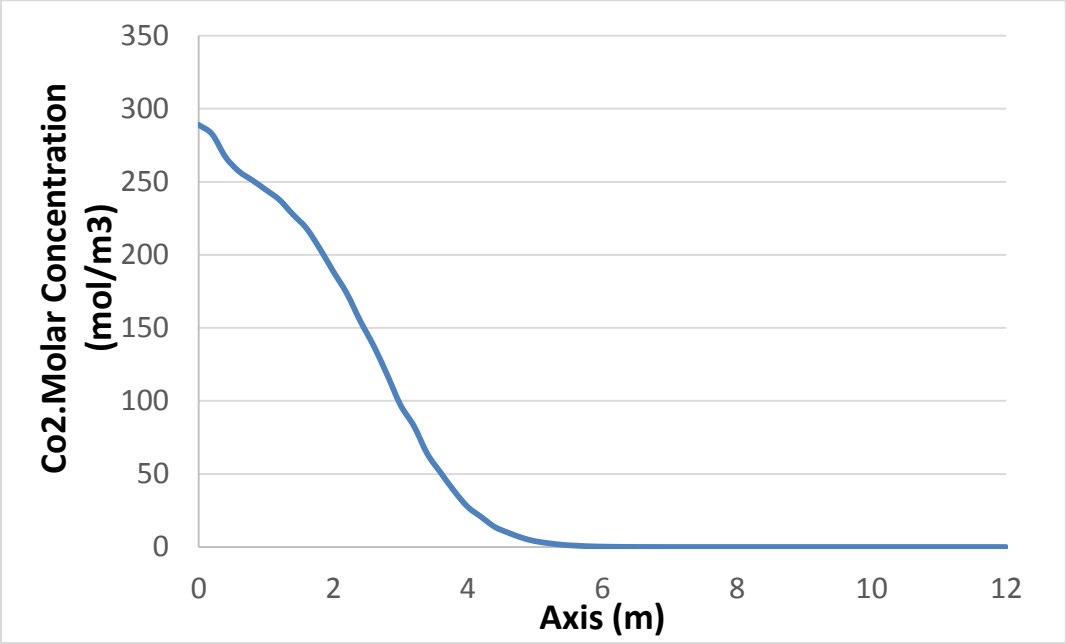

(a) T=40s

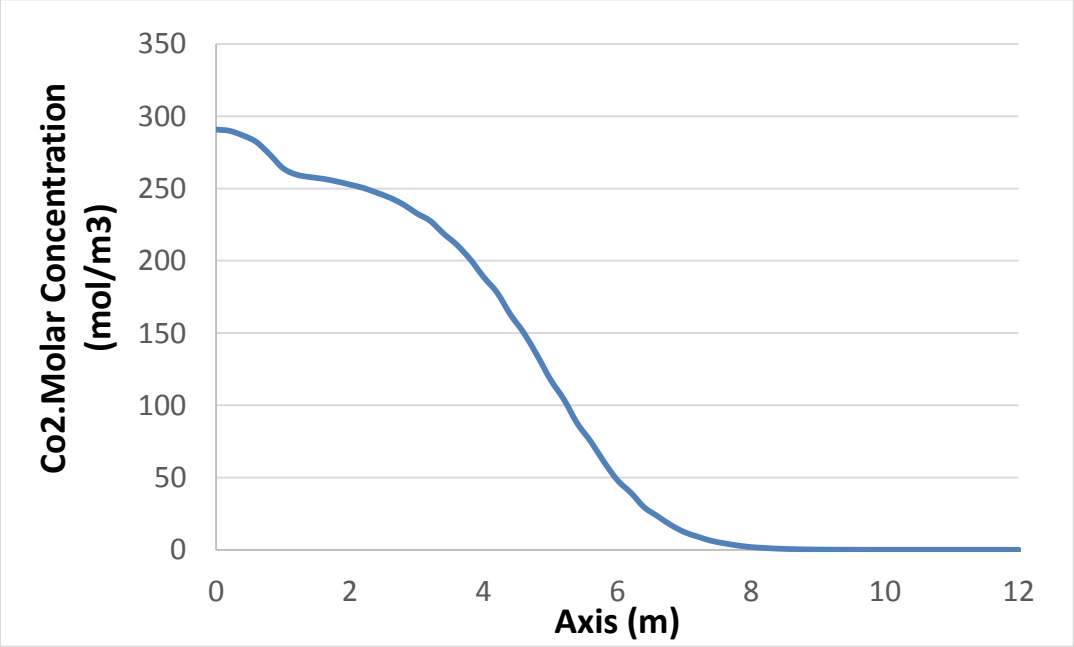

(b) T=80s

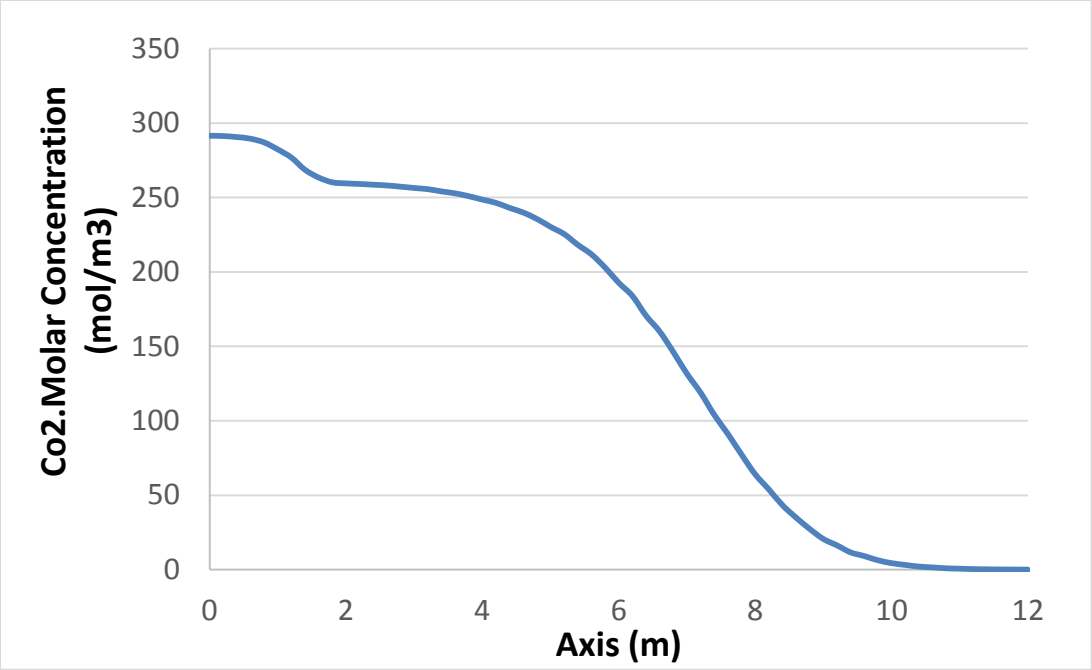

(c) T=120s

Figure 5-43 CO_2 molar concentration alone bed Axis

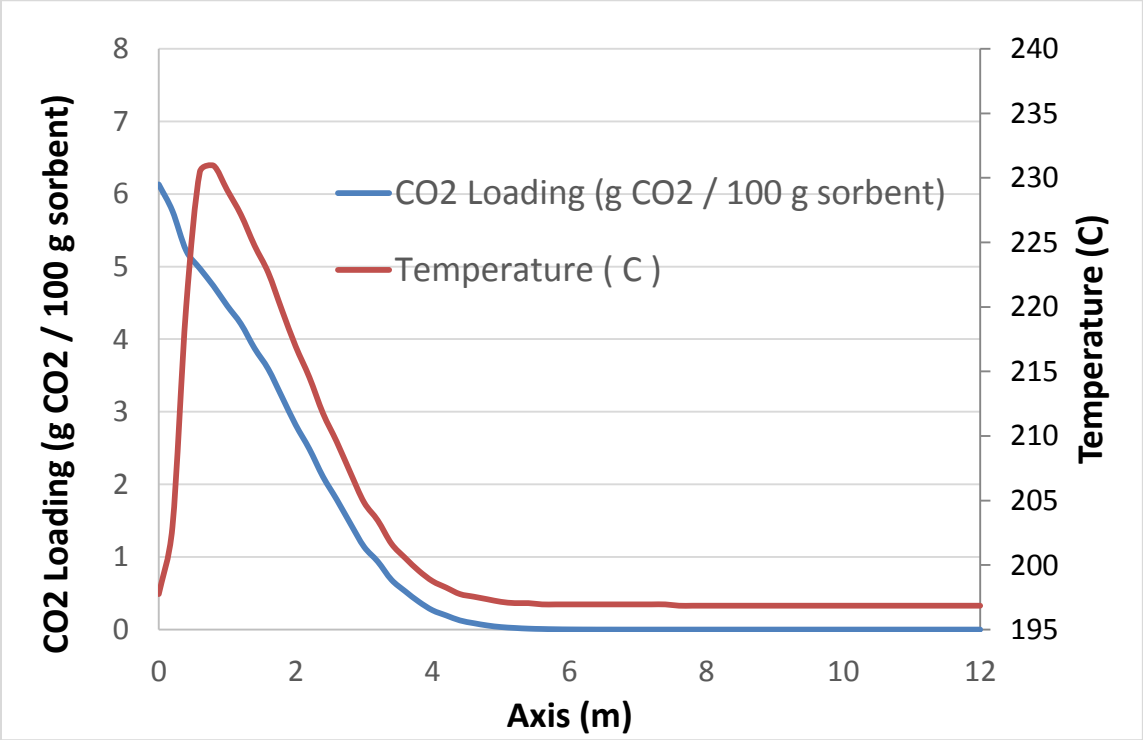

(a) T=40s

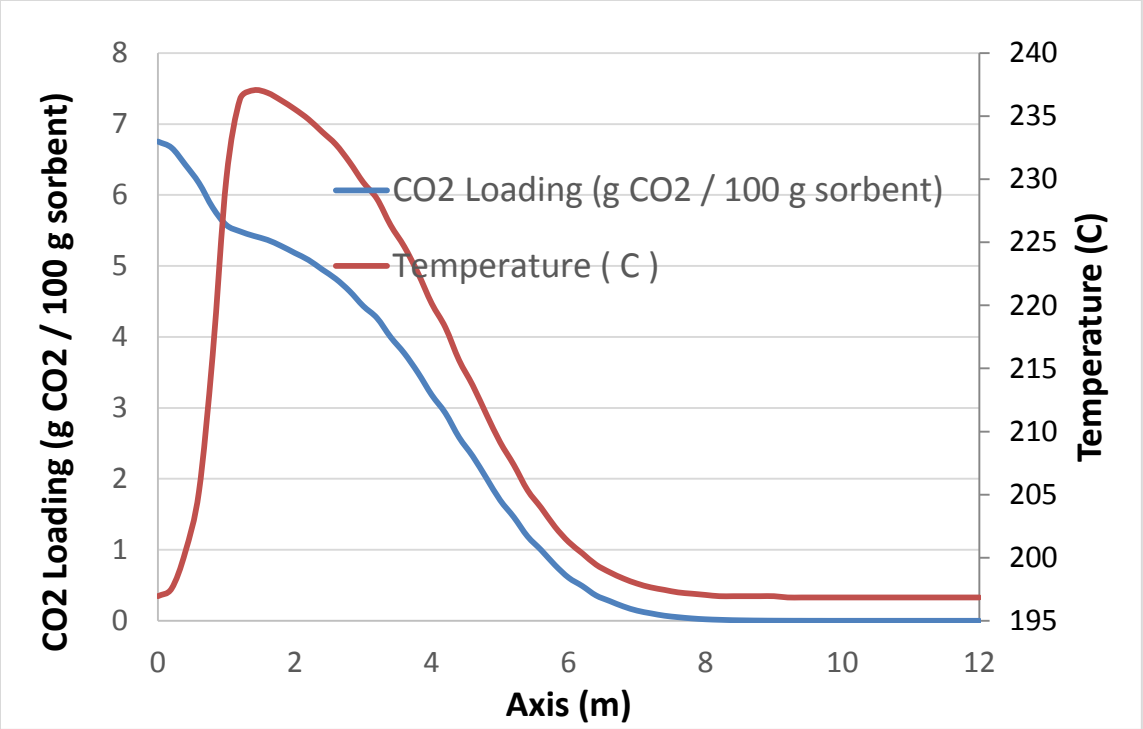

(b) T=80s

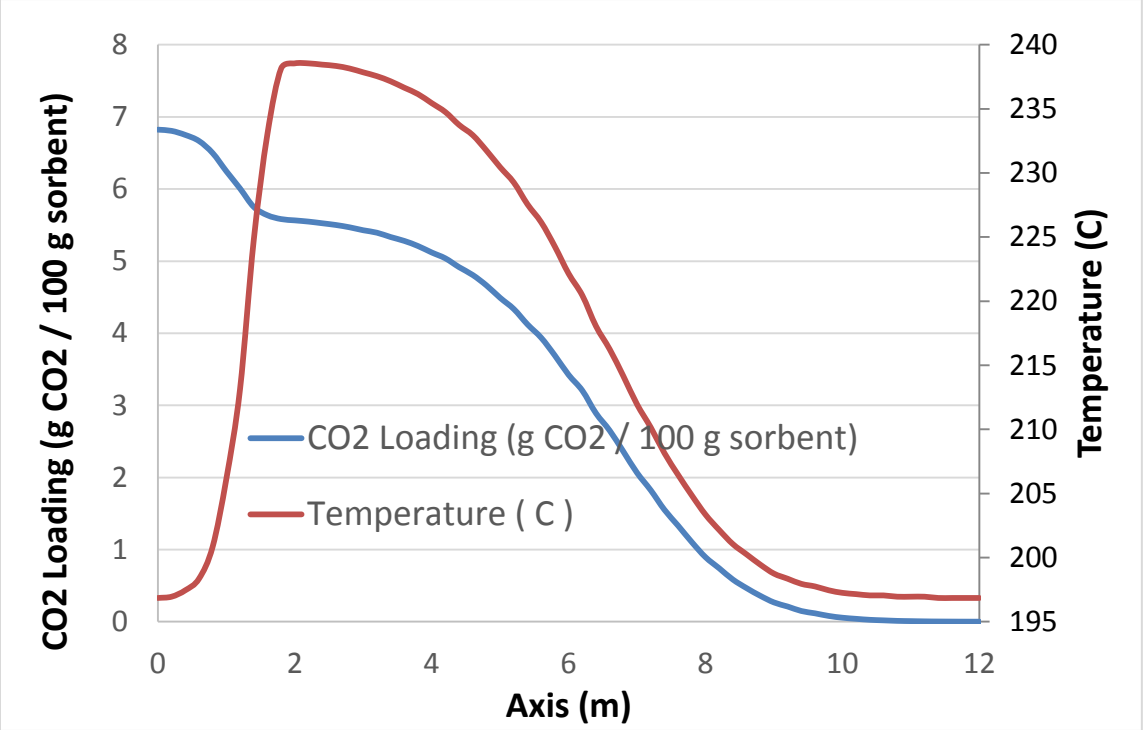

(c) T=120s

Figure 5-44 CO_2 molar concentration alone bed axis

The CFD model is also capable of predicting pressure drop across the bed. Since the volumetric flow rate is relatively low at high operating pressure during the adsorption step and the total gas flow rate decreases as the CO_2 is adsorbed while the syngas propagates through the bed, the highest pressure drop across the reactor bed is reasonably low at around 0.75 bar (11 psi) as shown by Figure 5-45, a reasonable value for plant operation without requiring downstream syngas gas compression.

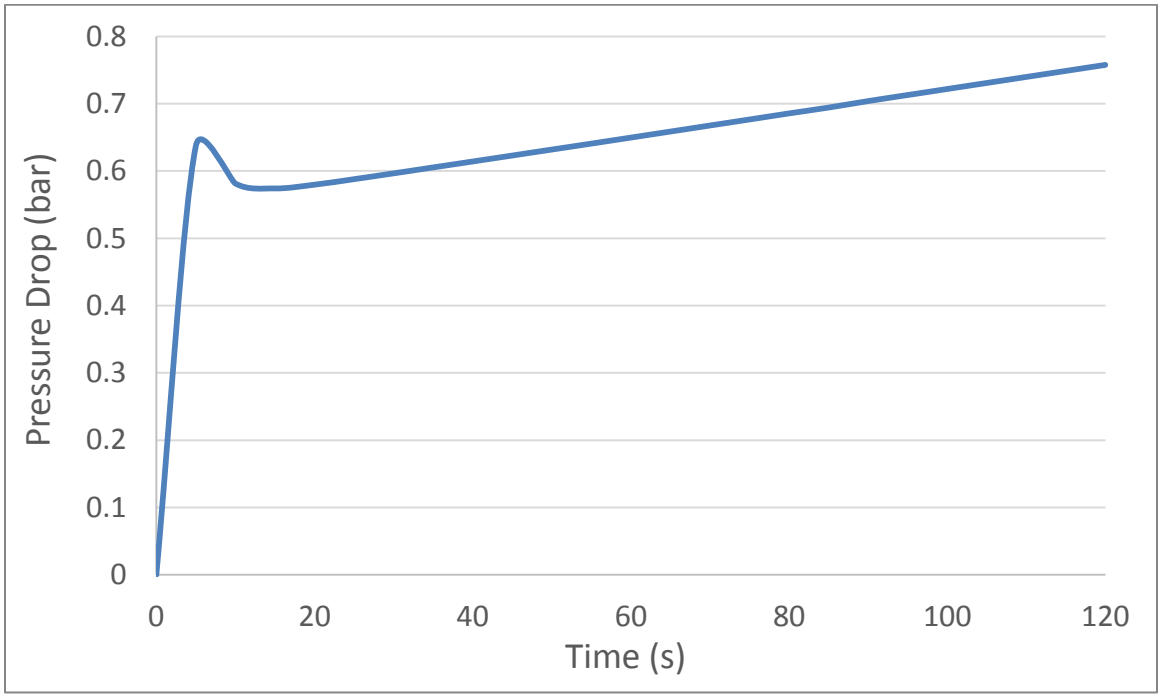

Figure 5-45 Pressure drop during adsorption step

For the purge process, assuming 120 seconds' desorption, 4 levels of purge steam flow rates were evaluated, ¼, ½, ¾, and 1 times the syngas flow rate. Figure 5-46 shows the CO_2 loading capacity at the beginning and at the end of purge step. As expected, more CO_2 is recovered from the solid sorbent when purge steam flow rate increases,

which effectively reduce CO_2 partial pressure. Figure 5-47 quantitatively indicates that with purge steam flow rate higher than ½ of the syngas flow rate, the impact of increasing the purge steam on recovery rate becomes small. Thus, purge stream about ½ of the syngas flow rate is recommended for this particular operating conditions.

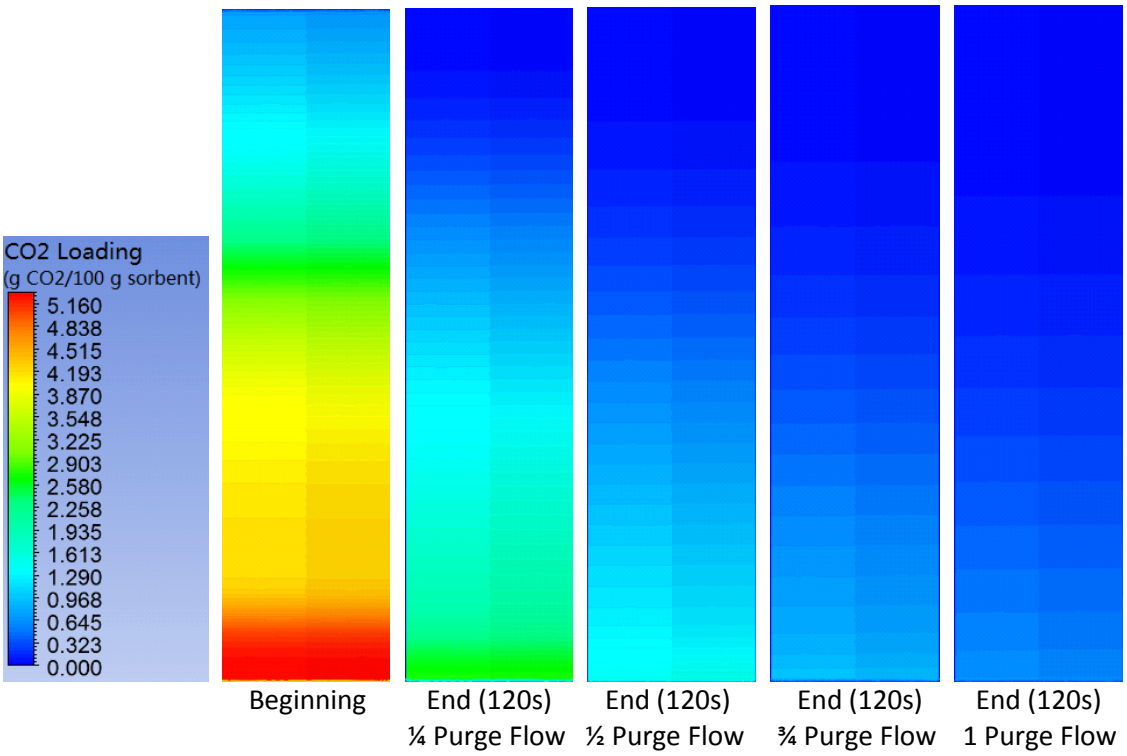

Figure 5-46 CO_2 loading at purge step

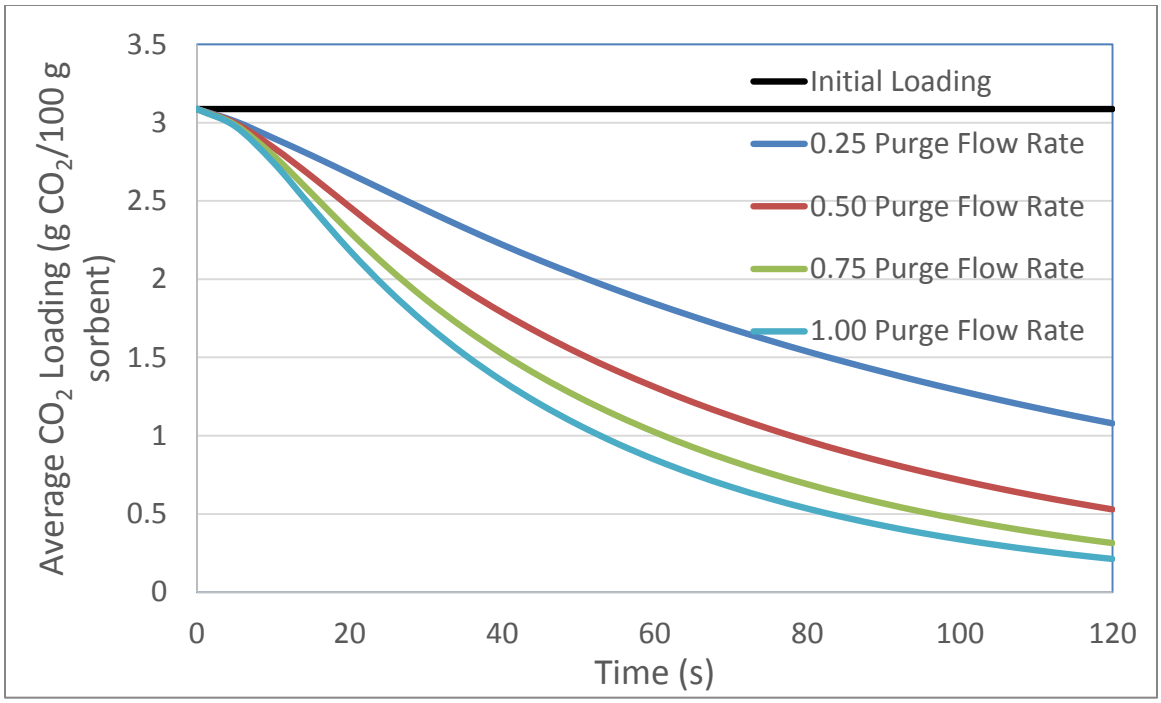

Figure 5-47 Average CO_2 loading at purge step

Besides CO_2 recovery rate, pressure drop is a major concern for the steam purge operation. Fixed bed operates under PSA mode, and steam purging occurs at lower pressure with high volumetric flow rate through the bed resulting in a much higher pressure drop across the bed than that under the high pressure adsorption operation. Figure 5-48 shows the pressure drop for four purge steam flow rate. At the beginning of purge step, gases in the bed are still. When steam starts to flow, the pressure drop starts increasing and the released CO_2 from the sorbent further increases the volumetric flow rate and the pressure drops. After about 10s, the CO_2 desorption rate decreases and the pressure drop slowly reduces. Thus, in order to minimize the supply pressure of the purge steam to reduce the power penalty in the steam turbine, smaller purge flow rate with effective CO_2 recovery rate is preferred.

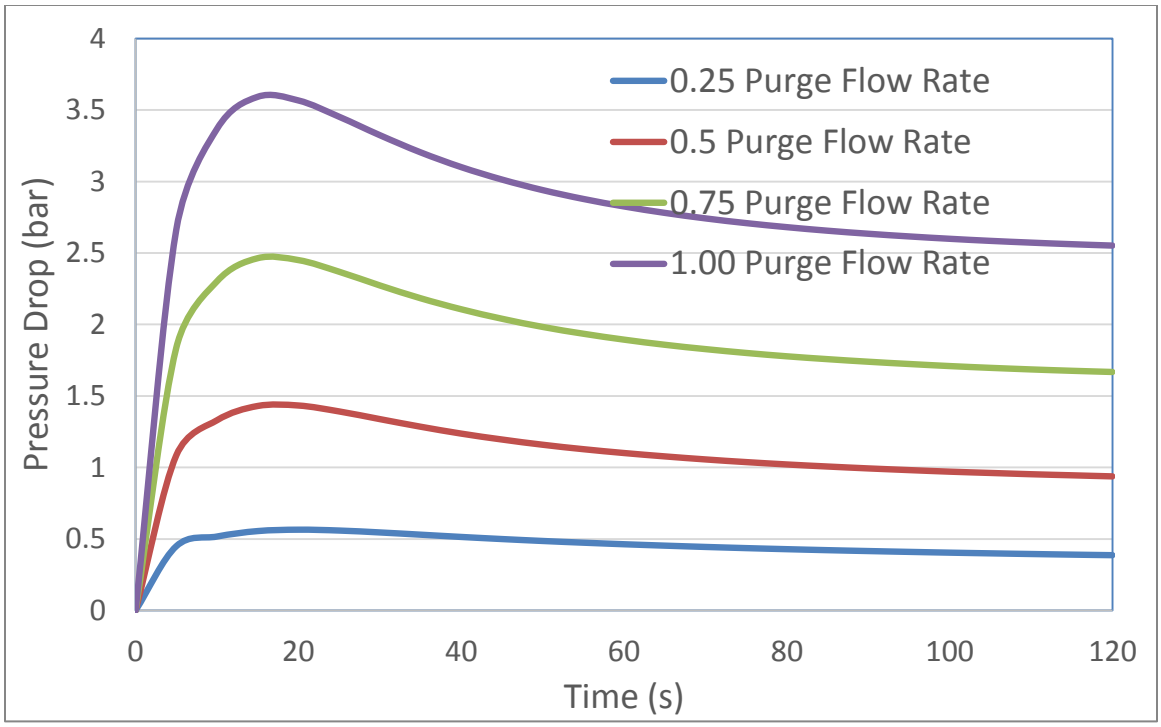

Figure 5-48 Pressure drop cross the bed at purge step

5.4.2 Results and Discussion for Combined WGS and CO_2 Capture Technology

The proposed design for a commercial size cylindrical column reactor for combined WGS and CO_2 capture, is shown in Figure 5-49. Top 20% and bottom 20% of the reactor is packed with solid sorbent while and the middle section is loaded with a mixture of solid sorbent (95 vol%) and WGS catalyst (5 vol%). Geometrical parameters and bed inlet conditions obtained from Aspen Plus® simulation of the IGCC are listed in Table 5-13 and Table 5-14.

The sensitivities of the performance of the combined WGS and CO_2 adsorption reactor on bed geometry, space velocity, adsorption kinetics and purge flow rate are

expected to be similar to the CO_2 adsorption only unit in terms of CO_2 breakthrough, CO_2 loading capacity, and pressure drop. However, as discussed in Section 5.3, WGS reaction occurs quickly and mainly at the bottom section of the mixture (catalyst + adsorbent) zone, and the temperature rise due to the WGS reaction can deactivate both the sorbent and the catalyst with the appearance of local hot spots. Cooling water injection into the reactor bed in the form of a fine mist would be an effective tool for thermal management of the reactor beds. Cooling strategy is the major concern of this combined technology. In the CFD simulations, water injection is introduced by a H_2O source term and a heat sink term to represent the impacts on mass and energy balances.

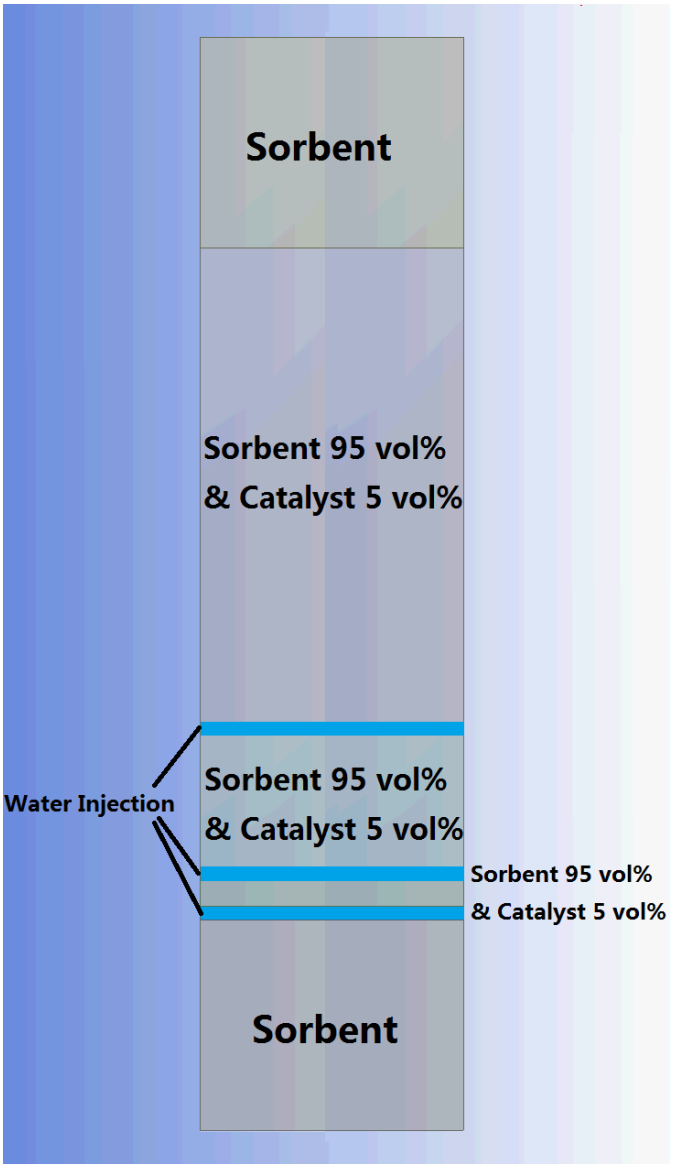

Figure 5-49 Combined WGS and CO_2 capture commercial size reactor

Table 5-13 Bed geometry

Diameter	3 m
Length	12.45 m
Each Water Injection Height	0.15 m
Space Velocity	0.01 s^{-1}

Table 5-14 Bed inlet conditions for combined WGS and CO_2 capture

Temperature	207C
Pressure	34.65 bar
Mole fraction	
CO_2	0.335
CO	0.075
H_2O	0.138
H_2	0.412
N_2	0.04

5.4.2.1 Sensitivity Study of Water Injection Strategy

In this study three water injection zones, at top, middle and bottom of the bed (see Figure 5-49) were simulated to remove the heat generated by the WGS reaction. Since the WGS reaction occur mostly at the bottom of the mixture zone of catalyst and sorbent, all three injection zones are located upstream of the mixture zone. The quantity of total water injection is calculated by Aspen Plus® to maintain an overall isothermal operation. Three cooling water injection options are evaluated as shown by Table 5-15. In the first option, the entire water is injected in the zone with no injection into the two other zones. In, the second option, 2/3 of the water is injected at the bottom zone and the remaining 1/3 in the mid zone. In the third option, water injection is evenly distributed among the three zones. In order to evaluate the cooling effectiveness, a simulation without water injection is also made.

Table 5-15 Water injection options for combined WGS and CO_2 capture

	No Water Injection	1 Water Injection	2 Water Injections	3 Water Injections
Top (kg/s)	0	0	0	0.27
Mid (kg/s)	0	0	0.27	0.27
Bottom (kg/s)	0	0.81	0.54	0.27

Figure 5-50 presents the CO_2 breakthrough curve for each of the three water cooling option as well as the comparison case without water injection. Since the total amount of solid sorbent and total water injected is the same for all the three cooling cases, the corresponding CO_2 breakthrough curves overlap each other. Because no water injected in the comparison case, the space velocity is slightly lower than other cases, which results in a slightly larger CO_2 breakthrough time.

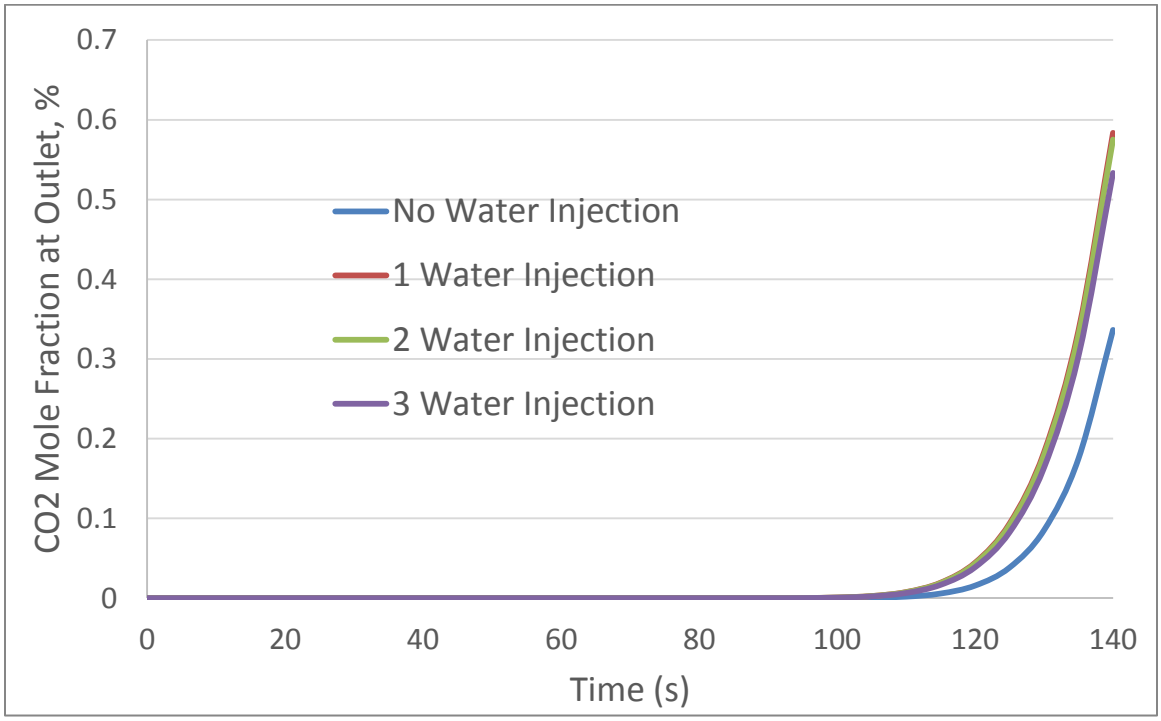

Figure 5-50 CO2 breakthrough for different cooling options

Table 5-16 shows that the average CO_2 loading for various water injection options are very close. Less CO is converted into CO_2 in the case without water injection, so that the CO_2 loading is relatively lower than the cases with water injection.

Table 5-16 Average CO_2 loading (g CO_2/100 g sorbent) for different cooling options

	No-Water-Injection	1-Water-Injection	2-Water-Injections	3-Water-Injections
Average CO_2 Loading (g CO2/100 g sorbent)	3.932	4.015	4.005	3.997

Temperature distribution of each water injection strategy is presented in Figure 5-51. Reactor bed without cooling water injection exhibits a high temperature zone with peak temperature of 284K. The 1-water-injection operation reduces the temperature significantly but creates a low temperature zone. The 3-water-injection option has a better temperature profile but the top water injection zone appears to be unnecessary since very small amount of heat is generated in that region. The 2-water-injection operation offers the best temperature distribution without giving rise to any high or low temperature regions.

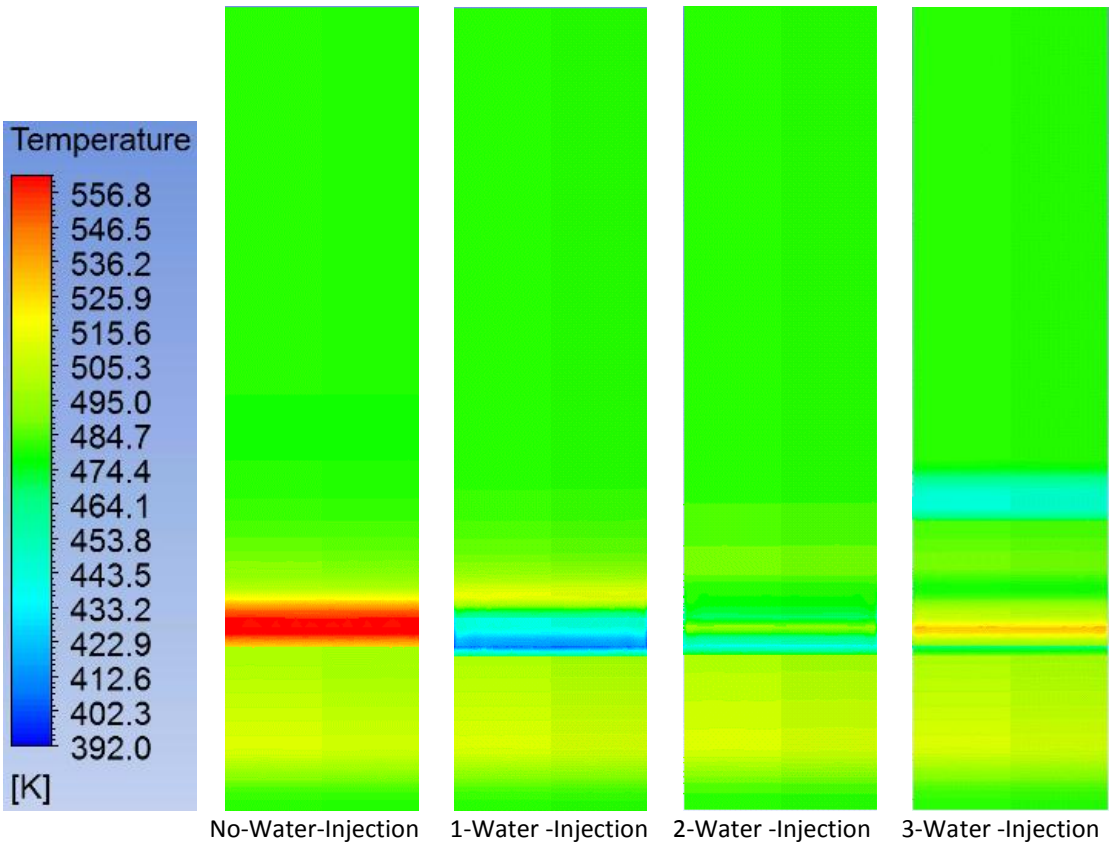

Figure 5-51 Temperature distribution for different cooling options

5.4.2.2 Discussion on Bed Performance

The 2-water-injection option is selected for further analyses. Figure 5-52 shows the species distribution across the bed at 40s, 80s, and 120s. CO_2 concentration decreases as the gases enter the bed. Due to the WGS reaction, a peak in the CO_2 concentration occurs as CO converts to CO_2 before its concentration gradually approaches zero. Correspondingly, CO decreases rapidly when the gas enters the combined zone of sorbent and catalyst. The two peaks observed in the H_2O profile represent water injection. Immediately after the peaks, H_2O concentration decreases due to rapid WGS reaction. Decarbonized syngas exiting the bed consists of mainly H_2 and H_2O.

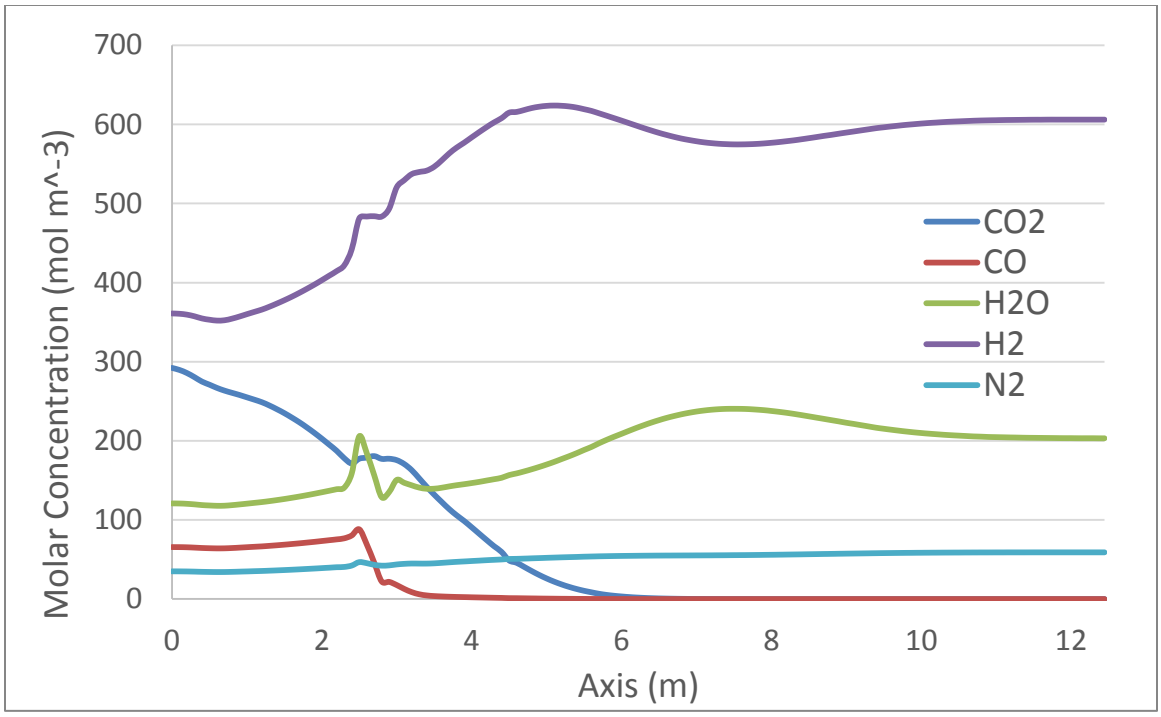
Molar Concentration (mol m^-3)
700
600
500
400
300
200
100
0
0
2
4
6
8
10
12
Axis (m)
CO2
CO
H2O
H2
N2

(a) T=40s

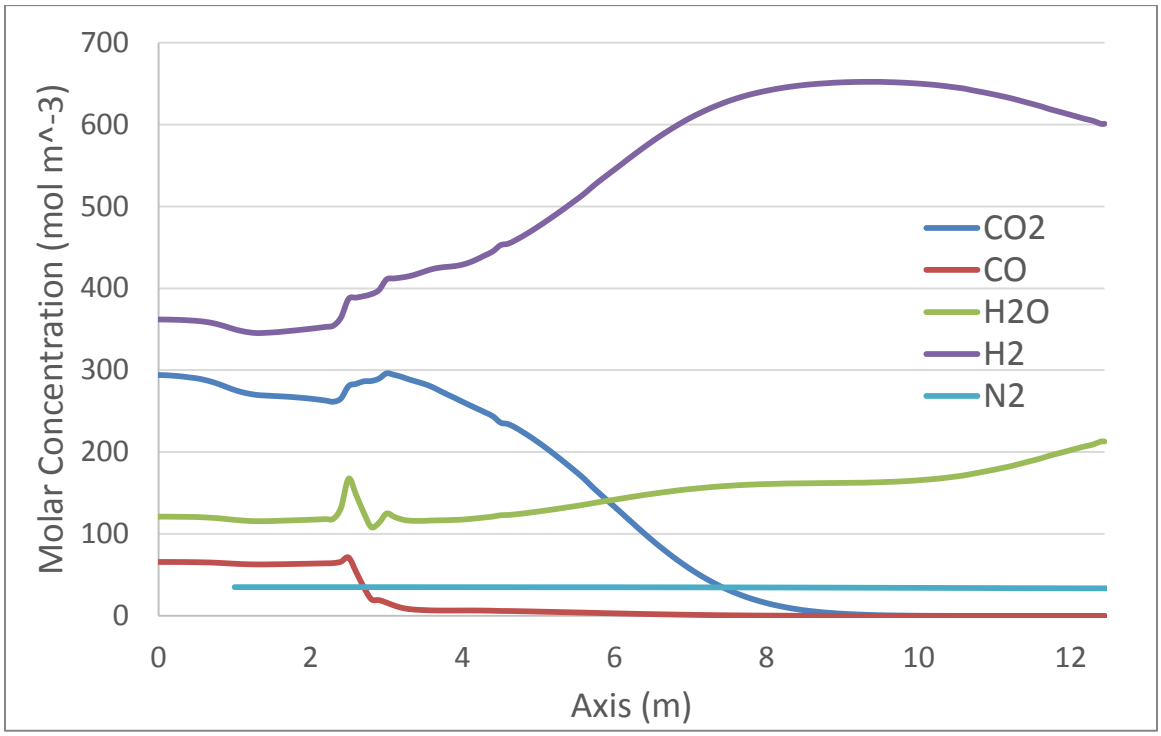
Molar Concentration (mol m^-3)
700
600
500
400
300
200
100
0
0
2
4
6
8
10
12
Axis (m)
CO2
CO
H2O
H2
N2

(b) T=80s

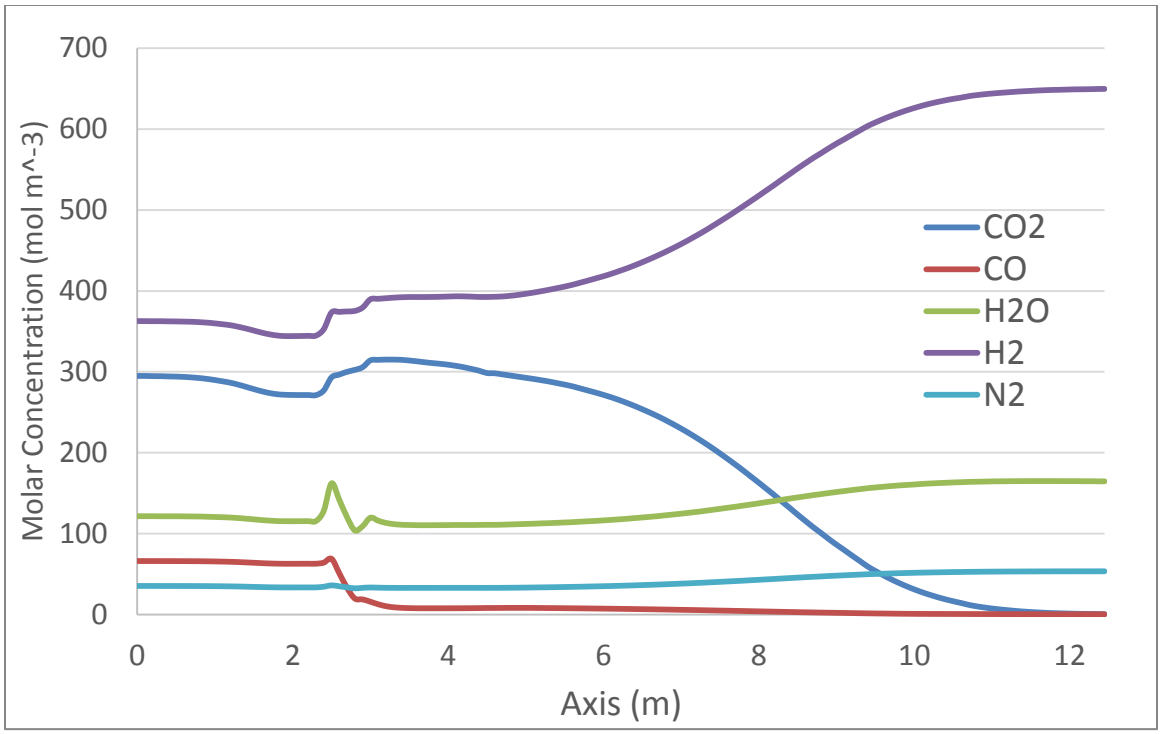

(c) T=120s

Figure 5-52 Species distribution across a reactor bed

Figure 5-53 shows the temperature distribution across the combined WGS and CO_2 adsorption reactor for the 2-water-injection design option. The two temperature dips observed in the plots represent the two water injections. Heat generated by WGS is effectively suppressed and the highest temperature rise anywhere in the bed is less than 40C, this initial temperature rise occurring due the CO_2 adsorption process.

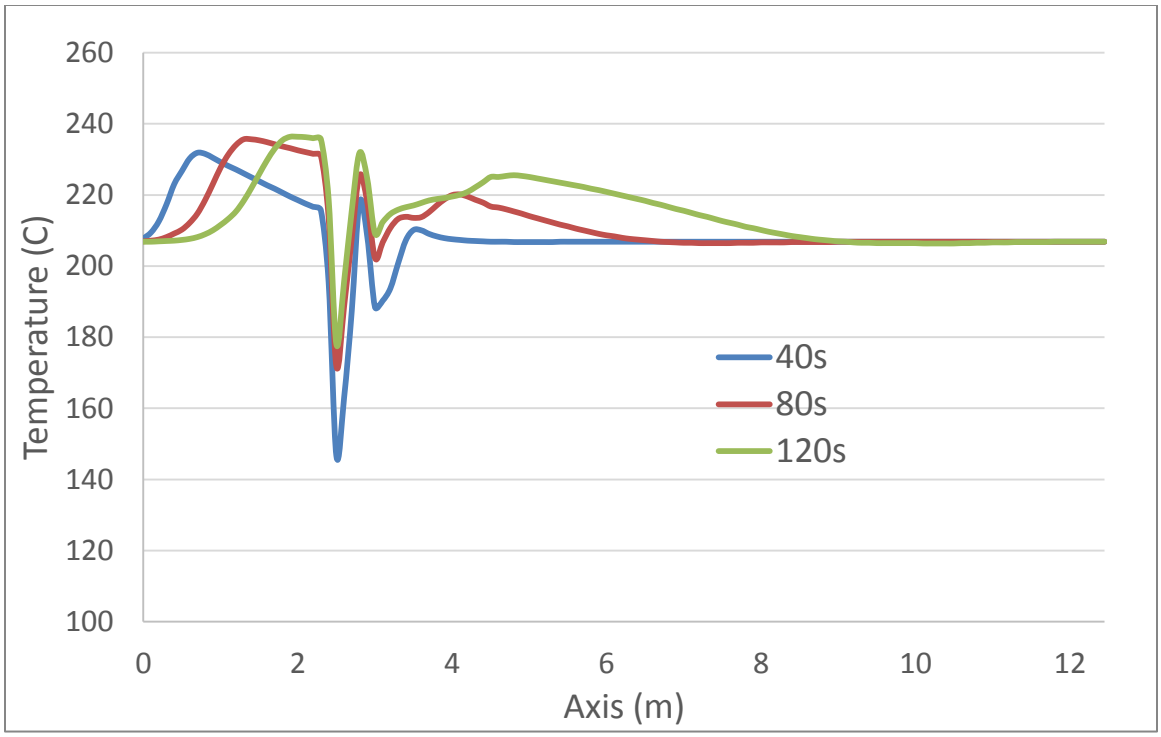

Figure 5-53 Temperature distribution of combined WGS and CO_2 adsorption

Figure 5-54 shows the CO_2 loading across the bed. The introduction of water into the bed mixture bumps up the CO_2 loading because WGS equilibrium moves toward the direction of CO_2 production when more H_2O is available, which means that cooling water introduction not only serves for cooling purpose but also benefits conversion of CO into CO_2 and further increases level of carbon capture.

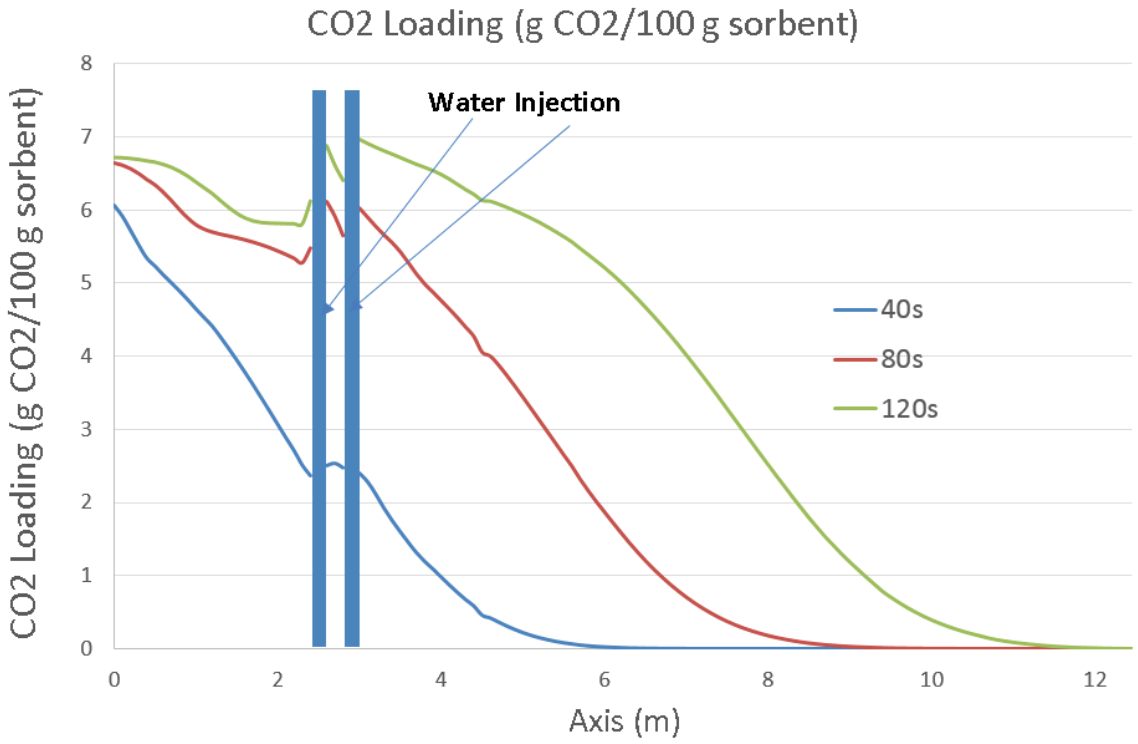

Figure 5-54 CO_2 loading distribution of combined WGS and CO_2 adsorption

5.4.3 Case Study of the Application of Solid Sorbent CO_2 Capture Technology in IGCC Plants

This subsection discusses the application of CFD simulation of both solid sorbent CO_2 capture alone technology and combined WGS and solid sorbent CO_2 capture technology in the IGCC plants described in Section Chapter 5. The process design of CO_2 capture unit, and reactor bed design and operation are two major focuses.

5.4.3.1 CO_2 Capture Process Design

Reactor beds are arranged in multiple trains, and the beds in each train work together cyclically. Based on the total syngas flow rate of the two IGCC systems (Case 2

and Case 3) described in Section Chapter 5 and using reasonable bed sizes, 3 trains of reactor beds and 8 beds for each train are selected for both Case 2 and Case 3 for solid sorbent CO_2 capture alone technology and combined WGS and solid sorbent CO_2 capture technology respectively. Each train undergoes cyclic operation with the designed time intervals as shown in Figure 5-55: two beds under adsorption step and two beds under desorption/purge stem at any time, with the duration for both adsorption step and purge step of 120 s which is a reasonable time for valve manipulation; after adsorption, the bed goes through three depressurization equalization steps with other beds under pressurization equalization steps to fully utilize the high pressure gas remaining in the bed; co-current blow-down to reduce the pressure to purge pressure level after depressurization equalization; decarbonized syngas introduced for final pressurization after pressurization equalization.

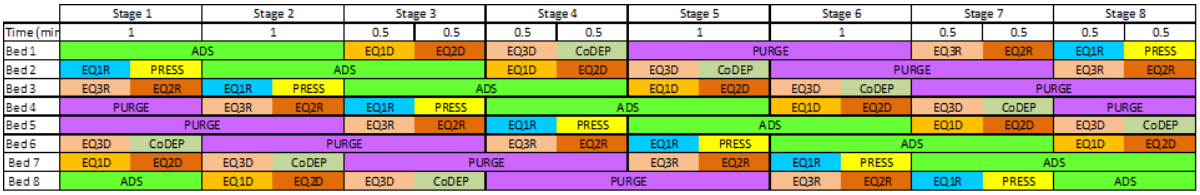

Figure 5-55 Cycle scheme of solid sorbent based CO_2 capture

Figure 5-56 schematically shows the solid sorbent based CO_2 capture subsystem in the IGCC. Syngas feed combined with blow-down recycle gas enters the adsorption bed, with CO_2 lean syngas exiting at bed outlet. After 3 steps of depressurization equalization and co-current blow-down for both reducing pressure and blowing out residual gases,

steam purge releases the CO_2 absorbed in the solid sorbents. The CO_2 rich desorption product is then sent for condensation and compression.

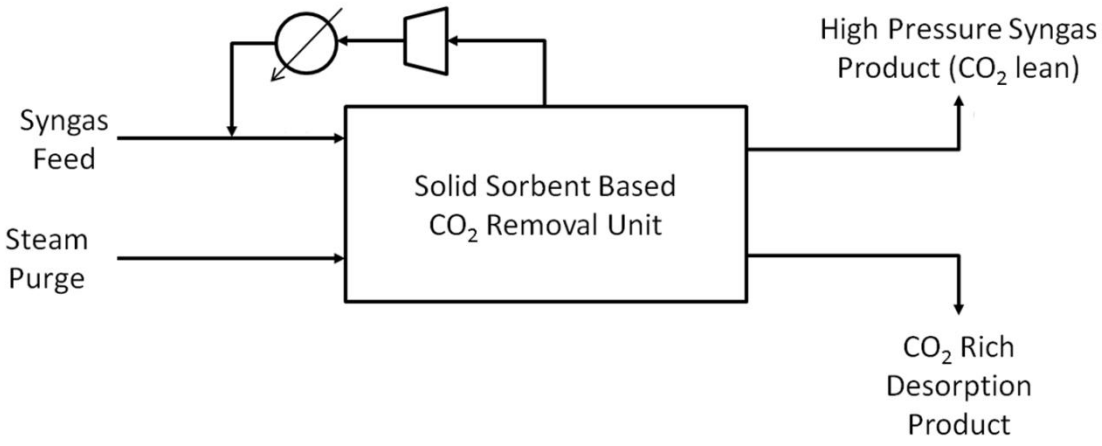

Figure 5-56 Block flow diagram of solid sorbent CO_2 Capture sub-system

5.4.3.2 Reactor Bed Design and Sizing

Syngas bed inlet conditions for a single reactor for adsorption step is obtained from Aspen Plus® simulation and presented in Table 5-17. Reactor bed is designed as a cylindrical column. For CO_2 capture alone, the columns are packed with solid sorbent; for combined WGS and CO_2 capture, the columns are packed with both catalyst and solid sorbent, similar to Figure 5-49 but the top water injection zone is eliminated.

Table 5-17 Syngas bed inlet conditions of a single reactor for adsorption step

	CO_2 Capture Alone	Combined WGS and CO_2 Capture
Temperature	196C	207C
Pressure	34.3 bar	34.65 bar
Flow Rate	1.69 kmol/s	1.38 kmol/s
Mole fraction		
CO_2	0.325	0.335
CO	0.007	0.075
H_2O	0.247	0.138
H_2	0.388	0.412
N_2	0.033	0.04

The diameter of reactor bed is kept at 3.96 m to meet the vertical clearance requirement for bridges so that the reactor can be shipped. Cyclic CFD simulation of adsorption, depressurization equalization, blow-down, purge, pressurization equalization and final pressurization are performed till it reaches a steady state. Various bed heights are tested. The bed height which results in a decarbonized syngas with CO_2 mole fraction (at bed exit during adsorption step) of about 1% is selected. Table 5-18 shows the final design bed geometry for both CO_2 capture alone and combined WGS and CO_2 capture.

Table 5-18 Bed geometry

	CO_2 Capture Alone	Combined WGS & CO_2 Capture Alone
Diameter	3.96 m	3.96 m
Length	20 m	15.3 m
Each Water Injection Height	N/A	0.15 m

The operating pressure for the adsorption alone reactor is slightly lower than the combined reactor due to pressure drop of a second WGS reactor included upstream of the CO_2 removal unit. The CO_2 mole fraction or partial pressure is also lower (see Figure 5-57) since for the adsorption alone case, a large amount of steam is added before the syngas enters WGS reactors. Therefore, CO_2 loading capacity on g CO_2/100 g sorbent basis for CO_2 capture alone is lower than combined WGS and CO_2 capture as shown by Figure 5-58, and in order to maintain comparable amounts of CO_2 capture, reactor size is larger for the CO_2 capture alone case.

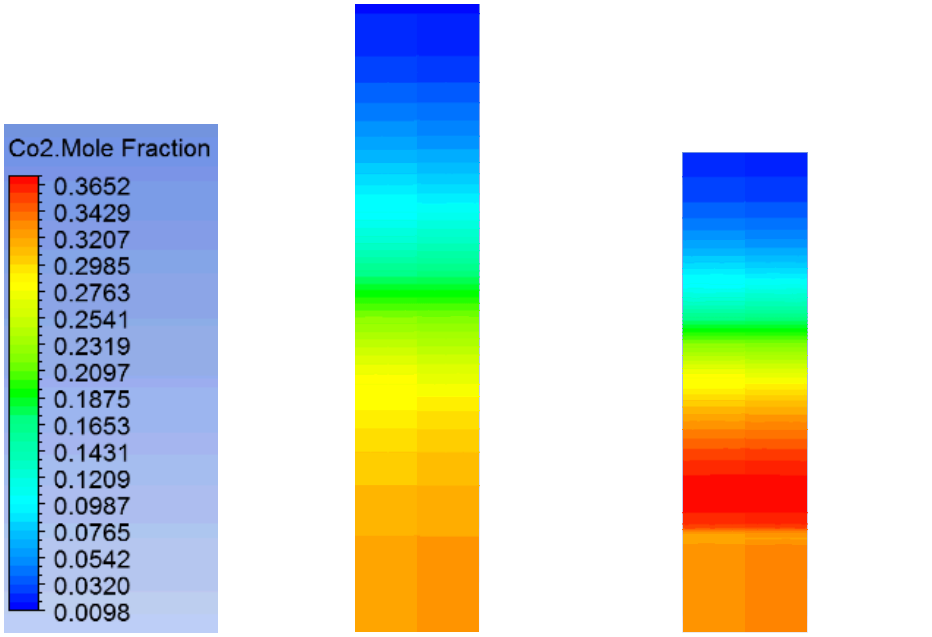

Figure 5-57 CO_2 mole distribution at the end of adsorption step

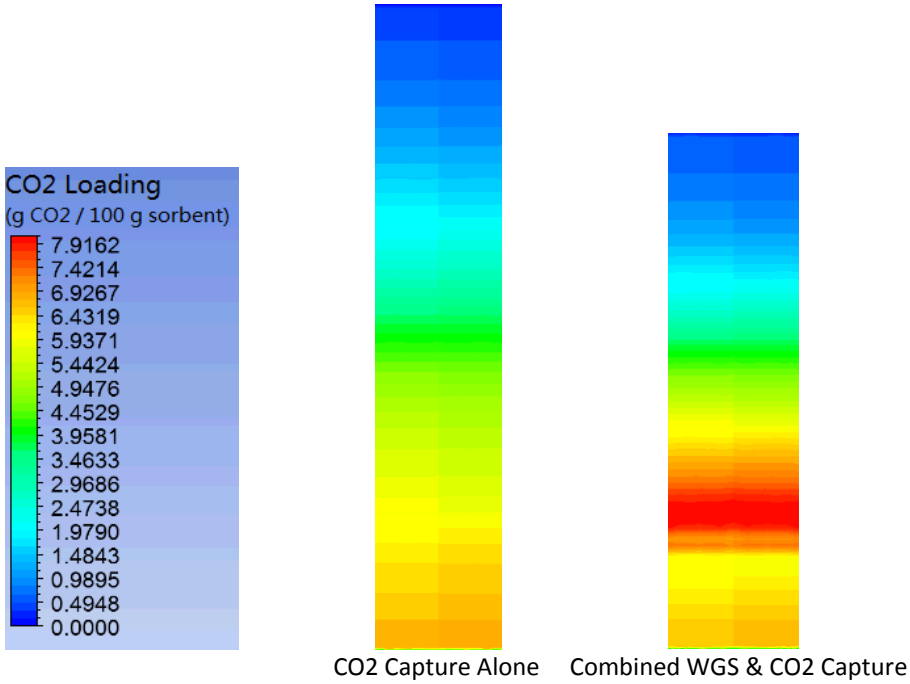

Figure 5-58 CO_2 loading at the end of adsorption step

Temperature distribution for adsorption step is shown by Figure 5-59 and Figure 5-60. Due to cyclic operation, the initial temperature profile is affected by previous cycles. For both CO_2 capture scenarios, as time evolves temperature increases across the beds. For CO_2 capture alone bed temperature ranges between 180C and 225C, for combined WGS and CO_2 capture bed temperature ranges between 130C and 230C, both within the active temperature range of the solid sorbent as well as the catalyst.

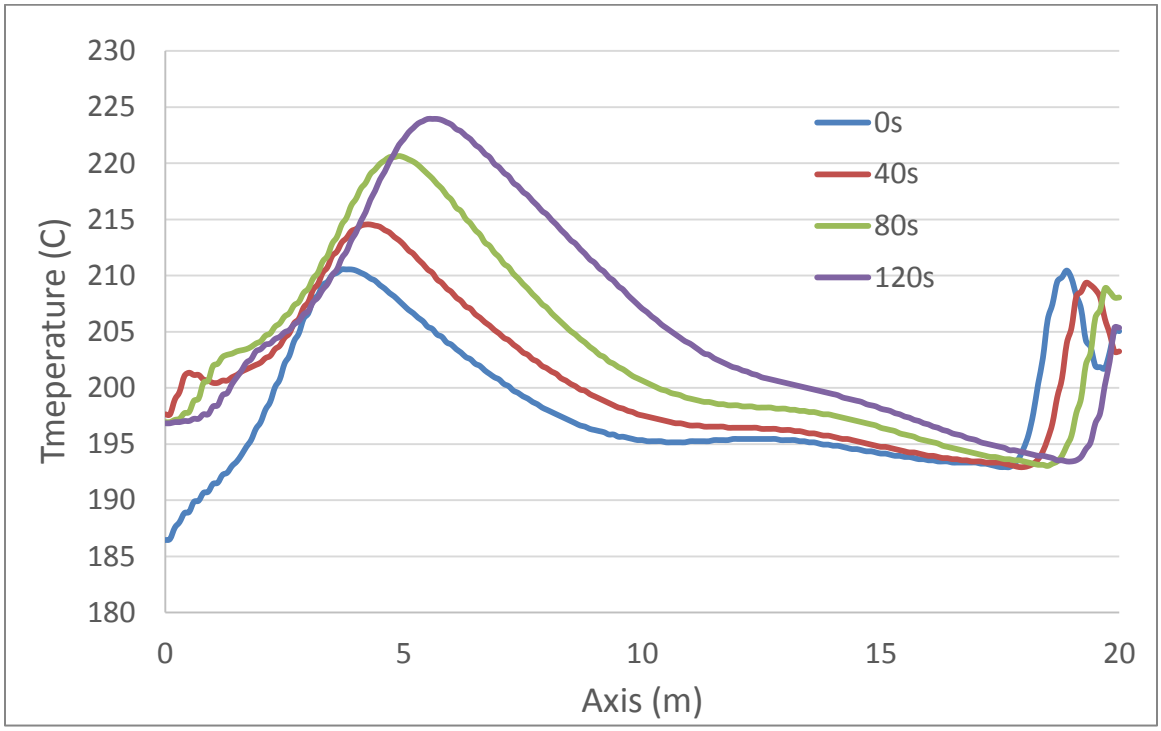

Figure 5-59 Temperature profile for adsorption step of CO_2 capture alone

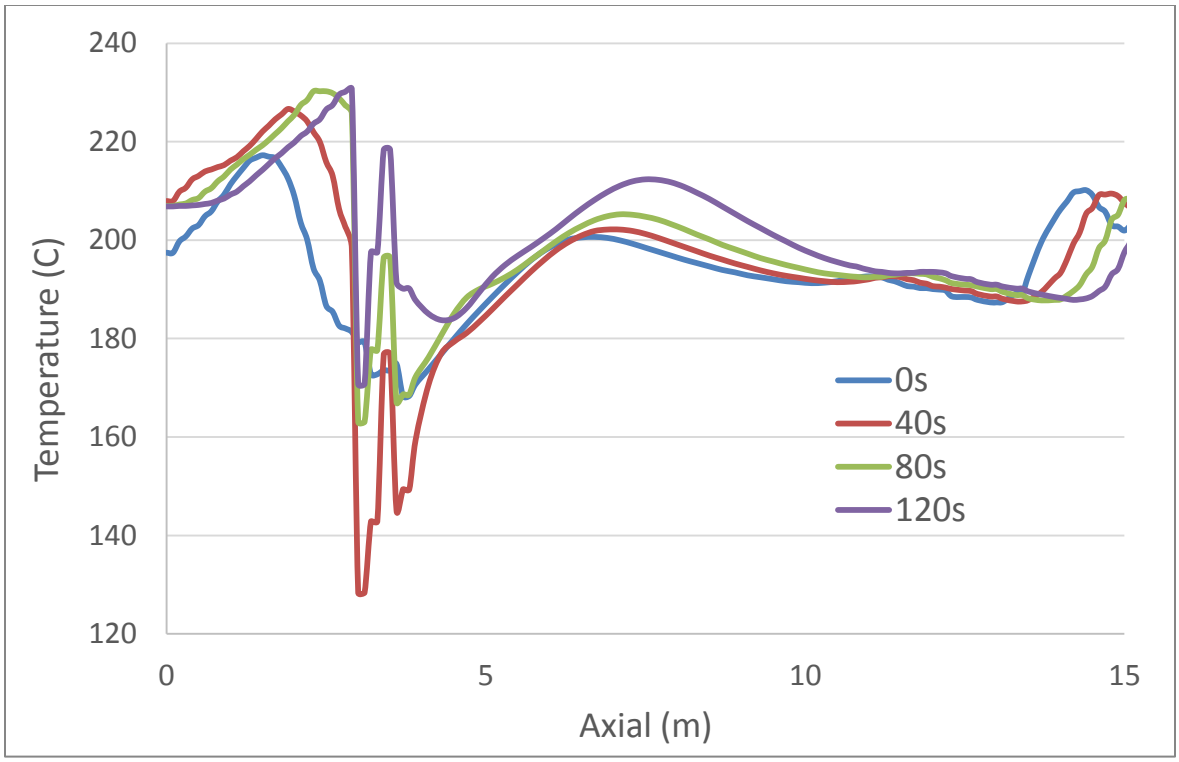

Figure 5-60 Temperature profile for adsorption step of combined WGS and CO_2 capture

Pressure drop of adsorption and purge steps for both CO_2 capture alone and combined WGS and CO_2 capture are shown by Figure 5-61. Since the bed height of the combined technology is lower, the corresponding pressure drops are lower than those for CO_2 capture alone. For CO_2 capture alone reactor, the maximum pressure drops are 1.05 bar and 1.40 bar for adsorption and purge step respectively. For combined technology, the maximum pressure drops are 0.62 bar and 1.20 bar for adsorption and purge step respectively.

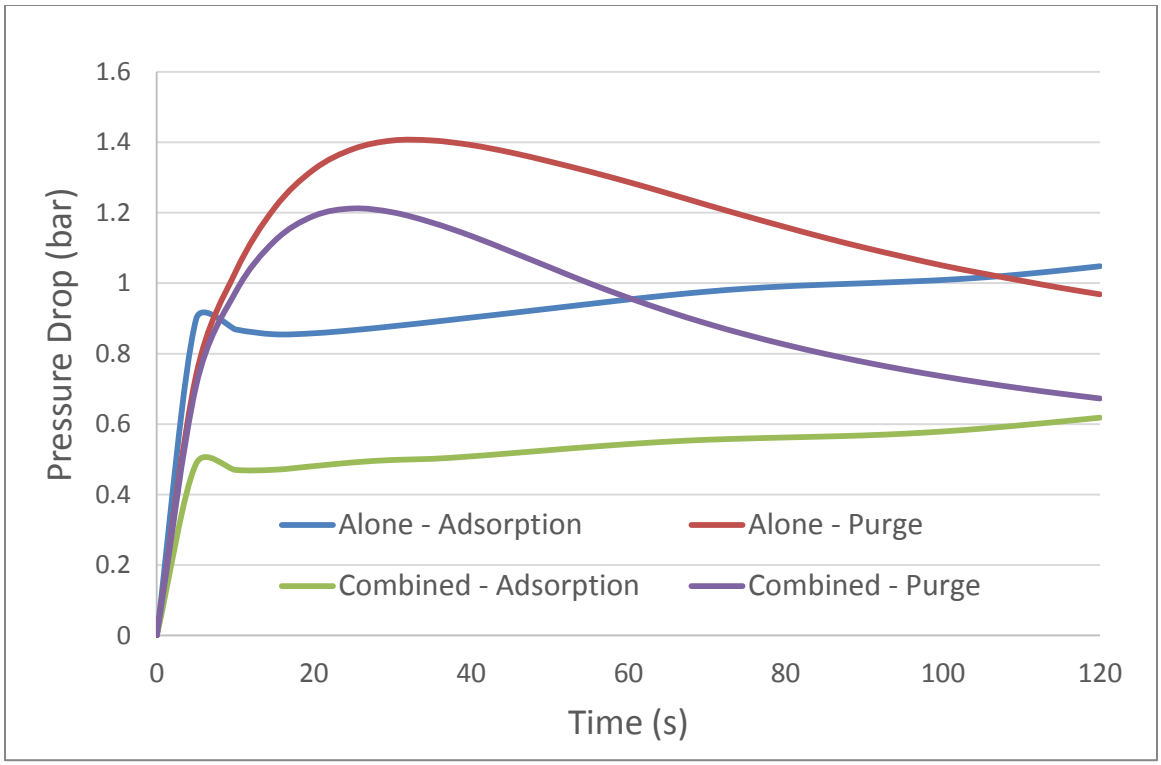

Figure 5-61 Pressure drop across the reactor bed

5.5 Summary

This chapter presents work on IGCC with solid sorbent CO_2 capture technologies. Two technology approaches are investigated, CO_2 capture alone and combined WGS and CO_2 capture. System analysis of IGCCs using this CO_2 capture approach is conducted to understand the advances at a system level. In comparison with Selexol^{TM} CO_2 capture, due to high moisture content in decarbonized syngas solid sorbent CO_2 capture requires smaller ASU unit as well as lower syngas diluent nitrogen compression power. In addition, solid sorbent CO_2 capture unit itself consumes less power than Selexol^{TM} unit. Therefore, the IGCC plant efficiency for solid sorbent CO_2 capture alone and combined WGS and CO_2 capture is higher than that for Selexol^{TM} CO_2 capture technology, by 2.77% and 3.27%, respectively. Difference in the moisture content of decarbonized syngas also results in performance difference between the two solid sorbent based CO_2 capture cases. Combining the effects of steam saving for power generation and slightly larger ASU unit and nitrogen compression, the IGCC with combined WGS and CO_2 capture technology has an overall plant efficiency of 34.31% which is slightly higher than that of the plant using CO_2 capture alone technology at 33.81%.

A CFD model was developed to understand the operating conditions, thermal management and reactor design of solid sorbent CO_2 capture reactors. Adsorption model is based on Langmuir-Freundlich Isotherm and linear driving force model. The WGS reaction rate equation is obtained from literature with the effect of gas internal diffusion added by introducing an internal effectiveness factor. The CFD model is

validated with experimental data for CO_2 capture alone and combined WGS and CO_2 capture. It is found that the CO_2 breakthrough time or CO_2 loading capacity is independent of reactor geometry as long as the space velocity is constant and within practical limits. Adsorption rate is the control step for CO_2 capture using the solid sorbent with a result that the solid sorbent bed is not fully utilized. However, low space velocity can increase the loading of the sorbent. One effective way to improve the performance of solid sorbent CO_2 capture is to increase the potential of adsorption and the adsorption rate by increasing mass diffusion rate within the porous structures and increasing functional groups in the porous surfaces. CFD model was applied to determine the operating conditions, reactor dimensions and thermal management for both solid sorbent based CO_2 capture alone technology and WGS and CO_2 capture technology.

Chapter 6 Co-Feeding and Co-Production for IGCC Using Advanced Technologies

Biomass is carbon neutral renewable energy, and co-production of fuels in power plants can play an important role in mitigating global warming due to the synergy in coproducing electricity and chemicals. This Chapter investigates conceptual designs for such integrated gasification combined cycle (IGCC) plants with carbon capture using the adsorption technology along with other advanced technologies under development. A major focus is selection of sub-systems and integration of the advanced technologies. Thermal performance and economics of the resulting plant configurations are assessed, and a particular focus is the quantitative analyses of co-feeding biomass along with coal and co-production. This chapter focusses primarily on H_2 co-production but co-production of Fischer-Tropsch (F-T) Liquids and ethanol, are also addressed.

6.1 Design Basis

6.1.1 Feedstock Specification

When looking at the U.S., there are large coal reserves available for power generation. About half the coal produced in the U.S. is bituminous containing from 65% to 85% carbon and resulting in a high energy density. At the other end of the spectrum, low rank lignite is another major coal resource, accounting for 7% of total U.S. produced coal [160]. Significant differences in heating value and ash, sulfur and moisture content between these two types of coals result in different gasification and overall plant

performances. Thus, these two major coal types are selected to cover each end of the spectrum.

Biomass residues, short rotation woody crops and herbaceous energy crops are under consideration as the primary biomass feedstocks for gasification. Biomass residues are heavily limited by harvest season, collection and transportation and thus are not suitable for large scale biomass only IGCC applications. On the other hand, short rotation woody crops and herbaceous energy crops grown on purpose can provide constant and significant supply of the biomass resource for power generation. They can grow on marginal or degraded lands and avoid competition over agricultural lands, as promoted by the Conservation Reserve Program (CRP) [161] led by the U.S. Department of Agriculture (USDA) Natural Resources Conservation Service (NRCS). Hybrid poplar, a short rotation woody crop, and switchgrass, an herbaceous energy crop, have been widely planted on CRP lands [162], [163]. Besides, hybrid poplar and switchgrass are fast growing crops, and they have been successfully utilized in gasification facilities [164]. Thus, these two biomass feedstocks are selected for this study.

Co-feeding of the biomass along with coal appears to be a strategy for building large scale IGCCs which can take advantage of economies of scale. Furthermore, this strategy can circumvent any seasonal variability in the supply of biomass; the coal rate may be increased to compensate for the reduction in biomass supply as long as the feed handling system is properly designed.

Table 6-1 Coal properties

	Bituminous		Lignite	
Coal Name	Illinois No. 6 (Herrin)		North Dakota Beulah-Zap	
Mine	Old Ben		Freedom	
Proximate Analysis1	Dry Basis, %	As Received, %	Dry Basis, %	As Received, %
Moisture	0	11.12	0	36.08
Ash	10.91	9.7	15.43	9.86
Volatile Matter	39.37	34.99	41.49	26.52
Fixed Carbon	49.72	44.19	43.09	27.54
Total	100	100	100	100
Ultimate Analysis	Dry Basis, %	As Received, %	Dry Basis, %	As Received, %
Carbon	71.72	63.75	61.88	39.55
H_2	5.06	4.5	4.29	2.74
Nitrogen	1.41	1.25	0.98	0.63
Sulfur	2.82	2.51	0.98	0.63
Chlorine	0.33	0.29	18 ppmW [169]	12 ppmW [169]
Ash	10.91	9.7	15.43	9.86
Moisture	0	11.12	0	36.08
Oxygen	7.75	6.88	16.44	10.51
Total	100	100	100	100
Heating Value	Dry Basis	As Received	Dry Basis	As Received
HHV, kJ/kg	30,531	27,135	24,253	15,391
LHV, kJ/kg	29,568	26,172	23,334	14,803
Trace Components				
Mercury, ppm		0.18 [23]		0.116

Illinois No. 6 is utilized as the representative bituminous coal while the lignite is from N. Dakota. All data presented for these feedstocks except that for the Hg content of Illinois No. 6 coal and Cl content of N. Dakota lignite are taken from US Department of Energy (DoE) Funding Opportunity Number: DE-FOA0000496 [165]. Data for the hybrid poplar (or woody biomass) is obtained from DoE/NETL Report 2012/1547 [166]. Data for the switchgrass is obtained from DoE/NETL Report 2012/1546 [167]. The moisture content for the switch grass corresponds to covered field drying. Table 6-1 and Table 6-2 summarize the coal properties and biomass properties respectively. The relative amount of biomass in the co-feed cases is proposed at 30% of the total feed on a dry weight

basis based on successful operation of the Shell gasifier with coal and biomass mixtures [168].

Table 6-2 Biomass properties

	Woody Biomass		Switchgrass	
Ultimate Analysis	Dry Basis, %	As Received, %	Dry Basis, %	As Received, %
Carbon	52.36	26.18	42.60	36.21
Hydrogen	5.60	2.80	6.55	5.57
Nitrogen	0.37	0.19	1.31	1.11
Sulfur	0.03	0.02	0.01	0.01
Chlorine	0.10 [170]	0.05 [170]	0.04 [171]	0.03 [171]
Ash	1.38	0.69	7.41	6.30
Moisture	0.00	50.00	0.00	15.00
Oxygen	40.16	20.08	42.08	35.77
Total	100.00	100.00	100.00	100.00
Heating Value	Dry Basis	As Received	Dry Basis	As Received
HHV, kJ/kg	19,627	9,813	18,113	15,396
LHV, kJ/kg	18,464	9,232	16,659	14,161

6.1.2 Design Basis

ISO ambient conditions are utilized for Illinois No. 6 bituminous coal studies: 15°C dry bulb temperature, 60% relative humidity, and sea-level barometric pressure. Since the lignite is from N. Dakota and lignite is typically not transported over significant distances due to its much lower energy density, ambient conditions for these set of cases are more specific to N. Dakota: 4.4°C dry bulb temperature, 40% relative humidity, and elevation of 579 m above sea level.

The coal only based IGCC plants developed to quantify the merits of cofeeding biomass and coproduction, capture 90% of the carbon present in the particulate free syngas, while the biomass cofed cases capture 80% of the carbon to take credit for the

renewable nature of the biomass feedstock, consistent with DoE Funding Opportunity Number: DE-FOA0000496 [165]. Even with this lower amount (80%) of carbon capture for biomass cofed cases (with 30% by weight of the total feed as biomass on a dry basis), substantially lower CO_2 emissions on a net MW basis are realized.

Co-produced H_2 is specified to be industrial grade or gas turbine fuel, but not Fuel Cell Hybrid Vehicle quality. The molar based purity is 99.95%.

For electricity and H_2 cases, the criteria used in setting the split between electricity and the co-product is:

$$\frac{\text{Net WM } \times 3.6 \times 10^6 \text{ KJ/(hr MW)}}{\text{Net WM } \times 3.6 \times 10^6 \text{ KJ/(hr MW)} + \text{KJ HHV Co} - \text{product}} = 50\%$$

6.2 Advanced Technology Identification

A major goal of this investigation is to identify advanced technologies for all the IGCC plant cases for commercial operation in the 2025 time frame. The major focus areas for integration are: air separation unit (ASU), gas cleanup, and combined cycle power generation.

6.2.1 Advanced Technology Identification

To achieve efficiency or performance gain from technology advancements, various promising technologies under development are identified. The main emphasis is to improve not only the performance of individual equipment but also overall plant cost and identify synergistic thermal integration of different plant subsections. Table 6-3 summarizes the technologies selected for major plant subsections for the electricity only and for the co-production IGCCs.

Air separation technology. The conventional ASU technology which uses cryogenic separation has a significant parasitic power consumption, as much as 15% of the IGCC gross power output [39]. Ion transport membrane (ITM) air separation technology [39], [172], [173] selected for this study has the potential for reducing both the power consumption and capital cost by as much as 30%. Highly selective ceramic membranes are used for the ITM process to separate O_2 from hot compressed air. At the operating temperature of 800 to 900°C, O_2 on the feed side (air) is ionized on the surface of the membrane and diffuses through the membrane as ions forming oxygen molecules on the permeate side. The pressure at the feed side is in excess of 14 bar and low to sub-

atmospheric pressure on the permeate side. The chemical potential (or O_2 partial pressure for ideal gases) gradient is the driving force for transporting O_2 from one side to the other. Compared with conventional cryogenic ASU, ITM with its higher operating temperature and pressure can achieve better integration with the advanced gas turbines which have higher pressure ratios.

Gasifier. A dry feed gasifier is employed in this study since it is more suitable for biomass as well as the lignite. A Siemens type dry feed, entrained flow, slagging, single stage, down-flow gasifier operating at a pressure of 40 bar is selected. This gasifier like the Shell gasifier is flexible with regard to feedstock, and can utilize coal as well as biomass [30]. In addition, the Siemens gasifier is simpler in design and multiple feed nozzles are available.

Biomass Pretreatment. To reduce the efficiency penalty of drying the biomass feedstocks, vapor recompression [174] (heat pump) technology is selected which recovers the latent heat in the evaporated moisture. Pyrolysis has been proposed in order to increase the friability of the biomass to assist in the milling operation but this added step results in a more complex plant since the process produces tars and oils that need to be treated or fed as an additional feed to the gasifier. Here, the pretreatment simply consists of drying the feedstock flowed by milling; the drying process increases the friability and the corresponding higher milling power requirement (derived from experimental data [175], [176]) is justified from a simplicity of design standpoint.

Gasifier feeding. A solids pump [177], [178] is identified to pressurize the milled solid fuel and introduce it into the gasifier while utilizing recycle CO_2 as inerting and injection gas to transport the solids into the gasifier. A solids pump has advantages over conventional lock hoppers such as controlled, continuous delivery of coal, and less gas losses.

Raw syngas scrubbing. The dry scrubbing option is an evolving technology but due to the significant uncertainties with respect to producing a syngas clean enough to meet the specifications of the advanced gas turbine, this technology is first compared with the conventional wet scrubbing option to quantify if a significant advantage does exist for the dry scrubbing option as discussed in the following section.

Syngas desulfurization [41]. In current state-of-the-art IGCC with carbon capture and storage (CCS), the syngas is desulfurized as well as decarbonized by scrubbing with a refrigerated physical solvent such as in the Selexol™ process. The syngas fed to this unit is cooled to near ambient temperatures to produce an H_2S rich acid gas which is provided to the Claus process for producing elemental sulfur byproduct. In this study, regenerable ZnO process operating around 260°C is employed for desulfurization, which eliminates the irreversibilities associated with cooling the syngas to near ambient temperatures when integrated with other downstream high temperature processes. The regenerator off-gas containing SO_2 is processed to produce H_2SO_4 byproduct.

Syngas mercury removal. A regenerable sorbent process [28] operating at much higher temperatures than the conventional sulfided activated carbon bed is selected to

remove mercury content making it compatible with the above described desulfurization as well as other downstream processes.

Syngas shifting. Two stages of syngas shifting are employed in this study consisting of a high temperature shift reactor followed by a low temperature shift reactor to react the CO with the H_2O vapor present in the syngas and additional steam added to form H_2 (and CO_2). Since the upstream desulfurization process does not completely desulfurize the syngas (Siriwardane et. al. [41] report < 10 ppmv H_2S plus COS remains), a sulfur tolerant catalyst is required. The two reactors operate adiabatically with intercooling while recovering the heat for the steam cycle.

Syngas CO_2 separation. As mentioned previously, current state of the art IGCCs with CCS typically separate CO_2 using a low temperature physical solvent scrubbing process [23], while the fixed-bed sorption process [42] operates at much higher temperatures, around 200°C. By separating CO_2 at a higher temperature, the irreversibilities associated with cooling the gas to near ambient temperatures are reduced. CO_2 desorbed from the sorbent by regeneration with steam is processed for further purification.

Combined Cycle Power Generation. H class gas turbine based combined cycle serves as power-island for electricity generation in this study. The H class gas turbine [179] is currently offered for natural gas operation (with a firing temperature of 1430°C) and it is assumed that this advanced steam cooled gas turbine will be offered for syngas applications in the future.

H_2 Purification. For co-production cases, a high purity H_2 co-product is produced from the H_2 rich decarbonized syngas in a conventional pressure swing adsorption (PSA) unit which operates near ambient conditions, the H_2 leaving the plant battery limits via pipeline near ambient temperatures. The tail gas leaving the PSA is compressed and combined with the syngas fed to the gas turbine.

Table 6-3 Plant subsection technology

Plant Unit	**Technology**
Air Separation	Ion Transport Membrane (ITM) Oxygen technology
Gasifier	Siemens type dry-feed entrained-bed operating at commercially offered operation pressure of ~41 bar and not at higher unproven pressure
Biomass Pretreatment	Drying using Vapor Recompression and Size Reduction by Milling
Gasifier feeding	Solids pump
Raw Syngas Scrubbing	Wet scrubbing as evaluated in screening study section
Syngas Desulfurization	Warm gas process such as RTI's ZnO process
Syngas Mercury Removal	Warm gas process such as TDA's regenerable sorbent process
Syngas Shifting	Sulfur tolerant catalyst
Syngas CO_2 Separation	Warm gas process such as TDA's regenerable sorbent process
Power Island	H Class gas turbine based combined cycle
H_2 Purification	Decarbonized syngas purified in PSA

6.2.2 Screening Analyses for IGCC Plant Integration

Screening analyses are conducted for raw syngas scrubbing options consisting of wet versus dry, the ITM integration with the gas turbine, and to determine the co-produced H_2 purity specification are described next.

Gas Cleanup. The wet scrubbing option consists of the following commercially proven units in the gas cleanup section of the IGCC upstream of the syngas shift unit: (1) cooling of the syngas exiting the gasifier at 1371°C to 677°C while generating high pressure steam, (2) barrier filter for removal of coarser particulates, (3) wet direct contact water scrubbing to remove remaining particulates and water soluble components including alkalis and chlorides, (4) preheating of the scrubbed gas from 189°C to 260°C followed by desulfurization using the regenerable ZnO process, and (5) cooling the desulfurized syngas to 250°C followed by mercury removal using the sorption process.

The dry scrubbing option consists of the following units in the gas cleanup section of the IGCC upstream of the syngas shift unit: (1) injection of aluminosilicates [180] into the raw syngas above 1000°C to react with alkalies by the following reaction: NaCl + $0.5Al_2O_3 + 3SiO_2 + 0.5H_2 + 0.5CO \rightarrow NaAlSi_3O_8 + HCl + 0.5C$, (2) cooling of the syngas to 800°C while generating high pressure steam, (3) passing the syngas through a halide filter-reactor containing nacholite, NaHCO3, to remove the halogens from the syngas by the reaction: $NaHCO_3 + HCl \rightarrow NaCl + H_2O + CO_2$, (4) further cooling of the syngas to 399°C while generating high pressure steam, (5) removal of particulates using monolithic ceramic filter [181] at 399°C which has been shown to have a separation efficiency of 99.999% in raw syngas applications, (6) spray water cooling of the syngas to 238°C, (7) preheating of the gas from 238°C to 260°C followed by desulfurization using the RTI regenerable ZnO process, and (8) cooling the desulfurized syngas to 250°C followed by mercury removal using the sorption process.

Compared to wet scrubbing, the dry scrubbing IGCC system shows only a half a percent decrease in plant net heat rate. Due to the low efficiency gain while the required technologies for high temperature halogen, alkali and particulate removal are highly developmental, the wet scrubbing option is selected.

Air Separation. Figure 6-1 through Figure 6-4 depict the four concepts investigated for the integration of the ITM with the gas turbine and Table 6-4 summarizes the impact on the relative heat rate of the IGCC for these various integration concepts as compared to the cryogenic ASU based IGCC. Case 1 preheats the depleted air against the extracted air, prior to returning it to the gas turbine. Cases 2 and 3 return the depleted air to the gas turbine at the same temperature as the air extracted from the gas turbine compressor discharge in order to minimize the impact on the gas turbine. This is accomplished by the generation of high pressure (HP) steam. Cases 3 and 4 return the depleted air to the gas turbine at the same pressure as the air extracted from the gas turbine compressor discharge without reducing the gas turbine pressure ratio. This booster compressor, however, requires inlet temperatures that are quite high. An axial compressor with design conditions similar to the HP stages of the gas turbine compressor would be suitable for this high temperature operation. Generation of HP steam to reduce the temperature of the depleted air returned to the gas turbine, however, negatively impacts the overall plant performance by as much as a 1% heat rate penalty. Inclusion of a booster compressor does improve the plant performance. The Case 4 configuration which returns the depleted air at the higher temperature and utilizes the high temperature booster compressor shows the highest plant performance

with approximate 4.0% decrease in overall plant heat rate over the cryogenic ASU based IGCC, and is selected.

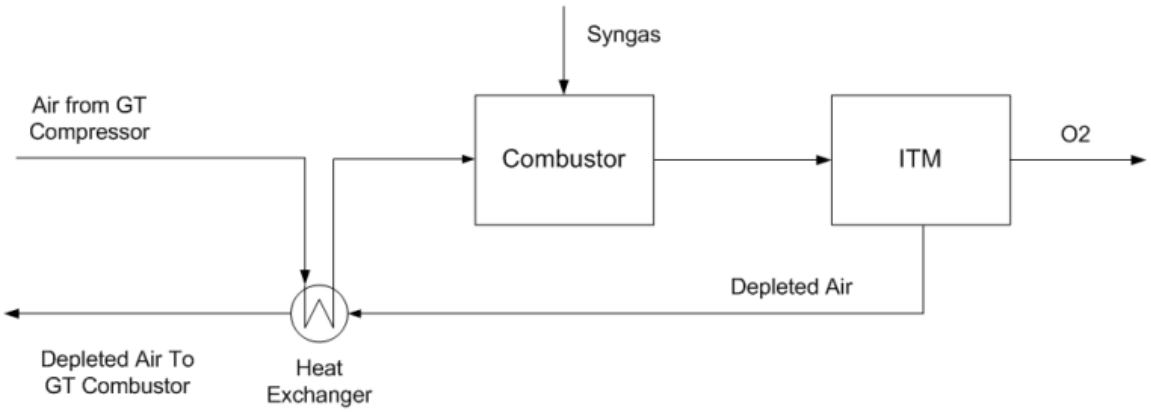

Figure 6-1 Block flow diagram – ITM integration for case 1

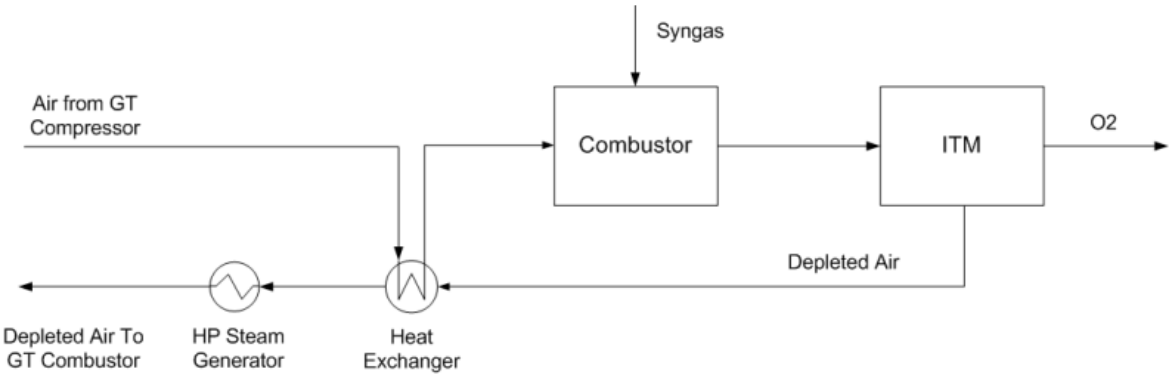

Figure 6-2 Block flow diagram – ITM integration for case 2

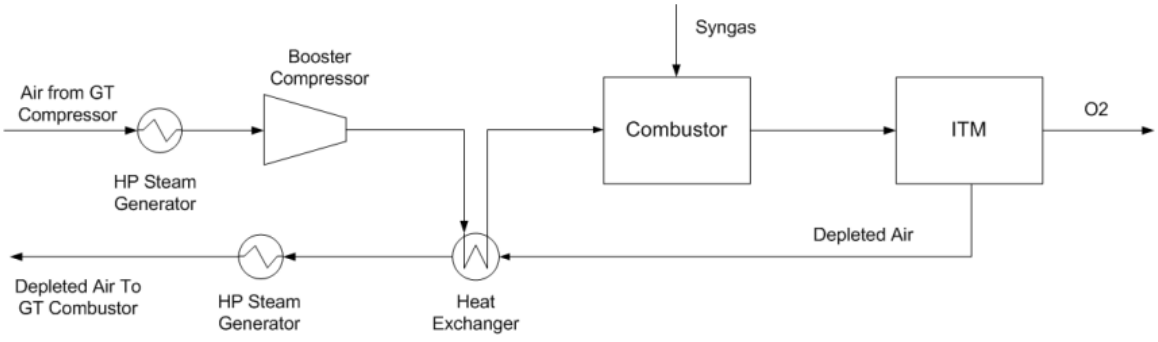

Figure 6-3 Block flow diagram – ITM integration for case 3

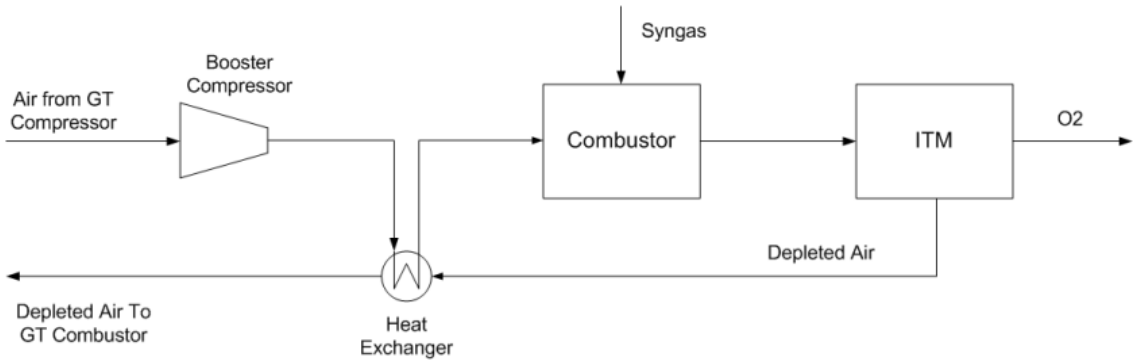

Figure 6-4 Block flow diagram – ITM integration for case 4

Table 6-4 Impact of ITM and gas turbine integration concepts on plant heat rate

	Case 0 (Cryogenic)	Case 1 (ITM)	Case 2 (ITM)	Case 3 (ITM)	Case 4 (ITM)
ITM Configuration	-	w/o HPS Producer	with HPS Producer	with HPS Producer	w/o HPS Producer
	-	w/o Booster Compressor	w/o Booster Compressor	with Booster Compressor	with Booster Compressor
Air Temperature to Booster Compressor, °C	-	-	-	362	485.5
Air and Depleted Air Mixture Temperature, °C	485.5	548.8	485.6	485.5	550.0
Decrease in Net Plant Heat Rate over Case 0, %	-	3.374	2.588	2.944	4.013

H_2 purity. A screening analysis is conducted to select the co-produced H_2 purity specification, i.e., industrial grade consisting of 99.95% H_2 versus decarbonized fuel gas for off-site gas turbines. The industrial grade H_2 as described previously is produced using a PSA unit to purify the decarbonized syngas. In the alternate case, a portion of the decarbonized syngas leaving the warm gas CO_2 removal unit is simply cooled while separating out the moisture and then exported for off-site gas turbines. The loss in electrical power output when producing industrial grade H_2 is about 2.3% compared with producing decarbonized fuel gas for export, with both options gasifying the same

amount of feedstock and exporting the same amount of energy (Lower Heating Value / LHV basis) contained in the exported co-product. The significantly higher revenue stream associated with the industrial grade H_2 offsets the increase in cost due to the addition of the PSA and the small loss in electrical power output and therefore, industrial grade H_2 is chosen for the H2 co-production cases.

6.3 Plant Configuration and Integration Concepts

6.3.1 Electricity only IGCCs

The resulting overall process scheme for the electricity only coal-fed IGCC plants with CCS using the advanced technologies is depicted in Figure 6-5 and only the advanced technologies subsystems are described in the following. Stream data for raw syngas and decarbonized syngas are presented in Table 6-5 and Table 6-6.

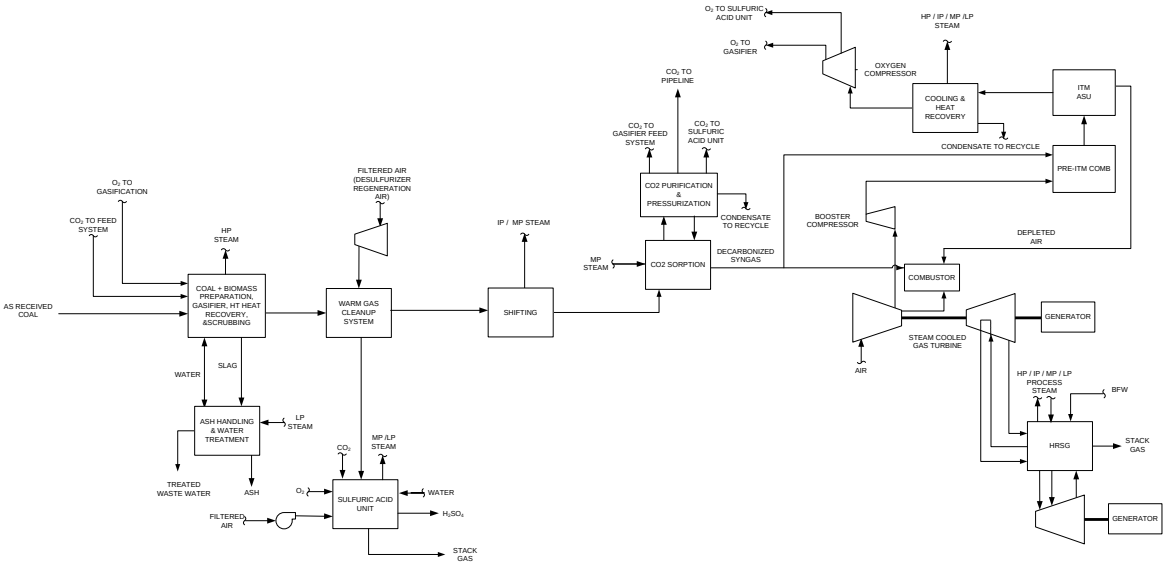

Figure 6-5 Block flow diagram – electricity only IGCC plants with CCS

Table 6-5 Raw syngas

Coal Type	Bituminous	Lignite	Bituminous	Lignite	Bituminous	Lignite	Bituminous	Lignite
Biomass Type	None	None	None	None	Wood	Wood	Grass	Grass
Co-product	None	None	H_2	H_2	H_2	H_2	H_2	H_2
Temperature, C	189	191	189	191	189	190	189	190
Pressure, bar	40.68	40.68	40.68	40.68	40.68	40.68	40.68	40.68
Flow Rate, kmol/hr	17775	17703	25680	23272	24205	22248	24904	22907
Mole Frac, %								
N_2	0.30	0.30	0.30	0.30	0.30	0.20	0.40	0.30
H_2	23.70	20.00	23.70	20.00	22.50	19.50	23.40	20.40
CO	37.40	39.20	37.40	39.20	38.60	40.00	37.90	39.40
CO_2	4.60	5.60	4.60	5.60	5.00	5.90	4.70	5.50
H_2O	33.40	34.60	33.40	34.60	33.20	34.20	33.10	34.10
H_2S	0.60	0.20	0.60	0.20	0.40	0.20	0.40	0.20
COS	0.10	0.00	0.10	0.00	0.00	0.00	0.00	0.00

Table 6-6 Decarbonized syngas to gas turbine combustor

Coal Type	Bituminous	Lignite	Bituminous	Lignite	Bituminous	Lignite	Bituminous	Lignite
Biomass Type	None	None	None	None	Wood	Wood	Grass	Grass
Co-product	None	None	H_2	H_2	H_2	H_2	H_2	H_2
Temperature, C	252	254	244	245	239	239	238	238
Pressure, bar	34.82	34.82	34.82	34.82	34.82	34.82	34.82	34.82
Flow Rate, kmol/hr	16390	16068	15827	14359	16409	15131	16591	15293
Mole Frac, %								
N_2	0.30	0.30	0.50	0.40	0.40	0.30	0.50	0.50
H_2	60.70	59.10	61.20	59.50	56.00	54.60	56.40	55.00
CO	1.30	1.30	2.00	2.00	1.80	1.80	1.90	1.90
CO_2	2.70	3.00	4.10	4.40	9.80	10.30	9.70	10.20
H_2O	34.90	36.30	32.20	33.70	32.00	33.00	31.50	32.50

Air Separation Unit (ASU). Feed to the ITM is extracted from the gas turbine compressor, further compressed to 25.7 bar in a booster compressor, and then heated up in an interchanger against the depleted air stream followed by further heating to 850°C by directly firing decarbonized syngas into the air stream. It then enters the membrane separation unit which is modeled using methodology developed by Air Products and Chemicals, Inc. [182]. Permeate oxygen stream is cooled in a heat recovery steam generator (HRSG) while generating HP, intermediate pressure (IP) and low pressure (LP) steam. Finally it is cooled against cooling water and then compressed by a

multistage intercooled compressor before it is provided to the gasifier and the H_2SO_4 unit, while non-permeate oxygen-depleted air is recycled back to the gas turbine.

Gasification and Syngas Cleanup. The dry feedstock is transported by CO_2 (and not N_2 as is done in conventional IGCCs utilizing a cryogenic ASU) and is fed to the gasifiers along with O_2 and steam via a top-mounted feed injector. Almost complete conversion (99.5%) of feedstock carbon occurs at temperature 1300°C to 1400°C. Hot raw syngas and liquid slag are discharged from the gasifier reaction chamber and the raw gas is cooled to 677°C in a radiant syngas cooler while generating HP steam. Coarser particulates are removed from raw syngas by barrier filter operating at this same temperature of 677°C [183], followed by spraying recycled water to remove water soluble components including alkalis and chlorides while cooling down the gas to 189°C. The slag discharges into a water bath at the bottom of the radiant syngas cooler and is cooled to temperature of around 220°C and the molten slag solidifies. The vitrified slag granulates accumulating in the water bath are discharged via a lock hopper. The gas is then fed through a fixed bed of nacholite sorbent for the removal of halides. The syngas is then preheated in a feed/effluent interchanger and desulfurized by the regenerable ZnO process such as that developed by RTI [41] operating at 260°C by the overall reactions: $H_2S + ZnO = ZnS + H_2O$ and $COS + ZnO = ZnS + CO_2$. The regenerator off-gas containing SO_2 obtained by the reaction: $ZnS + O_2 = ZnO + SO_2$, is fed to a H_2SO_4 unit to produce a saleable byproduct. The desulfurized syngas after cooling in the feed/effluent interchanger enters fixed-bed sorption process such as that developed by TDA [28] for Hg removal. Some of the NH_3 and HCN are also captured by this sorbent.

Syngas Shifting and Decarbonization. The purpose of this unit is to convert most of the CO in the syngas to H_2 by means of the water gas shift reaction: $CO + H_2O = H_2 + CO_2$. This conversion step is crucial to the overall carbon capture of the IGCC plant. NH_3 in the feed passes through the shift reactor unchanged and without affecting the catalyst performance. On the other hand, HCN will be hydrogenated to CH_4 and N_2. Sufficient steam is injected into the syngas and then fed to a fixed bed shift reactor and the heat evolved by the exothermic shift reaction is used to generate IP and medium pressure (MP) steam. The syngas is then fed to a second shift reactor for further conversion and the effluent from this second reactor is cooled to a temperature of about 200°C while generating MP steam. The syngas is then combined with recycle gas exiting the CO2 purification unit and then fed to the TDA fixed-bed sorption unit [42], [184] for decarbonizing the syngas. Regeneration is accomplished utilizing steam. The mixture consisting of desorbed CO_2, steam and residual syngas is cooled in a series of heat exchangers consisting of generating LP steam, vacuum condensate / makeup boiler feed water (BFW) heating and finally trim cooling against cooling water. The gas is then compressed, cooled while recovering bulk of the heat for vacuum condensate / makeup BFW heating, dehydrated and fed to a purification unit. The purification may be done cryogenically or simply fed to a catalytic oxidizer to burn off the combustibles present in this crude CO_2 stream depending on the required Ar content of the final CO_2 product. The purified CO_2 stream is then split into various fractions as required for in-plant usage (such as gasifier feed transport), and pressurized to the required pressures. The decarbonized syngas leaving the adsorption unit at a temperature of about 250°C with

its accompanying steam is supplied to the gas turbine along with the depleted air from the ASU.

Power Block. The combined-cycle power block consisting of the H class gas turbine exhausts into the HRSG which provides steam for the reheat steam turbine. In addition to the above equipment, the power block includes the associated vacuum condensate system, integral deaerator (as part of the HRSG), blowdown system and miscellaneous supporting facilities (boiler chemical injection and demineralized water package).

The performance on decarbonized syngas of this H class gas turbine [43] was developed in a previous study utilizing commercially available gas turbine modelling software, Thermoflex. A model was set up in Thermoflex utilizing published performance by General Electric (GE) for their 7H gas turbine [179] on natural gas and then this model was "operated" in off-design mode to obtain an estimate of its performance on syngas while limiting the blade surface temperatures at the same values as those for the calibrated natural gas case. This resulted in a decrease in the firing temperature of the gas turbine from 1428°C on natural gas to 1392°C on the syngas. The decarbonized syngas and the depleted air from the ASU are injected into the gas turbine combustor through separate nozzles. The steam enters the HP section of the steam turbine at 166.5 bar/538°C. Exhaust from the HP section is reheated to 538°C before admitting it to the IP section. The surface condenser uses circulating cooling water from the cooling towers while the makeup water for the steam system is sprayed directly into the condenser.

6.3.2 Electricity and H_2 Co-production IGCCs

The plant configuration for electricity and H_2 co-production IGCC plants is depicted in Figure 6-6. Stream data for raw syngas and decarbonized syngas to gas turbine combustor are presented in Table 6-5 and Table 6-6. The co-production IGCC configuration is similar to the previously described scheme for electricity only IGCC plants. Major differences in the configuration are described in the following:

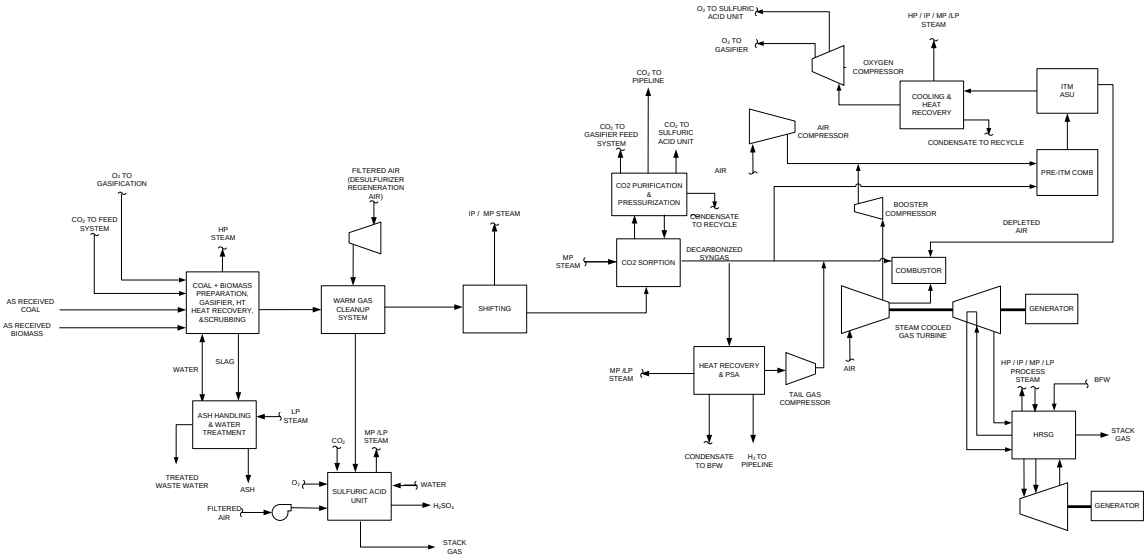

Figure 6-6 Block flow diagram – electricity and H_2 co-production IGCC plants CCS

Air Separation. Since a significant portion of the syngas is utilized for producing the co-product stream, the relative size of the gasification island in relation to the power island is much larger than that in the Electricity Only case. This results in the amount of air that may be extracted from the gas turbine not being sufficient for the ASU, since the maximum amount that may be extracted is typically limited to 50% of the total gas turbine inlet air for reasons such as not starving the gas turbine combustor of its liner

cooling medium. Thus, a compressor is included in the ASU to supply the additional air required by the ASU.

Biomass Receiving and Handling. In cases where woody biomass is a co-feed, hybrid poplar logs are received at the plant by truck and are unloaded using dedicated forklifts. The first step in size reduction consists of chipping the wood which is then sent to storage. In cases where switchgrass is a co-feed, the field dried switchgrass is received at the plant by truck as bundled bales. The trucks are again unloaded using dedicated forklifts and switchgrass storage consists of covered bales with allowances for water drainage. Each bale is wrapped in plastic net to prevent them from breaking during handling. The biomass is transferred from long term storage to short term storage, equivalent to 72 hours of uninterrupted production. In the case of switchgrass, from short term storage, the bales are conveyed to an unwrapping station and then to the biomass preparation and feed system. For this study it is assumed that there are no logistical barriers to transporting the required tonnages of either of the biomass feedstocks.

H_2 Co-production. The H_2 rich decarbonized syngas is fed to a PSA unit to produce the high purity co-product meeting the specifications as defined in the design basis. The tail gas from the PSA is compressed and combined with the fuel gas to the gas turbine.

6.4 Results and Discussion

Table 6-7 summarizes the thermal performance of the electricity only and the H_2 coproduction cases. A graphical comparison is presented in Figure 6-7 through Figure 6-9 showing the power generations, consumptions and thermal efficiencies of these cases. The plant feed rates for each of the cases are determined to fully load the gas turbine.

Table 6-7 Performance summary of IGCC plants

Coal Type		Bituminous	Lignite	Bituminous	Lignite	Bituminous	Lignite	Bituminous	Lignite
Biomass Type		None	None	None	None	Wood	Wood	Grass	Grass
Co-product	UNITS	None	None	H_2	H_2	H_2	H_2	H_2	H_2
	KG/HR (DRY)	122,902	150,832	177,565	198,287	132,053	142,341	138,913	150,546
Coal Feed Rate	MT/D (DRY)	2,950	3,621	4,262	4,760	3,170	3,417	3,334	3,614
	KG/HR (DRY)	0	0	0	0	0	0	59,534	64,520
Grass Feed Rate	MT/D (DRY)	0	0	0	0	0	0	1,429	1,549
	KG/HR (DRY)	0	0	0	0	56,594	61,003	0	0
Wood Feed Rate	MT/D (DRY)	0	0	0	0	1,358	1,464	0	0
Total HHV Input	GJ/HR	3,753	3,659	5,422	4,810	5,143	4,650	5,320	4,821
Gas Turbine Power Output	KW	318,000	312,928	318,000	312,928	318,000	312,928	318,000	312,928
Steam Turbine Power Output	KW	147,382	140,679	162,653	143,166	159,346	143,595	165,137	149,308
Total Gross Power Output	KW	465,382	453,607	480,653	456,094	477,346	456,523	483,137	462,236
Total Auxiliary Consumption	KW	66,550	80,057	103,344	137,330	129,342	154,607	110,652	136,110
Total Net Power Output	KW	398,833	373,550	377,310	318,764	348,004	301,916	372,484	326,126
Co-product Produced	MT/D	0	0	229	194	211	183	226	198
Co-product HHV	106 KJ/H	0	0	1,357	1,148	1,252	1,086	1,341	1,174
Decarbonized Syngas HHV	KJ/M3	7,521	7,322	7,518	7,319	7,103	6,935	7,157	6,989
Net Power Efficiency[2] HHV	%	38.26	36.76	25.05	23.86	24.36	23.37	25.20	24.36
Net Power Heat Rate	KJ/KWH	9,410	9,795	14,371	15,089	14,780	15,403	14,283	14,782
H2 Efficiency[3] LHV	%	0	0	21.84	20.96	21.38	20.63	22.22	21.62
Net Equivalent Power Efficiency[4], Converting 60% H2 LHV	%	38.26	36.76	37.74	35.96	36.70	35.21	37.98	36.70
Electricity / Total Energy	%	100.0	100.0	50.0	50.0	50.0	50.0	50.0	50.0
Carbon Captured	%	90.0	90.0	90.0	90.0	80.0	80.0	80.0	80.0
Condenser Cooling Duty	106 KJ/H	686.03	626.77	771.21	643.40	758.21	651.08	796.74	689.94
Raw Water Use	M3/MIN	13.18	12.90	17.06	15.41	15.57	14.16	15.92	14.45

[2] Net Power Efficiency = Net Power Produced Expressed in Thermal Units / Total Plant Feedstock HHV

[3] H_2 Efficiency = H_2 Product LHV / Total Plant Feedstock LHV

[4] Net Equivalent Power Efficiency = (Net Power Produced Expressed in Thermal Units + 0.6 X H_2 Product LHV) / Total Plant Feedstock HHV

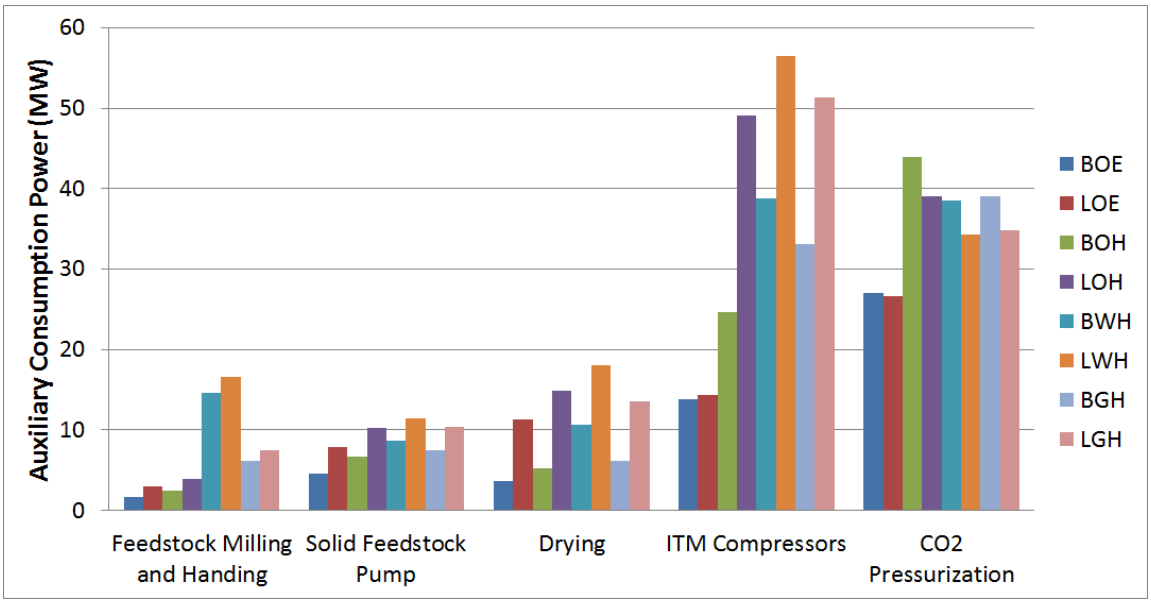

Figure 6-7 Major power consumptions[5]

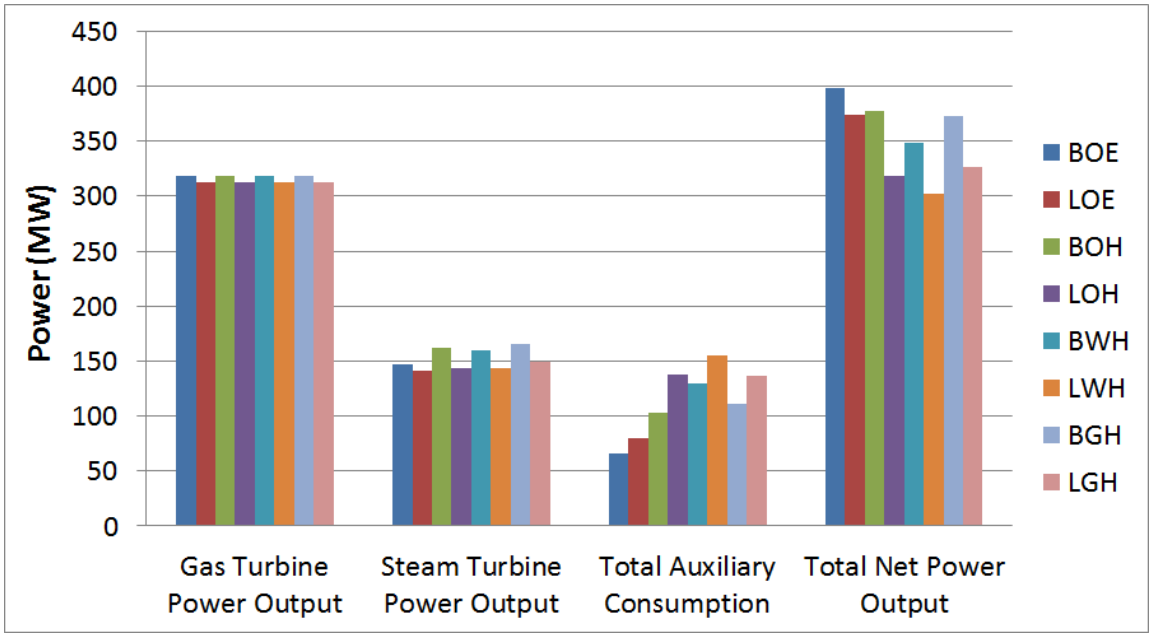

Figure 6-8 Power output and consumption

[5] Abbreviations (e.g. BOE, LOE etc.) represent various IGCCs. 1st letter represents coal type, B is bituminous, L is lignite. 2nd letter represents biomass type, O is none biomass, W is woody biomass, G is switchgrass. 3rd letter represents coproduction option, E is electricity only case, H is H_2 coproduction case.

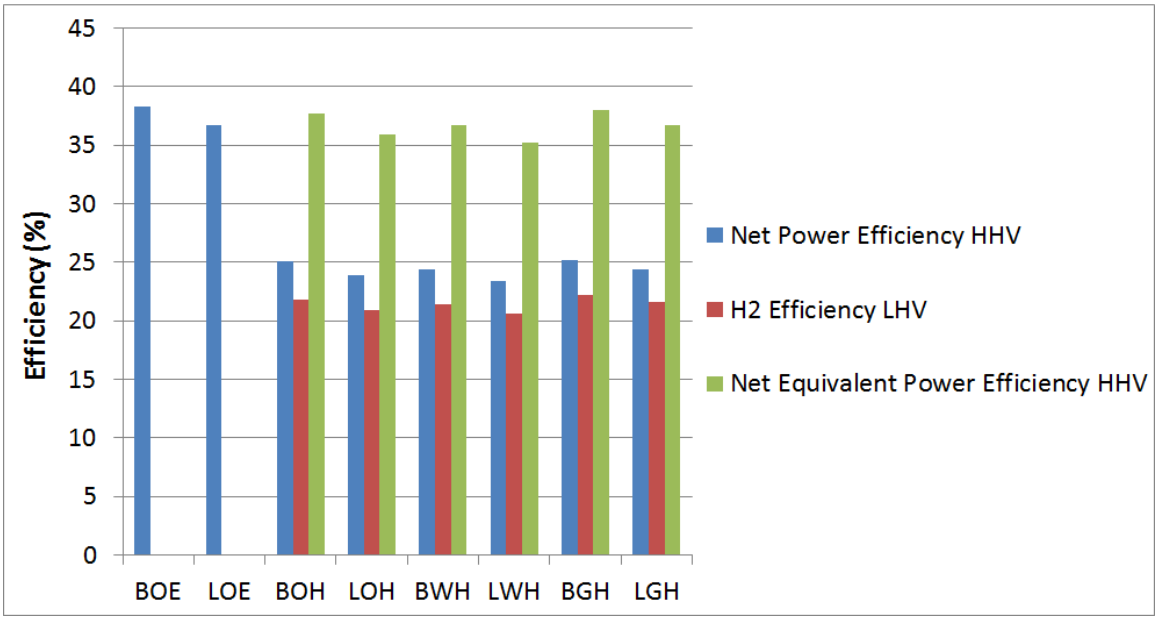

Figure 6-9 Plant efficiency

6.4.1 Electricity Only IGCC Performance

Due to the higher heating value or HHV of the bituminous coal than the lignite, the bituminous case shows a higher net power efficiency of 38.26% (HHV basis) versus 36.76% (HHV basis) for the lignite case. The fully loaded gas turbine output of 312,928 KW for the lignite case is lower than that for the bituminous case at 318,000 KW due to the higher elevation of the lignite plant.H_2 Co-producing IGCC Performance

The comparison is first made between coal based (without biomass) plants for electricity only and for H_2 co-production. As described previously in the design basis section, electricity and H_2 equally divide the total energy output (H_2 on an HHV basis) for

co-production cases, while the gas turbine operates at the same full load as electricity only cases. Therefore, feedstock input for co-production scenario is significantly higher than electricity only scenario as shown in Table 6-7. Figure 6-7 compares the five major auxiliary power consumptions of the plant. Power for feedstock milling and handling which increases primarily with the feedstock flow rate on an "as-received" basis and the power for solid feedstock pump which increases with the dried feedstock flow rate are significantly larger for co-production IGCC plants. The power for the feedstock drying operation in addition to being dependent on the feedstock flow rate is also a function of the feed moisture content which is higher for the lignite. Similarly, the absolute amount of CO_2 captured is significantly higher for the co-production cases since the feedstock flow rate is higher, resulting in the increased power consumption for CO_2 pressurization. There is a significant increase in ITM compression power for co-production IGCC plants also due not only to the increase in feedstock (requiring more O_2 for gasification), but also due to the added air compressor to limit the amount of air extraction from the gas turbine to 50%. These explain the larger total auxiliary consumption in Figure 6-8 for co-production IGCC plants. On the power generation side, since the gas turbine is fully loaded, the combined cycle power outputs are comparable. The net result is that the total net power output for co-production IGCC plants is lower as shown in Figure 6-8 and due to higher feedstock input, a significant drop in net power efficiency for the co-production cases as can be seen in Figure 6-9.

Next an incremental analysis is presented for assessing the merits of H_2 co-production. Consider a coal fed co-producing IGCC as comprised of two sections, namely

an electricity section and a H_2 section, with the electricity section producing only electric power with a power efficiency of the coal only IGCC. The equivalent coal feed for the electricity section can then be calculated. The equivalent coal feed rate to the H_2 section which produces "only H_2" is then the remaining portion of total coal feed. The conversion efficiency of the H_2 section, therefore, is defined as the ratio of energy in the H_2 stream and energy in this equivalent coal stream (both on LHV basis). The conversion efficiencies of H_2 are presented by Figure 6-10. H_2 section efficiencies are 63.25% and 59.72% for bituminous and lignite co-production cases respectively which are comparable to that of a steam methane reforming (SMR) H_2 plant [185] which has an efficiency of about 67% at the same CO_2 emission level (kg CO_2 / kg H_2) [185], [186] despite coal being a much dirtier fuel.

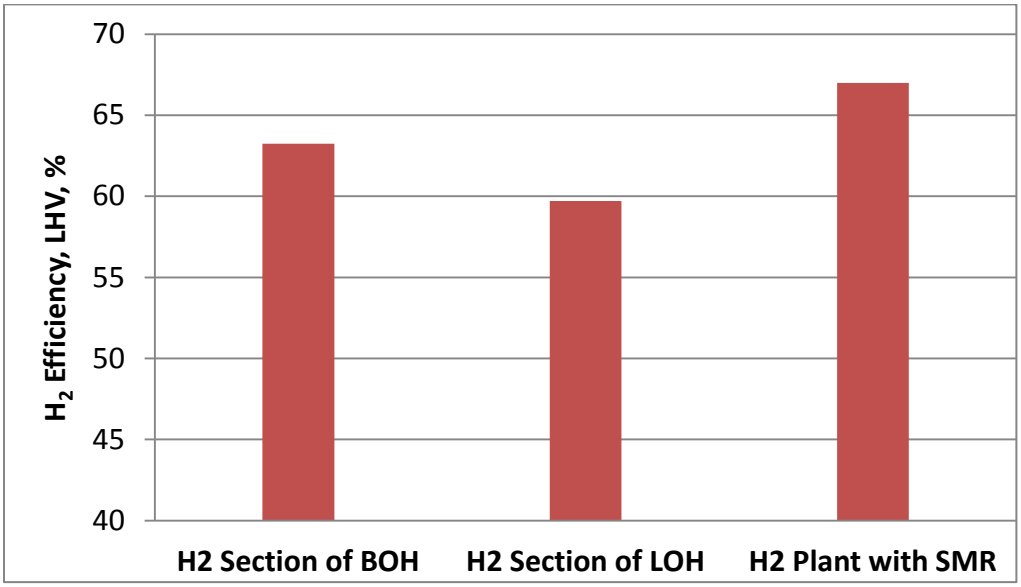

Figure 6-10 Conversion efficiencies of H_2

6.4.2 Biomass Co-feeding IGCC Performance

Next, a comparison is made between the different feedstocks for the H_2 co-production scenario. Co-feeding cases utilize coal (70% dry basis) and biomass (30% dry basis) feedstocks. Incremental analyses are conducted by decoupling coal and biomass in the co-feeding cases.

As mentioned previously, due to the higher elevation for the lignite cases, the gas turbine output is lower, resulting in a lower exhaust flow and consequently lower steam generation rate and steam turbine power output (shown in Figure 6-8). The steam turbine output shows no significant variation to the type of feedstock for a given plant location, the same gas turbine being used in all cases and fully loaded to the site specific conditions. The first three auxiliary power consumptions presented in Figure 6-7 for the biomass cofired cases are significantly higher than the corresponding coal only cases for the same reasons mentioned previously, i.e., being dependent on the feedstock flow rate and its moisture content. The majority of the power consumption of the ITM compressor in the co-production cases is due to the power consumed by the extra air compressor. To maintain a comparable air flow rate feeding the ITM, flow rate of the extra compressor increases with decreasing gas turbine inlet air flow rate and lowering fuel heating value. As shown in Table 6-7, lignite cases produce lower heating value decarbonized syngas due to LHV of lignite than bituminous coal, resulting in higher ITM compressor power. For a given coal, woody biomass cofed cases consume highest ITM compressor power for the same reason while switchgrass cofed cases consume the second largest. Regarding CO_2 pressurization, coal based plants which capture 90% of

total carbon consume relatively higher power for CO_2 compression than biomass cofed plants which capture 80% of total carbon. Bituminous cases for H_2 co-production utilize more CO_2 pressurization power compared with lignite cases due to higher carbon content for bituminous than lignite. The net power efficiencies for co-production cases as shown in Figure 6-9 are around 25%, significantly lower than the electricity only cases since a significant amount of energy leaves in the H_2. H_2 efficiencies (defined as the ratio of LHV of H_2 and LHV of the total feedstock, i.e, used in the production of electricity and the coproduct) for bituminous cofed co-production cases range from 21.38% to 22.22%, and those for lignite cases range from 20.63% to 21.62%. To account for energy in both electricity and H_2 on an equivalent basis, net equivalent power efficiency is calculated using an efficiency of 60% for converting the H_2 LHV to electricity. The net equivalent power efficiencies for bituminous cofed co-production cases then range from 36.70% to 37.98%, close to the efficiency of the bituminous fed electricity only case of 38.26%; while the net equivalent power efficiencies for lignite cofed co-production cases range from 35.21% to 36.70%, which are again close to the efficiency of the lignite fed electricity only case of 36.76%.

Next an incremental analysis is presented for assessing the merits of co-feeding biomass. Consider a biomass co-feeding and H_2 co-producing IGCC as being composed of a coal feeding section and a biomass feeding section, and coal feeding section operates with the same performance as coal only IGCC H_2 co-production plant. The resulting performances of the biomass feeding sections are shown in Table 6-8, indicating that the plant performance of biomass co-feeding plants with 80% carbon capture are

competitive with coal feeding plants with 90% carbon capture. Woody biomass co-feeding plants have lower net power efficiency and H_2 efficiency than coal feeding plants, while switchgrass co-feeding plants have better performance. The differences between woody biomass co-feeding plants and switchgrass co-feeding plants are due to the differences in their composition. Moisture content of woody biomass is 50%, much larger than that of switchgrass at 15% since it is field dried before it is received at the plant; thus woody biomass co-feeding plants consume lager power for feedstock milling and drying. In addition as described previously in this section, woody biomass produces a lower heating value decarbonized syngas resulting in higher ITM compressor power. Therefore, from an efficiency standpoint, woody biomass co-feeding is less competitive than field dried switchgrass co-feeding.

Table 6-8 Plant Performance of Biomass Feeding Sections of Co-feeding Cases

Case Designation	BOH	LOH	Bio Section of BWH	Bio Section of LWH	Bio Section of BGH	Bio Section of LGH
Net Power Efficiency HHV, %	25.05	23.86	21.86	21.99	25.83	25.92
H_2 Efficiency LHV, %	21.84	20.96	19.66	19.68	23.81	23.79

6.4.3 Economic Analyses

Capital costs, operating and maintenance costs, and the cost for transporting, storing, and monitoring of the CO_2 are evaluated to develop the relative economics for electricity only and co-production IGCC plants as shown in Table 6-9 and Table 6-10.

The 1st year levelized cost of electricity for the two electricity only (bituminous and lignite) cases were first developed using methodology described in the DoE/NETL Report

2010/1397 [23]. Next, the co-produced H_2 cost was determined to result in the same 1st year levelized cost of electricity as the corresponding electricity only case (i.e., with the same coal).

The cost of the bituminous coal was taken as $42.09/Metric Ton (as received) [23], while the cost of the lignite was taken as $12.04/ Metric Ton (as received) [187].

The cost of woody biomass was obtained by applying the cost correlation below [166] with X = (1 – biomass moisture fraction) * (as received biomass feed) [Metric Ton per day]:

Hybrid Poplar Cost ($/dry MT) = 1.252*10-11*X3 – 2.949*10-7*X2 + 3.476*10-3*X + 128.1

The cost of switchgrass was obtained by applying the cost correlation below [167] with X = switchgrass production, dry Metric Ton/day:

Switchgrass Cost ($/dry MT) = 1.418*10-11*X3 – 3.338*10-7*X2 + 3.934*10-3*X + 94.05

Larger biomass feedstock rates require larger areas of cultivation and, in turn, higher cost for collection and transportation to the plant. Therefore, the cost correlations for hybrid poplar and switchgrass both show an increase in cost when increasing the plant feed rate.

The resulting cost of woody biomass ranged from $132.37/dry MT to $133.35/dry MT, and that of switchgrass ranged from $99.09/dry MT to $100.33/dry MT. Due to this rather small variation, the costs of woody biomass and switchgrass for economic analysis were held constant at $132.28/dry MT (or $120/dry ST) and $99.21/dry MT (or $90/dry ST) respectively.

The first year cost of electricity (COE) calculated for the bituminous coal is $102.9/MWh while that for the lignite is $108.1/MWh. The calculated cost of H_2 ranged from $1.42/kg to $2.77/kg depending on the feedstock, which is lower than the DoE announced H_2 cost goal of $3.00/kg in July 14, 2005 [188]. Lin [189] also pointed out that a H2 price below $3/kg is preferable. Specifically looking at various feedstocks, lignite cofed H_2 co-production cases result in higher COE and higher cost of H_2 compared to bituminous cases. Due to the relatively higher cost of biomass feedstock, biomass cases show a higher H_2 cost with woody biomass feedstock having a higher H_2 cost than switchgrass.

Table 6-9 Plant cost and economics for electricity only cases

(Year 2007 $)

Feedstock	Bituminous	Lignite
Net Power, kW	398,833	373,550
Plant Cost, $1000		
Fuel Preparation System	146,555	213,044
Air Separation Unit	42,117	44,014
Gasification System	320,397	328,403
Gas Cleanup and Conditioning Systems	267,384	251,914
Power Island	184,749	180,513
Co-production Unit	-	-
General Facilities	155,693	153,790
Total Plant Cost (TPC), $1000	1,116,895	1,171,678
Total Fixed operating cost for Initial Year, $1000/yr	45,236	47,169
Total Variable Operating Costs for Initial Year, $1000/yr	71,207	56,962
1st Year Cost of Electricity (COE), $/MWh	102.9	108.1

Table 6-10 Plant cost and economics for electricity and H_2 co-production cases

(Year 2007 $)

Coal Type	Bituminous	Lignite	Bituminous	Lignite	Bituminous	Lignite
Biomass Type	None	None	Wood	Wood	Grass	Grass
Co-product	H_2	H_2	H_2	H_2	H_2	H_2
Net Power, kW	377,310	318,764	348,004	301,916	372,484	326,126
Plant Cost, $1000						
Fuel Preparation System	189,609	258,007	229,090	277,762	206,916	258,715
Air Separation Unit	54,495	53,312	52,982	51,765	52,874	51,644
Gasification System	414,522	397,712	395,131	380,333	409,788	395,272
Gas Cleanup and Conditioning Systems	354,720	310,678	312,981	277,303	316,469	279,842
Power Island	191,486	181,404	188,015	179,399	189,492	180,841
Co-production Unit	10,736	9,506	10,121	9,117	10,619	9,628
General Facilities	175,684	166,857	170,780	163,733	173,222	166,128
Total Plant Cost (TPC), $1000	1,391,251	1,377,476	1,359,100	1,339,412	1,359,380	1,342,070
Total Fixed Operating Cost for Initial Year, $1000/yr	54,834	54,512	53,852	53,302	53,929	53,464
Total Variable Operating Costs + Co-product Credit for Initial Year, $1000/yr	3,812	-23,477	-12,566[6]	-30,558	5,393	-12,360
H_2 Cost for Initial Year, $/kg	1.42	1.69	2.39	2.77	1.83	2.08
1st Year Cost of Electricity (COE), $/MWh	102.9	108.1	102.9	108.1	102.9	108.1

[6] Negative values are due to the credit for the coproduct.

6.5 Co-production of Transportation Fuels

Co-production of two other fuels in IGCC, namely F-T Liquids and ethanol is investigated in this section. F–T liquids could be processed in existing refineries while displacing petroleum and the refined products introduced into the market place at the present time or in the near term without requiring changes to the existing infrastructure. Fuel grade ethanol (97.7 mol% ethanol mixed with other alcohols resulting in an average carbon number of 2.01) could potentially serve in the not so distant future or could be phased in by blending with conventional liquid fuels. To be consistent with H_2 co-production cases, these co-production IGCCs are co-fed with biomass (30% by weight of the total feed on a dry basis), 50% of the energy exported is in the form of electricity, and 80% of the carbon produced are captured. Both bituminous and lignite are evaluated, while switchgrass is the sole biomass considered.

6.5.1 Plant Configurations

The plants are configured with the same promising technologies under development consistent with the previous cases with the main objective being to improve not only the performance of individual plant subsections but also the overall plant cost by identifying synergistic thermal integration of different plant subsections. Thus, the advanced technology subsystems are the same as in the H_2 co-production IGCCs as described previously. Only the F-T liquids synthesis and ethanol synthesis are described in the following.

F-T Liquids Synthesis. Once-through synthesis of co-products such as F–T liquids and ethanol while supplying the unconverted gas to the gas turbine has been shown to be advantageous but in the context of no CCS. These advantages include avoiding the buildup of inerts in the feed to the synthesis reactor, and eliminating the large recycle compressor and associated equipment for the unconverted gas. Since the plant designs for this research do require a significant degree of CCS, a screening analysis is first conducted to quantify the effect of purge rate from the synthesis loop on the overall system efficiency. For an F–T liquids co-production plant, it is found that the electrical heat rate is increased by as much as 1.46% when the purge rate is increased to 10% of the total recycle. When the purge rate becomes higher than a threshold amount, decarbonization of the purge gas is also required to limit the overall plant carbon emissions to the required value. The reduction in efficiency is due to the requirement for shifting and reforming the purge gas before the carbon may be captured as CO_2 which creates major irreversibilities from a thermodynamic standpoint. These additional equipment end up also penalizing the plant cost on a net basis. It should also be noted that with the ITM technology utilized for air separation in this work, the inerts buildup due to a reduction in the purge rate is less significant than for a plant utilizing cryogenic air separation.

The resulting plant configuration is depicted in Figure 6-11. A fraction of the clean syngas before it enters a 2^{nd} shift reactor is combined with a fraction of the unshifted syngas in order to obtain the specified H_2/CO ratio of about 1 [190] for the synthesis reactor feed gas, and passed through a bed of ZnO sandwiching a COS hydrolysis

catalyst to remove the trace amounts of sulfur compounds present. The desulfurized syngas is then expanded through a power recovery turbine to near synloop pressure (nominally at 24 barA) and combined with the synloop recycle syngas. The combined stream is then cooled in a series of heat exchangers, fed to an amine wash unit to remove most of the CO_2, and preheated in a feed/effluent interchanger before being fed to a slurry reactor with Fe based catalyst particles suspending in an inert hydrocarbon liquid (a mineral oil). The mineral oil acts as a temperature moderator and a heat removal medium, transferring the heat of reaction from the catalyst surface via the liquid slurry to boiling water in an internal tubular heat exchanger. IP steam is generated from the heat. The major overall reactions occurring are: $(2n+1)\ H_2 + n\ CO = H\text{-}(CH_2\text{-})_n\text{-}H + n\ H_2O$ and $CO + H_2O = CO_2 + H_2$. The reactor effluent at 260°C is cooled in a series of heat exchangers including the feed/effluent interchanger. The condensate collected is fed to the product stabilization unit which consists of a column to remove the dissolved light ends. The recycle gas which contains CH_4 and other undesirable hydrocarbons (undesirable in the context of maximizing the F-T liquids) is compressed and fed to an autothermal reformer to convert the hydrocarbons back to H_2 and CO. The F-T liquids contain significant amounts of high molecular weight waxes and require hydrocracking to produce lower molecular weight hydrocarbons followed by distillation for separating out the naphtha, diesel, and lighter molecular weight hydrocarbon fractions. It is assumed that these operations will be conducted at an existing refinery.

Ethanol Synthesis. The results obtained for the F–T liquids synthesis loop with respect to minimizing the purge rate are assumed to apply to ethanol co-production

where shifting and reforming of the unconverted gas is also required. The resulting plant configuration is depicted in Figure 6-12. As in the previous case, a fraction of the clean syngas before it enters the 2nd shift reactor is combined with a fraction of the unshifted syngas but to obtain a higher H_2/CO ratio of 2.0 at the synthesis reactor inlet. Again, the combined gas is passed through a bed of ZnO sandwiching a COS hydrolysis catalyst to remove the trace amounts of sulfur compounds present. The desulfurized syngas is then expanded through a power recovery turbine to near synloop pressure which is lower in this case (14 barA at the synthesis reactor outlet) and combined with the synloop recycle syngas. The combined stream after cooling in a series of heat exchangers and removal of most of the CO_2 in an amine wash, is preheated in a feed/effluent interchanger before being fed to a fixed bed reactor containing Rh based catalyst. The exothermic reaction heat is transferred to boiling water in an internal tubular heat exchanger to generate IP steam. The major overall reactions occurring are: $2n\ H_2 + n\ CO = C_n\ H_{2n}+1\ OH + (n-1)\ H_2O$ (with n predominantly = 2), $3\ H_2 + CO = CH_4 + H_2O$ and $CO + H_2O = CO_2 + H_2$. The reactor effluent at 285 C is cooled in a series of heat exchangers including the feed/effluent interchanger. The recycle gas which contains CH_4 and CH_3OH is compressed and fed to an autothermal reformer to convert these compounds back to H_2 and CO in order to maximize the production of the ethanol. The condensate collected is fed to the purification unit which consists of a set of energy saving heat integrated distillation columns (HP and LP columns with the condenser of the HP column providing heat for the reboiler of the LP column) to produce the azeotropic mixture of C_2H_5OH and H_2O which is then dehydrated using molecular sieves to meet the required specifications.

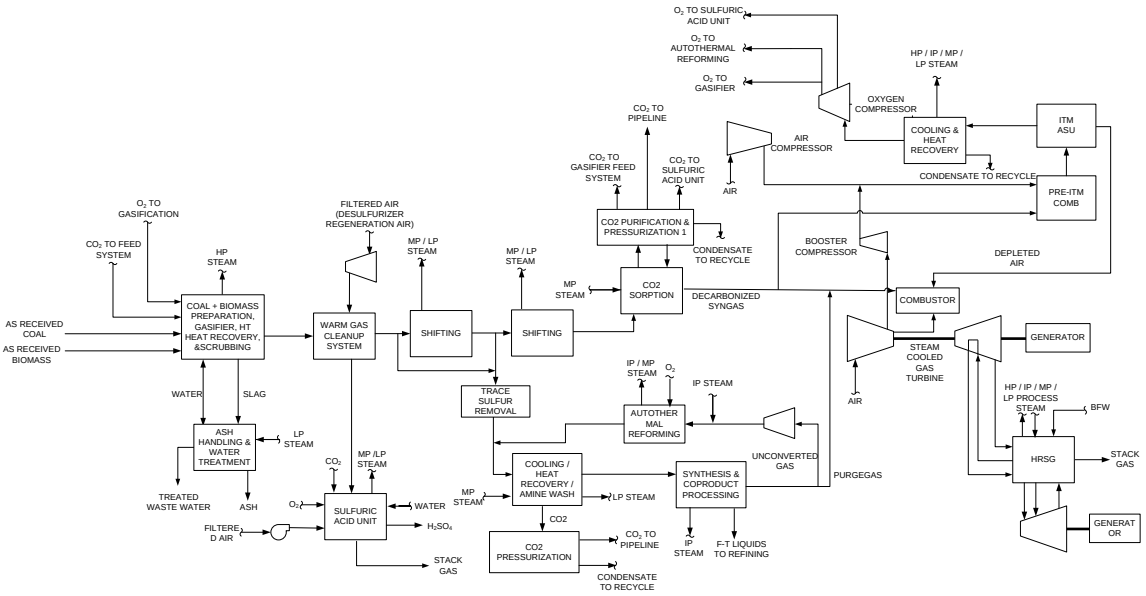

Figure 6-11 Block flow diagram – electricity and Fischer-Tropsch liquids co-production IGCC plants CCS

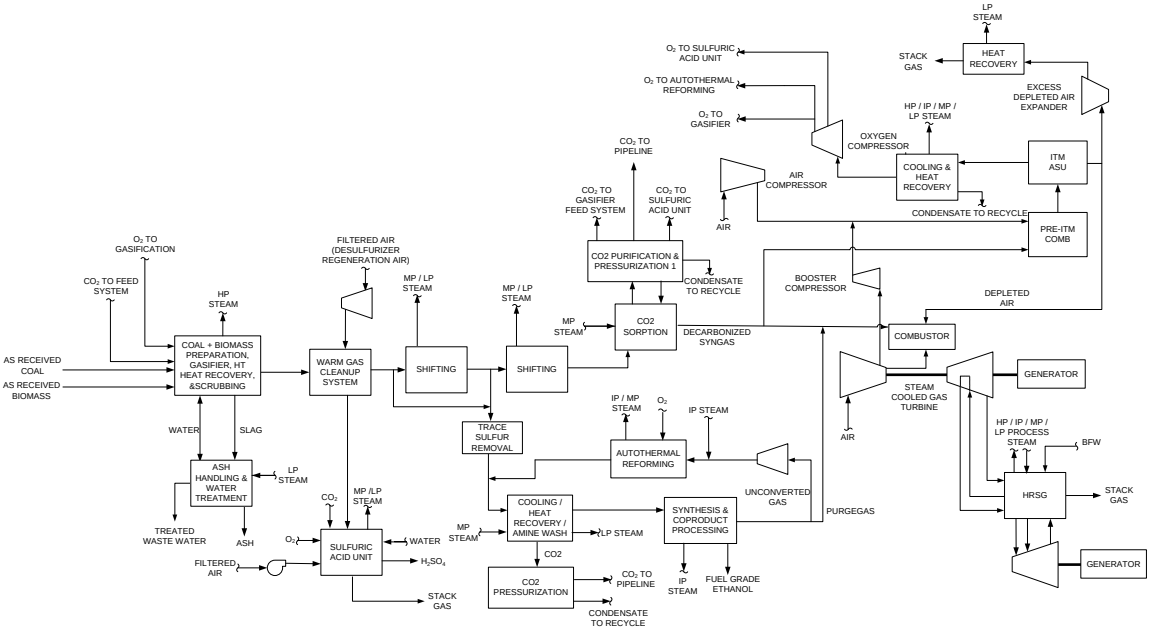

Figure 6-12 Block flow diagram – electricity and ethanol co-production IGCC plants CCS

6.5.2 Plant Performance

Table 6-11 and Table 6-12 summarize the plant performances for the bituminous and the lignite cases. As in the H_2 co-production IGCCs, the plant feed rates for each of the cases are determined to fully load the H class gas turbine under the site specific ambient conditions and 50% of the energy exported is in the form of electricity. The electrical efficiencies for F–T co-production cases are higher than those for the ethanol co-production cases but it should be noted that the ethanol co-production cases produce the finished co-product while the F–T co-production cases produce a co-product that requires further processing in a refinery. The cross comparison of the thermal performance between the various co-product cases is further complicated by the fact that the carbon footprint is not the same when carbon leaving with the co-product is accounted for. The lower efficiency of the ethanol cases is partly due to a low per pass conversion (<10 mol% of the CO and ~15 mol% of the recycled methanol which is co-synthesized in the reactor) to ethanol (and higher alcohols) requiring a large recycle rate. The thermal efficiency and consequently the overall plant economics can be enhanced if the methanol formed is not recycled to the synthesis reactor but purified and sold as an additional co-product. The efficiency of both the F–T and the ethanol cases can be enhanced if the CH_4 formed during synthesis is sold as an additional co-product, substitute natural gas after separation and purification. The impact on plant economics however is dependent on the prevailing natural gas price which is being impacted by shale gas prices.

Table 6-11 Plant thermal performance - bituminous coal cases

Co-feed		None	Switchgrass	
Co-product	Units	None	F-T Liquids	Ethanol
Coal feed rate	kg/h (dry)	122,902	127,566	136,880
	tonne/D (dry)	2,950	3,062	3,286
Biomass feed rate	kg/h (dry)	-	54,671	58,663
	tonne/D (dry)	-	1,312	1,408
Total HHV input	GJ/h	3,753	4,886	5,243
Gas turbine power output	kW	318,000	318,000	318,000
Steam turbine power output	kW	147,382	166,963	126,491
Total gross power output	kW	465,382	484,963	444,491
Total auxiliary consumption	kW	66,550	159,926	221,944
Net power output	kW	398,833	325,037	222,547
Net power efficiency, HHV	%	38.26	24.0	15.3
Net power heat rate, HHV	kJ/kWh	9,410	15,032	23,557
Co-product produced	tonne/D	-	593	621
Co-product HHV	GJ/h	-	1,157	792
Electricity/(Electricity + Co-product HHV)	%	100	50	50
Carbon captured	%	90.0	80.0	80.0
Surface condenser duty	GJ/h	686.03	921.52	456.76
Raw water use	M^3/m	13.18	17.58	18.70

Table 6-12 Plant thermal performance - lignite cases

Co-feed		None	Switchgrass	
Co-product	Units	None	F-T Liquids	Ethanol
Coal feed rate	kg/h (dry)	150,832	140,462	152,134
	tonne/D (dry)	3,621	3,372	3,652
Biomass feed rate	kg/h (dry)	-	60,198	65,200
	tonne/D (dry)	-	1,445	1,565
Total HHV input	GJ/h	3,659	4,498	4,871
Gas turbine power output	kW	312,928	312,928	312,928
Steam turbine power output	kW	140,679	154,071	120,758
Total gross power output	kW	453,607	466,999	433,686
Total auxiliary consumption	kW	80,057	179,200	225,758
Net power output	kW	373,550	287,798	207,928
Net power efficiency, HHV	%	36.76	23.04	15.37
Net power heat rate, HHV	kJ/kWh	9,795	15,628	23,429
Co-product produced	tonne/D	-	529	586
Co-product HHV	GJ/h	-	1,032	748

Electricity/(Electricity + Co-product HHV)	%	100	50	50
Carbon captured	%	90.0	80.0	80.0
Surface condenser duty	GJ/h	626.77	807.58	415.49
Raw water use	M^3/m	12.90	15.97	17.03

6.5.3 Economic Analyses

Table 6-13 and Table 6-14 present the plant cost estimates and results of the economic analysis for the bituminous and the lignite cases. The first year cost of electricity calculated for the bituminous coal is $103/MWh while that for the lignite is $108/MWh. The calculated cost of the F–T liquids ranges from $77.8/bbl to $86.6/bbl (or $0.0177 to 0.0197/MJ LHV) depending on the feedstock, which is comparable to the projected longer term market price of crude oil at ~$80/bbl (or ~$0.0172/MJ LHV) when supply and demand reach a new equilibrium [191]. The cost of the fuel grade ethanol ranges from $4.84/gal to $4.91/gal, while it ranged from $2.20/gal to $3.70/gal in a DoE funded study conducted by Louisiana State University [192]. The Louisiana State University study consisted of a significantly larger plant than this study and benefited from economies of scale as well the gasification plant feedstock which was Illinois No. 6 coal without the biomass cofeeding. When the plant size in this study is scaled up to similar size as in the Louisiana State University study, cost of the alcohol is then reduced to a range of $3.24/gal to $4.28/gal.

Table 6-13 Plant cost estimates and economics - bituminous coal cases (Year 2007 $)

Co-feed	None	Switchgrass	
Co-product	None	F-T Liquids	Ethanol
Net Power, kW	398,833	325,037	222,547
Plant Cost, $1000			
Fuel Preparation System	146,555	194,935	204,792
Air Separation Unit	42,117	51,797	60,691
Gasification System	320,397	386,060	405,581
Gas Cleanup and Conditioning Systems	267,384	200,855	207,671
Power Island	184,749	187,633	184,098
Co-production Unit	-	117,836	446,073
General Facilities	155,693	166,539	164,139
Total Plant Cost (TPC), $1000	1,116,895	1,305,656	1,673,045
Total Fixed Operating Cost for Initial Year, $1000/yr	45,236	53,591	67,195
Total Variable Operating Costs, $1000/yr	71,207	121,191	138,158
1st Year Cost of Electricity (COE), $/MWh	102.9	102.9	102.9
Co-product Cost for Initial Year, $/kg	-	$77.85/bbl	$4.91/gal

Table 6-14 Plant cost estimates and economics - lignite cases (Year 2007 $)

Co-feed	None	Switchgrass	
Co-product	None	F-T Liquids	Ethanol
Net Power, kW	373,550	287,798	207,928
Plant Cost, $1000			
Fuel Preparation System	213,044	246,459	260,622
Air Separation Unit	44,014	50,971	58,966
Gasification System	328,403	376,547	398,185
Gas Cleanup and Conditioning Systems	251,914	172,580	183,110
Power Island	180,513	180,666	178,204
Co-production Unit	-	108,804	384,246
General Facilities	153,790	160,356	158,701
Total Plant Cost (TPC), $1000	1,171,678	1,296,385	1,622,033
Total Fixed Operating Cost for Initial Year, $1000/yr	47,169	53,336	65,328
Total Variable Operating Costs, $1000/yr	56,962	101,302	116,257
1st Year Cost of Electricity (COE), $/MWh	108.1	108.1	108.1
Co-product Cost for Initial Year, $/kg	-	$86.56/bbl	$4.84/gal

6.6 Summary

Conceptual designs for electricity and H_2 and other fuels co-production IGCC plants with CCS via coal and biomass mixtures using advanced technologies are investigated. These conceptual designs identify ITM air separation, dry feed gasifier, warm gas cleanup processes, H class gas turbine, regenerable CO_2 sorbents technology as attractive technologies for plants to be built in the 2025 time frame. Two types of coal (bituminous and lignite) and two types of biomass (woody biomass and switchgrass) are evaluated. Performance evaluations are conducted for electricity only IGCCs, and net power efficiencies varied from 36.76% to 38.26%. For co-production IGCCs, H_2 efficiencies ranged from 20.63% to 22.22%, and net equivalent power efficiencies ranged from 35.21% to 37.98%. Sensitivity analyses on the feedstock mixtures show that for co-production cases, characteristics of feedstocks such as HHV and moisture content have significant effect on feed rate and auxiliary power consumptions for a given product amount. Incremental analyses show that H_2 co-produced in the IGCC has a competitive performance comparable to an SMR H_2 plant, and biomass co-feeding has competitive performance to coal. The levelized COE for the bituminous coal studies is \$102.9/MWh while that for the lignite studies is \$108.1/MWh. The calculated cost of H_2 ranged from \$1.42/kg to \$2.77/kg depending on the feedstock. Collection and transportation of biomass result in a relatively higher feedstock cost resulting in a higher cost of H_2.

Two other types of fuels are considered, F–T liquids and ethanol. Two types of coal (bituminous and lignite) along with switchgrass as the biomass co-feed are again included. The electrical efficiency for F–T co-production is higher than that for the ethanol co-production but it should be noted that the ethanol co-production plants produce the finished co-product while the F–T co-production plants produce a co-product that requires further processing in a refinery. The cross comparison of the thermal performance between the various co-product cases is further complicated by the fact that the carbon footprint is not the same when carbon leaving with the co-product is accounted for. The calculated cost of the F–T liquids ranges from $77.8/bbl to $86.6/bbl (or $0.0177 to 0.0197/MJ LHV) depending on the feedstock, which is comparable to the projected longer term market price of crude oil at ~$80/bbl (or ~$0.0172/MJ LHV) when supply and demand reach a new equilibrium. It should be noted, however, that F–T liquids do not contain any sulfur or nitrogen or inorganic compounds. The cost of the ethanol is higher than the current price of gasoline in the U.S., and thus the ethanol co-production may not appear to be as attractive as the other options at these scales, primarily due to the much lower plant efficiency. However, from a life cycle greenhouse gas emissions standpoint, ethanol produced with biomass co-feeding and CCS, has a lower carbon footprint than gasoline or diesel, especially when derived from petroleum.

Chapter 7 Summary, Conclusions and Recommendations

7.1 Summary

This dissertation focuses on development and evaluation of advanced technologies toward clean coal power generation relative to both CO_2 mitigation and water usage reduction.

As a near-term CO_2 mitigation strategy, retrofitting of a subcritical pulverized coal (PC) power plant with post-combustion CO_2 capture technologies is first investigated. Advanced solid sorbent CO_2 capture technology is evaluated by comparing with state-of-the-art amine CO_2 capture. The design of the solid sorbent based CO_2 capture system is optimized for integration to minimize plant modifications and the associated downtime (i.e., the integration of the CO_2 capture process with the steam cycle is minimized. Results show that a PC power plant with solid sorbent CO_2 capture has better thermal performance, less water usage and lower cost of electricity than a plant using amine based CO_2 capture). The evaluation of four levels of CO_2 capture indicates that the net plant efficiency decreases linearly or net heat rate increases linearly with CO_2 capture level, while due to economies of scale, power required decreases per unit of CO_2 captured. In terms of water usage, it is demonstrated that a combined wet/dry cooling system proposed in this study, with the entire exhaust from the low pressure (LP) steam turbine condensed by an air-cooled condenser, can significantly reduce water usage compared to a pure wet cooling system, i.e., employing wet cooling towers.

Mathematical models are developed, validated and applied to the proposed wet/dry combined cooling system for a PC power plant retrofitted with solid sorbent CO_2 capture. It is predicted by the model simulation that ambient conditions have significant impacts on the performance of a combined cooling system. Two operating strategies are considered: 1. fixed number of wet cooling tower cells while varying fan speed; 2. changing the number of tower cells at fixed air flow rate for each cell. It is found that the second operation strategy can achieve improved combined cooling system performance, and it is also suitable for plant retrofitting scenarios since adequate wet cooling tower cells would be available in the existing plant.

An advanced clean coal utilization for central power generation is the integrated gasification combined cycle (IGCC). The major focus of advanced IGCC technologies for this study is pre-combustion solid sorbent CO_2 capture. Two technology approaches were investigated, i.e. CO_2 capture alone and combined WGS and CO_2 capture, by comparing with Selexol^{TM} CO_2 capture. The decarbonized syngas leaving the solid sorbent CO_2 capture technology provided as fuel to the gas turbine, has higher moisture content requiring a smaller air separation unit (ASU) unit as well as lower power compression for the nitrogen added as a thermal diluent for NO_x control in the gas turbine. In addition, solid sorbent CO_2 capture unit itself consumes less power. Therefore, the IGCC plant efficiency with solid sorbent CO_2 capture is greater than that with Selexol^{TM} CO_2 capture. Moisture content of the decarbonized syngas also results in performance difference between the two solid sorbent based CO_2 capture technologies. The net effect of combining the effects of savings in steam usage with a slightly larger

ASU unit and nitrogen requirement for syngas dilution for the IGCC with combined water gas shift (WGS) and CO_2 capture technology, is that its plant efficiency is slightly increased over the plant using CO_2 capture alone technology, 34.31% versus 33.81%.

A computational fluid dynamics (CFD) model is developed, validated and applied to understand the operating conditions, thermal management and reactor design of solid sorbent CO_2 capture reactors. It is found that the CO_2 breakthrough time or CO_2 loading capacity is independent of reactor geometry as long as the space velocity is constant. Adsorption rate is the control step for CO_2 capture using solid sorbent, and break through occurs before the solid sorbent near the exit of the bed is fully utilized due to bulk transfer of the CO_2 in the axial direction. However, lower space velocities can increase loading of the sorbent. One effective way to improve the performance of solid sorbent CO_2 capture is to increase the potential of adsorption and adsorption rate by increasing mass diffusion rate in porous structures and increase functional groups in porous surfaces. CFD model was applied to predict the operation conditions, reactor design and thermal management of both solid sorbent based CO_2 capture alone technology and WGS and CO_2 capture technology.

Toward renewable energy utilization and facing energy security challenges, future technology direction of IGCC may be co-feeding and co-production. Firstly, conceptual designs for electricity and H_2 coproduction IGCC plants are investigated with carbon capture and storage (CCS) via coal and biomass mixtures using advanced technologies, including ITM air separation, dry feed gasifier, warm gas cleanup processes, H class gas

turbine, and regenerable CO_2 sorbents technology. Two types of coal (bituminous and lignite) and two types of biomass (woody mass and switchgrass) are evaluated. Sensitivity analyses on the feedstock mixtures show that for coproduction cases, characteristics of feedstocks such as HHV and moisture content have significant effect on feed rate and auxiliary power consumption for a given product amount. Incremental analyses show that H_2 coproduced in the IGCC has a competitive performance comparable to a natural gas fed steam methane reforming (SMR) H_2 plant, and biomass cofeeding has competitive performance to coal. Both plant efficiency and economic performance of each IGCC plant are evaluated. The calculated cost of H_2 ranged from $1.42/kg to $2.77/kg depending on the feedstock. Collection and transportation of biomass result in a relatively higher feedstock cost and a higher cost of H_2.

Two other types of co-producs are considered, Fischer-Tropsch (F–T) liquids and ethanol. Two types of coal (bituminous and lignite) along with switchgrass as the biomass cofeed are included. The electrical efficiency for F–T coproduction is higher than that for the ethanol coproduction. The calculated cost for F-T liquids ranged from $77.8/bbl to $86.6/bbl, depending on the feedstock, which is comparable to the projected longer term market price of crude oil at ~$80/bbl when supply and demand reach a new equilibrium. In addition, F–T liquids contain no sulfur or nitrogen or inorganic compounds. The cost of the ethanol is higher than the current price of gasoline in the U.S., and thus the ethanol coproduction may not appear to be as attractive as the other options at these scales. However, from a life cycle greenhouse gas emissions standpoint, ethanol produced with biomass cofeeding and CCS, have a

lower carbon footprint than gasoline or diesel, especially when the gasoline or diesel are derived from petroleum.

7.2 Conclusions

Major conclusions drawn from this dissertation research work are summarized as follows:

- In terms of PC plant retrofit, solid sorbent based post-combustion CO_2 capture technology exhibits advantages over amine based post-combustion CO_2 capture system on thermal performance, water usage and economics.

  Compared to amine CO_2 capture, solid sorbent CO_2 capture technology requires significantly less steam for sorbent regeneration, which makes it more independent from steam cycle and beneficial for plant retrofitting. Solid sorbent CO_2 capture system saves 45% of the steam used for LP steam turbine power generation, thus, thermal performance is significantly improved. In addition, since it requires less cooling capacity, the water usage (per MW basis) of a plant using solid sorbent CO_2 capture technology is almost 17% lower than the amine based PC plant. The calculated levelized cost of electricity is increased from \$60.5/MWh without CO_2 capture to \$124.3/MWh for amine based capture while that with the solid sorbent based capture is much lower at \$115.8/MWh.

  The net plant efficiency decreases linearly or net heat rate increases linearly with increased CO_2 capture level for a PC power plant with solid sorbent CO_2 capture. Due to economies of scale, power required decreases from 374 kWh/Tonne for 30% CO_2 capture to 283 kWh/Tonne for 90% CO_2 capture.

- Ambient conditions have significant impacts on the performance of a combined wet/dry cooling system. Operating strategy consisting of changing number of tower cells at fixed air flow rate for each cell showed improved combined cooling system performance.

  Empirical models typically employed are not able to precisely predict the performance of cooling systems under various ambient conditions. Detailed mathematical models have been developed and validated for both wet cooling tower and air-cooled condenser, and applied to a combined wet/dry cooling system for a PC power plant retrofitted with solid sorbent CO_2 capture.

  It was predicted by the model simulation that ambient conditions have significant impacts on the performance of a combined cooling system. If using the operating strategy of keeping a fixed number of wet cooling tower cells while varying air-cooled condenser fan speed to vary air flow rate, the Coefficient of Performance (COP), which is ratio of total power consumption by the cooling system and total heat rejected, reduces from 111 to 19 by increasing ambient temperature from 10C to 20C. COP decreases from 68.7 to 48.6 as relative humidity increases from 30% to 90% while the ambient temperature remains at 15C. An alternative operating strategy consisting of changing the number of tower cells at fixed air flow rate for each cell showed that improved combined cooling system performance can be achieved, i.e. at 20C ambient temperature the COP is 29.3 vs. 18.8 for fixed cooling

tower cells operation. These changes in cooling system would further affect the performance of a PC plant as a whole.

- IGCC plant using solid sorbent based CO_2 capture technologies has better plant performance and lower cost of electricity than that using Selexol^{TM} CO_2 capture.

  In comparison with Selexol^{TM} CO_2 capture, IGCCs equipped with solid sorbent CO2 capture consume less power, and have high moisture content in decarbonized syngas which leads to smaller ASU unit as well as lower nitrogen compression power for syngas dilution. Therefore, the IGCC plant efficiency for solid sorbent CO_2 capture alone and combined WGS and CO_2 capture is bigger than that for Selexol^{TM} CO_2 capture technology' by 2.77 and 3.27 percentage points, or a reduction by 8.2% and 9.5% in heat rate in heat rate respectively. Steam content in decarbonized syngas also results in the performance difference between the two solid sorbent based CO_2 capture technologies. Combining the effects of steam saving for power generation and slightly larger ASU unit and nitrogen compression for IGCC with the combined WGS and CO_2 adsorption capture technology, the net effect is its plant efficiency is 34.31%, slightly larger than the plant efficiency using separate WGS and CO_2 adsorption capture technology at 33.81%. In terms of economics, 1st Year Levelized Cost of Electricity for three IGCCs: with Selexol^{TM} technology, with solid sorbent CO_2 capture alone and with combined WGS and solid sorbent CO_2 capture are $127.8/MWh, $114.5/MWh and $112.5/MWh respectively.

- CFD simulation using ANSYS FLUENT with User Defined Functions (UDFs) is capable of handling the complex physics in a fixed bed reactor for solid sorbent CO_2 capture technologies.

  Solid sorbent CO_2 capture is a complex process because of the interactions between fluid mechanics, heat and mass transfer, water vaporization, adsorption equilibrium and kinetics, and WGS reaction kinetics. In the CFD simulation model using ANSYS FLUENT, fluid mechanics and heat and mass transfer are handled by fluid solver, while water vaporization, adsorption equilibrium and kinetics as well as WGS reaction kinetics are all introduced by UDFs as mass/energy source terms. Adsorption model is based on Langmuir-Freundlich Isotherm and linear driving force model. WGS reaction kinetics was obtained from literature; however, the effect of gas internal diffusion is accounted for by introducing internal effectiveness factor in the model. The CFD model is validated with experimental data for CO_2 breakthrough time and temperature profile for CO_2 capture alone and combined WGS and CO_2 capture.

- CFD simulation provided insight into optimizing the operation and performance of adsorption/desorption process of solid sorbent CO_2 capture fixed bed reactor.

  The validated CFD model is applied to investigate the operation and performance of a solid sorbent CO_2 capture fixed bed reactor. It is found that CO_2 breakthrough time or CO_2 loading capacity is independent of reactor geometry as long as the space velocity is constant. Adsorption rate is the controlling step for solid sorbent CO_2

capture. Due to axial mass transfer of CO_2, the downstream solid sorbent is not fully utilized when CO_2 breaks through at bed exit. One approach to increase the loading of the sorbent is to reduce space velocity. Reducing space velocity for each bed however increases the number of reactors required in an IGCC which leads to comparable or even lager total quantity of solid sorbent. Thus, it is not advantageous to pursue a design with very low space velocities due to the negative effects on plant economics. One effective way to improve the performance of solid sorbent CO_2 capture is to increase the potential of adsorption and adsorption rate by increasing mass diffusion rate in porous structures and increasing functional groups in porous surfaces. Pressure drop is a big concern for regeneration or purge step, since the bed operates under relatively lower pressure which results in high volumetric flow rate. A reactor design with a low aspect ratio should be pursued to reduce the pressure drop since it was found from the CFD simulations that the sorbent loading and breakthrough time were not affected significantly by changing the aspect ratio.

- <u>CFD simulation benefits the design of cooling strategy for combined WGS and solid sorbent CO_2 capture fixed bed reactor.</u>

  CFD simulation reveals that majority of CO is converted into CO_2 when the un-shifted syngas first contacts the catalyst, and this fast reaction rate leads to significant heat release and temperature increase. Cooling water injection in the form of fine water mist is required to cool down the temperature so that both

catalyst and solid sorbent can operate optimally. Different cooling options have been evaluated. A 2-water-injection-zone option is demonstrated to be effective as thermal management strategy to prevent significant temperature increase in a reactor bed for the combined WGS and solid sorbent CO_2 capture.

- CFD simulation is capable of fixed bed reactor sizing for both solid sorbent CO_2 capture alone and combined WGS and solid sorbent CO_2 capture technologies.

  With limited experimental data and experience in large-scale reactor design, CFD simulation is able to size the bed and define the cooling strategy for a given syngas flow rate entering the fixed bed reactor under steady state operation.

- Co-production IGCC plants with CCS via coal and biomass mixtures using advanced technologies are competitive to typical advanced IGCCs, and co-feeding and co-production IGCC is preferable for renewable energy utilization and energy security. The coproduction fuels are competitive in cost compared with market price.

  For electricity only advanced IGCCs, the net power efficiencies varied from 36.76% to 38.26% compared to about 30.00% for a state-of-the art IGCC with current technologies. For H_2 co-production IGCCs, the net equivalent power efficiencies ranged from 35.21% to 37.98%. The calculated cost of H_2 ranged from $1.42/kg to $2.77/kg depending on the feedstock. In terms of F-T liquids and ethanol co-production, the calculated cost for F-T liquids ranged from $77.8/bbl to $86.6/bbl, depending on the feedstock, which is comparable to the projected longer term

market price of crude oil at ~$80/bbl when supply and demand reach a new equilibrium. In addition, F–T liquids contain no sulfur or nitrogen or inorganic compounds. The cost of the ethanol is higher than the current price of gasoline in the U.S. However, from a life cycle greenhouse gas emissions standpoint, ethanol produced with biomass cofeeding and CCS, has a lower carbon footprint than gasoline or diesel, especially when these are derived from petroleum.

7.3 Recommendations for Future Work

Recommendations for future research work on advanced clean coal technologies for central power generation (especially advanced cooling systems for plant heat rejection and solid sorbent technologies for CO_2 capture) are summarized in the following:

- Wet cooling tower control strategy in various ambient conditions might have impact on process streams. This change would affect the performance of the power plant as a whole system. In current analysis, this change is assumed to be negligible. To fully understand the ambient conditions' impact on not only cooling system itself but also plant performance, evaluation of changes on process side and corresponding changes in plant performance should be investigated.
- Current CO_2 adsorption isotherm and adsorption kinetics are obtained from experimental tests conducted under a CO_2 partial pressure of 0.83 bar (12psi). CO_2 adsorption performance varies significantly with pressures due to pressure's impact on porous surface diffusivity. Darken theory has been adopted to scale the data to higher pressures but its validity may not hold for pressures that correspond to those in modern IGCCs, which are as much as 40% higher than that used in generating the experimental data. The impact of higher pressure on surface diffusivity may be quite different. Additional experimental data is necessary to confirm the validation of Darken theory.
- WGS reaction kinetics is obtained from literature, and internal effectiveness factor is introduced to account for mass diffusion within catalyst pellets. However, the WGS

reaction model itself under the specific operating conditions corresponding to the combined WGS and CO_2 adsorption reactor has not been validated by experiments. To confirm the validation of this model, additional experimental test need to be conducted on the specific catalyst pellets, so that the hot temperature spots can be precisely predicted and specific cooling strategy can correspondingly be improved.

- In the current CFD simulation for combined WGS and solid sorbent CO_2 capture, water injection is modeled as a vapor source in mass transport equation and a heat sink in energy transport equation. This approach can effectively ensure the mass balance and energy balance. However, effectiveness of water vaporization (i.e., taking into account any heat/mass transfer limitations to phase change and dispersion) is not considered. A detailed 3-D water injection spray model would be helpful in the design of the reactor to ensure that water mist droplets do not impinge upon the catalyst or sorbent.
- For commercial size reactors using solid sorbent CO_2 capture technologies, the effect of heat loss on reactor walls is significant in a real power plant application which results in temperature variation on radial direction and might further leads to changes on solid sorbent performance, catalyst performance and performance of reactor for CO_2 capture. Future work on various thermal boundary conditions of the wall would be helpful for the design and operation of a real fixed bed CO_2 capture reactor in PC or IGCC power plants.
- The commercial sized solid sorbent CO_2 capture fixed bed reactor was sized by the ANSYS FLUENT CFD model using stream data predicted by overall plant simulations

using Aspen Plus®. An iterative technique is required between the two models since one of purge streams exiting the reactor is recycled back to the reactor, while in this investigation, the number of iterations was limited. Directly linking ANSYS FLUENT with Aspen Plus® is recommended in order to achieve more precise reactor performance prediction and overall plant simulation.

Bibliography

[1] J. Conti and P. Holtberg, “International Energy Outlook 2013,” Energy Information Administration (EIA), 2013.

[2] S. J. Xu and W. J. Thomson, “Oxygen permeation rates through ion-conducting perovskite membranes,” *Chem. Eng. Sci.*, vol. 54, no. 17, pp. 3839–3850, Sep. 1999.

[3] “Gasifipedia,” *DoE/NETL*. [Online]. Available: http://www.netl.doe.gov/research/coal/energy-systems/gasification/gasifipedia/low-emissions. [Accessed: 21-Dec-2014].

[4] K. Goto, K. Yogo, and T. Higashii, “A review of efficiency penalty in a coal-fired power plant with post-combustion CO2 capture,” *Appl. Energy*, vol. 111, pp. 710–720, Nov. 2013.

[5] P. G. Cifre, K. Brechtel, S. Hoch, H. García, N. Asprion, H. Hasse, and G. Scheffknecht, “Integration of a chemical process model in a power plant modelling tool for the simulation of an amine based CO2 scrubber,” *Fuel*, vol. 88, no. 12, pp. 2481–2488, Dec. 2009.

[6] L. M. Romeo, S. Espatolero, and I. Bolea, “Designing a supercritical steam cycle to integrate the energy requirements of CO2 amine scrubbing,” *Int. J. Greenh. Gas Control*, vol. 2, no. 4, pp. 563–570, Oct. 2008.

[7] A. Samanta, A. Zhao, G. K. H. Shimizu, P. Sarkar, and R. Gupta, “Post-Combustion CO 2 Capture Using Solid Sorbents: A Review,” *Ind. Eng. Chem. Res.*, vol. 51, no. 4, pp. 1438–1463, Feb. 2012.

[8] N. Hedin, L. Andersson, L. Bergström, and J. Yan, “Adsorbents for the post-combustion capture of CO2 using rapid temperature swing or vacuum swing adsorption,” *Appl. Energy*, vol. 104, pp. 418–433, Apr. 2013.

[9] M. L. GRAY, J. S. HOFFMAN, D. C. HREHA, D. J. FAUTH, S. W. HEDGES, K. J.

CHAMPAGNE, and H. W. PENNLINE, “Parametric Study of Solid Amine Sorbents for the Capture of Carbon Dioxide,” *Energy & fuels*, vol. 23, no. 5, pp. 4840–4844.

[10] R. Siriwardane and C. Robinson, “Liquid-Impregnated Clay Solid Sorbents for C O2 Removal from Postcombustion Gas Streams,” *J. Environ. Eng.*, vol. 135, no. 6, pp. 378–385, Jun. 2009.

[11] M. Sarker, D. Chowdhury, and I. Hossain, “Power Generation from Coal-A review,” *J. Chem. Eng.*, vol. 27, no. 2, pp. 50–54, Jan. 2014.

[12] J. D. Mondol, D. McIlveen-Wright, S. Rezvani, Y. Huang, and N. Hewitt, “Techno-economic evaluation of advanced IGCC lignite coal fuelled power plants with CO2 capture,” *Fuel*, vol. 88, no. 12, pp. 2495–2506, Dec. 2009.

[13] M. Kanniche and C. Bouallou, “CO2 capture study in advanced integrated gasification combined cycle,” *Appl. Therm. Eng.*, vol. 27, no. 16, pp. 2693–2702, Nov. 2007.

[14] P. CHIESA, S. CONSONNI, and T. KREUTZ, “Co-production of hydrogen, electricity and CO from coal with commercially ready technology. Part A: Performance and emissions,” *Int. J. Hydrogen Energy*, vol. 30, no. 7, pp. 747–767, Jul. 2005.

[15] T. KREUTZ, R. WILLIAMS, S. CONSONNI, and P. CHIESA, “Co-production of hydrogen, electricity and CO from coal with commercially ready technology. Part B: Economic analysis,” *Int. J. Hydrogen Energy*, vol. 30, no. 7, pp. 769–784, Jul. 2005.

[16] C.-C. Cormos, “Evaluation of energy integration aspects for IGCC-based hydrogen and electricity co-production with carbon capture and storage,” *Int. J. Hydrogen Energy*, vol. 35, no. 14, pp. 7485–7497, Jul. 2010.

[17] J. M. Beér, “Combustion technology developments in power generation in response to environmental challenges,” *Prog. Energy Combust. Sci.*, vol. 26, no. 4–6, pp. 301–327, Aug. 2000.

[18] Y. A. ÇENGEL and M. A. BOLES, *Thermodynamics - An engineering approach*, 5th ed. McGraw-Hill, 2002.

[19] P. Forzatti, “Present status and perspectives in de-NOx SCR catalysis,” *Appl. Catal. A Gen.*, vol. 222, no. 1–2, pp. 221–236, Dec. 2001.

[20] P. S. Nolan, “Flue Gas Desulfurization Technologies for Coal-Fired Power Plants,” in *Coal-Tech 2000 International Conference*, 2000.

[21] J. Katzer and E. Al., “The future of coal: an interdisciplinary MIT study,” Cambridge, MA, 2007.

[22] J. Phillips, “U.S. Program for Advanced Ultrasupercritical (A-USC) Coal Fired Power Plants.” 2011.

[23] J. Black, “Cost and Performance Baseline for Fossil Energy Plants - Volume 1: Bituminous Coal and Natural Gas to Electricity,” DOE/NETL- 2010/1397. US, 2010.

[24] W. . Castle, “Air separation and liquefaction: recent developments and prospects for the beginning of the new millennium,” *Int. J. Refrig.*, vol. 25, no. 1, pp. 158–172, Jan. 2002.

[25] J. Repasky, L. Anderson, V. Stein, P. Armstrong, and E. Foster, “ITM Oxygen technology: scale-up toward clean energy applications,” in *International Pittsburgh Coal Conference 2012*, 2012.

[26] C. Higman and M. van der Burgt, *Gasification*. Gulf Professional Publishing, 2011.

[27] J. Phillip, “Different types of gasifiers and their integration with gas turbines,” in *The Gas Turbine Handbook*, DOE/NETL, 2006.

[28] G. Alptekin, J. Lind, R. Amalfitano, and R. Copeland, “Sorbents for mercury removal from coal-derived synthesis gas,” in *Proceedings of Twentieth Annual International Pittsburgh Coal Conference*, 2003.

[29] D. Gray, J. Plunkett, S. Salerno, C. White, and G. Tomlinson, “Current and Future IGCC Technologies—A Pathway Study Focused on Non-Carbon Capture Advanced Power Systems R&D Using Bituminous Coal,” DOE/NETL-2008/1337, US, 2008.

[30] “Siemens Fuel Gasification Technology,” 2008. .

[31] H. J. van der Ploeg, T. Chhoa, and P. L. Zuideveld, “The Shell Coal Gasificaion Process for the US Industry,” *Gasification Technology Conference*. Washington DC, USA.

[32] A. D. Rao, G. S. Samuelsen, and Y. Yi, “Gas Turbine Based High-efficiency ‘Vision 21’ Natural Gas and Coal Central Plants,” *Proc. Inst. Mech. Eng. Part A Power Energy*, vol. 219, no. 2, pp. 127–136, 2005.

[33] M. Li, A. D. Rao, and G. Scott Samuelsen, “Performance and costs of advanced sustainable central power plants with CCS and H2 co-production,” *Appl. Energy*, vol. 91, no. 1, pp. 43–50, 2012.

[34] C.-C. Cormos, “Hydrogen and power co-generation based on coal and biomass/solid wastes co-gasification with carbon capture and storage,” *Int. J. Hydrogen Energy*, vol. 37, no. 7, pp. 5637–5648, 2012.

[35] K. S. Cory and B. G. Swezey, “Renewable Portfolio Standards in the States: Balancing Goals and Implementation Strategies,” National Renewable Energy Laboratory/US Department of Energy Technical Report, NREL/TP-670-41409, 2007.

[36] “California Energy Commission.” [Online]. Available: www.energy.ca.gov.

[37] R. P. O’Hayre, S.-W. Cha, W. Colella, and F. B. Prinz, *Fuel Cell Fundamentals*. New York: John Wiley & Sons, 2006.

[38] R. von Helmolt and U. Eberle, “Fuel cell vehicles: Status 2007,” *J. Power Sources*, vol. 165, no. 2, pp. 833–843, 2007.

[39] J. M. Repasky, E. P. Foster, P. A. Armstrong, V. E. Stein, and L. L. Anderson, “ITM Oxygen Development for Advanced Oxygen Supply,” *Gasification Technologies Council*. San Francisco, California, USA.

[40] L. Rosen, N. Degenstein, M. Shah, J. Wilson, S. Kelly, J. Peck, and M. Christie, “Development of oxygen transport membranes for coal-based power generation,”

Energy Procedia, vol. 4, no. 0, pp. 750–755, 2011.

[41] R. V Siriwardane, D. C. Cicero, S. Jain, Raghubir, P. Gupta, and B. S. Turk, "Durable Zinc Oxide-Based Regenerable Sorbents for Desulfurization of Syngas in a Fixed-Bed Reactor," *Fifth international symposium on gas cleaning at high temperature*. .

[42] G. Alptekin, S. Dietz, A. Jayaraman, M. Dubovik, and R. Amalfitano, "A Low Cost, High Capacity Regenerable Sorbent for CO2 Capture," *A&WMA's 102nd Annual Conference & Exhibition*. Detroit, MI, USA.

[43] A. D. Rao and D. J. Francuz, "An evaluation of advanced combined cycles," *Appl. Energy*, vol. 102, no. 0, pp. 1178–1186, 2013.

[44] P. Klimantos, N. Koukouzas, A. Katsiadakis, and E. Kakaras, "Air-blown biomass gasification combined cycles (BGCC): System analysis and economic assessment," *Energy*, vol. 34, no. 5, pp. 708–714, May 2009.

[45] A. Valero and S. Usón, "Oxy-co-gasification of coal and biomass in an integrated gasification combined cycle (IGCC) power plant," *Energy*, vol. 31, no. 10–11, pp. 1643–1655, 2006.

[46] C.-C. Cormos, A.-M. Cormos, and S. Agachi, "Power generation from coal and biomass based on integrated gasification combined cycle concept with pre- and post-combustion carbon capture methods," *Asia-Pacific J. Chem. Eng.*, vol. 4, no. 6, pp. 870–877, Nov. 2009.

[47] C.-C. Cormos, A. Padurean, and P. S. Agachi, "Technical evaluations of carbon capture options for power generation from coal and biomass based on integrated gasification combined cycle scheme," *Energy Procedia*, vol. 4, no. 0, pp. 1861–1868, 2011.

[48] L. Tock and F. Maréchal, "Co-production of hydrogen and electricity from lignocellulosic biomass: Process design and thermo-economic optimization," *Energy*, vol. 45, no. 1, pp. 339–349, Sep. 2012.

[49] D. Sofia, P. Coca Llano, A. Giuliano, M. Iborra Hernández, F. García Peña, and D. Barletta, "Co-gasification of coal–petcoke and biomass in the Puertollano IGCC

power plant," *Chem. Eng. Res. Des.*, vol. 92, no. 8, pp. 1428–1440, Aug. 2014.

[50] M. Tijmensen, "Exploration of the possibilities for production of Fischer Tropsch liquids and power via biomass gasification," *Biomass and Bioenergy*, vol. 23, no. 2, pp. 129–152, Aug. 2002.

[51] X. Wang, Y. Xiao, S. Xu, and Z. Guo, "Predicting the Performance of System for the Co-production of Fischer-Tropsch Synthetic Liquid and Power from Coal," *J. Eng. Gas Turbines Power*, vol. 130, no. 1, p. 011401, Jan. 2008.

[52] C. Yue, Y. Shi, and N. Cai, "Technical and Economic Evaluation for the Fischer-Tropsch Liquids and Electricity Co-production System Based on Coal Gasification," in *International Colloquium on Environmentally Preferred Advanced Power Generation*.

[53] G. LIU, E. D. LARSON, R. H. WILLIAMS, T. G. KREUTZ, and X. GUO, "Making Fischer-Tropsch Fuels and Electricity from Coal and Biomass: Performance and Cost Analysis," *Energy & fuels*, vol. 25, no. JANFEV, pp. 415–437.

[54] R. Williams, E. Larson, and H. Jin, "Comparing climate-change mitigating potentials of alternative synthetic liquid fuel technologies using biomass and coal," in *proceedings of the Fifth Annual Conference on Carbon Capture and Sequestration*, 2006.

[55] R. H. Williams, E. D. Larson, G. Liu, and T. G. Kreutz, "Fischer–Tropsch fuels from coal and biomass: Strategic advantages of once-through ('polygeneration') configurations," *Energy Procedia*, vol. 1, no. 1, pp. 4379–4386, Feb. 2009.

[56] T. G. Kreutz, E. D. Larson, G. Liu, and R. H. Williams, "Fischer-Tropsch Fuels from Coal and Biomass," *25th Annual International Pittsburgh Coal Conference*. Pittsburgh, Pennsylvania, USA.

[57] W. G. I. of the I. P. on C. Change, B. Metz, O. Davidson, H. de Coninck, M. Loos, and L. Meyer, "IPCC, 2005: IPCC Special Report on Carbon Dioxide Capture and Storage." Cambridge University Press, 2005.

[58] A. B. Rao and E. S. Rubin, "A Technical, Economic, and Environmental Assessment of Amine-Based CO 2 Capture Technology for Power Plant Greenhouse Gas

Control," *Environ. Sci. Technol.*, vol. 36, no. 20, pp. 4467–4475, Oct. 2002.

[59] A. S. Bhown and B. C. Freeman, "Analysis and status of post-combustion carbon dioxide capture technologies.," *Environ. Sci. Technol.*, vol. 45, no. 20, pp. 8624–32, Oct. 2011.

[60] M. Wang, A. Lawal, P. Stephenson, J. Sidders, and C. Ramshaw, "Post-combustion CO2 capture with chemical absorption: A state-of-the-art review," *Chem. Eng. Res. Des.*, vol. 89, no. 9, pp. 1609–1624, Sep. 2011.

[61] S. Chakravati, A. Gupta, and B. Hunek, "Advanced technology for the capture of carbon dioxide from flue gases," in *1st National Conference on Carbon Sequestration*, 2001.

[62] "UOP Selexol Technology for Acid Gas Removal," 2009. [Online]. Available: http://www.uop.com/?document=uop-selexol-technology-for-acid-gas-removal&download=1. [Accessed: 11-Nov-2015].

[63] M. Li, "Detailed fuel cell modeling for coal-based integrated gasification fuel cell system design and analysis," UNIVERSITY OF CALIFORNIA, IRVINE, 2010.

[64] G. Alptekin, "A Low Cost, High Capacity Regenerable Sorbent for Pre-combustion CO2 Capture," Pittsburgh, PA, and Morgantown, WV (United States), Sep. 2012.

[65] H. Herzog, J. Meldon, and A. Hatton, "Advanced post-combustion CO2 capture," Clean Air Task Force, 2009.

[66] Oilgae, "Capture of CO2 Emissions Using Algae."

[67] M. Zhao, A. I. Minett, and A. T. Harris, "A review of techno-economic models for the retrofitting of conventional pulverised-coal power plants for post-combustion capture (PCC) of CO 2," *Energy Environ. Sci.*, vol. 6, no. 1, pp. 25–40, Dec. 2013.

[68] R. Shao and A. Stangeland, "Amines used in CO2 capture-health and environmental impacts," Bellona report, 2009.

[69] “Econamine FG Plus Process.” [Online]. Available: http://www.fluor.com/econamine/Pages/efgprocess.aspx. [Accessed: 10-Nov-2015].

[70] P. Versteeg and E. S. Rubin, “A technical and economic assessment of ammonia-based post-combustion CO2 capture at coal-fired power plants,” *Int. J. Greenh. Gas Control*, vol. 5, no. 6, pp. 1596–1605, Nov. 2011.

[71] Y. Huang, M. Wang, P. Stephenson, S. Rezvani, D. McIlveen-Wright, A. Minchener, N. Hewitt, A. Dave, and A. Fleche, “Hybrid coal-fired power plants with CO2 capture: A technical and economic evaluation based on computational simulations,” *Fuel*, vol. 101, pp. 244–253, Nov. 2012.

[72] R. Veneman, H. Kamphuis, and D. W. F. Brilman, “Post-Combustion CO2 capture using supported amine sorbents: A process integration study,” *Energy Procedia*, vol. 37, pp. 2100–2108, 2013.

[73] L. M. Romeo, I. Bolea, and J. M. Escosa, “Integration of power plant and amine scrubbing to reduce CO2 capture costs,” *Appl. Therm. Eng.*, vol. 28, no. 8–9, pp. 1039–1046, Jun. 2008.

[74] T. J. Tarka, J. P. Ciferno, M. L. Gray, and D. Fauth, “CO2 Capture Systems Using Amine Enhanced Solid Sorbents,” in *5th Annual Conference on Carbon Capture & Sequestration*, 2006.

[75] M. T. Ho, G. W. Allinson, and D. E. Wiley, “Reducing the Cost of CO 2 Capture from Flue Gases Using Pressure Swing Adsorption,” *Ind. Eng. Chem. Res.*, vol. 47, no. 14, pp. 4883–4890, Jul. 2008.

[76] J. Zhang, P. A. Webley, and P. Xiao, “Effect of process parameters on power requirements of vacuum swing adsorption technology for CO2 capture from flue gas,” *Energy Convers. Manag.*, vol. 49, no. 2, pp. 346–356, Feb. 2008.

[77] S. Sjostrom and H. Krutka, “Evaluation of solid sorbents as a retrofit technology for CO2 capture,” *Fuel*, vol. 89, no. 6, pp. 1298–1306, Jun. 2010.

[78] H. Krutka, S. Sjostrom, and M. Richard, “Topical Report 4: Conceptual 500 MW Design,” ADA Environmental Solutions. Littleton, Colorado, 2011.

[79] S. Sjostrom, H. Krutka, T. Starns, and T. Campbell, “Pilot test results of post-combustion CO2 capture using solid sorbents,” *Energy Procedia*, vol. 4, pp. 1584–1592, 2011.

[80] M. Ajhar, M. Travesset, S. Yüce, and T. Melin, “Siloxane removal from landfill and digester gas - a technology overview.,” *Bioresour. Technol.*, vol. 101, no. 9, pp. 2913–23, May 2010.

[81] W. Breckenridge, A. Holiday, J. O. Y. Ong, and C. Sharp, “Use of Selexol® process in coke gasification to ammonia project,” in *Proceedings of the Laurance Reid Gas Conditioning Conference*, 2000, pp. 397–418.

[82] A. Jayaraman, G. Alptekin, R. Copeland, S. Dietz, and M. Bonnema, “Highly Efficient Pre- combustion Sorbent Based Carbon Capture System,” in *the International Colloquium on Environmentally Preferred Advanced Power Generation*, 2014.

[83] E. R. van Selow, P. D. Cobden, P. A. Verbraeken, J. R. Hufton, and R. W. van den Brink, “Carbon Capture by Sorption-Enhanced Water−Gas Shift Reaction Process using Hydrotalcite-Based Material,” *Ind. Eng. Chem. Res.*, vol. 48, no. 9, pp. 4184–4193, May 2009.

[84] R. W. Stevens, A. Shamsi, S. Carpenter, and R. Siriwardane, “Sorption-enhanced water gas shift reaction by sodium-promoted calcium oxides,” *Fuel*, vol. 89, no. 6, pp. 1280–1286, Jun. 2010.

[85] R. Allam, R. Chiang, J. Hufton, P. Middleton, E. Weist, and V. White, “Development of the sorption enhanced water gas shift process,” in *Carbon dioxide capture for storage in deep geologic formations, Volume 1*, D. C. Thomas and S. M. Benson, Eds. Elsevier Ltd, 2005, pp. 227–256.

[86] L. BARELLI, G. BIDINI, F. GALLORINI, and S. SERVILI, “Hydrogen production through sorption-enhanced steam methane reforming and membrane technology: A review,” *Energy*, vol. 33, no. 4, pp. 554–570, Apr. 2008.

[87] K. Johnsen, H. J. Ryu, J. R. Grace, and C. J. Lim, “Sorption-enhanced steam reforming of methane in a fluidized bed reactor with dolomite as -acceptor,”

Chem. Eng. Sci., vol. 61, no. 4, pp. 1195–1202, Feb. 2006.

[88] K. Y. Foo and B. H. Hameed, "Insights into the modeling of adsorption isotherm systems," *Chem. Eng. J.*, vol. 156, no. 1, pp. 2–10, Jan. 2010.

[89] E. Turiel, C. Perez-Conde, and A. Martin-Esteban, "Assessment of the cross-reactivity and binding sites characterisation of a propazine-imprinted polymer using the Langmuir-Freundlich isotherm," *Analyst*, vol. 128, no. 2, pp. 137–141, Feb. 2003.

[90] J.-Y. Yoon, H.-Y. Park, J.-H. Kim, and W.-S. Kim, "Adsorption of BSA on Highly Carboxylated Microspheres—Quantitative Effects of Surface Functional Groups and Interaction Forces," *J. Colloid Interface Sci.*, vol. 177, no. 2, pp. 613–620, Feb. 1996.

[91] A. Serbezov and S. V. Sotirchos, "Particle-bed model for multicomponent adsorption-based separations: application to pressure swing adsorption," *Chem. Eng. Sci.*, vol. 54, no. 23, pp. 5647–5666, Dec. 1999.

[92] C. Chou and W.-C. Huang, "Simulation of a Four-Bed Pressure Swing Adsorption Process for Oxygen Enrichment," *Ind. Eng. Chem. Res.*, vol. 33, no. 5, pp. 1250–1258, May 1994.

[93] A. Serbezov and S. V. Sotirchos, "Multicomponent Transport Effects in Sorbent Particles under Pressure Swing Conditions," *Ind. Eng. Chem. Res.*, vol. 36, no. 8, pp. 3002–3012, Aug. 1997.

[94] K. S. Knaebel and F. B. Hill, "Pressure swing adsorption: Development of an equilibrium theory for gas separations," *Chem. Eng. Sci.*, vol. 40, no. 12, pp. 2351–2360, Jan. 1985.

[95] G. F. Fernandez and C. N. Kenney, "Modelling of the pressure swing air seperation process," *Chem. Eng. Sci.*, vol. 38, no. 6, pp. 827–834, 1983.

[96] Y. N. I. Chan, F. B. Hill, and Y. W. Wong, "Equilibrium theory of a pressure swing adsorption process," *Chem. Eng. Sci.*, vol. 36, no. 2, pp. 243–251, 1981.

[97] L. H. Shendalman and J. E. Mitchell, “A study of heatless adsorption in the model system CO2 in He, I,” *Chem. Eng. Sci.*, vol. 27, no. 7, pp. 1449–1458, Jul. 1972.

[98] B. Sankararao and S. K. Gupta, “Modeling and simulation of fixed bed adsorbers (FBAs) for multi-component gaseous separations,” *Comput. Chem. Eng.*, vol. 31, no. 10, pp. 1282–1295, Oct. 2007.

[99] K. S. Hwang, J. H. Jun, and W. K. Lee, “Fixed-bed adsorption for bulk component system. Non-equilibrium, non-isothermal and non-adiabatic model,” *Chem. Eng. Sci.*, vol. 50, no. 5, pp. 813–825, Mar. 1995.

[100] J.-H. Park, H.-T. Beum, J.-N. Kim, and S.-H. Cho, “Numerical Analysis on the Power Consumption of the PSA Process for Recovering CO 2 from Flue Gas,” *Ind. Eng. Chem. Res.*, vol. 41, no. 16, pp. 4122–4131, Aug. 2002.

[101] F. V. S. Lopes, C. A. Grande, and A. E. Rodrigues, “Activated carbon for hydrogen purification by pressure swing adsorption: Multicomponent breakthrough curves and PSA performance,” *Chem. Eng. Sci.*, vol. 66, no. 3, pp. 303–317, Feb. 2011.

[102] J. A. Delgado, M. A. Uguina, J. L. Sotelo, and B. Ruíz, “Modelling of the fixed-bed adsorption of methane/nitrogen mixtures on silicalite pellets,” *Sep. Purif. Technol.*, vol. 50, no. 2, pp. 192–203, Jun. 2006.

[103] N. S. Raghavan, M. M. Hassan, and D. M. Ruthven, “Numerical simulation of a PSA system using a pore diffusion model,” *Chem. Eng. Sci.*, vol. 41, no. 11, pp. 2787–2793, 1986.

[104] R. Rajasree and A. . Moharir, “Simulation based synthesis, design and optimization of pressure swing adsorption (PSA) processes,” *Comput. Chem. Eng.*, vol. 24, no. 11, pp. 2493–2505, Nov. 2000.

[105] E. A. Mason and A. P. Malinauskas, *Gas transport in porous media: the dusty-gas model. Vol. 17.* Elsevier Science Ltd, 1983.

[106] R. Jackson, *Transport in porous catalysts. Vol. 4.* New York: Elsevier Science & Technology, 1977.

[107] S. V. Sotirchos, “Multicomponent diffusion and convection in capillary structures,” *AIChE J.*, vol. 35, no. 12, pp. 1953–1961, Dec. 1989.

[108] R. T. Yang, *Gas Separation by Adsorption Processes*. Elsevier Science, 2013.

[109] S. Sircar and J. R. Hufton, “Why Does the Linear Driving Force Model for Adsorption Kinetics Work?,” *Adsorption*, vol. 6, no. 2, pp. 137–147.

[110] F. W. Leavitt, “Non-isothermal adsorption in large fixed beds,” *Chem. Eng. Prog.*, vol. 58, no. 8, pp. 54–59, 1962.

[111] L. M. Sun, P. Le Queré, and M. D. Levan, “Numerical simulation of diffusion-limited PSA process models by finite difference methods,” *Chem. Eng. Sci.*, vol. 51, no. 24, pp. 5341–5352, Dec. 1996.

[112] F. Augier, C. Laroche, and E. Brehon, “Application of computational fluid dynamics to fixed bed adsorption calculations: Effect of hydrodynamics at laboratory and industrial scale,” *Sep. Purif. Technol.*, vol. 63, no. 2, pp. 466–474, Oct. 2008.

[113] S. A. Nouh, L. K.K., and S. A.M., “Modeling and Simulation of Fixed Bed Adsorption Column using Integrated CFD Approach,” *Journal of Applied Sciences*. Asian Network for Scientific Information, 10-Nov-2010.

[114] J. Xiao, L. Tong, D. Cossement, P. Bénard, and R. Chahine, “CFD simulation for charge–discharge cycle of cryo-adsorptive hydrogen storage on activated carbon,” *Int. J. Hydrogen Energy*, vol. 37, no. 17, pp. 12893–12904, Sep. 2012.

[115] D. G. Kröger, *Air-cooled Heat Exchangers and Cooling Towers, Volume 1*. PennWell Books, 2004.

[116] J. C. Kloppers and D. G. Kröger, “Cooling Tower Performance Evaluation: Merkel, Poppe, and e-NTU Methods of Analysis,” *J. Eng. Gas Turbines Power*, vol. 127, no. 1, p. 1, Jan. 2005.

[117] J. C. Kloppers and D. G. Kröger, “A critical investigation into the heat and mass transfer analysis of counterflow wet-cooling towers,” *Int. J. Heat Mass Transf.*, vol. 48, no. 3–4, pp. 765–777, Jan. 2005.

[118] F. Merkel, “Verdunstungskühlung,” *VDI-Verlag*, 1925.

[119] H. B. Nottage, “Merkel’s cooling diagram as a performance correlation for air-water evaporative cooling systems,” *ASHVE Trans.*, vol. 47, pp. 429–448, 1941.

[120] F. Osterle, “On the analysis of counter-flow cooling towers,” *Int. J. Heat Mass Transf.*, vol. 34, no. 4–5, pp. 1313–1316, Apr. 1991.

[121] H. Jaber and R. L. Webb, “Design of Cooling Towers by the Effectiveness-NTU Method,” *J. Heat Transfer*, vol. 111, no. 4, p. 837, Nov. 1989.

[122] M. Poppe and H. Rögener, “Berechnung von rückkühlwerken,” *VDI Wärmeatlas*, p. pp. Mi., 1991.

[123] T. W. Baard, “Performance characteristics of expanded metal cooling tower fill.” Stellenbosch : Stellenbosch University, 1998.

[124] C. Bourillot, “TEFERI: numerical model for calculating the performance of an evaporative cooling tower,” Aug. 1983.

[125] N. Williamson, M. Behnia, and S. Armfield, “Comparison of a 2D axisymmetric CFD model of a natural draft wet cooling tower and a 1D model,” *Int. J. Heat Mass Transf.*, vol. 51, no. 9–10, pp. 2227–2236, May 2008.

[126] R. Al-Waked and M. Behnia, “CFD simulation of wet cooling towers,” *Appl. Therm. Eng.*, vol. 26, no. 4, pp. 382–395, Mar. 2006.

[127] Y. Gudmundsson, “Performance evaluation of wet-cooling tower fills with computational fluid dynamics.” Stellenbosch : Stellenbosch University, 01-Mar-2012.

[128] J. Liu, Y. Hu, D. Zeng, and W. Wang, “Optimization of an air-cooling system and its application to grid stability,” *Appl. Therm. Eng.*, vol. 61, no. 2, pp. 206–212, Nov. 2013.

[129] H. Zhao, H. Wu, and L. Cao, “Analysis on the Back-Pressure Optimum Operation of the Direct Air-Cooled Condenser,” in *2011 Asia-Pacific Power and Energy Engineering Conference*, 2011, pp. 1–4.

[130] H. Zhao and L. Cao, “Study on the Optimal Back-Pressure of Direct Air-Cooled Condenser in Theory,” in *2009 Asia-Pacific Power and Energy Engineering Conference*, 2009, pp. 1–4.

[131] M. Finkenrath, J. Smith, and D. Volk, “CCS Retrofit: Analysis of the Globally Installed Coal-Fired Power Plant Fleet.” OECD Publishing, 29-Mar-2012.

[132] G. Alptekin, A. Jayaraman, and R. Copeland, “Post-Combustion CO2 Capture System for Existing Coal-fired Power Plant, Project Review (DE-FE-0007580),” in *NETL CO2 Capture Technology Meeting*, 2013.

[133] T. J. Skone, “Carbon Dioxide Capture from Existing Coal-Fired Power Plants,” DOE/NETL-401/110907. US., 2007.

[134] S. K. Tyagi, A. K. Pandey, P. C. Pant, and V. V. Tyagi, “Formation, potential and abatement of plume from wet cooling towers: A review,” *Renew. Sustain. Energy Rev.*, vol. 16, no. 5, pp. 3409–3429, Jun. 2012.

[135] J. E. Braun, “Methodologies for the Design and Control of Central Cooling Plants,” University of Wisconsin-Madison, 1988.

[136] D. I. Stevens, “Analysis of Liquid-Desiccant Systems and Component Modeling,” University of Wisconsin-Madison, 1988.

[137] F. Bosnjakovic and K. F. Knoche, *Technische Thermodynamik, Part 1*. Springer-Verlag, 2013.

[138] W. M. Simpson and T. K. Sherwood, “Performance of small mechanical draft cooling towers,” *Refrig. Eng.*, vol. 52, no. 6, pp. 525–543, 1946.

[139] B. A. Qureshi and S. M. Zubair, “A complete model of wet cooling towers with fouling in fills,” *Appl. Therm. Eng.*, vol. 26, no. 16, pp. 1982–1989, Nov. 2006.

[140] T. Muangnoi, W. Asvapoositkul, and S. Wongwises, “An exergy analysis on the performance of a counterflow wet cooling tower,” *Appl. Therm. Eng.*, vol. 27, no. 5–6, pp. 910–917, Apr. 2007.

[141] X. Li, Y. Li, and J. E. Seem, “Dynamic Modeling of Mechanical Draft Counter-Flow Wet Cooling Tower With Modelica,” in *ASME 2010 Dynamic Systems and Control Conference, Volume 2*, 2010, pp. 687–694.

[142] L. D. Berman, *Evaporative cooling of circulating water*. Pergamon press, 1961.

[143] ASHRAE, “Cooling towers,” in *ASHRAE Systems and Equipment Handbook*, 2000.

[144] P. Amick, “E-Gas Technology 2013 Outlook,” 2013.

[145] DOE/NETL, “CB&I E-GAS™ GASIFIERS.” [Online]. Available: http://www.netl.doe.gov/research/coal/energy-systems/gasification/gasifipedia/egas. [Accessed: 12-Nov-2015].

[146] J. Butz, J. Lovell, T. Broderick, R. Sidwell, C. Turchi, and A. K. Kuhn, “Evaluation of Amended Silicate, Sorbents for Mercury Control,” in *Joint EPRI DOE EPA Combined Utility Air Pollution Control Symposium, The Mega Symposium*, 2003.

[147] D. Do Duong, *Adsorption Science and Technology: Proceedings of the Second Pacific Basin Conference on Adsorption Science and Technology : Brisbane, Australia, 14-18 May 2000*. World Scientific, 2000.

[148] A. Kapoor and R. T. Yang, “Surface diffusion on energetically heterogeneous surfaces,” *AIChE J.*, vol. 35, no. 10, pp. 1735–1738, Oct. 1989.

[149] A. Kapoor and R. T. Yang, “Surface diffusion on energetically heterogeneous surfaces—an effective medium approximation approach,” *Chem. Eng. Sci.*, vol. 45, no. 11, pp. 3261–3270, 1990.

[150] R. J. Umpleby, S. C. Baxter, Y. Chen, R. N. Shah, and K. D. Shimizu, “Characterization of Molecularly Imprinted Polymers with the Langmuir−Freundlich Isotherm,” *Anal. Chem.*, vol. 73, no. 19, pp. 4584–4591, Oct. 2001.

[151] G. Alptekin, A. Jayaraman, R. Copeland, S. Dietz, M. Bonnema, M. Schaefer, and M. Cesario, “Novel warm gas CO2 capture technology for IGCC power plants,” *Prepr. Pap.-Am. Chem. Soc., Div. Fuel Chem*, vol. 58, no. 1, 2013.

[152] Y. Choi and H. G. Stenger, “Water gas shift reaction kinetics and reactor modeling for fuel cell grade hydrogen,” *J. Power Sources*, vol. 124, no. 2, pp. 432–439, Nov. 2003.

[153] G. Alptekin, “Impact of Contaminants Present in Coal-Biomass Derived Synthesis Gas on Water-gas Shift and Fischer-Tropsch Synthesis Catalysts,” Pittsburgh, PA, and Morgantown, WV (United States), Sep. 2012.

[154] H. S. Fogler, *Elements of Chemical Reaction Engineering*. Upper Saddle River, New Jersey: Prentice Hall PTR, 2005.

[155] M. E. Davis and R. J. Davis, *Fundamentals of Chemical Reaction Engineering*. Courier Corporation, 2012.

[156] R. E. Cunningham and R. J. J. Williams, *Diffusion in Gases and Porous Media*. Boston, MA: Springer US, 1980.

[157] B. Poling, J. Prausnitz, and J. O. Connell, *The Properties of Gases and Liquids*, vol. 27. McGraw Hill Professional, 2000.

[158] W. Kast and C.-R. Hohenthanner, “Mass transfer within the gas-phase of porous media,” *Int. J. Heat Mass Transf.*, vol. 43, no. 5, pp. 807–823, Mar. 2000.

[159] M. Kaviany, *Principles of Heat Transfer in Porous Media*. Springer Science & Business Media, 2012.

[160] “Different Coal Ranks.” .

[161] “Conservation Reserve Program.” .

[162] M. Downing, D. Langseth, R. Stoffel, and T. Kroll, “Large-Scale Hybrid Poplar

Production Economics: 1995 Alexandria, Minnesota," *7th National Bioenergy Conference*. Nashville, Tennessee, U.S.A.

[163] V. R. Mulkey, V. N. Owens, and D. K. Lee, "Management of Switchgrass-Dominated Conservation Reserve Program Lands for Biomass Production in South Dakota," *Crop Sci.*, vol. 46, no. 2, pp. 712–720, 2006.

[164] D. L. Carpenter, R. L. Bain, R. E. Davis, A. Dutta, C. J. Feik, K. R. Gaston, W. Jablonski, S. D. Phillips, and M. R. Nimlos, "Pilot-scale gasification of corn stover, switchgrass, wheat straw, and wood: 1. Parametric study and comparison with literature," *Ind. Eng. Chem. Res.*, vol. 49, no. 4, pp. 1859–1871, 2010.

[165] "Advanced Gasification: Novel CO2 Utilization Systems, Low Rank Coal IGCC Optimization, and Improvements in Gasification Systems Availability and Costs." DoE Funding Opportunity Number: DE-FOA0000496.

[166] "Greenhouse Gas Reductions in the Power Industry Using Domestic Coal and Biomass Volume 2: Pulverized Coal Plants."

[167] M. Matuszewski, "Greenhouse Gas Reductions in the Power Industry Using Domestic Coal and Biomass - Volume 1: IGCC."

[168] E. van Holthoon, "Shell Gasification Processes," *Gasification Technology Conference*. San Francisco, California, USA, 2007.

[169] C. R. Crocker, S. A. Benson, M. J. Holmes, Y. Zhuang, J. H. Pavlish, and K. C. Galbreath, "COMPARISON OF SORBENTS AND FURNACE ADDITIVES FOR MERCURY CONTROL IN LOW-RANK FUEL COMBUSTION SYSTEMS," *Prepr. Pap.-Am. Chem. Soc., Div. Fuel Chem*, vol. 49, no. 1, p. 289, 2004.

[170] K. Umeki, K. Yamamoto, T. Namioka, and K. Yoshikawa, "High temperature steam-only gasification of woody biomass," *Appl. Energy*, vol. 87, no. 3, pp. 791–798, 2009.

[171] R. Lemus, E. C. Brummer, K. J. Moore, N. E. Molstad, C. L. Burras, and M. F. Barker, "Biomass yield and quality of 20 switchgrass populations in southern Iowa, USA," *Biomass and Bioenergy*, vol. 23, no. 6, pp. 433–442, 2002.

[172] A. R. Smith and J. Klosek, “A review of air separation technologies and their integration with energy conversion processes,” *Fuel Process. Technol.*, vol. 70, no. 2, pp. 115–134, 2001.

[173] R. J. Allam, C. J. McDonald, V. White, V. E. Stein, and M. Simmonds, “Oxyfuel conversion of refinery process equipment utilising flue gas recycle for CO2 capture,” *Greenh. Gas Control Technol.*, vol. 7, 2004.

[174] “Vapor Recompression to Recover Low Pressure Waste Steam.” .

[175] J. Kobayashi, Y. Itaya, S. Tsukada, K. Mizuno, M. Ueda, H. Morikawa, T. Sugimoto, Y. Ueda, Y. Oshika, and N. Kobayashi, “Drying technology for woody biomass for fine grinding by vibration mills,” *Asia-Pacific J. Chem. Eng.*, vol. 2, no. 2, pp. 83–89, 2007.

[176] S. Mani, L. G. Tabil, and S. Sokhansanj, “Grinding performance and physical properties of wheat and barley straws, corn stover and switchgrass,” *Biomass and Bioenergy*, vol. 27, no. 4, pp. 339–352, 2004.

[177] D. L. Bonk and A. Hay, “Stamet Solids Pump Feeds Coal into 210 psig in a DOE Supported Project,” 1995.

[178] D. Aldred, T. Saunders, and G. Shirey, “Results of DOE Funded Research to Achieve Continuous Injection of Solid Fuels into Advanced Combustion and Gasification System Pressures,” *2003 Gasification Technology Conference*. .

[179] R. K. Matta, G. D. Mercer, and R. S. Tuthill, *Power Systems for the 21st Century-“ H” Gas Turbine Combined-cycles*. GE Power Systems, 2000.

[180] S. D. Sharma, M. Dolan, A. Y. Ilyushechkin, K. G. McLennan, T. Nguyen, and D. Chase, “Recent developments in dry hot syngas cleaning processes,” *Fuel*, vol. 89, no. 4, pp. 817–826, 2010.

[181] R. A. Martin, B. Gardner, X. Guan, and H. Hendrix, “Power system development facility: high temperature high pressure filtration in gasification operation,” in *Proceedings of 5th International Symposium on Gas Cleaning at High Temperature*.

[182] P. A. Armstrong, “Method for Predicting Performance of an Ion Transport Membrane Unit-Operation,” *Air Prod. Chem. Inc., Pennsylvania, USA*, 2002.

[183] B. Bishop and N. Raskin, “CeraMem Filter Development Program,” *Advanced Coal-Fired Power Systems ’96 Review Meeting*. Morgantown, West Virginia, USA, 1996.

[184] R. J. Copeland, G. Alptekin, M. Cessario, S. Gebhard, and Y. Gerhanovich, “A novel CO2 separation system,” *The Eighth International Symposium on Transport Phenomena and Dynamics of Rotating Machinery*. Honolulu, HI, USA, 2000.

[185] L. K. Rath, “Assessment of Hydrogen Production with CO2 Capture Volume 1: Baseline State-of-the-Art Plants.”

[186] SRI, *PEP Yearbook International*. Menlo Park, CA, USA: SRI International, 1985.

[187] J. B. Black, “Cost and Performance Baseline for Fossil Energy Plants Volume 3a: Low Rank Coal to Electricity: IGCC Cases.”

[188] “DOE Announces New Hydrogen Cost Goal, July 14, 2005,” 2005. [Online]. Available: http://www1.eere.energy.gov. [Accessed: 25-Dec-2012].

[189] Z. Lin, C. W. Chen, J. Ogden, and Y. Fan, “The least-cost hydrogen for Southern California,” *Int. J. Hydrogen Energy*, vol. 33, no. 12, pp. 3009–3014, 2008.

[190] Bechtel-group-Inc., “Slurry Reactor design studies: slurry vs. fixed-bed reactors for Fischer–Tropsch and methanol; final report. DoE contract DE-AC22-89PC89867.,” Pittsburgh Energy Technology Center, 1990.

[191] CNNMoney, “Why oil could rebound to $80. Yes, $80.” [Online]. Available: http://money.cnn.com/2015/01/09/investing/oil-price-bottom/index.html. [Accessed: 11-Nov-2015].

[192] J. J. Spivey, “FINAL TECHNICAL REPORT: Catalytic Process for the Conversion of Coal-derived Syngas to Ethanol (DOE Award: DE-FC26-06NT43024),” 2011.